THE
PHYSICAL REVIEW

A Journal of Experimental and Theoretical Physics Established by E. L. Nichols in 1893

VOL. 55, NO. 11 JUNE 1, 1939 SECOND SERIES

An X-Ray Study of the Changes that Occur in Malleable Iron During the Process of Fatiguing

RAYMOND G. SPENCER
Albion College, Albion, Michigan

(Received April 17, 1939)

Carefully prepared test bars of malleable iron have been fatigued; x-ray diffraction patterns were taken of each specimen at intervals as fatiguing progressed. This study shows that, when malleable iron is fatigued below its endurance limit, no changes in internal structure that are detectable by the camera used occur after the first few cycles. However, when malleable iron is fatigued above its endurance limit, marked changes do occur. Appreciable changes may occur during the first few cycles of fatiguing. Changes then take place comparatively slowly during the major part of the fatiguing process. These changes proceed at an accelerated rate as the specimen approaches failure. The changes consist of (1) rotation of some of the grains, (2) introduction of strains in some of them, and (3) fragmentation of some of the grains into sizes small enough so that they arrange themselves with random orientation. These changes are all readily detectable with the camera used.

INTRODUCTION

IT is highly desirable, from a theoretical as well as a practical point of view, to know just what changes in structure occur in metals during the process of fatiguing. If changes in internal structure do occur, it is important to know whether they take place only when the metal is fatigued at a stress above its endurance limit or at all values of the fatiguing stress. Since x-rays are one of the best tools that scientists have at their disposal with which to study internal structure of matter, it is natural to attempt to use them to study fatigue. During the last three years, the author has been working on the problem and is of the opinion that very useful information can be obtained by taking diffraction patterns of metals at intervals as fatiguing progresses. Studies of several different metals have been made and some of the results are sufficiently conclusive to report in detail at this time. This paper will be confined to the results obtained by studying malleable iron. Results pertaining to other metals will be reported at a later date.

Some of the earliest experiments in this field were performed by Dehlinger,[1] who investigated the changes produced in cold-rolled copper and silver sheets by repeated bending. Barrett[2] has given a critical review of the literature up to 1936, including a rather complete bibliography. During the last few years Gough and Wood,[3, 4] and Barrett[2, 5] have done careful and extensive

[1] U. Dehlinger, Naturwiss. **17**, 545 (1929).
[2] Charles S. Barrett, "The Application of X-ray Diffraction to the Study of Fatigue in Metals," Am. Soc. for Metals, Preprint, October, 1936.
[3] H. J. Gough and W. A. Wood, Proc, Roy. Soc. **A154**, 510–539 (1936).
[4] H. J. Gough and W. A. Wood, Proc. Roy. Soc. **A165**, 358–371 (1938).
[5] C. S. Barrett, *Metals and Alloys*, **8**, 13–21 (1937).

work and reported their findings. Unfortunately, the results of these workers are in sufficient disagreement to lead to quite different conclusions.

Preparation and Fatiguing of the Specimens

Samples of properly annealed malleable iron were used. (An x-ray diffraction pattern will reveal conclusively whether or not malleable iron is properly annealed.) Each specimen was machined to one-half-inch diameter. A constriction of circular contour was then machined near one end, the smallest diameter of this constriction being $\frac{3}{8}$ of an inch. The last half-dozen cuts with the lathe tool while machining the constriction were each about 0.001 of an inch deep. The specimen was then polished with fine aloxite cloth. Finally, the specimen was etched with acid to remove any metal that might have become strained during the machining and to remove the finely powdered iron and abrasive dust which had become imbedded in the surface of the metal. With this type of surface, the specimen has a lower fatigue limit than it would have if it had been polished and not etched. However, crystallites which have been broken up by machining and polishing and those which have had strains introduced in them must be removed from the sample or the results will be confusing. A study of such a surface should reveal what changes occur due to the repeated stresses of fatiguing not confused with strains that have been produced by other processes before fatiguing has started.

The specimens were fatigued in an ordinary rotating beam machine in my laboratory. They were removed from the machine at intervals as fatiguing progressed and diffraction patterns taken of them.

The Camera

The main part of the camera consists of a casting into which two one-half-inch holes, spaced three inches apart, were bored to receive and hold the specimen. The specimen and camera were marked so that the specimen could be removed and replaced in the camera in exactly the same position. Thus, the x-ray beam impinged upon the same part of the specimen each time an exposure was made. An ordinary collimator which produced a beam of circular cross section was affixed to the casting. The x-ray beam struck the specimen near the middle of the constriction at a point on its smallest circumference or at a point which was subjected to the maximum stress. However, it must be admitted that the x-ray beam did not necessarily strike the point where the maximum strain occurred or where the first fatigue crack would start. It is obvious that, because of the slightly nonhomogeneous structure of the specimen, the greatest strain may occur at any point on the smallest circumference, and not necessarily in the area surveyed by the x-ray beam. A flat film was placed so as to receive the rays diffracted from the 211 planes in a direction nearly perpendicular to the film. This arrangement made the camera quite fast. The films shown in this paper were exposed 30 minutes. The $K\alpha$ line from an iron target was used.

Results

Figure 1(A) is the pattern from specimen No. 1, which has been subjected to 1000 cycles of fatigue at a stress just under the endurance limit. Fig. 1(B) is a pattern from the same specimen after it had been subjected to 10,000,000 more cycles of fatigue under the same conditions.

Figure 2(A) is the pattern from specimen No. 2 before fatiguing was started. Fig. 2(B) is the pattern from the same sample after it had been subjected to 1000 cycles at a stress slightly greater than the endurance limit. Fig. 2(C) is the pattern from the same specimen after 500,000 cycles, Fig. 2(D) after 2,000,000 cycles, and Fig. 2(E) after 2,300,000 cycles. The specimen broke after 2,500,000 cycles. Fig. 2(F) is the pattern from the broken end of the specimen.

Figure 3(A) is the pattern from specimen No. 3 after it had been subjected to 1000 cycles of fatigue at a stress greater than the stress applied to specimen No. 2. Fig. 3(B) is the pattern from the same specimen after 500,000 cycles, Fig. 3(C) after 750,000 cycles, Fig. 3(D) after 1,000,000 cycles and Fig. 3(E) after 1,200,000 cycles. The specimen broke after 1,300,000 cycles. Fig. 3(F) is the pattern taken with the x-ray beam impinging on the broken end.

FIG. 1. X-ray pattern from specimen No. 1 after (A) (1000 fatigue cycles) and (B) (10,000,000 additional fatigue cycles). Stress just under endurance limit.

DISCUSSION OF THE RESULTS

Figure 1(B), taken after 10,000,000 cycles of fatiguing just under the endurance limit for the specimen, is an exact duplicate of Fig. 1(A), taken after 1000 cycles. Each of these two patterns has the same number of spots distributed in the same way. Corresponding spots in the two patterns have the same intensity and structure as nearly as can be seen by the naked eye. Evidently, no changes in the internal structure of malleable iron, which are detectable by this camera, occur after the first few cycles of fatiguing if the specimen is fatigued below the endurance limit. This is in agreement with Gough and Wood's[3] results obtained with mild steel, but in disagreement with the general conclusion drawn by Barrett.[2, 5] Neither Gough and Wood nor Barrett worked with malleable iron.

Figure 2(B), taken from specimen No. 2 after 1000 cycles of fatiguing at a stress slightly above the endurance limit, has several more spots than Fig. 1(B), taken before fatiguing started. One might assume from this that some of the crystallites rotate slightly and some of them break up into smaller units during the first few cycles of fatiguing. This is in agreement with some of Gough and Wood's[3, 4] findings. Fig. 2(C) and Fig. 2(D) are not markedly different from 2(B) or from each other. Fig. 2(E) shows that some of the crystallites have been broken down into small enough fragments to assume nearly random orientation and some of them are severely strained as is indicated respectively by a more marked background in the line and blurring of the spots that remain in the line. A condition like that indicated by Fig. 2(E) always indicates that the specimen is approaching failure very rapidly. Evidently, after the first few cycles of fatiguing, changes take place very slowly during the major part of the fatiguing, but as the specimen approaches failure changes, consisting of the incidence of marked grain distortion and some fragmentation, take place more and more rapidly as the specimen approaches failure. While grain distortion and fragmentation is more marked in some specimens than others, they always precede failure of the specimen. Fig. 2(F) was taken with the x-ray beam impinging upon the broken end of the specimen. It indicates fragmentation of nearly all the grains to a very small size randomly oriented and possessing strains of an undetermined amount.

Gough and Wood[4] state that failure may be preceded by a complete fragmentation of the grains down to a limiting size of 10^{-4} to 10^{-5} cm. with completely random orientation. The writer finds, in the case of malleable iron, that much of this fine fragmentation is associated with the formation of fatigue cracks and with the actual rupture of the specimen. The fine fragmentation indicated in Fig. 2(F) was, of course, produced by the actual breaking of the specimen.

The patterns in Fig. 3 show about the same characteristics as are shown in Fig. 2. The changes took place more rapidly in this specimen because it was stressed more severely. Figs. 3(A), (B) and (C) are not markedly different from each other. Fig. 3(D) indicates marked distortion of the crystallites but very little grain fragmentation. Severe grain distortion as shown by this pattern probably always precedes fine fragmentation. Fig. 2(E) indicates very marked fragmentation of the grains. Fatigue cracks were visible at the time this pattern was taken. Fig. 2(F) again indicates that fragmentation is produced by the process of rupture.

The term "distortion" as used above refers to changes in the grains which causes a blurring of the spots. These changes may consist of an actual bending of atomic planes over an entire grain, the bending of atomic planes over a part of a grain or of "block displacement" of one part of a grain with respect to the other part. It is difficult, and sometimes impossible, to distinguish between these effects by studying a diffraction pattern.

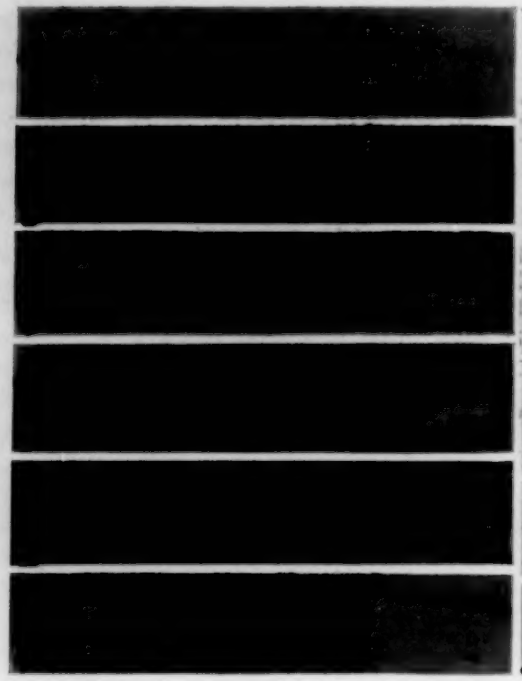

FIG. 2. X-ray pattern from specimen No. 2. Stress just over endurance limit. (A) before fatigue. (B) after 1000 cycles. (C) 500,000. (D) 2,000,000. (E) 2,300,000. (F) from broken end.

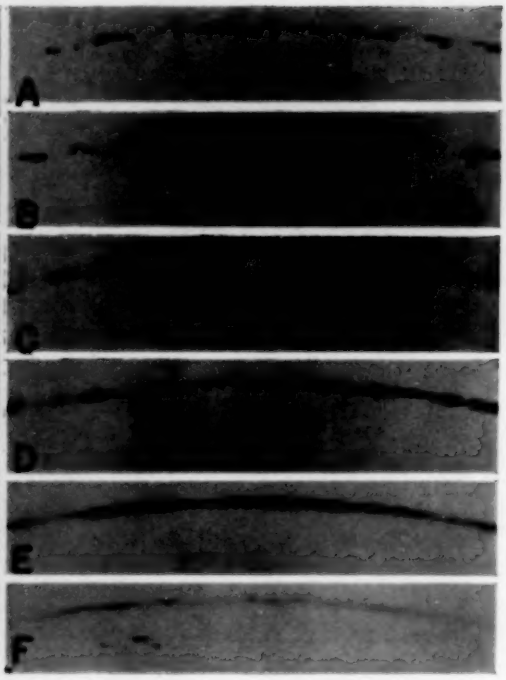

FIG. 3. X-ray pattern from specimen No. 3. Stress greater than that for sample No. 2. (A) after 1000 fatigue cycles. (B) 500,000. (C) 750,000. (D) 1,000,000. (E) 1,200,000. (F) from broken end.

CONCLUSIONS

It appears to be reasonable to draw the following conclusions. (1) When malleable iron is fatigued below its endurance limit no appreciable changes occur in its internal structure after the first few cycles of fatiguing. (2) When it is fatigued at a stress greater than its endurance limit, appreciable rotation of the grains and some splitting of the grains may occur during the first few cycles. (3) Very slight changes in internal structure occur during the major part of the fatiguing process. (4) As the specimen approaches failure very marked grain distortion occurs followed by fragmentation of some of the grains to small enough size to approach random orientation. (5) The formation of fatigue cracks or rupture makes very fine fragments of all the grains adjacent to the fatigue crack or rupture.

ACKNOWLEDGMENTS

It is a pleasure to acknowledge that this study was made possible by grants of money by the Trustees of the Horace H. Rackham and Mary A. Rackham Fund. All of the apparatus, equipment and supplies used were paid for with the money made available by these grants.

The Rossi Transition Curve for Small Angle Showers*

W. M. NIELSEN, J. E. MORGAN, *Duke University, Durham, North Carolina*

AND

K. Z. MORGAN, *Lenoir Rhyne College, Hickory, North Carolina*

(Received April 17, 1939)

Measurements have been made of 7° and 28° cosmic-ray shower production in iron up to thicknesses of approximately 320 g/cm². A comparison of the data here presented and measurements previously reported for 38° showers leads to the conclusion that there is no significant difference in the ratio of counting rates at the first maximum of the Rossi transition curve to that under 200 g/cm² for either large or small angle showers. It is concluded that the processes which are responsible for the character of the transition curve under large thicknesses of material are not necessarily restricted to small angles.

1. INTRODUCTION

EVER since the early investigation of Rossi[1] the production of cosmic-ray showers in various materials has been the subject of numerous investigations.[2] These studies have involved the use of G-M counters in various geometrical arrangements and, in general, are in very good agreement as to most of the important features of the transition curve. The well-known first maximum of the transition curve is qualitatively in agreement with what one would expect on the view that such showers are the result of multiplication processes associated with ordinary electrons and quanta. Current theories as to the properties of such particles are unable, however, to account for showers under large layers of material. We have expressed the view based on G-M counter[3] and cloud-chamber[4] studies that a considerable number of such showers, particularly the small ones, are produced by light particles which must be secondary to the penetrating component of the cosmic radiation.

Quite recently Bothe and Schmeiser[5] in a series of interesting papers have presented evidence which they have interpreted as showing that the prominence of the so-called second maximum of such transition curves is a marked function of the angular spread of the detected showers, being more prominent for small angle showers. The significance of these observations has already attracted a good deal of theoretical interest[6] because of their possible relation to the generation of a considerable number of penetrating particles (mesotrons) under large layers of materials. Because of this fact and because of the very direct relation of this work to our investigations referred to above, we have made measurements of small angle (7°) and large angle (28°) showers under layers of iron up to a thickness of approximately 320 g/cm².

2. EXPERIMENTAL ARRANGEMENT AND RESULTS

In the present series of measurements, the experimental techniques are essentially the same as those used in previously reported work with G-M counters from this laboratory. The arrangement of counters is shown in the insert of Fig. 1, which has been drawn to scale. Fourfold coincidences between the inner group of counters and between the outer four counters were counted as 7° and 28° showers, respectively.*

It is well known that this counter arrangement increases the importance of the material com-

* A report on this work was presented at the New York meeting of the American Physical Society, February, 1939.

[1] B. Rossi, Zeits. f. Physik **82**, 151 (1933).

[2] See, for example, such summaries as H. Geiger, Ergebn. d. Exakt. Naturwiss. **14**, 42 (1935); Darol K. Froman and J. C. Stearns, Rev. Mod. Phys. **10**, 133 (1938).

[3] K. Z. Morgan and W. M. Nielsen, Phys. Rev. **52**, 564 (1937); W. M. Nielsen, J. Frank. Inst. **226**, 601 (1938).

[4] J. I. Hopkins, W. M. Nielsen and L. W. Nordheim, Phys. Rev. **55**, 233 (A) (1939).

[5] K. Schmeiser, Naturwiss. **25**, 173 (1937); K. Schemiser and W. Bothe, Naturwiss. **25**, 669–670 (1937); K. Schmeiser and W. Bothe, Ann. d. Physik **32**, 161 (1938).

[6] W. Heitler, Proc. Roy. Soc. **A166**, 529 (1938); W. Heisenberg and H. Euler, Ergebn. d. Exakt. Naturwiss. **17**, 1–69 (1938); G. Wentzel, Phys. Rev. **54**, 869 (1938).

* We are using the terms 7° and 28° showers in the sense heretofore given them in the cosmic-ray literature. Actually the angles may be greater; the length of the counters was 20 cm.

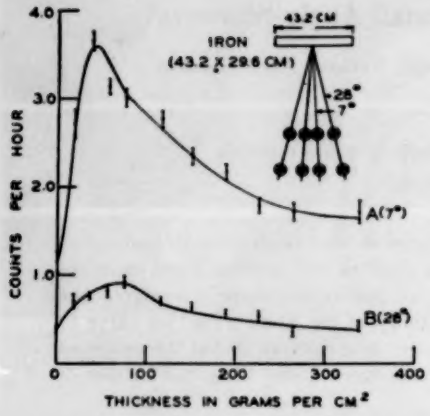

FIG. 1. Fourfold coincidence counting rate of 7° and 28° showers as a function of material thickness in grams per square centimeter. Area of iron plates 43.2×29.6 cm.

pared to the background count as measured by the ratio of the counting rate at the first maximum of the transition curve to the counting rate with no scattering material above the counters.

We have also made similar measurements of 7° and 28° showers generated in layers of iron of twice the cross-sectional area shown in Fig. 1. We felt this was necessary in order to remove the major portion of the background due to showers coming in at appreciable angles with the vertical. The data under these conditions are shown in Fig. 2.

There are considerable differences between the transition curves here presented and those reported by Bothe and Schmeiser, and we shall therefore discuss them in some detail.

DISCUSSION

There has been considerable discussion[5, 7] in the literature as to the existence of a real second maximum in the Rossi transition curve. These investigations have indeed indicated a hump in the curve at a thickness of approximately 200 g/cm² in a considerable number of cases. It is also true that generally the departure from a smooth curve in the region in question is rather small. In the work of Bothe and Schmeiser the shower curves for the smaller angles have been drawn in such a way as to indicate two well-defined peaks. One of us[3] has emphasized that the important conclusion from the work of Bothe and Schmeiser is not that a deviation from a smooth curve seems to be indicated, but rather that there seems to be a progressive increase in the ratio of the counting rate at approximately 200 g/cm² to that at the first maximum, as one goes from the larger to the smaller angle shower curves. The data of Bothe and Schmeiser for the smaller angles show a counting rate at about 200 g/cm² comparable to that at the first maximum. Clearly if the processes which are responsible for the possible second maximum are of such a character as to be largely confined to small angles and are of increasing importance at large thicknesses of material, we should expect just such a change. In our discussion which follows we are only interested in this feature of the curves.

The curves *A* of Figs. 1 and 2 appear quite normal and are very similar, as discussed later, to earlier measurements in this laboratory and elsewhere. One very difficult question in any discussion of the Rossi transition curve is the treatment of the background. We have tried to remove, insofar as possible, complications of this kind by using a counter arrangement which is most sensitive to twofold showers from above, and have thereby obtained a relatively high ratio between the number of showers produced in sufficiently thick layers of iron to the background count. It is also clear that such an arrangement is more effective in the absorption of the background count than one which detects

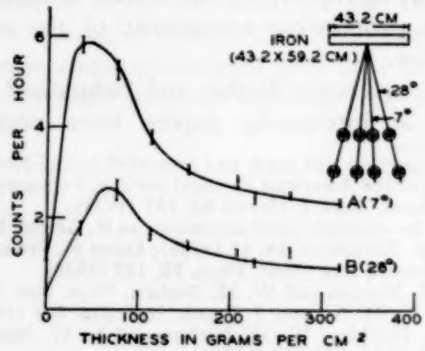

FIG. 2. Fourfold coincidence counting rate of 7° and 28° showers as a function of material thickness in grams per square centimeter. Area of iron plates 43.2×59.2 cm.

[7] J. N. Hummel, Naturwiss. **22**, 170 (1934); H. Kulenkampff, Physik. Zeits. **35**, 996 (1934); H. Maass, Physik. Zeits. **35**, 858 (1934); A. Drigo, Ricerca. Scient. **5**, 88 (1934); M. Ackelmann, Naturwiss. **22**, 169 (1934); J. Clay, A. van Germert and J. T. Wiersma, Physica **7**, 627 (1936).

only two- or threefold coincidences. That very few of the coincidences are due to higher multiple showers from the sides was shown by placing absorbing materials at the sides of the counters in which case the counting rate was sensibly unaltered. We are therefore fairly certain that the measured counting rates give a qualitative indication of the effects caused by the presence of the iron above the counters. Curves *A* and *B* of Figs. 1 and 2 are quite parallel and give no apparent evidence for a relatively larger counting rate under the larger thicknesses of material for the showers of smaller angular divergence.

This last conclusion is more forcefully shown by a comparison of the 7° curve of Fig. 1 with some of our earlier measurements[3] of the Rossi curve in which the angle subtended at the lower layers of material was 38°, and the actual counting rates (including background) have been divided by 2.5 for comparison purposes in Fig. 3. The curves are essentially alike. There is certainly no evidence here for a relatively increased counting rate at large thicknesses on the 7° curve.

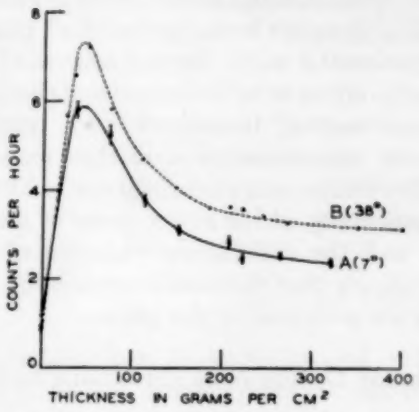

FIG. 3. A comparison of the data of curve *A* of Fig. 1 (full curve) with measurements previously reported, reference 3, (dashed curve) the ordinates of which have been divided by 2.5 for comparison purposes.

The question naturally arises as to why two series of experiments such as those of Bothe and Schmeiser and those here presented should lead to such apparently different results. We have therefore modified our technique by connecting the two upper counters together as shown in Fig. 4. A similar arrangement was used by Bothe and Schmeiser. In this case triples are counted. The curve is not unlike that of Bothe and Schmeiser for 7° showers. In this case the added counting rate due to the iron is relatively very much less compared to the very large background. While Bothe and Schmeiser attempted to avoid complications caused by the background count, we are inclined to believe they have underestimated its importance in their work. Certainly it is significant that our own measurements show that the relatively high counting rate at large thicknesses is peculiar to an arrangement relatively insensitive to showers from the scattering material above it. We are therefore forced to conclude that our own measurements show that there is no significant difference in the ratio of counting rates at the first maximum to that under 200 g/cm² of iron, for either large or small angle showers, and that the processes which are responsible for the character of the transition curve under large thicknesses of a material are not necessarily restricted to small angles.

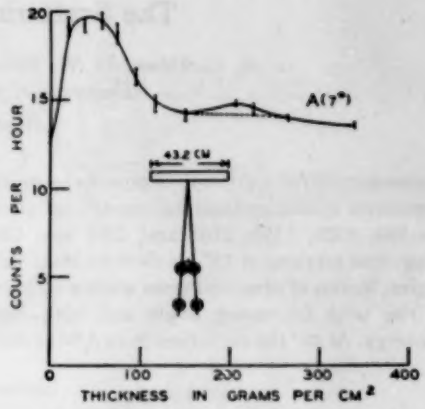

FIG. 4. Threefold coincidence counting rate of 7° showers from iron.

The writers are indebted to Mr. Charles George for aid in the taking of data.

The Scattering of Protons by Protons

R. G. HERB, D. W. KERST,* D. B. PARKINSON† AND G. J. PLAIN
University of Wisconsin, Madison, Wisconsin

(Received April 19, 1939)

The cross section for scattering of protons by protons has been measured at angles from 15° to 45° for protons of energies 860, 1200, 1390, 2105 and 2392 kev. Observed scattering cross sections at 15° are close to Mott values for all energies. Ratios of observed cross section to Mott cross section rise with increasing angle and with increasing proton energy. At 45° the ratio rises from 3.90 at 860 kev to 42.9 at 2392 kev. At 1830 kev measurements were made at scattering angles up to 60° and the scattering cross section showed the theoretically expected asymmetry (cos θ) about 45°. As a check on the proton-proton measurements the scattering of protons from argon and krypton was investigated with protons of energies between 850 kev and 2440 kev.

INTRODUCTION

THE scattering of protons by protons was investigated by Tuve, Heydenburg and Hafstad[1] in 1936 using protons in the energy region between 600 kev and 900 kev. At small scattering angles their observed yields were fairly close to the Mott values, but at large angles they found that the ratio of observed yield to Mott yield rises with voltage and reaches a value of approximately 4 at 900 kev and 45°. Breit, Condon and Present[2] found that the results of THH could be fitted by assuming an attractive interaction between protons in the ^1S state. They were able to determine the magnitude of this interaction within fairly close limits and found that it is nearly the same as that between a proton and a neutron in a ^1S state. Breit, Condon and Present showed that accurate scattering measurements over a wide voltage region might offer the possibility of an accurate determination of the range of the ^1S interaction between protons.

Upon completion of the generator at Wisconsin in April, 1936, Professor Breit pointed out the desirability of extending the measurements of THH to the higher energies available at this laboratory. Measurements were started early in January, 1937 and by August, 1937 data had been obtained over the energy range from 900 kev to 2400 kev. The data were sufficiently consistent, but it was thought that the results might be subject to systematic errors. Improvements were made in apparatus and several months were then spent in a thorough investigation of all phases of the experimental work. Several sources of small systematic errors were discovered and eliminated, and experimental techniques were improved. Scattering measurements were then made over the entire energy range from 860 kev to 2392 kev. The consistency of the entire series of measurements and the satisfactory outcome of check work indicate that the results are reliable. These results are presented in this paper.

GENERAL DESIGN OF SCATTERING CHAMBER

The scattering chamber used in these experiments is shown in Figs. 1 and 2. High velocity protons from the generator pass through an aluminum foil covering a hole in disk *A*. This foil separates the main vacuum system from the scattering chamber, which contained hydrogen at a pressure of about 11 mm Hg during most of the scattering measurements. After passing through the collimating slit system the proton beam goes through the chamber, through aluminum foil *F*, and into collector cup *G*. The region around the collector cup is evacuated so that ionization currents cannot vitiate measurements of proton current.

The ionization chamber for detection of scattered protons is equipped with an analyzing slit system which limits the effective scattering volume to a small region near the center of the chamber, and which selects only protons which are scattered into a small angular region. A graduated disk serves as a support for the

* Now at the University of Illinois, Urbana, Illinois.
† Now at the Bell Telephone Laboratories, New York, New York.
[1] M. A. Tuve, N. P. Heydenburg and L. R. Hafstad, Phys. Rev. **50**, 806 (1936).
[2] G. Breit, E. U. Condon and R. D. Present, Phys. Rev. **50**, 825 (1936).

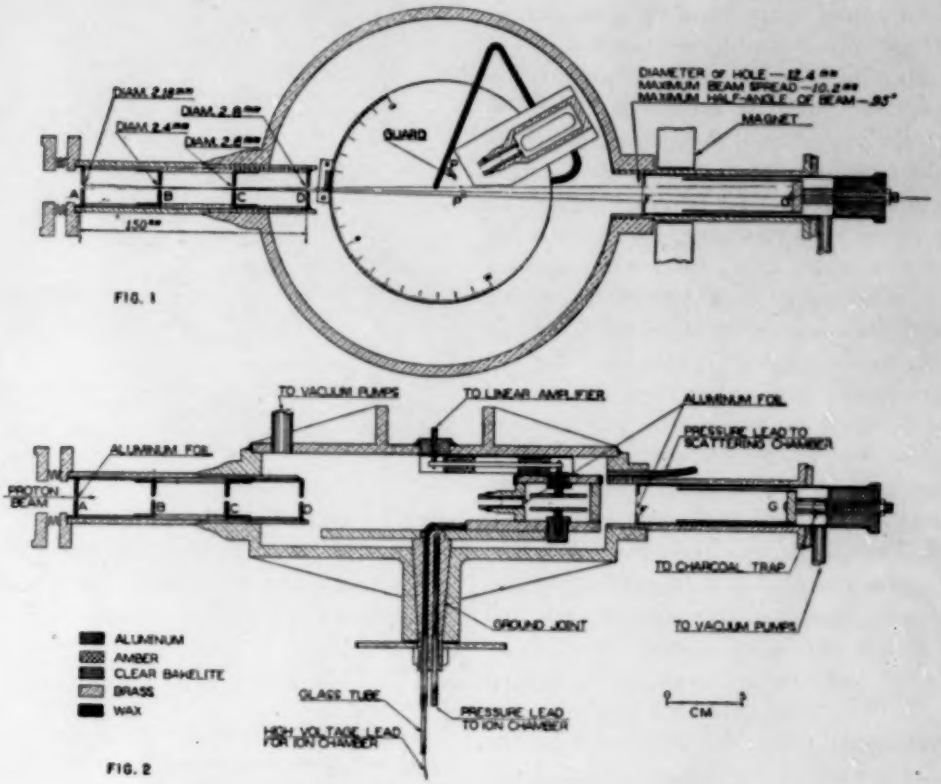

FIGS. 1 and 2. Two views of proton scattering chamber.

ionization chamber. It can be rotated through a ground joint and angular settings can be read through a window in the cover of the scattering chamber. An aluminum foil covers a hole at the inner end of the slit system and isolates the ionization chamber. During scattering experiments the ionization chamber is filled with air at pressures up to approximately one-half atmosphere. Pulses from the ionization chamber go to a linear amplifier, which is connected through a scaling circuit to a counter.

MECHANICAL DETAILS OF SCATTERING CHAMBER

The scattering chamber and its cover are brass castings. They were first turned down to approximately the desired dimensions, were annealed by a heat treatment, and then were allowed to age for a period of five weeks before the final turning. In finishing the holes for the two necks which carry the collimating slit system and the collector cup system the procedure was as follows: The chamber was clamped to the carriage of a lathe. A boring bar was mounted so as to turn between centers, and the two holes were bored (equal diameters) without unclamping the chamber. These holes were therefore accurately in line.

For good geometry the axis of the collimating slit system must intersect the axis about which the ionization chamber turns and must be perpendicular to it. For accurate fulfillment of these requirements the following procedure was used in finishing the hole for the ground brass plug: A mandrel of solid cold-rolled steel 20 inches long was accurately turned between centers to a tight slip fit in the holes for the two necks and was put in place with its ends protruding through the holes. The chamber was mounted in a four-jaw chuck and a sensitive gauge (Universal dial indicator) was mounted on the carriage about 3 inches off center with its stem pointed toward the chuck. As the chuck was turned and the mandrel swung over the ball of the gauge the maximum gauge deflection was noted. The chuck was then turned a half revolution and the maximum gauge

deflection was noted as the mandrel again moved past the gauge. The back of the chamber rested against studs which had been threaded into the face of the chuck and by means of these the chamber was adjusted until the gauge deflections were equal to within approximately 0.0002 inch. This adjustment provided for perpendicularity of the two axes referred to above. To provide for intersection of the two axes a further adjustment was made. The gauge was mounted on the carriage with its stem vertical and with its ball below center by an amount slightly less than the radius of the mandrel, and the chuck was turned so that the mandrel was horizontal. The carriage was moved so that the ball of the gauge passed beneath one end of the mandrel where it protruded from the chamber and the gauge deflection was noted. The gauge was then moved to the other end of the mandrel and the deflection was again noted. These measurements were repeated after the chuck had been turned through an angle of 180° and the chamber was adjusted until gauge deflections at each end of the mandrel were equal to within 0.0002 inch for the two angular positions of the chamber. Since adjustment for intersection of the axes disturbed the adjustment for their perpendicularity it was necessary to make successive repetitions of the two adjustments until both requirements were accurately fulfilled. With the chamber thus adjusted the tapered hole for the ground plug was finished.

Heavy-walled brass tubing turned inside and outside was used for the two necks. They were turned to a press fit for the holes and were soldered into place with the least possible heating of the chamber. Greater dependability would have been assured if the necks had been soldered into place before the final turning, but this method could not be used because the complete chamber could not be swung in the largest of the lathes available.

The ground plug and rotating disk were roughed out, soldered together, and the system was then mounted on a lathe between centers for the final turning. A dividing head dependable to 0.01 degree was used for graduating the rotating disk. Graduation lines on both disk and vernier index were fine and accurately made, and settings on an integral tenth degree could be made to within approximately 0.01 degree. A spring washer clamped by a nut held the ground plug in place, and a gear reduction system was provided to facilitate accurate angular setting.

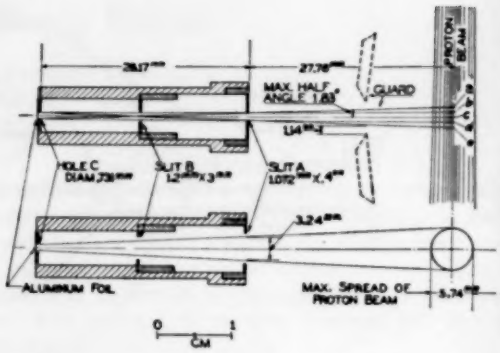

FIG. 3. Analyzing slit system set perpendicular to the proton beam. This slit system slips into the nose of the ionization chamber. The two possible positions of the guard are outlined by a broken line.

IONIZATION CHAMBER

The nose, front face and two sides of the ion chamber were machined as a unit from a solid brass block. Plates for the back end and base were fastened with screws and soldered. The top plate (removable) was fastened by screws and was sealed with wax. For alignment of the ion chamber a solid brass mandrel was turned to form a tight slip fit into the neck of the scattering chamber, and one end was turned down to a tight slip fit into the nose of the ion chamber. By means of a special arbor the ion chamber could be mounted on a lathe. The base plate was faced off until the mandrel could be slipped into the nose of the ion chamber with the ion chamber clamped in place on the graduated disk, with grease on the ground plug, and with the mandrel extending through the neck and across the scattering chamber. This gave assurance that the axis of the analyzing slit system passed through the point of intersection of the axis of the collimating neck with the axis of the rotating disk. With the ion chamber clamped in place, holes were drilled, and the base of the ion chamber was pinned to the disk. Four screws were provided to clamp the base of the ion chamber to the disk, since the pins were only for alignment.

The brass tube carrying the collimating disks was machined from solid rod (tight slip fit into neck), and precautions were taken to assure that the inner surface was made accurately concentric with the outer surface. The collimating disks were made of hard aluminum sheet which machines easily, and the holes were accurately centered. Two holes were drilled through the ground plug, one for the high voltage lead and one for a gas line, to the ionization chamber. The gas line extends approximately radially through the disk, and connection is made to the ionization chamber.

Slit System

Figure 3 shows the analyzing slit system. It was made to have a tight slip fit into the nose of the ionization chamber. Hole C was turned on a lathe with a fine tool and was therefore accurately centered with respect to the outer cylindrical surface of the slit system. The hole was beveled with the smaller diameter toward the inside, and the aluminum foil was placed over the outer edge of the hole so that protons could not go through the foil in a small region around its edge. Slits A and B were made of brass 0.2 mm thick and were finished with a fine file. Slit B was made sufficiently large so that it did not define the incoming proton stream. As shown in Fig. 3 (lower view), slit A is sufficiently long so that the entire width of the proton beam is included in the effective scattering volume, and it was therefore not essential to provide accurate centering of the slit along this dimension with respect to the outer surface of the cylindrical holder. However, the edges of slit A shown in the upper view of Fig. 3 define the effective scattering volume and determine the average scattering angle. The slit defined by these edges must be accurately centered with respect to the holder. To check the centering of slit A the holder was inserted into a hole (slip fit) in a brass block and a cross hair of a comparator was set on, and parallel to one slit edge. The cylindrical holder was then turned through 180° and the comparator was adjusted until the cross hair was on the second edge. By successive repetition of this procedure the slit was shown to be off center by less than 0.01 millimeter. Slit-edge roughness limited the accuracy of the check, but the limit set on the accuracy of centering is very satisfactory.

The thickness of the scattering volume measured along the central axis of the proton beam is determined by the width of slit A. When the slit system is perpendicular to the central axis of the beam any element of area in the plane of hole C can see a section of the beam of thickness $T=2bR_0/h$ where $2b$ is the width of slit A, h is the distance from hole C to slit A, and R_0 is the distance from hole C to the center of the proton beam. When the slit system is set at any angle θ with respect to the proton beam the effective target thickness, measured along the axis of the beam will be $T/\sin\theta$. The solid angle Ω subtended by the hole C is given by A/R_0^2 where A is the area of hole C. If Y is the number of counts for a given number N of incident protons, then $Y=T\Omega\sigma Nn/\sin\theta$ where n is the number of target protons per cm³ and σ is the scattering cross section per unit solid angle. Substituting for T and Ω this expression becomes

$$Y=2bANn\sigma/R_0h\sin\theta=Nn\sigma G/\sin\theta$$

or $\sigma=Y\sin\theta/NnG$ where $G=2bA/R_0h$ is a geometric constant which must be accurately determined by measurement.

The diameter of hole C was measured with a Zeiss microscope equipped with a scale (AA objective, 20X eyepiece calibrated by Zeiss, 0.1-mm scale). The hole was not round (maximum variation of diameter 2 percent), but the edge was smooth and sharp. Readings were taken at uniformly spaced intervals of 15°, and values of the area were consistent to within 0.3 percent.

Measurement of the width of slit A caused difficulty because of surface roughness. Accurately ground knife edges would have been more satisfactory than the slit used. A comparator was tried for this measurement, but it proved to be less satisfactory than the Zeiss microscope. Microscope readings of the width were taken at intervals of 0.2 mm along the length of the slit. Within a central region 2 mm wide (1 mm from each side of the center) the maximum variation in width was 0.8 percent, and the average width, obtained April, 1938, was 1.0725 mm. Most of the protons will enter in this region, but taking into consideration the maximum possible spread of the main proton beam (5.74 mm at center of

chamber) protons can enter this slit in a region 3.24 mm long. The average width of the outer region was 1.065 mm, but since most of the protons enter the central region the value 1.072 mm was assumed for the width of the slit. A micrometer comparator was used to determine the distance from slit A to hole C. This determination is dependable to within approximately 0.1 percent. For determining the distance from slit A to the center of the scattering chamber the microscope of a comparator was sighted on the end of the slit system, the ion chamber was turned through 180°, and the carriage was then moved to the new position of the slit system. This gave double the distance desired, and the value determined in the April, 1938 measurements for the distance in question was 27.76 mm (dependable to better than 0.1 percent).

All measurements were made several times, and by at least two persons before scattering observations were started. In April, 1937 these measurements were gone into more thoroughly. Three persons worked approximately a week on the determinations before they were considered dependable. The values obtained were: $T=2.12$ mm, $\Omega=1.344\times10^{-4}$ steradian, and $G=2.850\times10^{-6}$ cm. In April, 1938 three persons again spent several days on the measurements. Techniques were improved and the final values obtained were: $T=2.129$ mm, $\Omega=1.341\times10^{-4}$ steradian, and $G=2.855\times10^{-6}$ cm. The April, 1938 value of G is considered to be more reliable than those obtained previously and was used for computation of the final data. Estimates of the probable error involved in the measurements are difficult to make. In spite of the time spent on check work and the precautions taken, small systematic errors may still be present. It is considered unlikely, however, that the final value of G is off by more than 0.5 percent.

For convenience in the experimental work the proton-proton scattering yield Y was expressed in counts per microcoulomb of incident protons per mm of oil pressure. The value of N was computed to be 6.250×10^{12} protons per microcoulomb using $e=4.80\times10^{-10}$ e.s.u. The value of n was found to be 4.492×10^{15} atoms per cm^3 at 0°C per mm of oil pressure. The oil density was assumed to be 0.864 which is the density of Apiezon oil B at 26°. In computing n the value 6.023×10^{23} was used for Avogadro's number. Substitution of the values of G, N and n into the expression for σ gives $\sigma=Y\sin\theta\times1.247\times10^{-24}$ cm^2.

In computing the expression for σ a number of approximations were used which must be given some consideration. The scattering angle θ was taken as the angle between the central axes of the collimating slit system and the analyzing slit system. The maximum half-angle spread of the collimated proton beam is 0.95°. The maximum half-angle spread allowed by the analyzing slit system is 1.83° in the plane determined by axes of the slit systems. If $d^2Y/d\theta^2$ were zero, where Y is the scattering yield, the experimental values of σ would not be affected by the angular spread of the slit systems. At large scattering angles effects are negligible since $d^2Y/d\theta^2$ is small for Rutherford scattering, and it is still smaller for proton-proton scattering yields. Calculations in the paper by Breit, Thaxton and Eisenbud show that at 15° $d^2Y/d\theta^2$ is sufficiently large to cause an appreciable shift in experimental values of σ. At 20° the effect is also appreciable at the low proton energies.

Other factors in addition to those described can affect the experimental values of σ. A thorough analysis of the problem is given in the paper by Breit, Thaxton and Eisenbud in this issue. They find that because of the approximations used in computing σ experimental values of the scattering cross section are probably too high by about 2.5 percent at 15° and by about half that amount at 20° in the lower energy region. These corrections were not applied to the data. The approximate expression was used for σ and no adjustments were made in experimental values.

Errors due to imperfections in the mechanical construction of the scattering chamber appear to be entirely negligible. After completion of the scattering measurements the chamber was examined to see if warping had taken place during the two years it was used. The collimating slit system was removed and mandrels of cold-rolled steel having tight slip fits in the collimating neck were used for checking alignment of the apparatus. The axis of the graduated disk was found to be 0.067° off from perpendicularity with respect to the axis of the collimating neck. The position of the analyzing slit system depends on the thickness of the grease film on the ground

plug and with a very thin film the axis of this slit system was 0.20 mm below (orientation of Fig. 2) the axis of the collimating neck. Errors due to these two imperfections add but they are entirely negligible. With the ionization chamber set at an indicated angle of 15° the true scattering angle is 0.002° greater because of these imperfections. At larger scattering angles the angular shifts are smaller. When the apparatus was first assembled the vernier index (Fig. 1) was not accurately set to read true scattering angle. It was set only approximately since it seemed desirable to determine the zero angle or angle of symmetry by yield measurements. Scattering measurements showed that the yield values were very nearly equal when angular settings were made at $+14.8°$ and $-15.2°$ where angles on one side of the beam are referred to as positive and angles on the other side as negative. In all yield measurements the angular reading $-0.2°$ was taken as the true zero angle and in making a measurement at 30°, for example, angular settings were made at $+29.8°$ and at $-30.2°$.

During the examination of the chamber a mandrel, inserted in the collimating neck, was used to check the angle of symmetry. One end of the mandrel was turned down to give a tight slip fit in the nose of the ionization chamber. With the mandrel in place pushed into the nose of the ionization chamber the angular reading of the vernier index was $-0.2°\pm0.015°$. Thus the zero angle determined by mechanical alignment agreed with the zero angle determined by scattering measurements. When the mandrel was first tried the grease film on the ground plug was very thin and the ground plug had to be pushed inward about 0.2 mm before the mandrel would enter the nose of the ionization chamber. Grease was then applied to the plug and after a short period of "working in" the ion chamber was at the proper level so that the mandrel entered the nose with the ground plug seated. The zero angle reading was again $-0.2°\pm0.015$.

The axis of the graduated disk was found to be displaced by 0.05 mm from the axis of the collimating neck, but errors due to this displacement are entirely negligible because of the following considerations. First, the check on the zero angle showed that when the reading of the vernier index was $-0.2°$ the axis of the analyzing slits coincided with the axis of the collimating neck and thus angular readings were accurate. Second, the distance R_0 from hole C to the center of the scattering chamber enters only to the minus first power in G and it was taken as one-half the distance between diametrically opposite positions of hole C. At each angle θ equal numbers of counts were taken at $+\theta$ and $-\theta$ and thus errors cancel out except for second-order effects which are smaller than one part in 10^6.

The hole covered by foil F was found to be 0.4 mm off center with respect to the axis of the collimating neck but allowing for this displacement protons in the beam defined by the collimating slits could come no closer than 0.7 mm to the edge of the hole.

Aluminum Foils

Aluminum foil $\sim1.44\times10^{-4}$ cm thick was used to cover the hole over the collector cup chamber, and also to cover hole C, Fig. 3. For the hole over the collimating slits, aluminum foil with a thickness of $\sim0.97\times10^{-4}$ cm was used. Foils were cut sufficiently large so that they overlapped the supporting disks well. After a foil had been centered over a hole its edge was wetted with a 2-percent solution of collodion in amyl acetate applied with a small brush. This application caused the foil to adhere to the supporting disk and to stretch out smoothly over the hole. Red sealing wax was then applied around the edge of the foil to form a ring which covered the foil near its edge and extended over the supporting disk. As the wax cooled it stretched the foil tight and left it smooth. A careful examination was then made to see that no wax had flowed past the edge of the disk where it would block out part of the hole. To plug small holes in the foils they were painted with a 5-percent solution of collodion in amyl acetate. This solution was spread on as evenly as possible and measurements showed that the energy loss of protons in the collodion film was less than 5 kev for protons in the energy region of 900 kev. For an accurate determination of the absorption thickness of the foil over hole A the following procedure was used. The collector cup and the chamber which surrounds it were removed from the scattering chamber and another collector cup with a

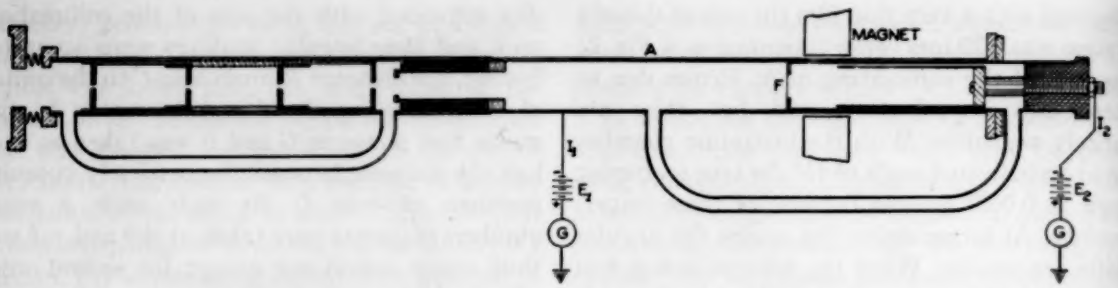

FIG. 4. Apparatus for checking the method of measuring proton current.

calcium fluoride crystal at its base was substituted. To prevent the crystal from charging up when bombarded by protons it was covered with fine mesh nickel gauze. With the scattering chamber evacuated the gamma-ray yield was investigated in the region of the 862-kev and the 927-kev fluorine resonances, and the generator voltages at which these resonances appeared were accurately determined. These measurements gave the energy loss of protons at only two voltages, but the energy loss at any other voltage could then be determined by means of the "range in aluminum *versus* proton energy" curve which had been previously determined.[3] Determination of the absorption thickness of the foil over hole *A* was complicated further because of the formation of a carbon deposit on the foil which increased in thickness with bombardment time. In early proton scattering measurements no correction was made for this additional absorption thickness and the results were therefore inaccurate. During the course of the final measurements which yielded the results given in this paper periodic determinations were made of foil thickness. The carbon deposit was assumed to increase in thickness linearly with bombardment time, and its thickness was determined for each series of scattering experiments.

The absorption thickness of newly installed foils for disk *A* varied from 54 kev to 46 kev for emergent protons of 862 kev, and absorption thickness was found to increase on the average by 1 kev for each scattering run where "run" is used to designate a series of yield measurements as a function of scattering angle at constant voltage. Each run required approximately 3½ hours of bombardment time. The final absorption thicknesses of the two foils used after July 28 were 74 kev and 60 kev.

[3] D. B. Parkinson, R. G. Herb, J. C. Bellamy and C. M. Hudson. Phys. Rev. **52**, 75 (1937).

MEASUREMENT OF PROTON CURRENT

Only a negligible fraction of protons are scattered out of the main beam in going through the hydrogen. The beam has a maximum possible spread of 10.2 mm at aluminum foil *F*, Fig. 1, and the foil covers a hole 12.4 mm in diameter. Charge due to protons entering collector cup *G*, Fig. 1, was stored on a condenser when scattered protons were being counted. A magnetic field of 600 gauss (position of magnet shown in Fig. 1) prevented secondary electrons from vitiating charge measurement. Special contact points on a charge and discharge key were arranged so that when one button was pressed the Cenco counter started, and charge started accumulating on the condenser. Pressing a second button stopped the counter and discharged the condenser through a ballistic galvanometer. A 1-microfarad mica condenser was used, and when taking data the potential on the condenser was never allowed to build up to more than 10 volts. The charge and discharge key was enclosed in a de-humidified case, and the lead from the collector cup was supported by paraffin blocks. Before taking data the system was checked for leakage in the following way. A small "*C*" battery with a tap at approximately 10.5 volts was used for charging the condenser, and the ballistic galvanometer deflections were determined as a function of time between charge and discharge. In the final measurements on scattering yield these checks showed that with the values of condenser voltage and leakage time used in obtaining data leakage could not give an error of more than 0.2 percent.

The charge and discharge key was provided with hard rubber insulation and with tungsten contact points. Tests were frequently made with a constant voltage from a battery for charging the condenser, and ballistic galvanometer deflections were always consistent to within 0.1 percent for all voltages tried.

When taking data on proton scattering the potential of the collector cup becomes positive with respect to the surrounding cylinder which is grounded, and if the region around the cup is not well evacuated, ionization current will cause charge leakage. A charcoal trap was provided for the region around the collector cup. Before taking data on proton scattering, this trap was heated by a special furnace and was well outgassed. A stopcock in the lead to the vacuum system was then closed, and the trap was immersed in liquid air. To check for ionization currents the following procedure was used. The yield of scattered protons was determined in the usual way by taking approximately 10,000 counts at a particular angle and voltage. Then a 10½ (sometimes 22½)-volt battery was connected in the lead to the collector cup, and scattering yield was determined first with the collector cup negative with respect to the condenser and then with the polarity of the battery reversed. Reversing the connections of the battery reverses the direction of an ionization current, and since the battery voltage was as high as or higher than the maximum voltage on the condenser, effects of ionization current on yield determinations should have been magnified several times. This check was frequently used after completion of a series of proton scattering yields. When foil F, Fig. 1, was in good condition no check showed any ionization current, and

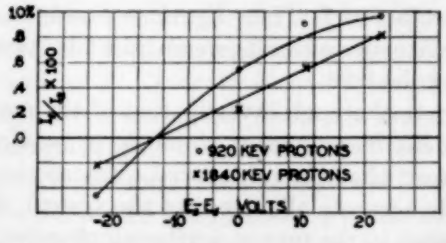

FIG. 5. Current measurement test: foil over collector cup, no foil over collimating slits. I_1/I_2 is the ratio of current from chamber A to current from the collector cup. (E_2-E_1) is the potential difference between the collector cup and the chamber. The slopes of the curves are probably due entirely to ionization current.

with 10,000 counts a yield change of 1 percent would have been detected. Changing the potential on the collector cup should also change a secondary electron current, and since the change in yield was less than 1 percent when a 22½-volt battery was used the effect of secondary electrons on proton scattering results must have been negligible.

The dependability of the method of current measurement might be questioned because of the

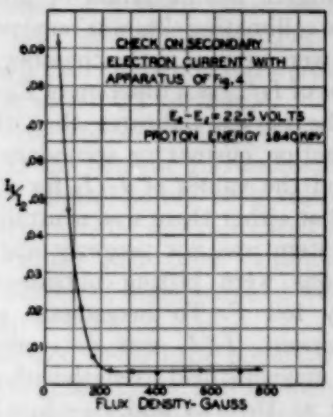

FIG. 6. Showing variation of I_1/I_2 with the strength of the magnetic field used for suppression of secondary electron currents. In proton scattering work a field of 600 gauss was used.

possibility that an appreciable fraction of the protons are neutral as they leave the aluminum foil and enter the collector cup. As neutralization effects could not be easily investigated with the proton scattering set up, the arrangement shown in Fig. 4 was used. This arrangement also provided the opportunity for further checks on secondary electron currents and ionization currents. The collimating slit system and the collector cup with its surrounding chamber were removed from the scattering chamber and were installed in this apparatus with distances from collimating slits to foil and collector cup the same as in the scattering chamber. The same magnet was used for suppression of secondary electrons as in the scattering apparatus, and the magnet was placed in the same position with respect to the end of the collector cup. Chamber A was ordinarily kept at a potential of -45 volts (E_1) to prevent entrance of secondary electrons. Proton current entering chamber A is given by I_1+I_2, and if the collector cup system were

perfect I_1 would be zero. The apparatus was well insulated and, when tests were made with no protons entering the chamber, no leakage currents could be detected. In proton scattering experiments the potential of the collector cup rises from zero to a maximum of 10 volts (average of 5 volts) as the condenser charges, and the chamber around the collector cup is grounded. In this check work E_2-E_1 was varied from $+22\frac{1}{2}$ volts to $-22\frac{1}{2}$ volts, and the ratio I_1/I_2 was determined.

To investigate neutralization of protons the foil over the collimating slits was removed so that no protons were neutral in the chamber A. Fig. 5 shows ratios of I_1/I_2 as a function of E_2-E_1. The slope of the curves indicates that there was either ionization current or secondary electron current, and the values of I_1/I_2 for $E_2-E_1=0$ indicates that either there was neutralization or else the system was not properly aligned, and some protons were hitting outside the hole covered by foil F. To investigate secondary electron current, I_1/I_2 was determined as a function of magnetic field strength with generator voltage set at 1840 kv and $E_2-E_1=22\frac{1}{2}$ volts (Fig. 6). Since I_1/I_2 showed no change as the magnetic field was decreased from 760 gauss to 250 gauss it seems safe to conclude that secondary electron current was negligible, and that the slopes of the curves of Fig. 5 must have been due to ionization current. Further considerations as explained below substantiated this conclusion. In obtaining the experimental results shown in Fig. 5 the test chamber was connected to the main vacuum system which was at a pressure of approximately 10^{-5} mm Hg with the ion source running. Rough computations showed that ionization currents of a few tenths of one percent should be obtained.

Values were obtained for I_1/I_2 as a function of E_2-E_1 with the collimating slit foil in place and with foil F removed. For this experiment the apparatus was modified so that the test chamber could be isolated from the main vacuum system, and a charcoal trap was used in an attempt to improve vacuum conditions. Results of one run are shown in Fig. 7. Values of I_1/I_2 vary only slowly with E_2-E_1 which shows that ionization currents were small, yet the pressure was much higher than that maintained in the collector cup chamber during proton scattering measurements.

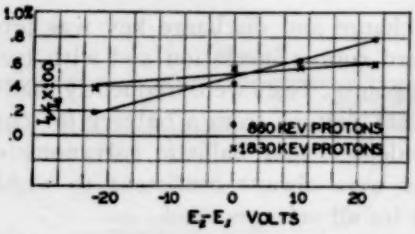

FIG. 7. Current measurement test: no foil over collector cup, foil over collimating slits. Showing I_1/I_2 as a function of E_2-E_1. Since foil F was removed for this work neutralization of protons could have given no contribution to I_1. During this work the vacuum in the test chamber was better than for the work of Fig. 5 and ionization currents were smaller.

At the conclusion of this run, when the test chamber was connected to the main vacuum system, the ionization gauge showed a pressure rise of 10^{-6} mm Hg. In similar checks after all proton scattering runs which were included in the final data the pressure rise was never greater than 5×10^{-8} mm Hg.

Since foil F was not in place during the experiment giving the data shown in Fig. 7, neutralization of protons could give no contribution to I_1. A comparison of the results shown in Fig. 7 with the results of Fig. 5 indicates that neutralization effects must be small, probably negligible. Further experiments were tried with both foils in place, but these data yielded little additional information.

When the apparatus was removed from the generator it was examined for alignment. The hole which is ordinarily covered by foil F was found to be off center with respect to the axis of the slit system. No accurate measurement was made of the displacement, but careful sighting through the system showed that a small percentage of protons coming through the collimating slits could miss the hole. It is probable that the finite values of I_1/I_2 for $E_2-E_1=0$ and the lack of consistency in results were caused by protons missing the hole.

A more thorough investigation of the method of current measurement would have required a new test chamber of special construction to provide accurate alignment of the system. Since alignment in the proton scattering chamber was satisfactory, this error could not have entered. It seems safe to conclude that the collector cup system used for proton scattering could have introduced an error no greater than 0.5 percent.

Calibration of Ballistic Galvanometer

As explained previously, current from the collector cup flows onto a mica condenser while scattered protons are being counted, and charge is measured by means of a ballistic galvanometer. The ballistic galvanometer was equipped with an Ayrton shunt providing a number of different sensitivities, three of which were used in proton scattering measurements. After careful adjustment had been made for linearity of the ballistic galvanometer its sensitivity varied by less than 0.1 percent for deflections in the region between 30 cm and 50 cm (50-cm scale, 170 cm from galvanometer). During measurements on proton-proton scattering only this region of the scale was used, and a constant value was assumed for sensitivity.

The capacity of the mica condenser was not accurately known, and after investigation there seemed to be difficulty in obtaining an accurate determination of its value. To make the calibration of the ballistic galvanometer independent of the capacity of the mica condenser the following method was used. Current from a 400-volt B eliminator supplied by a Raytheon voltage regulator was fed onto the mica condenser through a high resistance (S.S. White resistors). This current was measured by a calibrated galvanometer, and it was fed onto the condenser through the charge and discharge key in exactly the same way that proton current flows onto the condenser during proton scattering experiments. The current was allowed to flow for a known time, and it was then interrupted by the key, and the condenser was discharged through the ballistic galvanometer. Several periods of current flow were used ranging from ½ minute to 4 minutes to check the consistency, and several values of current were used for each calibration. Current was read at 5, 10, or 15 second intervals, and readings were averaged. With this system the ballistic galvanometer was calibrated for each of the sensitivities used in scattering experiments.

A careful search was made for possible systematic errors. Leakage was found to be negligible from any part of the system. Ordinarily in the calibration work the current galvanometer was connected in the ground lead of the mica condenser, but it was changed to the high voltage terminal of the condenser, and results were not changed. Tests showed that the measurement of time for a minute interval was dependable to approximately 0.02 percent. For calibration of the current galvanometer a known fraction of the voltage of a dry cell was picked off by a voltage divider (Leeds and Northrup resistance boxes), and current was fed through a 100,000-ohm resistance box to the galvanometer. The e.m.f. of the dry cell was determined immediately before use by means of a Wolff potentiometer and a standard cell, and all resistances used were checked on a Post Office box and were found to be accurate to within 0.1 percent.

During the course of the proton scattering experiments the ballistic galvanometer was calibrated five times. Before each calibration the current galvanometer was calibrated with standard cells which had been calibrated at the National Bureau of Standards and were reserved for calibration work.

There seemed to be little possibility that the calibration of the ballistic galvanometer could be off by more than 0.3 percent, but after completion of the scattering experiments it was thought advisable to try an entirely different method of calibration. A General Radio precision air condenser with a maximum capacity of 1435.66 $\mu\mu$f was charged to high voltage (maximum 400 volts) by B batteries, and was discharged through the ballistic galvanometer. The air condenser was calibrated especially for this work by the General Radio Company. Voltage was measured by a voltmeter which was calibrated at the Standards Laboratory of the University of Wisconsin. Values were determined for the sensitivity of the ballistic galvanometer with five different condenser settings ranging from 917.31 $\mu\mu$f to 1435.66 $\mu\mu$f. Potentials in the region of 390 volts and in the region of 280 volts were used. The percentage differences between these values of the sensitivity and the "current-time" value ranged from -0.88 percent to -0.42 percent with an average of -0.76 percent.

No investigation was made of the cause of the discrepancy since the air condenser method was not very satisfactory for precise work. The maximum charge available gave a deflection of less than half-scale with the galvanometer set for maximum sensitivity. The current-time method

was least accurate with the ballistic galvanometer at maximum sensitivity, and in proton scattering experiments this sensitivity was never used. In computing proton scattering yields the "current-time" values for the sensitivity of the ballistic galvanometer were used.

Measurement of Proton Energies

The generating voltmeter used for measurement of generator voltage has been described in previous publications.[4] For calibration of the voltmeter the gamma-ray yield from lithium was investigated and the value 440 kev was assumed for the energy position of the resonance. In recent calibrations diatomic ions were used and the generator voltage at which the lithium resonance appeared was assumed to be 880 kev. Calibrations were made with lithium on May 17 and on August 15, and the calibration was checked by investigation of the 862-kev fluorine resonance on August 17, August 26, September 17 and October 8.

During the course of the experimental work carried out since the construction of the generator frequent checks have been made on the performance of the voltmeter and no departure from linearity has ever been detected. In work on the 927-kev fluorine resonance with protons and hydrogen diatomic ions no shift was observed in the sensitivity of the voltmeter between 927 kev and 1854 kev although a shift of 0.2 percent could have been detected. Proton scattering yields from krypton serve as a rough check on the linearity of the voltmeter up to 2473 kev (2440 kev-protons at the center of the scattering chamber). Because of difficulty in the measurement of proton current the krypton results do not set close limits on the linearity of the voltmeter, but they indicate that the voltmeter could have changed in sensitivity by no more than 0.5 percent between 1850 kev and 2470 kev.

Since May 1938 the current output of the generating voltmeter has remained constant to within 0.1 percent at 7.035×10^{-10} amp. per kilovolt. The galvanometer used for measuring current from the voltmeter has changed in sensitivity several times during the past year, but during the final work on proton scattering galvanometer sensitivity was checked frequently, usually before a series of scattering measurements, and this instrument could have caused no error in voltage measurement. Proton energies were corrected for absorption loss in the foil over the collimating slits and a correction was applied for absorption loss in the gas between the foil and the center of the scattering chamber. It is believed that the greatest uncertainty in the values assumed for the proton energies at the center of the scattering chamber is due to the uncertainty in the position of the "440 kev" lithium resonance which was used for calibration of the generating voltmeter.

Detection of Scattered Protons

A linear amplifier of the Dunning type was used for detection of scattered protons. Voltage for the high potential plate of the ionization chamber was supplied by a voltage regulator circuit. Usually this potential was set at about 700 volts. The first stage of the amplifier was mounted on the scattering chamber, and the 259B-tube was carried by a heavy piano wire spring which served as a floating support. The scattering chamber was rigidly clamped to a heavy support (weight 500 lb.) which rested on sponge rubber, and the chamber was connected to the magnetic analyzer by a sylphon bellows. Very little change in amplifier background could be noticed when the generator was started. A constant check on noise level and pulse size was maintained by means of a cathode-ray oscilloscope which was connected to the output stage of the amplifier. Pulses from the amplifier were fed into a scale-of-ten counter,[5] and the output pulses from the scaling circuit were fed into an 885 recorder circuit which operated a Cenco high impedance counter. A set of earphones was connected across the input (885) tube of the scaling circuit. *C* bias on the 885 tube was adjusted while watching the oscilloscope and listening to the breakdown of the tube by means of the earphones. For the smallest pulses obtained in the scattering measurements, those due to proton-proton scattering at 860 kev and 45 degrees, the ratio of pulse size to noise level was sufficiently great to give dependable counting.

[4] D. B. Parkinson, R. G. Herb, E. J. Bernet and J. L. McKibben, Phys. Rev. **53**, 642 (1938).

[5] D. W. Kerst, Rev. Sci. Inst. **9**, 131 (1938).

The entire counting arrangement caused very little trouble. Once during two years' work the scale-of-ten counter failed because of a punctured condenser, and at another time high humidity caused leakage in the scaling circuit which made the scaling ratio undependable. An accurate and convenient check on the scaling ratio can be made by feeding pulses at 120 cycles into the amplifier and by determining the number of output pulses per minute. This check was always made before and after taking data on proton scattering. Additional checks were also made occasionally. The scale-of-ten circuit was connected in parallel with a scale-of-eight circuit of standard design, and the two were found to check perfectly. The scaling ratio was also checked for counting rates much lower than any used in the proton scattering work, and the ratio was found to be dependable. The counting rate was always kept below 20 pulses per second (two pulses per second from scaling circuit), and since the longest time constant was 1/2000 second (input of scaling circuit) the correction for counts missed was negligible.

Air pressure in the ionization chamber was measured by means of a small dial gauge. For high energy protons the pressure was not critical and was usually set at about one-half atmosphere, and for the slowest protons the pressure was adjusted for maximum pulse size. At 860 kev and 45 degrees the optimum pressure was approximately $\frac{1}{8}$ atmosphere.

A considerable amount of check work was done on the counting system. Proton scattering yields were studied as a function of (1) counting speed, (2) pressure in the ionization chamber, (3) setting of the C bias of the input tube of the scaling circuit, (4) potential on the high voltage plate of the ionization chamber. All results indicated that the counting system was dependable.

Hydrogen Supply and Pressure Measurements

Hydrogen from a supply tank (commercial hydrogen) was passed through a palladium tube into the scattering chamber. A tungsten filament around the palladium tube served to control its temperature, and when filling the scattering chamber the filament was kept well below red heat. Hydrogen pressure in the chamber was measured by means of a manometer containing Apiezon oil B. One end of the manometer was connected to the vacuum system. The glass U-tube was made sufficiently large in diameter (inside diameter $\frac{1}{2}$ inch), so the effects of capillary attraction were negligible. A steel scale graduated in $\frac{1}{2}$ mm was mounted between the arms of the manometer, and oil levels were read by means of a telescope equipped with cross hairs mounted at a distance of $3\frac{1}{2}$ feet from the manometer. The telescope was well mounted, and readings of hydrogen pressure were always consistent to better than 0.1 percent. An Invar tape which was accurate to within 0.003 percent was used to check the steel scale and the steel scale was found to be off by less than 0.03 percent. The density of the Apiezon oil was carefully measured and was found to be 0.864 at 26 degrees C. This value checks the results of O. Beeck[6] to within 0.02 percent. A mercury thermometer held against the scattering chamber by Plasticine served to determine hydrogen temperature. To avoid errors due to changing room temperatures, hydrogen temperature and pressure were always read simultaneously. For convenience, pressures were reduced to P_0 (pressure at 0°C). The value of P_0 was found to remain constant when the temperature changed showing that the thermometer as mounted was dependable for determining hydrogen temperature. Values of hydrogen pressure P_0 are considered to be reliable to approximately 0.2 percent.

Slit Edge Scattering

When scattering experiments were first tried with the chamber evacuated a large yield was obtained at small angles due to scattering from slit edges. A consideration of the geometry showed that protons scattered from the edge of the last collimating slit could enter the ionization chamber if they were re-scattered from the edge of the first analyzing slit. To reduce the slit edge yield a beveled aluminum sheet 20 mm long by 9 mm wide was placed as shown in Fig. 1 and Fig. 3. It is mounted on an arm equipped with a toggle joint and is automatically swung from position P Fig. 1 to position P' as the ionization

[6] O. Beeck, Rev. Sci. Inst. **6**, 399 (1935).

TABLE I. *Proton-proton scattering results.*

DATE	PROTON ENERGY (KEV)	ANGLE 15°	20°	25°	30°	35°	40°	45°
Aug. 2	2392	2.56	1.286	1.000				0.498
Aug. 3	2392	2.56	1.312	1.010	0.839	0.704	0.604	
Aug. 4	2392	2.50	1.306	1.000	0.833	0.702	0.595	0.498
2392 Average		2.54	1.301	1.003	0.836	0.703	0.600	0.498
2392 Mott		2.262	0.5180	0.1626	0.06275	0.02880	0.01606	0.01162
Ratio		1.124	2.51	6.17	13.31	24.4	37.4	42.9
July 29	2105	2.95	1.376	1.050	0.858	0.740	0.600	0.530
July 30	2105	2.87	1.433	1.027	0.853	0.746	0.608	0.520
2105 Average		2.91	1.405	1.039	0.855	0.743	0.604	0.525
2105 Mott		2.925	0.6698	0.2102	0.08114	0.03720	0.02074	0.01501
Ratio		0.993	2.098	4.95	10.54	19.98	29.1	35.0
July 28	1840	3.37	1.454	1.084	0.876	0.737	0.643	0.540
Aug. 23	1848	3.36			0.892		0.637	
Aug. 5	1812	3.53	1.488	1.084	0.889	0.756	0.623	0.543
July 28	1830*	3.40	1.457	1.084	0.876	0.737	0.643	0.540
Aug. 23	1830*	3.43			0.892		0.637	
Aug. 5	1830*	3.48	1.482	1.084	0.889	0.756	0.623	0.543
Sept. 15	1830	3.38	1.480	1.058	0.881	0.729	0.636	
1830 Average		3.42	1.473	1.075	0.885	0.741	0.635	0.542
1830 Mott		3.871	0.8868	0.2784	0.1074	0.04929	0.02746	0.01986
Ratio		0.884	1.661	3.862	8.24	15.04	23.12	27.28
Oct. 5	1390	5.16	1.645	1.065	0.855		0.609	0.509
Oct. 7	1390	5.28	1.677	1.054	0.856	0.703	0.602	0.514
1390 Average		5.22	1.661	1.060	0.856	0.703	0.606	0.512
1390 Mott		6.720	1.538	0.4831	0.1865	0.08540	0.04760	0.03442
Ratio		0.777	1.080	2.196	4.59	8.23	12.74	14.88
Oct. 3	1200	6.70	1.866	1.043	0.800	0.672	0.576	0.476
Oct. 6	1200	6.69	1.857	1.020	0.799	0.682	0.565	0.478
1200 Average		6.70	1.862	1.032	0.800	0.677	0.571	0.477
1200 Mott		9.019	2.066	0.6485	0.2501	0.1147	0.06388	0.04620
Ratio		0.743	0.901	1.590	3.20	5.90	8.93	10.32
Sept. 30	854	13.55	2.77	1.044	0.641	0.493	0.420	0.345
Sept. 30	860*	13.38	2.75	1.044	0.644	0.499	0.424	0.349
Aug. 26	860	12.97	2.71		0.644		0.425	
Sept. 14	860	13.23	2.68	1.012	0.633	0.498	0.420	0.354
Sept. 16	860	13.20	2.71	1.026	0.649	0.501	0.416	0.349
860 Average		13.19	2.71	1.027	0.643	0.499	0.421	0.351
860 Mott		17.60	4.032	1.266	0.4882	0.2239	0.1245	0.08998
Ratio		0.750	0.672	0.811	1.317	2.229	3.38	3.90

chamber moves through the position of zero angle. Both positions of the guard were determined by stops which were accurately set by means of a special mandrel. The mechanism was ruggedly built and never caused any difficulty. Periodic checks were made of the stops, and they were always found to be satisfactory. After installation of the guard, measurements at 860 kev and at 1830 kev for angles from 15° to 45° with the chamber evacuated gave yields at each angle which were less than 0.05 percent of the corresponding yields obtained from hydrogen at the usual pressure.

HYDROGEN CONTAMINATION

Apiezon grease L was used for all stopcocks which were connected to the proton scattering chamber. American Express wax No. 2 was used for all wax joints inside the chamber and Picein was used on joints for which wax was applied to the outside of the chamber. In the early scattering experiments no trap was provided for condensation of vapors in the scattering chamber, and contaminants gave a large contribution to the scattering yield. The contribution of contaminants was reduced by the installation of a

liquid-air trap on the scattering chamber. An investigation of the scattering from contaminants was then made in the following way. After the chamber had been evacuated it was isolated, the trap was immersed in liquid air, and the contamination yield at 15° was studied as a function of time. After a period of approximately four hours the yield was investigated at two different voltages as a function of angle. Yields were found to increase approximately linearly with time and varied with angle and voltage according to the Rutherford formula.

During the experimental work on proton-proton scattering which gave the final results the contamination yields were measured and corrections were applied by the following method: After the scattering chamber had been filled with hydrogen to the desired pressure the generator voltage was set to give protons with an energy of 860 kev at the center of the scattering chamber, and the ionization chamber was set to detect protons scattered at 35°. Pressure in the ionization chamber was then adjusted so that pulses due to protons scattered by protons were of just sufficient size to permit accurate counting. Protons scattered by contaminant atoms suffered little loss in energy and gave large pulses which could be easily distinguished from the small proton-proton pulses by observation of the cathode-ray oscilloscope. For a determination of contamination yield large pulses were counted by visual observation while the regular counter system received a total of 2500 pulses. This contamination measurement was made immediately before and after each series of measurements on proton-proton scattering. From the observed contamination yields at 860 kev and 35° corrections were computed for all angles and voltages.

Procedure in Scattering Measurements

Difficulty in early measurements had shown the necessity for thorough check work, and in the scattering measurements giving the final data, the procedure was as follows: The charcoal trap (connection shown in Fig. 1) was heated by means of a furnace for a period varying from ¾ hour to 2 hours for thorough outgassing. During this time the apparatus and leads for measurement of proton current was checked for leakage, and the scale-of-ten counter was checked for reliability. Usually at this time the sensitivity of the voltmeter galvanometer was checked. After the charcoal trap had cooled the scattering chamber was pumped out to a pressure of approximately 2×10^{-6} mm Hg. The palladium tube for purification of hydrogen was then heated somewhat hotter than for the final filling for about five minutes, and the hydrogen was pumped out through the chamber. The palladium tube was then allowed to cool, and after the scattering chamber and hydrogen lead were again pumped down to a good vacuum, a stopcock was turned which isolated the chamber from the vacuum system. The palladium tube was then heated (heating filament not red) until the oil manometer connected to the chamber showed a pressure of approximately 180 mm. While the scattering chamber was being filled with hydrogen a flask of liquid air was put around the trap which was connected to the scattering chamber. Immediately after the chamber had been filled, liquid air was put around the charcoal trap, and the apparatus was then ready for scattering measurements. Before each series of scattering measurements generator voltage was first set to give 860-kev protons at the center of the scattering chamber, time was noted, and a determination was made of the contamination yield. The average initial contamination yield at 35° and 860 kev for all runs was 0.73 percent of the total yield. Generator voltage was then set for investigation of 1830-kev protons, and the scattering yield was determined at 15°. For this determination 12,000 counts were taken, 6000 on one side of the beam and 6000 on the other side. This standard yield served to interlock all scattering measurements and gave protection against errors

TABLE IA. *Percentage corrections to be applied to yield values because of the variation of oil density with temperature. Positive correction percentages are to be added to the yield values and negative corrections are to be subtracted.*

Proton energy kev	Scattering Angle						
	15°	20°	25°	30°	35°	40°	45°
2392	+0.22	+0.22	+0.22	+0.13	+0.13	+0.13	+0.22
2100	+ .22	+ .22	+ .22	+ .22	+ .22	+ .22	+ .22
1830	+ .11	+ .08	+ .08	+ .11	+ .08	+ .11	+ .08
1390	+ .05	+ .05	+ .05	+ .05	+ .05	+ .05	+ .05
1200	+ .14	+ .14	+ .14	+ .14	+ .14	+ .14	+ .14
860	− .05	− .05	− .05	− .05	− .05	− .05	− .05

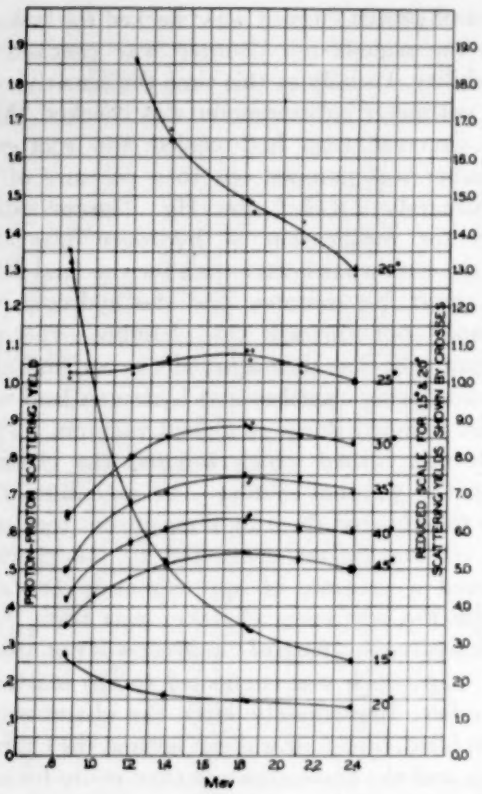

FIG. 8. Showing proton-proton scattering yields as a function of proton energy. The yield values of Table I are plotted with yields given in counts per microcoulomb of incident protons per mm oil pressure at 0°C. These values multiplied by $\sin\theta \times 1.247 \times 10^{-24}$ cm² give values of the scattering cross section σ. In plotting yield values which coincide or are very close circles of different diameters were used so that they can be distinguished.

which might be introduced by faulty apparatus or a shift in the sensitivity of some instrument. It served only to call attention to trouble and was not used to adjust other yield values. After completion of the standard check measurements, generator voltage was set to give protons at the center of the chamber of the energy desired for yield measurements. The usual order of procedure was to start at 15°, go progressively to larger angles up to 45° and then go back to 15° for a check measurement. Usually 12,000 counts were taken at 15°, 8000 counts at 45°, and at intermediate angles the number of counts was between the two values given above. At each angle half of the counts were taken on one side of the beam and half on the other. To guard against the introduction of systematic errors several series of measurements were made in different order. Yields at all angles were found to be independent of the order in which they were investigated. After completion of a series of yield measurements, which usually took from three to four hours, the voltage was again set to give 860-kev protons and another determination was made of the contamination yield (average, 2.3 percent of total). Since time was recorded frequently during a scattering run, the contamination correction could be computed for the yield at each scattering angle. This correction was always made although for large scattering angles and high voltage it was negligible. The generator was shut down after the contamination determination, and after the pressure in the main vacuum system dropped to a steady value (1 to 2×10^{-6} mm Hg), the pressure reading was watched while a stopcock was opened connecting the chamber around the collector cup to the vacuum system. This check was made after all measurements included in the final data, and in each case the pressure rise was less than 5×10^{-8} mm Hg. Other check work had shown that a pressure rise of the order of 1×10^{-6} mm Hg should be expected if pressure in the collector cup were sufficiently high to cause a noticeable shift in scattering yield.

The scale counter was again checked after completion of scattering measurements. Hydrogen pressure and temperature were usually measured twice during the course of the scattering measurements, and values of P_0 (pressure at 0°C) rarely differed by more than 0.1 percent.

All scattering measurements made before July 28, 1938 were discarded. These yields were considered to be unreliable since up to that time no measurements had been made of the absorption thickness of the carbon deposit on the collimation slit foil. Some of the results obtained before July 28, 1938 were off still further because of a shift in the sensitivity of the voltmeter galvanometer (galvanometer which measures the output of the generating voltmeter). All results on proton-proton scattering from July 28, 1938 up to the time of the last measurement on October 7, 1938 are included in the data shown in Table I and in Figs. 8 and 9. At least two separate runs were made at each voltage, and the runs were not made in regular order. For example, runs at 1830 kev, were made on July 28, August 5, August 23, and on September 15. The

results show no trend with time. For all of the measurements giving the final data (measurements after July 28) values of the hydrogen pressure P_0 were between 160 mm and 170 mm of oil. Previous work had shown that yields were independent of hydrogen pressure. With protons having an energy of 860 kev at the center of the scattering chamber two series of measurements were made. In the first of these, June 28, P_0 had the value 167.1 mm, and in the second, on June 29, the value of P_0 was 82.5 mm. Yields at all angles for these two runs agreed very closely, with a maximum difference between corresponding yields of 1.2 percent.

The aluminum foil over the collimating slits was replaced once during the course of the final measurements and yield values were unchanged. The absorption thickness of the first foil was measured on August 16 and was found to be 75 kev. Further use of this foil was considered undesirable because the energy spread introduced by straggling causes a shift in scattering yield which might have become appreciable for the lower part of the 860-kev to 2492-kev region. A new foil was installed August 23, and its absorption thickness was found to be 46 kev. Yield measurements at 1830 kev were made before and after August 23, and the values show no shift although small angle scattering yields at 1830 kev are sensitive to proton energy.

On September 17, the foil over hole C of the analyzing slit system was replaced and yield values showed no shift. The foil over the collector cup chamber was not replaced after July 28, but during the measurements made over a period of almost two years this foil was replaced several times and no replacement caused a noticeable shift in yield values.

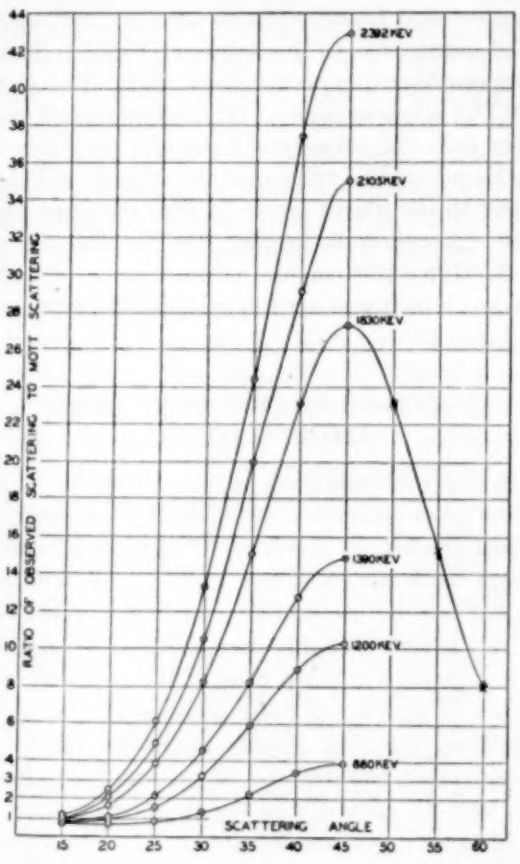

FIG. 9. Ratios of observed scattering yields to computed Mott values. The ratios of Table I are plotted.

RESULTS

Proton-proton scattering results obtained after July 28, 1938 are shown in Table I. Some measurements were made at 840 kev, but they were intended only for check work on the apparatus and are therefore not included in the tabulated results. One run at 860 kev was discarded because the contamination correction was three times as large as the average. Yield values at 15° and 1830 kev which were taken to provide a standard check are not included in the table. All other results obtained after July 28 are included, and except for the contamination correction experimental yield values were not adjusted before tabulation. For all but seven of the tabulated yield values 8000 or more protons were counted and for these seven the number of counts was between 7000 and 8000. For 44 percent of the values the number of counts was 9000 or more. Four series of measurements were made at energies slightly off from the standard values. The experimental energies and yield values are given for these runs, but before averaging the yield values they were adjusted to the standard energies. A star after an energy value indicates that the corresponding yield values have been adjusted (method of adjustment described below) from experimental values listed above.

The experimental yield values of Table I, unadjusted, are plotted in Fig. 8 to show the

variation of yield with voltage at constant angle. At all angles above 20° the yield goes through a maximum which appears to be at approximately 1650 kev for 25° and at approximately 1800 kev for higher angles. After the curves of Fig. 8 had been drawn in they were utilized for adjustment of yield values which had been taken at energies slightly off from the standard energies. A shift ΔY in a value was determined by multiplying the slope of the curve at that point by the required shift in energy. Since all of the adjustments were small this method was sufficiently accurate. After these adjustments had been made yield values were averaged, and each average was divided by the corresponding Mott value. For computing Mott values the tabulated values given by Breit, Condon and Present were used. Values of "ratio to Mott" in Table I are plotted in Fig. 9.

At 1830 kev two runs were taken up to scattering angles of 60°. Results are shown in Table II and in Fig. 9. One of the runs was taken on July 12, and the proton energy is not known to the accuracy which was obtained in the work after July 28, but the values shown in Table II are considered to be reliable since at 1830 kev large angle scattering yields change very slowly with proton energy. Yield values in the July 12 work at 30°, 35°, 40° and 45° were in very good agreement with the corresponding average yields of Table I. This agreement provided additional evidence for the reliability of the July 12 values shown in Table II.

The cross section for scattering of protons by protons should vary as $\cos\theta$ about the angle $\theta=45°$, and the "ratio to Mott" should be symmetric about 45°. This relation provided an opportunity for valuable checks on the geometrical accuracy of the proton scattering chamber and the accuracy of the apparatus for counting protons. Since a proton scattered at 30° has 87 percent of its original energy, and a proton scattered at 60° has only 25 percent of its original energy, agreement of the experimental "ratios to Mott" would indicate that protons over a wide energy range are accurately counted.

TABLE II. *Experimental results for scattering angles above 45°. The experimental "ratios to Mott" were compared with the average 1830-kev ratios of Table I for corresponding angles below 45°, and the percentage differences are given.*

	July 12			August 5		
Angle	Ratio to Mott	Percentage Difference	No. of Counts	Ratio to Mott	Percentage Difference	No. of Counts
50°	23.16	+0.17	9100	23.16	+0.17	7200
55°	14.90	−0.93	9100	15.23	+1.26	8000
60°	8.19	−0.61	6000	8.04	−2.43	7200

The curves of Fig. 9 and the tabulated values of Table II show that agreement is satisfactory. Percentage differences given in Table II show very little trend with angle and are approximately as great as should be expected from statistical fluctuations.

All values of Table I were computed with 0.864 as the density of Apiezon oil B. This value is correct at 26°C, but temperatures were slightly off from this value when the data were taken. The error was noticed after the curves of Fig. 8 and Fig. 9 were plotted. Table IA gives the percentage corrections which must be applied to the values of Table I to correct for the variation of oil density with temperature. Breit, Thaxton and Eisenbud have applied additional small corrections to the values of Table I. Their computation of expected Mott yield (Eq. (3.4) of BTE) is independent of fundamental constants other than the velocity of light and the value of the Faraday. The value of c, the velocity of light, enters to the fourth power in their equation and their correction is largely due to the use of $c=2.99796\times10^{10}$ cm/sec. rather than $c=3\times10^{10}$ cm/sec. which was used in computing the values of Table I.

Scattering of Protons by Argon and by Krypton

In the determination of proton-proton scattering cross sections a large number of absolute measurements are involved. All of these measurements, with the exception of generator voltage, appear to be dependable to 0.5 percent or better. Errors probably compensate one another to a large extent, but if most of the errors shifted values of scattering cross sections in the same direction, the final results might be off by a considerable amount. In an attempt to check the over-all accuracy of the method, scattering yields from argon and krypton were investigated.

The Coulomb field of an argon nucleus is sufficiently great so that scattering yields would

be expected to follow the Rutherford formula if there were no pronounced resonance penetration. Scattering yields from krypton were investigated as a check on the argon work since there seemed to be little possibility that krypton scattering yields would deviate from the Rutherford values. Argon and krypton for this work were obtained from the Linde Air Products Company. The argon was spectroscopically pure and was sealed in ½-liter Pyrex flasks. The krypton, sealed in 5-cc Pyrex bulbs, was guaranteed to contain less than 1.5 percent of xenon and negligible amounts of other impurities. Precautions were taken to avoid contamination of the gas when it was admitted to the scattering chamber, and scattering measurements were always made as soon as possible after the seal on the Pyrex container was broken. Accurate measurements of scattering yield from argon and krypton could not be made over a wide angular region because of the rapid variation of yield with angle. At 860 kev measurements were not attempted at angles below 20° or above 50°. For protons of 1830 kev or above the usable angular region was between 15° and 40° for the gas pressures chosen in most of the work. Expected yields were calculated under the assumption that the scattering obeyed the Rutherford formula, and these values were compared with experimental yield values.

Results from argon

The first measurements on argon were made with 1830-kev protons and with $P_0=27.5$ mm of oil. Results of these experiments are shown in the second column of Table III where percentage differences between observed yields and calculated Rutherford yields are given. The high yield values were disturbing since they indicated that the proton-proton measurements were inaccurate. Scattering yields were then investigated with protons having energies in the region of 1830 kev and 860 kev for several different values of argon pressure. All of the results are shown in Table III. The excess in observed yield values over calculated Rutherford values increases with argon pressure, and for a given pressure the excess in observed yield is greater at low voltage than at high voltage. Values in each of the rows of Table III were averaged, and the averages are plotted in Fig. 10.

TABLE III. *The scattering of protons by argon. Experimental scattering yields were compared to computed Rutherford yields and the percentage differences are given. All experimental yields were higher than Rutherford values and thus all tabulated percentages are positive. The Sept. 28 value 8.7* at 20° differs widely from the 30° and 40° values. Since an error in the reading of some instrument may have caused the discrepancy this value was not included in the average plotted in Fig. 10.*

Date	Argon Pressure P_0	Proton Energy kev	Scattering Angle 15°	20°	30°	40°	50°
Sept. 28	15.88	1826	6.0	6.6	3.6	2.3	—
Sept. 26	27.78	1830	4.5	5.0	1.3	2.6	—
Sept. 27	28.77	1830	5.7	5.0	4.5	2.8	—
Sept. 27	57.02	1819	—	6.3	8.0	9.4	—
Sept. 28	119.4	1832	—	8.7*	16.2	15.8	—
Sept. 27	15.46	866	—	3.2	7.8	4.7	3.6
Sept. 26	27.58	862	—	11.6	10.0	9.5	11.5
Sept. 27	54.73	846	—	25.1	26.0	24.5	23.7

A consideration of the variation in excess scattering as a function of argon pressure and proton energy indicated that the effect was caused by multiple small angle scattering which spread the main proton beam so that protons missed the hole covered by foil F, Fig. 1. Calculations by Professor Breit substantiated this assumption. Since the structure of the proton beam is not known, the percentage of protons which miss hole A cannot be calculated accurately. The variation of this percentage with proton energy and argon pressure also depends on the structure of the proton beam and cannot be calculated accurately. However, the calculations showed that if the beam spread is S_1 with the proton energy at E_1 and argon pressure at P_1, then with a proton energy $E_2=2E_1$ the beam spread S_2 should be equal to S_1 for $P_2=3.4P_1$. This relationship should be fairly independent of the structure of the beam for high argon pressure. The values of P_0 from curves A and B which give a percentage difference of 16 percent are 39 mm and 120 mm, respectively. Thus, for a constant beam spread the pressure had to be increased by a factor of 3.03 when the voltage was raised by a factor of 2.13. Considering the approximations used in the calculations the agreement is satisfactory.

The scatter in the points of the 1830-kev argon curve in the low pressure region is probably due partially to errors in pressure measurement since for $P_0=15$ mm the pressure measurement was not considered dependable to better than 1

percent. Inconsistent yield values may also be caused by changes in the structure of the main proton beam. The data of Table III show that for protons in the energy region of 860 kev the variation of scattering yields as a function of angle agree fairly well with the Rutherford formula. There are, however, some inconsistent values, but these may be due to variations in the structure of the proton beam which could cause changes in the percentage of protons that miss hole *A*. This source of difficulty would not be present in the proton-proton scattering work.

In high voltage argon measurements for which P_0 had the values of 27.78, 28.77 and 15.88 mm of oil the excess in observed yield relative to Rutherford yield is greater at 15° and 20° than at the higher angles.

For each of these runs the average of the 30° and 40° values shown in Table III was subtracted from the 15° value. The average of the differences obtained in this way for each of the three runs was 2.6 percent. When the 20° values were compared with the 30° and 40° values in the same way an average difference of 2.7 percent was obtained. The average difference of 2.6 percent for the 15° values is approximately what should be expected because of the finite size of the collimating and analyzing slits, but at 20° this average difference should be approximately 0.56 as great as at 15°. Thus the average 20° difference appears to be too large by 1.2 percent. This discrepancy also appears in the krypton results and may have been caused by some defect in one of the instruments used for the scattering measurements. If the curves of Fig. 10 are extrapolated to $P_0=0$ the yield values determined will be free from error due to spreading of the beam. Extrapolations are not very dependable because yield values for $P_0=15$ mm of oil are not accurate, and for lower pressures little is known about the form of the curves. It seems safe, however, to assume that the curves are horizontal at $P_0=0$ since the extreme outer edges of the beam must move out 0.7 mm before any protons can miss the hole over the collector cup. Reasonable extrapolations indicate that observed yields from argon do not differ from calculated Rutherford yields by more than about 2.5 percent.

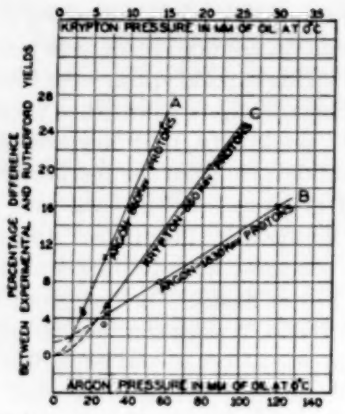
KRYPTON PRESSURE IN MM OF OIL AT 0°C
0 5 10 15 20 25 30 35
PERCENTAGE DIFFERENCE BETWEEN EXPERIMENTAL AND RUTHERFORD YIELDS
0 4 8 12 16 20 24 28
A
C
B
ARGON-ARGON PROTONS
KRYPTON-PROTON RECOILS
KRYPTON-KRYPTON PROTONS
ARGON PRESSURE IN MM OF OIL AT 0°C
0 20 40 60 80 100 120 140

FIG. 10. Percentage differences between experimental scattering yields from argon and krypton and computed Rutherford yields are plotted to show the variations of percentages difference with argon and krypton pressure. Values of Tables III and IV were averaged with respect to scattering angle to give the values for these curves.

Results from krypton

For most of the measurements with krypton the values of P_0 were between 8 and 9 mm of oil, and pressure measurements were dependable to about 1.5 percent. The xenon impurity could be responsible for an excess of 1.9 percent in observed yields over the calculated values. Because of these factors absolute yield values from krypton are not as dependable as the argon results. All results obtained after July 28 are shown in Table IV.

The variations of yield with angle shows approximately the same behavior as the argon results. Scattering yields from krypton for protons in the energy region of 860 kev were investigated at pressures of 8.73 and 20.76 mm of oil, and results are shown in Fig. 10. If the curve determined by these two points is extrapolated to $P_0=0$ the yield value obtained is in satisfactory agreement with the Rutherford value.

It was at first expected that for a given voltage the beam spread due to krypton (atomic number 36) at a pressure P should be the same as the spread due to argon (atomic number 18) at a pressure $4P$. Curves *C* and *A* show that the pressure at which argon gives a beam spread S is approximately 2.34 times the pressure at which krypton gives the same beam spread. The apparent discrepancy can be explained in

the following way: Calculations showed that multiple small angle scattering is chiefly responsible for the spread of the proton beam. Electronic screening will cause a considerable reduction in the cross section of nuclei for small angle scattering and calculations by Professor Breit show that the magnitude of the screening effect should increase with an increase in the atomic number of the target element. Results of these calculations, which are given in the section "Spread of Beam" of the paper by BTE, are in satisfactory agreement with the experimental results of Fig. 10.

Conclusion

The outcome of the scattering experiments with argon and krypton was disappointing. Because of the difficulty with measurement of the proton current the results do not serve as a close check on the accuracy of the proton-proton yields. The authors believe, however, that the proton-proton values are not greatly in error since results of other check work were for the most part satisfactory. Yield measurements at 1830 kev showed the expected variation about 45°. Yields were independent of hydrogen pressure, and the repeatability of yield values during the entire period of the final measurements tends to increase confidence in their reliability.

Because of the nature of the experiment an estimate of the probable error in the yield values is difficult to make and has not been attempted. The authors feel that their experimental work should be repeated with different apparatus and preferable at another laboratory. The work of Breit, Thaxton and Eisenbud in this issue demonstrates the remarkable possibilities presented by precise data on proton-proton scattering for quantitative information on the interaction potential between protons. More data of greater precision are needed before all of these possibilities can be utilized.

We are indebted to Dr. E. J. Bernet, Dr. R. J. Havens, Mr. R. E. Warren and Mr. C. M. Hudson for help in this work. Professor G. Breit suggested the problem and by his encouragement and advice during the course of the work contributed much to its success. Mr. J. R. Foerst and Mr. J. P. Johnson deserve much credit for their excellent work on the construction of the scattering chamber. Many details of the design are due to Mr. Foerst. We are indebted to the Wisconsin Alumni Research Foundation and to the American Philosophical Society for financial assistance.

Table IV. *The scattering of protons by krypton. Experimental scattering yields were compared to computed Rutherford yields and the percentage differences are given. All experimental yields were higher than Rutherford yields and thus all of the tabulated values are positive.*

Date	Krypton Pressure P_0	Proton Energy kev	Scattering Angle 15°	20°	30°	40°	50°
Aug. 8	9.14	2440	4.4	3.5	2.9	3.8	—
Aug. 8	9.07	1849	5.5	6.6	3.9	2.0	—
Oct. 13	8.09	1835	4.8	6.2	2.0	3.8	—
Oct. 13	8.06	864	—	4.9	4.5	6.0	6.0
Oct. 14	8.73	860	—	5.8	5.2	7.2	5.6
Oct. 14	20.76	850	—	—	17.4	20.5	23.0

Analysis of Experiments on the Scattering of Protons by Protons

G. BREIT, H. M. THAXTON AND L. EISENBUD*
University of Wisconsin, Madison, Wisconsin
(Received April 19, 1939)

The new observations of Herb, Kerst, Parkinson and Plain and of Heydenburg, Hafstad and Tuve are analyzed. No definite indication of a p wave anomaly or higher phase shifts is found. The s wave anomaly is the major effect observed. The phase shift K_0 responsible for it is compared with theoretical expectation using potentials which are constant (except for their Coulombian part) within distances 0.75, 1, 1.25 in units $e^2/mc^2=2.81\times10^{-13}$ cm. The first of these gives a too rapid and the last a too slow variation of K_0 with energy. The interaction radius e^2/mc^2 agrees with experiment much better than the others. The potential energy giving the best agreement with experiment, when superposed on the Coulomb energy within this distance, is determined within a few tenths of a percent and is 11.3 Mev. The Gauss error potential $Ae^{-\alpha r^2}$ with $\alpha=16$ and with 9×10^{-13} cm as the unit of length gives a too slow variation of K_0 with E. Experiment agrees decidedly better with $\alpha\sim20$. An over-all fit can be obtained with $\alpha=21.6$, $A=51.4\ mc^2$. The shortening of the range of force is about the same as that previously suggested by Rarita and Present from calculations on the binding energy of H^3. This is surprising since the discovery of the electric quadrupole moment of H^2 necessitates a revision of binding energy calculations. Conclusions about the range of force derivable from proton-proton scattering experiments are shown to be sensitive to a possible velocity dependence of the nuclear potential. The proton-proton and proton-neutron forces in ^1S states are compared and it is found that for both types of potentials the proton-proton interaction is less by approximately two percent. This difference is definitely outside the probable errors in the scattering experiments and is not very sensitive to velocity dependence.

The absence of p wave anomalies in the data from 1830 to 2400 kev is not sufficiently clear cut to claim a definite disagreement with Feenberg's inequality derived from saturation requirements with exchange forces. The effects expected are close to the consistency of the measurements.

The paper includes formulas and tables for the calculation of anomalies due to phase shifts, discussions of geometrical corrections and of some of the effects of experimental errors on the conclusions. Some of the features that may be learned by extensions to higher and lower energies are pointed out. An outline is given in the introduction.

I. INTRODUCTION

OBSERVATIONS on the anomalous scattering of protons by protons have been made by Wells,[1] White,[2] by Tuve, Heydenburg and Hafstad,[3] by Hafstad, Heydenburg and Tuve,[4] by Herb, Kerst, Parkinson and Plain[5] and by Heydenburg, Hafstad and Tuve.[6] The present paper concerns itself with the interpretation of the experiments paying special attention to the results obtained in the two recent papers just mentioned. The data of Herb *et al.* extend the knowledge of the scattering to an energy of 2.4 Mev for the incident protons. These observations as well as the new measurements of Heydenburg, Hafstad and Tuve have been made with improvements in technique which resulted in a high degree of internal consistency. The analysis of the observations made below indicates a high accuracy in the values of the phase shift K_0 responsible for the s wave scattering anomaly recorded in Tables XI, XII and plotted in Figs. 6 and 7. The values obtained in the two laboratories join smoothly at the energy 860 kev for the data of Herb *et al.* and 867 kev for the data of Tuve *et al.*

The extension of the energy region to 2400 kev made by Herb and collaborators enables one to determine an average range for the nuclear force responsible for the s wave anomaly. An over-all fit between 800 and 2400 kev makes an accuracy of ~5 percent seem possible. A "square well" potential with a width e^2/mc^2 and a depth $D=10.52$ Mev represents this region quite well. For the Gauss error potential an over-all fit from 670 kev to 2392 kev is obtained for $Ae^{-\alpha r^2}$ with $A=51.44$, $\alpha=21.59$ in nuclear units. Fits made with the Gauss error potential to different parts of the experimental curve vary by amounts

* Now at Princeton University.
[1] W. H. Wells, Phys. Rev. **47**, 591 (1935).
[2] M. G. White, Phys. Rev. **47**, 573 (1935).
[3] M. A. Tuve, N. P. Heydenburg and L. R. Hafstad, Phys. Rev. **49**, 402 (1936); **50**, 806 (1936).
[4] L. R. Hafstad, N. P. Heydenburg and M. A. Tuve, Phys. Rev. **51**, 1023 (1937); **53**, 239 (1938).
[5] R. G. Herb, D. W. Kerst, D. B. Parkinson and G. J. Plain, Phys. Rev. **55**, 603(A) (1939). Also paper in this issue. Referred to as HKPP in text.
[6] N. P. Heydenburg, L. R. Hafstad and M. A. Tuve, Phys. Rev. **55**, 603(A) (1939). Referred to as HHT in text.

illustrated in Table XIX which indicate 20 as the lower limit and 24 as the upper limit for α. Rarita and Present[7] have found it necessary to use a range corresponding to about $\alpha=20$ in order to account for the binding energy of H^3. They pointed out that with such a range the mass of He^4 should be expected to be smaller than the experimental value. The work of Margenau and Warren and Margenau and Tyrrell[7] has made it doubtful to what extent a shorter range is called for by the binding energy of H^3 since the difficulty according to them can be partly removed by suitable adjustments of the parameter g entering into the expression for nuclear forces. The new proton-proton scattering experiments show, however, that the range of force cannot be supposed to correspond to $\alpha=16$ as long as the interaction potential is supposed to be independent of velocity. It is surprising that the value obtained for α is so close to that obtained by Rarita and Present[7] from the binding energy of H^3 since this value gives a too small mass of He^4. The discovery of the electric quadrupole moment of H^2 recently made by Rabi and coworkers[8] makes the meaning of these binding energy calculations rather doubtful since the ^3S states are mixed with $^3D_1$. The effect of couplings of the $(\sigma_1\mathbf{r})(\sigma_2\mathbf{r})$ type which are demonstrated by the quadrupole moment has been already considered for the position of the ^3S and ^1S terms in the deuteron[9] and even for the relatively small magnitudes expected from relativistic considerations appreciable effects have been obtained. Larger effects should follow from the mesotron theory[10] and the connection of the range of force with binding energies is decidedly an open one. On the other hand, the ^1S state remains uncoupled to the others[11] so that this interaction can be investigated independently with the proton-proton and with the slow neutron-proton scattering experiments.

On the other hand, the scattering experiments do not give a unique answer to the question of range because of the possibility of velocity dependence.[12] It will be seen at the end of the paper that changes of the order of 1.6 percent of the depth of the potential well through an energy region of 2.4 Mev for incident protons would account for the observations using an old fashioned range of $\alpha=16$. The mesotron theories of nuclear forces in their usual form involve the arbitrary feature of "cutting off" which presumably introduces errors regarding velocity dependence since the relative importance of long and short wave-lengths is different for collisions with different energies of relative motion. This point is doubtless speculative and controversial but it was thought of interest to see in a purely empirical manner to what extent conclusions about range are affected by the introduction of a velocity dependence.

The saturation and stability arguments with exchange forces have led Feenberg[13] to the establishment of a lower limit for the repulsion in the ^3P state which should cause a small scattering anomaly to appear at two Mev. Here again the existence of the electric quadrupole of the deuteron changes the situation. The assumption regarding the possibility of representing nuclear

[7] W. Rarita and R. D. Present, Phys. Rev. **51**, 788 (1937); H. Margenau and D. T. Warren, Phys. Rev. **52**, 790 (1937); **52**, 1027 (1937); W. A. Tyrrell, Jr., and H. Margenau, Phys. Rev. **53**, 939(A) (1938); H. Margenau and W. A. Tyrrell, Phys. Rev. **54**, 422 (1938); W. Rarita and Z. I. Slawsky, Phys. Rev. **54**, 1053 (1938).

[8] I. I. Rabi, J. R. Zacharias, N. F. Ramsey, Jr., and J. M. B. Kellogg **55**, 595(A) (1939); J. M. B. Kellogg, I. I. Rabi, N. F. Ramsey, Jr., and J. R. Zacharias, Phys. Rev. **55**, 318 (1939).

[9] S. S. Share and G. Breit, Phys. Rev. **52**, 546 (1937); G. Breit, Phys. Rev. **51**, 248 (1937); **54**, 153 (1938). First *a priori* introduction of $(\sigma_1\mathbf{r})(\sigma_2\mathbf{r})$ terms for nuclear forces apart from magnetic effects was made by Wheeler, Phys. Rev. **50**, 643 (1936). See also E. Wigner Phys. Rev. **51**, 106 (1937). The existence of the quadrupole moment as an effect of these terms and other interesting effects have been discussed by J. Schwinger, Phys. Rev. **55**, 235 (1939). Chicago meeting American Physical Society, November 25, 1938.

[10] H. Yukawa, Proc. Phys. Math. Soc. Japan **17**, 48 (1935); H. Yukawa and S. Sakata, Proc. Phys. Math. Soc. Japan **19**, 1084 (1937); H. Yukawa, S. Sakata and M. Taketani, Proc. Phys. Math. Soc. Japan **20**, 319 (1938); H. Yukawa, S. Sakata, M. Kobayasi and M. Taketani, Proc. Phys. Math. Soc. Japan **20**, 720 (1938); N. Kemmer, Proc. Roy. Soc. **34**, 354 (1938); N. Kemmer, Proc. Camb. Phil. Soc. **34**, 354 (1938); H. Fröhlich, W. Heitler and N. Kemmer, Proc. Roy. Soc. **A166**, 154 (1938); H. J. Bhabha, Proc. Roy. Soc. **A166**, 501 (1938); W. Heitler, Proc. Roy. Soc. **A166**, 529 (1938).

[11] G. Breit, Rev. Sci. Inst. **9**, 63 (1938). See end of first column on p. 74. The ^1S term remains uncoupled to all other terms for two particles of spin $\frac{1}{2}$.

[12] J. A. Wheeler, Phys. Rev. **50**, 643 (1936). Here the possibility of velocity dependence for nuclear force is introduced.

[13] E. Feenberg, Phys. Rev. **52**, 667 (1937); See also G. Breit and E. Wigner, Phys. Rev. **53**, 998 (1938) for feasible upper limit on the repulsion.

forces as a mixture of Wigner, Heisenberg, Majorana and Bartlett interactions cannot be maintained any longer and this assumption was made in deriving the inequality. It appears unlikely, however, that the experiment could have concealed a negative phase shift of $-0.25°$ which is approximately the amount expected using the old fashioned theory with $\alpha=16$. Unfortunately the effect looked for is at the limit of experimental accuracy and a definite claim for the absence of such a phase shift cannot be made. A discussion of the evidence is given under "Possibilities at low and high energies and higher phase shifts" as well as in connection with Table XIV and Figs. 3, 4 and 5.

The paper is divided into two longer sections. The first is concerned with the handling of experimental material up to the point of obtaining the phase shifts and is called "Determination of Phase Shift from Experimental Data." The second is concerned with the interpretation of the phase shifts in terms of interaction potentials and is called "Calculation of the Potentials." The first part is less speculative than the second. In the first part the subdivisions are as follows.

1. Coefficients for the calculation of the scattering anomaly. Here tables and formulas are given for the calculation of the s wave anomaly in sufficient detail to make the analysis of experimental material easy in the future.

2. Effect of error consisting of a constant factor. Here the effect introduced into the value of the s wave phase shift K_0 due to an error consisting of a constant factor is calculated.

3. Effect of error in voltage. This is similar to 2.

4. Estimate of spread of beam due to collisions. The checks made by Herb *et al.* on the performance of the apparatus using argon and krypton scattering showed the presence of an effect of pressure. The spread of the beam due to collisions is estimated and is seen to be of the right order of magnitude. Multiple scattering is discussed.

5. Values of phase shift derived from experiment. (*a*) Explanation of tables. The experimental results are tabulated and the comparison of theoretical expectation is compared in this section with experiment. (*b*) Corrections due to geometry of apparatus. For low angle scattering corrections for geometry enter. They are of importance for conclusions regarding higher phase shifts. (*c*) Possible presence of p and d wave anomalies. Upper limits for their effect on K_0.

The second section contains the following subdivisions.

1. The proton-neutron interaction. (*a*) Square wells. Eqs. (8.2) and (8.3) for calculation of depth and Eq. (8.4) for scattering cross section of ^3S. Eqs. (8.5) and (8.6) for relation between depth and scattering cross section for ^1S. Connection with virtual level treatment in Eq. (8.8). (*b*) Expansions for wells of any shape. Eqs. (9.1) for Taylor expansion of logarithmic derivative in several parameters. (*c*) Formulas for neutron-proton potential for the Gauss error type interaction. Eqs. (10.1), (10.4), (10.6), (10.7), (10.8) and (10.9) for calculation of depth of proton-neutron potential corresponding to given scattering. Effect of neglecting tail of Gauss error potential in Eq. (10.91). (*d*) Intercomparison of numerical integrations used for proton-proton and proton-neutron potentials.

2. Coulomb effect for square wells. Calculations of phase shifts for proton-proton scattering are made with least trouble using "square wells" without Coulomb potential inside. Corrections for the Coulomb potential inside the well are made here. See Eq. (11.2) for effect of Coulomb potential on depth. Necessary quantities collected in Table XVI. Eq. (11.5) and Table XVII for calculation of phase shift with fixed depth superposed on Coulomb potential.

3. Adjustment of range and values obtained from experiment.

4. Comparison of proton-proton and proton-neutron interaction. See Tables XX, XXI.

5. Possibilities at lower and higher energies and evidence regarding p scattering. Some of the points which may be learned by extending experiments to lower and higher energies are discussed and the evidence regarding p scattering available at present is reviewed.

A table of Coulomb functions for $L=0$ is given in the appendix.

Notation

M = mass of proton; M_H = mass of hydrogen atom.

$\mu = M/2$ = reduced mass in the collision of two protons.
v = relative velocity of the two protons before the collision.
r = distance between protons.
E = kinetic energy of the incident proton.
E' = energy in frame of center of gravity = $E/2$.
$\Lambda = \hbar/\mu v$.
$k = 2\pi/\Lambda$, $\eta = e^2/\hbar v$, $\rho = kr$.
$L\hbar$ = angular momentum of colliding particles around common center of gravity.
P_L = Legendre function.
θ = scattering angle in the reference system of center of gravity.
$\Theta = \theta/2$ = scattering angle in the laboratory reference system.
F_L = regular solution of the differential equation for r times the radial wave function in a Coulomb field normalized so as to be asymptotic to a sine wave of unit amplitude at ∞.
K_L = phase shift defined by the asymptotic form of $\mathfrak{F}_L = r$ times the radial function in the actual field. The phase of $\mathfrak{F}_L$ minus that of F_L at large r is K_L.
G_L = irregular solution of the same equation as F_L having $K_L = \pi/2$.
σ = scattering cross section per unit solid angle in the laboratory system.
$\dot{\mathbf{P}}$ = scattering cross section per unit solid angle in the center of gravity system.
$(\Delta\mathbf{P})_0$ = change in $\mathbf{P}$ due to the s scattering anomaly.
$(\Delta\mathbf{P})_1$ = change in $\mathbf{P}$ due to the p scattering anomaly.
$(\Delta\mathbf{P})_2$ = change in $\mathbf{P}$ due to the d scattering anomaly including interference terms with K_0.
$\mathbf{P}_M$ = value of $\mathbf{P}$ using Mott's formula.
$\mathbf{X}$, $\mathbf{Y}$ defined by Eq. (1).
Y = yield of scattered protons, per microcoulomb, per mm oil pressure.
$\mathfrak{M} = (2\mu v^2/e^2)^2\mathbf{P}_M$ = quantity tabulated in Table I of BCP.
ρ_H = density of hydrogen in scattering chamber.
$2b$ = width of slit in analyzing system.
A = area of hole in analyzing system. Same symbol as depth of Gauss error potential.
R_0 = distance from hole to beam if beam is very narrow.
$\mathfrak{r}$ = distance from hole to center of beam if beam is wide.
$\mathfrak{h}$ = distance from hole to slit.
$\mathfrak{R} = \mathbf{P}/\mathbf{P}_M$ = ratio of scattering to that expected by Mott's formula.
$\dot{\rho}$ = radius of circular beam.
σ_{np} = scattering cross section of neutron having zero energy with a free proton.
$\sigma_{th} = 4\sigma_{np}$.
$F = r$ times radial function for proton-neutron collision.
E_3 = $-$energy of deuteron in normal state.
D_1, D_3 = depths of square wells representing, respectively, proton neutron interaction in the singlet and triplet states.
χ defined by Eq. (8.3).
r_0 = radius of square well.
a_1, a_3 = intercepts on axis of r of tangents to F for zero energy neutrons for singlet and triplet states.
$y = dF/Fdx$ or $d\mathfrak{F}/\mathfrak{F}dx$.
A, α = constants for Gauss error potential $Ae^{-\alpha r^2}$.
$\lambda = A/\alpha$.
$C = 0.577216$ = Euler's constant.
$C_0 = [2\pi\eta/(e^{2\pi\eta}-1)]^{\frac{1}{2}}$.
$C_L = [1/1.3\cdots(2L+1)][1+\eta^2/L^2]^{\frac{1}{2}}\cdots \times[1+\eta^2/1^2]^{\frac{1}{2}}C_0$.

II. Determination of Phase Shift from Experimental Data

1. Coefficients for the calculation of the scattering anomaly

The values of the coefficients of $\sin K_0 \cos K_0$ and $\sin^2 K_0$ in $\mathbf{P}/\mathbf{P}_M$ as given by Breit, Condon and Present[14] are not quite accurate enough for the discussion of the newer improved data. The relation between η and the energy in Mev as used there is slightly inaccurate because of the use of old values of e, h, m, M, c and it is difficult

[14] G. Breit, E. U. Condon and R. D. Present, Phys. Rev. **50**, 825 (1936). Referred to as BCP in text. See references to previous theoretical work in BCP. A more accurate comparison of the proton-proton and proton-neutron interactions was made by G. Breit and J. R. Stehn, Phys. Rev. **52**, 396 (1937). This paper is referred to as BS in the text.

to interpolate from the tables with sufficient accuracy. Values of the coefficients obtained by improved and more systematic calculations are listed below in Table I. It was found at times more convenient to interpolate from tables of the quantities $\mathbf{X}$, $2\mathbf{Y}/\eta$ defined by

$$\mathbf{X}=\mathbf{s}^{-2}\cos\alpha_0+\mathbf{c}^{-2}\cos\beta_0;$$
$$\mathbf{Y}=\mathbf{s}^{-2}\sin\alpha_0+\mathbf{c}^{-2}\sin\beta_0; \quad (1)$$
$$\alpha_0=\eta\ln\mathbf{s}^2;\quad \beta_0=\eta\ln\mathbf{c}^2$$

in the notation of BCP. The quantities $\mathbf{X}$, $2\mathbf{Y}/\eta$ are, therefore, also listed in the tables. The relations are

$$\sigma=4\mathbf{cP}, \quad (2)$$

$$(2\mu v^2/e^2)^2(\Delta\mathbf{P})_0=-\frac{2\mathbf{X}}{\eta}\sin K_0\cos K_0 + \left(\frac{4}{\eta^2}+\frac{2\mathbf{Y}}{\eta}\right)\sin^2 K_0\cdots, \quad (2.1)$$

$$\mathfrak{M}=(2\mu v^2/e^2)^2\mathbf{P}_M=\mathbf{s}^{-4}+\mathbf{c}^{-4} -\mathbf{s}^{-2}\mathbf{c}^{-2}\cos\eta\ln\mathbf{s}^2\mathbf{c}^{-2}, \quad (2.2)$$

$$\mathbf{P}=\mathbf{P}_M+(\Delta\mathbf{P})_0 \quad (2.3)$$

where σ is the collision cross section per unit solid angle for scattered as well as recoil protons. The values of $\mathfrak{M}$ are also tabulated. The quantities $-2\mathbf{X}/\eta\mathfrak{M}$, $4/\eta^2\mathfrak{M}+2\mathbf{Y}/\eta\mathfrak{M}$ can be used directly for the calculation of $\mathbf{P}/\mathbf{P}_M$. The relation of η to E as used in Tables I, II, III, IV, V is $\eta=0.15818(E/\text{Mev})^{-\frac{1}{2}}$. The conversion factor 0.15818 is not known with an accuracy corresponding to the number of figures used above. If, in future applications, it should be desired to correct the inaccuracy present in the conversion factors it is sufficient to attribute the values of the quantities given in the tables to the values of E that correspond to the tabulated values of η.

The conversion factors as used in the present paper correspond to the following values of the fundamental physical constants: $e/mc=1.7575\times10^7$, $e=4.8036\times10^{-10}$, $c=2.9986\times10^{10}$. C.g.s. electrostatic units are used here and below. The value of c, as used, is slightly incorrect. The more accurate value is 2.99796×10^{10}. This inaccuracy is of no practical consequence in the present work. From the above numbers one obtains $m=0.9115\times10^{-27}$. Using $R_\infty=109{,}737$ cm^{-1} for the Rydberg constant for infinite mass one obtains $h=6.628\times10^{-27}$, $\hbar=1.0549\times10^{-27}$, $e^2/\hbar c=1/137.08$. The quotient 1 Mev$/mc^2$ is determined by the above constants as $10^6(e/mc)/c^2=1/0.511(61)$. For the computation of η one needs besides the ratio M_H/m where M_H is the mass of the hydrogen atom. The Faraday constant $9648.9=e/Mc$ where M is the mass of the oxygen atom divided by 16. Using $M_H=1.0081\,M$ one obtains $M_H/m=1836.2$. It was assumed that it should be good enough to compute η by $\eta=(e^2/\hbar c)(c/v)=(e^2/\hbar c)c(M_H/2m)^{\frac{1}{2}}(mc^2/Ve)^{\frac{1}{2}}$ where V is the electrostatic difference of potential through which the protons have been accelerated. This gives $\eta=0.15810(E/\text{Mev})^{-\frac{1}{2}}$, $1/\eta=6.3251(E/\text{Mev})^{\frac{1}{2}}$. There is some question as to whether one should use the mass of the hydrogen atom or the mass of the proton in these calculations. The influence of extranuclear electrons is presumably negligible in the collision process itself but it has not been sufficiently investigated to be quite sure of this point. The incident particles must be practically entirely protons which do not have electrons permanently attached to them. From this point of view it would have been better to use M_H-m rather than M_H as the mass of the particles. On the other hand, there is spectroscopic evidence for M_H/m being close to 1838 which corresponds to $(M_H-m)/m=1837$. It appeared safest, therefore, to use $(M_H-m)/m=1836.2$ since this is close to the mean of 1835.2 and 1838. The remaining uncertainty in this number is probably of no importance for the present purpose particularly since it enters to the $\frac{1}{2}$ power. If the ratio of the mean mass of the oxygen atom and the mass of O^{16} is taken into account the ratio 1836.2 changes to 1835.7. The effect of the corresponding change in η is not taken into account in the tables.

For most work one can use Tables I and II to give by interpolation the values of the coefficients of $\sin K_0\cos K_0$ and $\sin^2 K_0$ for $\mathbf{P}/\mathbf{P}_M$. For better accuracy, particularly with graphs, Tables III and IV for $\mathbf{X}$ and $-2\mathbf{Y}/\eta$ are to be preferred. For the lowest energies in Table III the interval is not small enough to secure on interpolation a better accuracy in $\mathbf{X}$ than about two percent at $\Theta=15°$. It is unnecessary to have a better accuracy in this region since $\mathbf{P}/\mathbf{P}_M$ is nearly 1. For higher scattering angles Θ the

TABLE I.* *Values of* $2\mathbf{X}/\eta\mathfrak{M}$ *as functions of* E *and of scattering angle* Θ.

$\Theta=15°$	20°	25°	30°	35°	40°	42.5°	45°	E (KEV)	η
0.1764	0.4773	0.984	1.775	2.892	4.113	4.544	4.704	150	0.40822
.2555	.6190	1.218	2.139	3.426	4.820	5.307	5.488	200	.35353
.3224	.7396	1.417	2.453	3.889	5.435	5.974	6.174	250	.31621
.3811	.8459	1.595	2.733	4.305	5.988	6.574	6.791	300	.28865
.4336	.9418	1.755	2.987	4.684	6.494	7.124	7.356	350	.26724
.4814	1.0297	1.903	3.222	5.034	6.964	7.634	7.881	400	.24998
.5258	1.1112	2.041	3.441	5.356	7.404	8.112	8.373	450	.23569
.5662	1.197	2.170	3.648	5.672	7.820	8.563	8.838	500	.22359
.6423	1.328	2.408	4.029	6.245	8.591	9.402	9.701	600	.20411
.7105	1.455	2.625	4.378	6.769	9.298	10.172	10.493	700	.18897
.7730	1.572	2.826	4.701	7.257	9.956	10.887	11.230	800	.17676
.8311	1.682	3.013	5.003	7.715	10.572	11.558	11.921	900	.16666
.8856	1.785	3.190	5.289	8.144	11.155	12.192	12.574	1000	.15810
.820	1.660	2.977	4.945	7.623	10.45	11.43	11.79	880	.16854
.991	1.983	3.533	5.843	8.982	12.29	13.43	13.84	1210	.14373
1.077	2.148	3.816	6.302	9.676	13.23	14.45	14.90	1400	.13362
1.161	2.308	4.094	6.753	10.361	14.15	15.46	15.94	1600	.12499
1.251	2.480	4.391	7.237	11.094	15.15	16.54	17.05	1830	.11687
1.314	2.600	4.598	7.573	11.606	15.84	17.30	17.83	2000	.11179
1.349	2.668	4.716	7.764	11.897	16.24	17.73	18.28	2100	.10910
1.450	2.862	5.054	8.313	12.728	17.37	18.96	19.55	2400	.10205
1.634	3.216	5.669	9.313	14.24	19.43	21.21	21.87	3000	.091279
1.773	3.483	6.134	10.071	15.40	21.00	22.92	23.63	3500	.084508
1.902	3.732	6.566	10.78	16.47	22.45	24.51	25.26	4000	.079050
2.022	3.965	6.972	11.44	17.475	23.82	26.00	26.80	4500	.074529
2.136	4.185	7.356	12.06	18.43	25.115	27.41	28.25	5000	.070704

* The values of η given in the last column of this table were used also for the succeeding tables. The quantities calculated are functions of η directly rather than E.

accuracy of interpolation increases rapidly and similarly for higher energies.

The coefficients for the computation of effects of higher phase shifts K_1, K_2, $\cdots$ are given sufficiently accurately in BCP. The indications of the presence of such phase shifts are as yet not definite enough to make it necessary to have more accurate calculations.

At the end of Tables III, IV, V are given numerical formulas which express the values of $\mathbf{X}$, $-2\mathbf{Y}/\eta$, $\mathfrak{M}$ in terms of the energy E measured in Mev. These formulas are usually sufficiently accurate from 1000 kv on to $E=\infty$. They are obtained from the expansions

$$\begin{aligned}\mathbf{X}&=\mathbf{s}^{-2}+\mathbf{c}^{-2}-\frac{\eta^2}{2}[\mathbf{s}^{-2}(\ln \mathbf{s}^2)^2+\mathbf{c}^{-2}(\ln \mathbf{c}^2)^2]\\&\quad+\frac{\eta^4}{24}[\mathbf{s}^{-2}(\ln \mathbf{s}^2)^4+\mathbf{c}^{-2}(\ln \mathbf{c}^2)^4]-\cdots\\&=\mathbf{s}^{-2}+\mathbf{c}^{-2}-\frac{0.01250}{E}[\mathbf{s}^{-2}(\ln \mathbf{s}^2)^2+\mathbf{c}^{-2}(\ln \mathbf{c}^2)^2]\\&\quad+\frac{0.00002603}{E^2}[\mathbf{s}^{-2}(\ln \mathbf{s}^2)^4+\mathbf{c}^{-2}(\ln \mathbf{c}^2)^4]-\cdots,\end{aligned}\tag{3.1}$$

$$\begin{aligned}\frac{2\mathbf{Y}}{\eta}&=2[\mathbf{s}^{-2}\ln \mathbf{s}^2+\mathbf{c}^{-2}\ln \mathbf{c}^2]\\&\quad-\frac{\eta^2}{3}[\mathbf{s}^{-2}(\ln \mathbf{s}^2)^3+\mathbf{c}^{-2}(\ln \mathbf{c}^2)^3]\\&\quad+\frac{\eta^4}{60}[\mathbf{s}^{-2}(\ln \mathbf{s}^2)^5+\mathbf{c}^{-2}(\ln \mathbf{c}^2)^5]+\cdots\\&=2[\mathbf{s}^{-2}\ln s^2+\mathbf{c}^{-2}\ln c^2]\\&\quad-\frac{0.008332}{E}[\mathbf{s}^{-2}(\ln \mathbf{s}^2)^3+\mathbf{c}^{-2}(\ln \mathbf{c}^2)^3]\\&\quad+\frac{0.00001041}{E^2}[\mathbf{s}^{-2}(\ln \mathbf{s}^2)^5+\mathbf{c}^{-2}(\ln \mathbf{c}^2)^5]+\cdots,\end{aligned}\tag{3.2}$$

$$\begin{aligned}\mathfrak{M}&=\mathbf{s}^{-4}+\mathbf{c}^{-4}-\mathbf{s}^{-2}\mathbf{c}^{-2}\\&\quad+(\eta^2/2)\mathbf{s}^{-2}\mathbf{c}^{-2}(\ln(\mathbf{s}^2\mathbf{c}^{-2}))^2\\&\quad-(\eta^4/24)\mathbf{s}^{-2}\mathbf{c}^{-2}(\ln(\mathbf{s}^2\mathbf{c}^{-2}))^4+\cdots\\&=\mathbf{s}^{-4}+\mathbf{c}^{-4}-\mathbf{s}^{-2}\mathbf{c}^{-2}\\&\quad+(0.01250/E)\mathbf{s}^{-2}\mathbf{c}^{-2}(\ln(\mathbf{s}^2\mathbf{c}^{-2}))^2\\&\quad-(0.00002603/E^2)\mathbf{s}^{-2}\mathbf{c}^{-2}(\ln(s^2c^{-2}))^4+\cdots.\end{aligned}\tag{3.3}$$

TABLE II. *Values of* $4/\eta^2\mathfrak{M}+2\mathbf{Y}/\eta\mathfrak{M}$ *as function of E and of scattering angle* Θ.

$\Theta=15°$	20°	25°	30°	35°	40°	42.5°	45°	E (KEV)
−0.1916	−0.1247	0.2120	0.981	2.288	3.849	4.419	4.633	150
− .1731	− .0230	.4969	1.603	3.426	5.565	6.340	6.629	200
− .1472	.0869	.790	2.233	4.571	7.286	8.262	8.626	250
− .1171	.2012	1.089	2.868	5.719	9.009	10.187	10.625	300
− .0850	.3182	1.389	3.504	6.869	10.731	12.111	12.624	350
− .0514	.437	1.692	4.142	8.020	12.455	14.04	14.62	400
− .0165	.556	1.995	4.781	9.16	14.179	15.96	16.62	450
+ .0189	.677	2.300	5.421	10.32	15.90	17.89	18.62	500
.0911	.919	2.910	6.702	12.63	19.35	21.74	22.62	600
.1648	1.163	3.521	7.985	14.94	22.80	25.59	26.62	700
.2393	1.408	4.134	9.27	17.24	26.25	29.44	30.62	800
.3143	1.653	4.747	10.55	19.55	29.70	33.29	34.62	900
.3897	1.899	5.360	11.84	21.86	33.15	37.14	38.62	1000
.2994	1.604	4.624	10.30	19.09	29.01	32.52	33.82	880
.5489	2.416	6.65	14.53	26.71	40.40	45.23	47.02	1210
.693	2.884	7.82	16.98	31.09	46.95	52.55	54.62	1400
.846	3.378	9.05	19.55	35.71	53.86	60.26	62.62	1600
1.022	3.946	10.46	22.51	41.02	61.79	69.12	71.82	1830
1.152	4.365	11.50	24.69	44.95	67.66	75.66	78.63	2000
1.229	4.613	12.12	25.97	47.26	71.11	79.52	82.63	2100
1.459	5.353	13.96	29.83	54.18	81.46	91.07	94.63	2400
1.919	6.84	17.65	37.54	68.03	102.2	114.2	118.63	3000
2.303	8.07	20.73	43.98	79.58	119.4	133.4	138.64	3500
2.687	9.31	23.80	50.40	91.12	136.7	152.7	158.64	4000
3.072	10.55	26.88	56.84	102.67	153.9	172.0	178.65	4500
3.456	11.78	29.95	63.26	114.21	171.2	191.2	198.64	5000

TABLE III. *Values of* $\mathbf{X}$ *as function of E and of scattering angle* Θ. *In expansion E is in Mev.*

$\Theta=15°$	20°	25°	30°	35°	40°	42.5°	45°	E (KEV)
7.79	6.60	5.484	4.700	4.203	3.928	3.863	3.841	150
9.69	7.34	5.807	4.856	4.283	3.978	3.904	3.881	200
10.87	7.79	6.004	4.950	4.332	4.006	3.929	3.904	250
11.68	8.09	6.136	5.013	4.365	4.026	3.946	3.920	300
12.27	8.31	6.232	5.058	4.388	4.040	3.958	3.932	350
12.72	8.48	6.304	5.092	4.406	4.050	3.967	3.940	400
13.07	8.61	6.360	5.119	4.418	4.059	3.974	3.947	450
13.35	8.71	6.405	5.140	4.431	4.065	3.980	3.952	500
13.78	8.87	6.473	5.172	4.447	4.075	3.988	3.960	600
14.09	8.99	6.521	5.195	4.459	4.082	3.994	3.966	700
14.33	9.07	6.560	5.212	4.468	4.087	3.999	3.970	800
14.66	9.19	6.609	5.236	4.480	4.095	4.005	3.976	1000
14.48	9.13	6.582	5.223	4.473	4.090	4.002	3.973	880
14.89	9.28	6.645	5.253	4.489	4.100	4.010	3.980	1210
15.16	9.38	6.687	5.273	4.499	4.105	4.014	3.986	1600
15.32	9.44	6.712	5.285	4.505	4.109	4.018	3.988	2000
15.36	9.45	6.717	5.287	4.506	4.110	4.019	3.988	2100
15.44	9.48	6.730	5.293	4.509	4.112	4.020	3.990	2400
15.55	9.52	6.747	5.301	4.513	4.115	4.022	3.992	3000
15.66	9.56	6.764	5.309	4.517	4.117	4.024	3.994	4000
15.73	9.58	6.775	5.314	4.520	4.118	4.026	3.995	5000
16.00	9.68	6.816	5.333	4.530	4.124	4.031	4.000	
$-1.364/E$	$-0.492/E$	$\frac{-0.2083}{E}$	$\frac{-0.0975}{E}$	$\frac{-0.0500}{E}$	$\frac{-0.0297}{E}$	$\frac{-0.0254}{E}$	$\frac{-0.0240}{E}$	Expansion at $E=\infty$. In expansion E is in Mev.
$\frac{+0.02075}{E^2}$	$\frac{+0.00472}{E^2}$	$\frac{+0.00128}{E^2}$	$\frac{0.00038}{E^2}$	$\frac{+0.00012}{E^2}$	$\frac{+0.00004}{E^2}$	$\frac{+0.00003}{E^2}$	$\frac{+0.000024}{E^2}$	

TABLE IV. *Values of $-2Y/\eta$ as function of E and of scattering angle Θ. In expansion E is in Mev.*

$\Theta=15°$	20°	25°	30°	35°	40°	42.5°	45°	E (KEV)	$4/v^2$
65.46	32.45	18.22	11.27	7.71	5.991	5.600	5.472	150	24.003
69.12	33.55	18.60	11.42	7.77	6.021	5.619	5.488	200	32.005
71.39	34.22	18.83	11.51	7.81	6.032	5.633	5.501	250	40.006
72.89	34.67	18.98	11.56	7.83	6.041	5.639	5.506	300	48.007
74.02	34.99	19.09	11.61	7.84	6.050	5.646	5.512	350	56.008
74.88	35.23	19.18	11.63	7.86	6.06	5.65	5.519	400	64.009
75.50	35.42	19.24	11.66	7.87	6.06	5.66	5.52	450	72.01
76.03	35.59	19.29	11.68	7.88	6.06	5.66	5.52	500	80.01
76.85	35.81	19.37	11.71	7.89	6.07	5.66	5.53	600	96.01
77.42	35.97	19.43	11.73	7.90	6.07	5.66	5.53	700	112.02
77.84	36.09	19.47	11.74	7.90	6.08	5.66	5.53	800	128.02
78.42	36.26	19.53	11.77	7.91	6.08	5.68	5.53	1000	160.02
78.08	36.18	19.49	11.76	7.90	6.08	5.67	5.53	880	140.82
78.84	36.39	19.56	11.79	7.92	6.08	5.67	5.54	1210	193.63
79.27	36.53	19.62	11.81	7.92	6.08	5.67	5.54	1600	256.04
79.63	36.61	19.65	11.82	7.93	6.09	5.68	5.54	2000	320.05
79.71	36.62	19.66	11.82	7.94	6.09	5.68	5.54	2100	336.05
79.84	36.69	19.66	11.82	7.94	6.09	5.68	5.54	2400	384.05
80.00	36.74	19.68	11.82	7.94	6.09	5.68	5.54	3000	480.08
80.25	36.79	19.71	11.84	7.94	6.09	5.68	5.54	4000	640.11
80.35	36.83	19.72	11.84	7.94	6.09	5.68	5.54	5000	800.13
80.86	36.97	19.77	11.86	7.95	6.094	5.680	5.545		
$\frac{-2.457}{E}$	$\frac{-0.704}{E}$	$\frac{-0.238}{E}$	$\frac{-0.0891}{E}$	$\frac{-0.0356}{E}$	$\frac{-0.0161}{E}$	$\frac{-0.0123}{E}$	$\frac{-0.01110}{E}$	Expansion at $E=\infty$. In expansion E is in Mev.	
$\frac{+0.0224}{E^2}$	$\frac{+0.00405}{E^2}$	$\frac{+0.00088}{E^2}$	$\frac{+0.00021}{E^2}$	$\frac{+0.000054}{E^2}$	$\frac{+0.000014}{E^2}$	$\frac{+0.000008}{E^2}$	$\frac{+0.000006}{E^2}$		

TABLE V. *Values of $\mathfrak{M}$ as function of E and of scattering angle Θ. In expansion E is in Mev.*

$\Theta=15°$	20°	25°	30°	35°	40°	42.5°	45°	E (KEV)
216.4	67.79	27.29	12.97	7.121	4.679	4.164	4.000	150
214.4	67.05	26.98	12.84	7.073	4.669	4.162	4.000	200
213.2	66.59	26.79	12.76	7.045	4.663	4.160	4.000	250
212.4	66.28	26.66	12.71	7.026	4.658	4.159	4.000	300
211.8	66.06	26.57	12.67	7.012	4.655	4.158	4.000	350
211.3	65.89	26.50	12.64	7.002	4.653	4.158	4.000	400
211.0	65.76	26.45	12.62	6.999	4.651	4.157	4.000	450
211.0	65.65	26.41	12.60	6.988	4.650	4.157	4.000	500
210.2	65.49	26.34	12.58	6.978	4.648	4.157	4.000	600
209.9	65.38	26.29	12.56	6.971	4.646	4.156	4.000	700
209.7	65.29	26.26	12.54	6.966	4.645	4.156	4.000	800
209.4	65.17	26.21	12.52	6.959	4.644	4.156	4.000	1000
209.5	65.24	26.24	12.54	6.963	4.644	4.156	4.000	880
209.1	65.09	26.18	12.51	6.954	4.642	4.155	4.000	1210
208.7	64.93	26.11	12.48	6.944	4.640	4.155	4.000	2000
208.6	64.88	26.10	12.48	6.942	4.640	4.155	4.000	2400
208.4	64.84	26.08	12.47	6.940	4.639	4.155	4.000	3000
208.3	64.78	26.05	12.46	6.936	4.639	4.155	4.000	5000
208.0	64.68	26.01	12.44	6.930	4.638	4.154	4.000	
$\frac{+1.387}{E}$	$\frac{+0.494}{E}$	$\frac{+0.198}{E}$	$\frac{+0.0803}{E}$	$\frac{+0.0288}{E}$	$\frac{+0.00635}{E}$	$\frac{+0.00153}{E}$		Expansion at $E=\infty$. In expansion E is in Mev	
$\frac{-0.0200}{E^2}$	$\frac{-0.00421}{E^2}$	$\frac{-0.00096}{E^2}$	$\frac{-0.00020}{E^2}$	$\frac{-0.000030}{E^2}$	$\frac{-0.000002}{E^2}$				

In these expansions E is in Mev and $\eta E^{\frac{1}{2}}$ was taken to be 0.1581.

The number of counts expected according to Mott's formula is practically independent of the choice of fundamental constants. It can be expressed in terms of the Faraday constant, the velocity of light and the density of hydrogen in the scattering volume. In addition there enters $\mathfrak{M}$ of Eq. (3.3) which is 4 for $\Theta=45°$ at all energies and depends only little on the energy at other angles. For one microcoulomb of incident protons the yield of scattered protons is:

$$Y=10^{-35}\rho_H\left(\frac{e}{M_Hc}\right)c^4\frac{2bA}{R_0\mathfrak{h}}\mathfrak{M}(10^{-6}V_{abs})^{-2}\cot\Theta.$$

Here the absolute coulomb and absolute volt are used as units, ρ_H = density of hydrogen, c = velocity of light, M_H = mass of neutral hydrogen atom. The quantities A, $2b$, R_0, $\mathfrak{h}$ refer to the detector system for counting protons. The notation is A = area of hole, $2b$ = width of slit, R_0 = distance from hole to beam, $\mathfrak{h}$ = distance from hole to slit. Using $e/Mc=9648.9$ abs.-e.m.u. g-equiv.$^{-1}$, $c=2.99796\times10^{10}$ cm sec.$^{-1}$ and computing ρ_H for one mm of oil having density 0.864 with hydrogen at 0°C one obtains

$$Y_{abs}=581.0\frac{2bA}{R_0\mathfrak{h}}\mathfrak{M}(10^{-6}V_{abs})^{-2}\cot\Theta.$$

Here M is taken to be the mass of the average oxygen atom. Supposing that average hydrogen contains 0.04 percent of O_{17} and 0.20 percent O_{18} one has $M=(\frac{1}{16})\times1.000275\times$mass of O_{16} atom $=(1.000275/1.00813)M_H$. The density of hydrogen at 0°C and normal atmospheric pressure was taken as 8.988×10^{-5} g/cm^3; the presence of deuterium was neglected. Boyle's law was assumed, and normal atmospheric pressure was used as the pressure due to 760 mm of mercury having density 13.5951 with the acceleration due to gravity having the value 980.665 cm sec.$^{-2}$. The deviation of the acceleration of gravity in Madison (980.365 cm sec.$^{-2}$) from the standard was taken into account. In international volts and coulombs (International volt = 1.00045 abs. volt; International coulomb = 0.99993 abs. coulomb)

$$Y_{intern}=580.5\frac{2bA}{R_0\mathfrak{h}}\mathfrak{M}(10^{-6}V_{intern})^{-2}\cot\Theta. \quad (3.4)$$

This is the Mott yield per international microcoulomb of incident protons neglecting the geometrical corrections which will be discussed later. The final adjustments to the reduction of data from both laboratories have been made from the above formula.

The assumption of the validity of Boyle's law and the compressibility of Apiezon oil B (the latter has been pointed out by Mr. L. E. Hoisington) introduce small errors in the above constant. The compressibility of oil presumably makes it necessary to decrease the above number by about 0.01 percent. Assuming the equation between volume and pressure for hydrogen to be $pv=0.99938+0.00062p$, with p in atmospheres, one has for small v; $1/v=1.00062p$. The above result should be increased therefore by 0.06 percent on account of the inaccuracy of Boyle's law. Both of these corrections were omitted as insignificant.

2. Effect of error consisting of constant factor

Because of an error in the measurement of the slit system through which the protons are admitted to the ionization chamber there may be present in the measurements an error consisting of a factor which does not depend on the scattering angle. Errors in the operation of the scale-often counter that do not depend on the pulse size entering the amplifier are independent of scattering angle. Similarly some of the errors in the calibration of the Faraday cage used for measuring the primary current enter in the same way for angles and errors in the operation of the Faraday cage during the scattering measurements may depend on the primary energy but should be independent of the scattering angle. Similarly an error in the measurement of the pressure comes under the present head. An effect of an error in the measurement of the energy of the incident particles is also mainly of the nature of a constant factor for all angles but is slightly more complicated. It will be treated as a separate error in another section.

It is found on calculation that in the range 1400–2400 kev a factor independent of angle does not introduce an apparent presence of a p wave to an important degree. If the scattering is due to an s wave anomaly alone then a reasonably small error of this sort produces very nearly

the same error in K_0 at all scattering angles that are used in the experiments for determining K_0. This condition can be expected to persist at the higher energies because the Coulomb scattering becomes increasingly less important. Spherical symmetry in the system of the center of gravity which is characteristic of s scattering cannot be destroyed by an error which is independent of scattering angle and, therefore, a p wave anomaly cannot be introduced by such an error. On the other hand, in the lower energy region 600–900 kev, the Coulomb scattering becomes more important. The spherical symmetry of the scattering in the center of gravity system is then destroyed. A factor constant at all angles produces in this energy range effects on K_0 which depend on the scattering angle used. An apparent p wave anomaly can be introduced at these energies by such an error. Since one may expect theoretically that p and d anomalies increase with energy this circumstance is fortunate for judging experimental data as to presence in it of errors of this nature. For if the data indicate at the higher energies that the anomaly is due to s scattering alone then, even though the value of K_0 obtained from the data may be incorrect, there is no p scattering and, therefore, there should be no p scattering at the lower energies either. If, in addition, the 600–900-kev range shows no p scattering, then the absolute values in this voltage range must be right because otherwise a constant factor at all angles would introduce p scattering. There is at present no indication of a p wave in the 1400–2400-kev range and the above criterion can be used. Errors which are represented by a factor which depends on the scattering angle are, of course, not taken care of by the above type of test.

Let $\mathfrak{R}=\mathbf{P}/\mathbf{P}_M=$ then

$$\frac{\partial \mathfrak{R}}{\partial K_0}=-\frac{2\mathbf{X}}{\eta \mathfrak{M}}\cos 2K_0+\left(\frac{4}{\eta^2 \mathfrak{M}}+\frac{2\mathbf{Y}}{\eta \mathfrak{M}}\right)\sin 2K_0 \quad (4)$$

gives the sensitivity of $\mathfrak{R}$ to K_0 and

$$a_\Theta=(57.3°/100)/(\partial \mathfrak{R}/\mathfrak{R}\partial K_0);\ (\mathfrak{R}\rightarrow 1.01\mathfrak{R}) \quad (4.1)$$

represents the error in K_0 due to one percent error in $\mathfrak{R}$. In Table VI values of this error are listed for different scattering angles, energies and phase shifts. The latter were obtained from theoretical calculations with an interaction potential having a constant value through a distance e^2/mc^2. The negative of the potential energy (depth of well $=D$) within this distance in Mev is given in the last column. Outside the distance e^2/mc^2 the Coulomb field e^2/r was assumed to represent the potential energy. The phase shifts used correspond approximately to the experimental values. For $D=11$ Mev the phase shifts in this table were obtained by extrapolation from $D=10.0$ and $D=10.5$ Mev.

It is seen from the table that at $\Theta=15°$ and 20° the accuracy for determining K_0 is frequently poorer than at other scattering angles. For $K_0=34.8°$, $E=880$ kev, $\Theta=15°$ the accuracy is especially poor. This is because close to this energy the ratio $\mathfrak{R}$ is practically independent of K_0. At all energies the optimum range of angles for determining K_0 is around $\Theta=45°$. It should be pointed out again that at the higher energies the same percentage error in $\mathfrak{R}$ gives practically the same error in K_0 except at $\Theta=15°$ while from 1600 kev down there is a noticeable change in δK_0 with Θ.

The changes of sign in δK_0 which occur in Table VI are somewhat confusing, and it is at times better to express the results in terms of the percentage by which the apparent $\mathfrak{R}$ differs from the $\mathfrak{R}$ that is theoretically expected using the apparent K_0 as derived from the data at $\Theta=45°$. If the correct $\mathfrak{R}$ is changed at all angles into $(1+\epsilon)\mathfrak{R}=\mathfrak{R}'$, then the value of K_0 using $\Theta=\pi/4$ is $K_0+(\delta K_0)_{\pi/4}$ where

$$(\delta K_0)_{\pi/4}=\epsilon[\mathfrak{R}/(\partial \mathfrak{R}/\partial K_0)]_{\pi/4}.$$

From this phase shift the expected $\mathfrak{R}$ at other Θ is $\mathfrak{R}+(\partial \mathfrak{R}/\partial K_0)(\delta K_0)_{\pi/4}$. One has

$$\mathfrak{R}'/[\mathfrak{R}+(\partial \mathfrak{R}/\partial K_0)(\delta K_0)_{\pi/4}]$$
$$=1+(\epsilon/\delta K_0)[\delta K_0-(\delta K_0)_{\pi/4}]$$
$$=1+(\epsilon/a_\Theta)(a_\Theta-a_{\pi/4}). \quad (4.2)$$

The quantity $(a_\Theta-a_{\pi/4})/a_\Theta$ is thus the ratio of the apparent percentage deviation of $\mathfrak{R}$ from the value to be expected at scattering angle Θ from the apparent K_0 at $\Theta=45°$ to the percentage error in $\mathfrak{R}$. Values of this ratio are given in Table VII.

TABLE VI. *Values of error in phase shift K_0 in degrees due to one percent error in measured scattering.*

Θ=15°	20°	25°	30°	35°	40°	42.5°	45°	E (KEV)	K_0	D (MEV)
−2.3	−0.97	−0.51	−0.28	−0.16	−0.10	−0.087	−0.082	175	5.5°	10.395
−1.4	− .71	− .40	− .23	− .12	− .061	− .045	− .039	275	9.6°	10.395
−1.2	− .64	− .42	− .29	− .19	− .091	− .038	− .013	375	13.7°	10.395
−1.1	− .67	− .55	− .85	+ .34	+ .049	+ .023	+ .017	450	16.4°	10.395
−1.1	− .85	−3.1	+ .29	+ .088	+ .047	+ .041	+ .039	550	19.8°	10.395
−1.2	−2.2	0.50	.14	.083	.068	.065	.064	650	23.8°	10.500
−1.5	+3.1	.27	.12	.094	.085	.084	.083	750	26.6°	10.500
−2.2	+0.85	.21	.12	.11	.102	.101	.101	850	29.2°	10.500
−2.7	.70	.20	.13	.11	.11	.11	.11	880	30.0°	10.500
1.8	.30	.18	.16	.15	.15	.15	.15	1210	36.2°	10.500
0.94	.26	.19	.17	.17	.17	.17	.17	1400	39.0°	10.500
.66	.25	.20	.19	.19	.19	.19	.20	1600	41.4°	10.500
.51	.25	.21	.21	.21	.22	.22	.22	1830	43.8°	10.500
.46	.25	.22	.22	.22	.23	.23	.23	2000	45.1°	10.500
.43	.25	.23	.23	.23	.23	.24	.24	2100	45.7°	10.500
.39	.26	.24	.25	.25	.26	.26	.26	2400	47.6°	10.500

3. Effect of error in voltage

If the experiment is performed at an energy E and if there is only an s wave anomaly the ratio $\mathfrak{R}=\mathbf{P}/\mathbf{P}_M$ is given by Eqs. (2) with a suitable K_0. If the energy at the scattering volume is incorrectly judged to be

$$E'=E+\delta E$$

one obtains an apparent experimental value $\mathfrak{R}'$ for that ratio at the energy E'. This value corresponds to an apparent phase shift K_0' if Eqs. (2) are used. In this section

$$\delta K_0=K_0'-K_0$$

will be called the error in the phase shift. This nomenclature is not the best because it takes no account of the fact that at the energy E' the correct phase shift differs from K_0. This circumstance will be discussed later in connection with the variation of K_0 with E and the effect of a possible error in voltage on the magnitude of the interaction potential. It will then be seen that only a fraction of K_0 matters for conclusions drawn from experiments at the higher energies.

It is seen in Table V that $\mathfrak{M}$ changes very slowly with energy. It is thus sufficiently accurate to consider $\mathbf{P}_M$ as being proportional to E^{-2}. The apparent value of $\mathfrak{R}$ at energy E' is then

$$\mathfrak{R}'=(E'/E)^2\mathfrak{R}\cong(1+2\delta E/E)\mathfrak{R}.$$

This may be equated to

$$\mathfrak{R}+(\partial\mathfrak{R}/\partial E)\delta E+(\partial\mathfrak{R}/\partial K_0)\delta_{E,\Theta}K_0.$$

One obtains thus

$$\delta_{E,\Theta}K_0=(2\mathfrak{R}/E-\partial\mathfrak{R}/\partial E)\delta E/(\partial\mathfrak{R}/\partial K_0)\cdots. \quad (5)$$

Treating again $\mathfrak{M}$ as independent of the energy one has

$$\frac{\partial\mathfrak{R}}{\partial E}=-\frac{\sin K_0\cos K_0}{E\eta\mathfrak{M}}\left(\mathbf{X}-\eta\frac{\partial\mathbf{X}}{\partial\eta}\right)+\frac{\sin^2 K_0}{E\mathfrak{M}}\left(\frac{4}{\eta^2}+\frac{\mathbf{Y}}{\eta}-\frac{\partial\mathbf{Y}}{\partial\eta}\right). \quad (5.1)$$

TABLE VII. *Percentage by which apparent ratio to Mott is higher than value calculated from apparent phase shift K_0 determined at Θ=45° if at all angles the measured yields are too high by one percent and if the anomaly is due only to s scattering. Quantity tabulated is $(a_\Theta-a_{\pi/4})/a_\Theta$. Values of K_0 correspond to $r_0=e^2/mc^2$, D=10.5 Mev.*

Θ=15°	20°	25°	30°	35°	40°	42.5°	E (KEV)	K_0
1.04	0.85	0.46	0.164	0.043	0.008	0.002	880	30.0°
.92	.50	.14	.02	−.003	−.002	−.001	1210	36.2°
.81	.34	.064	−.0004	−.009	−.003	−.000	1400	39.0°
.70	.22	.015	−.019	−.013	−.004	−.001	1600	41.4°
.58	.12	.019	−.028	−.015	−.004	−.001	1830	43.8°
.50	.07	−.032	−.032	−.016	−.004	−.002	2000	45.1°
.46	.051	−.038	−.033	−.016	−.004	−.001	2100	45.7°
.34	−.001	−.052	−.037	−.017	−.003	−.001	2400	47.6°

TABLE VIII. *Values of error in phase shift K_0 in degrees due to one percent error in voltage of scattering volume.*

Θ=15°	20°	25°	30°	35°	40°	42.5°	45°	E (KEV)	K_0	D (MEV)
−4.6	−2.0	−1.05	−0.60	−0.36	−0.23	−0.20	−0.19	175	5.5°	10.395
−2.9	−1.5	−0.86	− .51	− .30	− .17	− .14	− .13	275	9.6°	10.395
−2.4	−1.4	− .91	− .65	− .46	− .26	− .15	− .10	375	13.7°	10.395
−2.3	−1.5	−1.19	−1.8	+ .63	+ .027	− .031	− .045	450	16.4°	10.395
−2.3	−1.8	−0.65	+0.51	+ .081	− .004	− .014	− .018	550	19.8°	10.395
−2.6	−4.6	+ .90	.17	.049	.018	.013	.012	650	23.8°	10.500
−3.2	+6.1	.41	.12	.055	.038	.035	.034	750	26.6°	10.500
−4.7	+1.6	.27	.10	.067	.056	.055	.055	850	29.2°	10.500
−5.7	1.26	.25	.10	.071	.063	.061	.061	880	30.0°	10.500
+3.6	0.43	.17	.12	.114	.113	.113	.114	1210	36.2°	10.500
1.7	.33	.17	.14	.14	.14	.14	.14	1400	39.0°	10.500
1.1	.29	.18	.16	.16	.16	.16	.16	1600	41.4°	10.500
0.83	.27	.19	.18	.18	.18	.19	.19	1830	43.8°	10.500
.71	.26	.20	.19	.19	.20	.20	.20	2000	45.1°	10.500
.66	.26	.20	.20	.20	.21	.21	.21	2100	45.7°	10.500
.56	.26	.22	.22	.22	.23	.23	.23	2400	47.6°	10.500

Computing this one obtains the numbers in Table VIII.

The phase shifts, energies and depths of well in Table VIII correspond to those in Table VI. The effect of an error in voltage is seen to become nearly independent of the angle at the higher energies. In this respect the effect of an error in voltage is very similar to that of an error due to a factor independent of angle.

The effect of an error in voltage is somewhat simpler when it is expressed in terms of the percentage by which the observed scattering at an angle Θ differs from the scattering to be expected, when only an s scattering anomaly is assumed and when the observed scattering at Θ=45° is used. This can be done using the numbers tabulated in Tables VI and VIII. The quantity recorded in the latter table is

$$b_\Theta = 0.573 E \delta_{E,\Theta} K_0 / \delta E. \tag{5.2}$$

The quantity $\mathfrak{R}$ is a function of K_0 and E and in the absence of exact knowledge of the voltage the value of $\mathfrak{R}$ theoretically expected at the angle Θ and the apparent energy E' using observations at $\Theta=\pi/4$ is

$$\mathfrak{R}(K_0+\delta_{E,\pi/4}K_0, E+\delta E) = \mathfrak{R}+(\partial\mathfrak{R}/\partial K_0)\delta_{E,\pi/4}K_0+(\partial\mathfrak{R}/\partial E)\delta E=\mathfrak{R}''.$$

The ratio of the apparent value $\mathfrak{R}'$ to this expected value $\mathfrak{R}''$ is then

$$\mathfrak{R}'/\mathfrak{R}''=1+(\partial\mathfrak{R}/\mathfrak{R}\partial K_0)(\delta_{E,\Theta}K_0-\delta_{E,\pi/4}K_0) =1+(\delta E/E)(b_\Theta-b_{\pi/4})/a_\Theta. \tag{5.3}$$

By means of Eq. (5.3) and Tables VI and VIII one can obtain the ratio $\mathfrak{R}'/\mathfrak{R}''$. The percentage by which the observed value at scattering angle Θ should differ from the value to be expected on the basis of measurements made at Θ=45° is seen to be the percentage of error in the voltage multiplied by

$$(b_\Theta-b_{\pi/4})/a_\Theta.$$

Values obtained in this way are tabulated in Table IX.

4. Estimate of spread of beam due to collisions. Discussion of pressure effects in argon and krypton. Multiple scattering

As the beam goes through the scattering chamber it becomes spread on account of the many small collisions that each bombarding particle makes with the hydrogen atoms of the gas. The purpose of the present section is to make estimates of the order of magnitude of the additions to the width of the beam due to this cause. The diameter of the beam must be kept somewhat smaller than the diameter of the foil used to admit the protons into the evacuated Faraday cylinder connected to the current integrator. The fluctuation of the direction of the beam due to changes in the accelerating tube makes it unnecessary to have more than estimates of order of magnitude.

The relatively numerous small angle collisions may be considered in first approximation as changing the direction of motion without chang-

ing the energy of the particle. The vector representing the velocity is changed at each collision through the addition of a small vector perpendicular to the initial direction and the probability of the occurrence of a single such change in a short path can be calculated by means of Rutherford's or Mott's scattering formula. For the first collision the change of direction occurs in a plane perpendicular to the original beam, but in later collisions it takes place in planes having slightly different directions. Since the total deflection is supposed to be small the change of orientation of the planes will be neglected. The additions to the velocity may then be considered as taking place in the same plane but each successive addition must be considered as taking place in a random direction with probabilities determined by Rutherford's formula. Instead of using the velocities one may also deal directly with vectors having absolute values equal to the angular deflections and drawn in the direction of the velocity changes. The problem is thus very similar to that of "random flights" in a plane.

A set of random radial displacements in a plane having equal magnitude α gives resultant displacements for which the Cartesian coordinates x, y, and distance, r, have $(r^2)_{Av}=(2x^2)_{Av}=(2y)^2{}_{Av}=(n\alpha^2)_{Av}$. For large n the average deviations of the squares correspond to a Gauss error distribution. It is shown in Rayleigh's *Theory of Sound*[15] that the distribution is of the Gauss error type even if one deals with the composition of a large number n of components with amplitude α, a large number n' of components with amplitude β, etc. The chance of a resultant displacement of amplitude between r and $r+dr$, is then according to Rayleigh

$$P(r)dr=2(n\alpha^2+n'\beta^2+\cdots)^{-1}r \times\exp\left[-r^2/(n\alpha^2+n'\beta^2+\cdots)\right]dr.$$

The number of deflections taking place in an infinitesimal angular range is, of course, not infinite and it is not justifiable to apply this formula since the numbers n, n', $\cdots$ are not infinite. It may, nevertheless, be expected to give the result approximately because the angular range may be divided into finite rather than infinitesimal intervals and because the validity of

$$(r^2)_{Av}=n\alpha^2+n'\beta^2+\cdots$$

does not depend on n, n', $\cdots$ having large values. In the remainder of the discussion $(r^2)_{Av}=(\theta^2)_{Av}$ (θ = angular deflection) will be calculated and it will be assumed that the distribution is not far from that given by Rayleigh's formula. Since the latter drops off steeply at and beyond $[(\theta^2)_{Av}]^{\frac{1}{2}}$, the values of this quantity will be used as estimates of the probable angular spread.

For scattering from a heavy nucleus such as that of argon Rutherford's formula applies. It will be supposed that the scattering by an atom of argon becomes zero when the impact parameter (distance from nucleus to orbital asymptote at ∞) is greater than some suitably chosen distance p of the order of nuclear dimensions. Corresponding to this distance there is an angle of minimum deflection ω which, when small, is given by

$$\omega=ZZ'e^2/Ep, \tag{6}$$

where Ze, $Z'e$ are the charges of the colliding nuclei and E is the kinetic energy of the scattered particle. The chance that one small angle collision should take place into an angular range θ, $\theta+d\theta$ on going through a thickness l of gas having n atoms per cm^3 is

$$K\theta^{-3}d\theta,$$

where

$$K=2\pi nl(ZZ'e^2/E)^2. \tag{6.1}$$

For large angles this is not true. The number of large angle collisions is, however, quite small and they will be neglected in studying the spreading of the beam. One has then

$$((\Sigma\theta)^2)_{Av}=K\int_{\omega}^{\theta_{\max}}\theta^{-3}\theta^2d\theta=K\ln(\theta_{\max}/\omega), \tag{6.2}$$

where $\theta_{\max}$, is a suitably chosen upper limit for elementary deflections that need to be taken into account. For an argon pressure of 60 mm of oil having a density 0.866 one has a pressure equal to that of 3.83 mm of mercury so that $n=2.70\times10^{19}\times3.84/760=1.36\times10^{17}$. For $E=2mc^2$ one has then $K=1.21\times10^{-4}$ for a path length $l=22$

[15] Lord Rayleigh, *Theory of Sound*, second edition (Macmillan Co., 1894), Vol. I, p. 41; G. N. Watson, *Bessel Functions* (Cambridge University Press, 1922), p. 419 for references.

cm. Assuming p = Bohr radius $= 0.528\times10^{-8}$ cm, one has at an energy of $2mc^2$ the value $\omega = 18e^2/2mc^2a_H = 9(e^2/\hbar c)^2 = 4.79\times10^{-4}$. The number of single deflections into $\Delta\omega$ is $\sim K\omega^{-3}\Delta\omega = 500\Delta\omega/\omega$. Thus practically every proton suffers several small angle collisions. Using $\theta_{max}=\pi/2$ one has $\ln(\theta_{max}/\omega)=8.1$ and using $\theta_{max}=1°$ $=1/57.3$ one has $\ln(\theta_{max}/\omega)=3.6$. The result is seen to be insensitive to the choice of θ_{max}. Using $\theta_{max}=\pi/2$ one obtains Table Xa. In the last row is given the quantity $2l\Delta\theta/3$. This is an approximate estimate of the linear spread of the beam. The root mean deviation $\Delta\theta$ is assumed here to give sufficiently well the direction of motion of the root mean deviation of the linear displacement Δx so that,

$$\Delta x = \Delta\theta\int_0^l (y/l)^{\frac{1}{2}}dy = 2l\Delta\theta/3.$$

This assumption is crude, but should be good enough for estimates of order of magnitude. The values in Table Xa are probably too high since $\theta_{max}=\pi/2$ is an overestimate. With $\theta_{max}=2°$ $=0.0349$ values given in Table Xb are obtained. These may still be somewhat too high because for this θ_{max} at $E=2mc^2$ one has $K\theta_{max}^{-2}=1.2\times10^{-4}/(0.035)^2=0.10$. There is, therefore, only a chance of 1/10 that a proton will be scattered into a 2° range at the rate at which scattering occurs at 2°. However, this chance increases rapidly towards smaller deflections.

In order to obtain the same spread at $E=4mc^2$ as at $E=2mc^2$, the pressure must be increased nearly four times so as to compensate by means of n the change in E and to obtain the same K. For $\theta_{max}=0.0349$ the factor $\ln_e(\theta_{max}/\omega)$ increases from 4.30 at $E=2mc^2$ to 5.00 at $E=4mc^2$. Hence the pressure should be increased in this case not quite by the factor four but by $4\times4.30/5.00$ $=3.4$. If $\theta_{max}=\pi/2$, the increase in pressure required to produce the same spread at $4mc^2$ at a higher pressure as at $2mc^2$ at a lower pressure is $4\times8.1/8.8=3.7$. The accidental fluctuations of the direction of the proton beam and the impossibility of knowing precisely its width make it difficult to determine just how the loss of some of the incident protons through multiple small angle scattering will affect the measurements at a given energy as the pressure is varied. A better test of the origin of the observed deviations is to vary the energy and the pressure in such a way as to obtain the same apparent deviation from Rutherford's scattering. Then according to the estimates just made the same deviations should be obtained at two Mev at a pressure of about $3.4p$ as at one Mev at a pressure p. These preliminary estimates will be improved presently by using Eq. (6.6).

In hydrogen at the pressures used the spread of the beam due to multiple small angle scattering should be much smaller than in argon because the large scattering anomaly at $\Theta=45°$ makes it unnecessary to have as large a small angle scattering in hydrogen. In this case the chance that one small angle collision should take place into an angle between Θ and $\Theta+d\Theta$ on going through a thickness l of gas having n atoms per cm³ is

$$K_H\Theta^{-3}d\Theta,$$

where

$$K_H = 2\pi nl(e^2/E)^2. \qquad (6.3)$$

For $E=2mc^2$ and a path length $l=22$ cm through hydrogen gas at 12 mm Hg pressure one has $n=8.5\times10^{17}$, $K_H=2.34\times10^{-6}$, $\omega=2.66\times10^{-5}$. The probable angular spread must be less than $[K\ln\pi/4\omega]^{\frac{1}{2}}=0.0049=0.28°$. The probable linear

TABLE IX. *Percentage by which apparent $\Re$ is higher than value calculated from apparent phase shift K_0 determined at $\Theta=45°$ if the voltage measurements are too high by one percent and if the anomaly is due only to S scattering. Quantity tabulated is $(b_\Theta - b_{\pi/4})/a_\Theta$. Values of K_0 correspond to $r_0=e^2/mc^2$, $D=10.5$ Mev.*

$\Theta=15°$	20°	25°	30°	35°	40°	42.5°	E (KEV)	K_0
2.09	1.72	0.95	0.34	0.090	0.017	0.003	880	30.0°
1.9	1.04	.33	.064	.004	−.002	−.002	1210	36.2°
1.7	0.74	.17	.014	−.009	−.003	−.001	1400	39.0°
1.5	.52	.085	−.013	−.015	−.005	−.001	1600	41.4°
1.3	.34	.021	−.029	−.020	−.006	−.001	1830	43.8°
1.1	.25	−.005	−.036	−.021	−.006	−.002	2000	45.1°
1.0	.21	−.018	−.039	−.020	−.006	−.001	2100	45.7°
0.84	.11	−.042	−.043	−.021	−.004	−.002	2400	47.6°

TABLE Xa. *Estimate of linear spread of proton beam with* θ_{max} *assumed to be* $\pi/2$.

$E=1mc^2$	$2mc^2$	$3mc^2$	$4mc^2$
$[((\Sigma\theta)^2)_{Av}]^{\frac{1}{2}}=3.4°$	1.8°	1.2°	0.93°
$\Delta x=2l\Delta\theta/3=0.88$ cm	0.46 cm	0.31 cm	0.24 cm

displacement must be less than 0.07 cm. According to Table X*b* this linear displacement corresponds to a pressure of $(0.07/0.33)^2\times 60$ mm $=3$ mm of argon at an energy of $2mc^2$. According to Fig. 10 of the paper of HKPP a pressure of 3 mm of argon at 860 kev shows no definite difference from Rutherford's scattering and may be in agreement with it. Although the evidence for this is not very definite it would be surprising if this error could be serious for hydrogen since there is good agreement of absolute yields in the overlap region between HHT and HKPP.

The above estimates are too crude for a comparison of argon and krypton scattering since screening is taken account of too roughly. An idea of the effect of screening can be obtained using the Thomas-Fermi field. The effective nuclear charge for force as a function of the distance r will be called $Z_e(r)$. For small deflections

$$\theta=(e^2/pE)\int_0^{\pi/2} Z_e(p/\cos\varphi)\cos\varphi d\varphi$$

and

$$\int nl\theta^2\sigma d\Omega$$

$$=K\int_{p(\min)}^{\infty}\left\{\int_0^{\pi/2} Z_e(p/\cos\varphi)\cos\varphi d\varphi\right\}^2 p^{-1}dp.$$

On account of the inapplicability of the formula for θ at large θ the integration over the distance of closest approach is cut off at a suitable $p_{\min}$. The Fermi-Thomas field gives $Z_e=Zf(\xi)$ with $\xi=Z^{\frac{1}{3}}r/(0.885a_H)$. The function $f(\xi)$ starts at $f=1$ for $\xi=0$, decreases roughly linearly up to $\xi=2$ and approaches $f=0$ asymptotically for large ξ. At $\xi=8$ it is ~ 0.1. The function will be approximated by

$$f(\xi)=A-B\xi \qquad (A, B>0)$$

through the region in which the above expression gives positive values. For larger ξ it will be supposed that $f=0$. This is admittedly an approximation. The integrations give

$$\int nl\theta^2\sigma d\Omega=KA^2\left[\frac{1}{2}\zeta_m^2\sin^2\zeta_m-\frac{5}{4}\sin^2\zeta_m\right.$$

$$\left.+\frac{3}{2}\zeta_m\sin\zeta_m\cos\zeta_m-\frac{3}{4}\zeta_m^2-\ln\cos\zeta_m\right], \quad (6.4)$$

where

$$\tan\zeta_m-\zeta_m=0.885a_HZ^{-4/3}(E/e^2)\theta_{max}/B,$$
$$\cos\zeta_m=(B/A)Z^{\frac{1}{3}}p(\min)/(0.885a_H). \quad (6.5)$$

The last equation determines ζ_m in terms of $p(\min)$ which is the smallest impact parameter admitted by the requirement of using a formula for θ valid only for small θ. The equation before last similarly determines ζ_m in terms of θ_{max}. The large value of $a_H/(e^2/E)$ makes the right side of Eq. (6.5) of the order of 100 which makes $\zeta_m\sim\pi/2$. Setting

$$\zeta_m=\pi/2-\epsilon$$

one has

$$1/\epsilon=0.885a_HZ^{-4/3}(E/e^2)\theta_{max}/B$$
$$+\pi/2+\cdots, \quad (6.5')$$

$$((\Sigma\theta)^2)_{Av}=KA^2[-5/4-\pi^2/16$$
$$+\ln(1/\epsilon)+\pi\epsilon+\cdots] \quad (6.6)$$

where K is given by Eq. (6.1). The result in the form of Eq. (6.6) is similar to Eq. (6.2). It is more suitable for the purpose of comparing krypton with argon because the screening is made to vary with Z in accordance with the Fermi-Thomas distribution. Using $\theta_{max}=\frac{1}{10}$, $B=\frac{1}{5}$, $A=1$ one has at 860 kev $1/\epsilon\leqq 1.40\times 10^4Z^{-4/3}$ which gives for the coefficient of KA^2 in Eq. (6.6) the values 2.92 for krypton and 3.83 for argon. The number of argon atoms n_A that would be expected to give the same effect as n_K krypton atoms should be therefore $n_A=4(2.92/3.83)n_{Kr}=3.0n_{Kr}$. The experimental ratio of the argon pressure to that of krypton for the same percentage difference from Rutherford is approxi-

TABLE Xb. *Estimate of linear spread of proton beam with* θ_{max} *assumed to be 2°.*

$E=1mc^2$	$2mc^2$	$3mc^2$	$4mc^2$
$[((\Sigma\theta)^2)_{Av}]^{\frac{1}{2}}=2.4°$	1.3°	0.91°	0.70°
$2l\Delta\theta/3=0.61$ cm	0.33 cm	0.23 cm	0.18 cm

mately 2.3. The discrepancy between these two numbers can be reduced by using a larger B. There is some justification for using a larger B because most of the contributions to $((\Sigma\theta)^2)_{Av}$ come from small p and the values of ξ that correspond to p_{min} are, with the above constants, 0.04 for krypton and 0.02 for argon. The values of $\xi_p = Z^{\frac{1}{2}}p/(0.885a_H)$ that make important contributions are <0.4 and one may therefore use the initial rectilinear portion of the $f(\xi)$ curve. For this $A=1$, $B=\frac{1}{3}$ are fair values. Also $\theta_{max}=1/20$ corresponds better to Table X*b* than $\theta_{max}=\frac{1}{10}$. Making these changes one obtains $n_A = 4(1.71/2.62)n_{Kr} = 2.6n_{Kr}$. This is not far from the experimental value $2.3n_{Kr}$. The coefficient of K in Eq. (6.6) is smaller than in the computation of Table X*b*. The difference is less than a factor 2 and does not affect seriously the linear spreads.

The scattering in argon at 860 kev can be compared with that at 1830 kev. Comparing the pressures giving 16 percent difference from Rutherford's formula one has a ratio 3.1. The ratio of energies is 2.13. The ratio of pressures expected on account of the variation of K with energy is therefore $4.5=(2.13)^2$. The ratio $4.5/3.1=1.5$ must be accounted for by the change in the bracket in Eq. (6.6). Here again it is favorable to assume a large B and a small θ_{max}. With $B=\frac{1}{3}$ and $\theta_{max}=1/20$, the bracket is 2.62 for 860 kev and $2.62+\ln_e 2.13=3.38$ for 1830 kev. The corrected expectation for the ratio of pressures is $(2.13)^2(2.62/3.38)=3.5$. This is in fair agreement with the experimental 3.1. Here, as in the comparison with krypton, the coefficient of K does not change quite as rapidly as experiment requires. It appears from the above comparisons that the large scattering observed at high pressures is due to the spreading of the beam. On the other hand, the agreement between expectation and experiment is sufficiently imperfect to allow at least partly another explanation.

Double scattering in which the first deflection is greater than 5° will be seen to contribute little. The percentage difference caused by it should vary as nZ^2/E^2. Experimentally n must be varied more slowly than Z^2/E^2 in order to give the same percentage difference. This speaks against attributing a large part of the effect to double scattering in which the first deflection is $>5°$. The chance that a proton will be scattered into a cone between θ_1 and θ_2 is $(K/8)(1/\sin^2\theta_1/2 - 1/\sin^2\theta_2/2)$. For a path of 10 cm at 860 kev through argon at 60 mm oil pressure $K/8=10^{-4}$. The total number of protons scattered beyond 5° is according to this 0.5 percent of the number of incident protons. The change in the proton energy due to argon recoil is negligible for such a small fraction of the whole number. The effect of the change in direction can be estimated from a formula for second-order corrections caused by the divergence of the beam which is considered at the end of the section on "Geometrical Corrections." According to this the fractional increase in the scattering due to spreading the proton beam uniformly on the surface of a cone is $25\theta^2/4\Theta^2$ where Θ is the angle between the axis of the cone and the central line of the analyzing system while θ is the scattering angle for the first deflection. It is assumed that the angle θ is small. The chance of θ being between θ and $\theta+d\theta$ is $Kd\theta/\theta^3$. The fractional increase in scattering is

$$(25K/4\Theta^2)\ln(\theta_{max}/\theta_{min}).$$

For $\theta_{max}=\pi/2$, $\theta_{min}=5°$, $\Theta=20°$ this gives for argon at 860 kev, with path length $l=10$ cm, at a pressure of 60 mm of oil an effect of 1.1 percent. Decreasing θ_{min} to 2.5° increases this to only 1.4 percent. This effect is seen to be not serious since the total deviation from Rutherford's formula is ~25 percent. There should be an additional smaller effect due to having a large deflection first and a small one afterwards. This effect is expected to be smaller because the distance from the analyzing slit to the beam is ~3 cm. Since for larger Θ these corrections decrease as Θ^{-2} they account for only a small part of the whole.

For double scattering in which the first deflection is of the order of 1° or less it ceases to have meaning to consider only double scattering because the spread of the beam due to multiple scattering is of this order of magnitude. It is also incorrect to use the expression $(25K/4\Theta^2)\ln(\theta_{max}/\theta_{min})$ for too small values of θ_{min} because it was supposed, in deriving it, that the major part of the beam suffered no deflection comparable with θ_{min}. The contributions due to

double scattering in which the first angle is very small will be considered, therefore, as part of the effect of multiple scattering at small angles followed by a large deflection. The fractional effect due to this cause is $(25/4)((\Sigma\theta)^2)_{Av}/\Theta^2$. For a path of 10 cm in argon at 60 mm oil pressure at 860 kev for $\Theta=20°$ the above expression gives 1.0 percent. This effect should have the same value for a given value of the expression (6.6) and the estimates of the way n varies with Z and E made for the effect of missing the Faraday cylinder apply to this effect also. Double scattering through larger angles as well as multiple scattering through small angles followed by a large angle deflection give, with the approximation used here, fractional increases which vary directly with the pressure. It is surprising that the experimental curve gives also a linear variation with pressure for the fractional increase, but it is difficult to predict the law of increase with pressure without knowing more about the structure of the beam. There appears to be no objection so far, therefore, to attributing the pressure effects in argon and krypton primarily to the spreading of the beam and the too low value for the number of incident protons.

5. Values of phase shift derived from experiment

Explanation of tables.—In Table XI are given values of the ratio to Mott $\mathfrak{R}$ as obtained from experiment by Herb, Kerst, Parkinson and Plain. These represent the mean of several observations at energies close to the value listed in the first column. Where necessary corrections have been applied by them for the rate of change of yield with voltage in reducing the values to a common energy. The table consists of six sections each section of which refers to one energy. The first line of each section gives the value of $\mathfrak{R}$ tabulated by HKPP in their Table I. The second line gives the corrections which have been applied to this $\mathfrak{R}$. The corrections are expressed in percentage of $\mathfrak{R}$ and are in each case a sum of corrections for temperature of oil used in the manometer and a correction for fundamental units. The latter was made so as to reduce the values to Eq. (3.4). It amounts to a uniform increase of all values by 0.381 percent. The corrections for oil temperature are listed by HKPP in their Table I(a) and have been added to the correction for fundamental units. The final corrected value of $\mathfrak{R}$ is listed in the third row. The fourth and fifth rows give values of $\mathfrak{R}$ for two values of K_0 differing by 1° and representing approximately the experimental values. The object in listing these numbers is to show the sensitivity of $\mathfrak{R}$ to K_0. In the sixth row are given values of K_0 obtained from each scattering angle on the assumption of a pure s anomaly. The arithmetic mean of the values so obtained from $\Theta=30°$, 35°, 40°, 45° stands in the sixth row and last column. The values of K_0 obtained for smaller scattering angles were not used in taking the mean because the accuracy in the determination of K_0 is expected to be poorer for them. It is satisfactory to note, however, that for $\Theta=25°$ the experimental mean K_0 and the derived K_0 agree quite well and that the only large deviations for $\Theta=20°$ are 0.6° for 1200 kev and 0.4° at 2105 kev. For $\Theta=15°$ the deviations from the mean are large and are probably due to the poor sensitivity caused by the predominance of Rutherford scattering and by the presence of a slight systematic error caused by the variation of the scattering yield within the scattering angle. The seventh line contains values of $\mathfrak{R}$ computed for the mean K_0 on the assumption of absence of higher phase shifts and the eighth gives the percentage difference of the observed (line 3) and computed $\mathfrak{R}$. This last line contains information regarding the presence of higher phase shifts.

The experimental values used above correspond to the calibration of the ballistic galvanometer for current measurement by the "current time method." In addition Herb *et al.* have used a calibration by the "air condenser method." The latter gives values of $\mathfrak{R}$ greater than the "current time" values by 0.76 percent. Reasons for considering the current time method as more reliable are given in the paper of HKPP. The effect of using the air condenser values is, therefore, not tabulated. An alternative interpretation of the data would consist in increasing all experimental values of HKPP by 0.38 percent. According to Table VII the percentage difference between the observed and computed $\mathfrak{R}$ (eighth row of each section in Table XI) will be affected at the higher energies by negligible amounts except at $\Theta=15°$ where ~ 0.2 percent would have to be added. The uncertainties in geometrical

TABLE XI. *Phase shift analysis of data of Herb, Kerst, Parkinson and Plain.*

	Θ=15°	20°	25°	30°	35°	40°	45°
				E=860 kev			
ℜ from HKPP	0.750	0.672	0.811	1.317	2.229	3.38	3.90
Corrections	.327%	.327%	.327%	0.327%	0.327%	0.327%	0.327%
Final ℜ	.752	.674	.814	1.321	2.236	3.39	3.91
ℜ (K_0=29°)	.724	.670	.811	1.288	2.184	3.278	3.821
ℜ (K=30°)	.721	.670	.853	1.394	2.395	3.608	4.211
K_0 from ℜ		29.45	29.07	29.31	29.25	29.34	29.23
Mean K_0 from Θ=30°, 35°, 40°, 45°=29.28°							
ℜ (K_0=29.28°)	0.723	0.673	0.823	1.318	2.243	3.370	3.930
Diff. obs. and comp. ℜ	4.0%	0.1%	−1.1%	0.2%	0.3%	0.6%	−0.5%

	Θ=15°	20°	25°	30°	35°	40°	45°
				E=1200 kev			
ℜ from HKPP	0.743	0.901	1.590	3.20	5.90	8.93	10.32
Corrections	.525%	.525%	0.525%	0.525%	0.525%	0.525%	0.525%
Final ℜ	.747	.906	1.598	3.22	5.93	8.98	10.37
ℜ (K_0=35°)	.715	.860	1.516	3.004	5.511	8.43	9.87
ℜ (K_0=36°)	.718	.888	1.605	3.209	5.897	9.02	10.56
K_0 from ℜ		36.60	35.92	36.05	36.08	35.93	35.72
Mean K_0 from Θ=30°, 35°, 40°, 45°=35.94°							
ℜ (K_0=35.94°)	.718	0.886	1.600	3.197	5.874	8.98	10.52
Diff. obs. and comp. ℜ	4.0%	2.3%	−0.1%	0.7%	0.96%	0.0%	−1.4%

	Θ=15°	20°	25°	30°	35°	40°	45°
				E=1390 kev			
ℜ from HKPP	0.777	1.080	2.196	4.59	8.23	12.74	14.88
Corrections	.436%	0.436%	0.436%	0.436%	0.436%	0.436%	0.436%
Final ℜ	.780	1.085	2.206	4.61	8.27	12.80	14.94
ℜ (K_0=38°)	.740	1.046	2.098	4.34	8.019	12.28	14.35
ℜ (K_0=39°)	.747	1.086	2.214	4.602	8.506	13.01	15.21
K_0 from ℜ		38.97°	38.93°	39.03°	38.51°	38.71°	38.69°
Mean K_0 from Θ=30°, 35°, 40°, 45°=38.76°							
ℜ (K_0=38.76°)	.745	1.076	2.186	4.539	8.389	12.83	15.00
Diff. obs. and comp. ℜ	4.7%	0.8%	0.9%	1.6%	−1.4%	−0.2%	−0.4%

	Θ=15°	20°	25°	30°	35°	40°	45°
				E=1830 kev			
ℜ from HKPP	0.884	1.661	3.862	8.24	15.04	23.12	27.28
Corrections	.491%	0.460%	0.460%	0.491%	0.460%	0.491%	0.460%
Final ℜ	.888	1.669	3.880	8.28	15.11	23.23	27.41
ℜ (K_0=43°)	.851	1.598	3.676	7.86	14.53	22.18	25.91
ℜ (K_0=44°)	.868	1.665	3.854	8.24	15.26	23.25	27.14
K_0 from ℜ		44.06°	44.14°	44.10°	43.79°	43.98°	44.22°
Mean K_0 from Θ=30°, 35°, 40°, 45°=44.02°							
ℜ (K_0=44.02°)	0.868	1.666	3.858	8.25	15.27	23.27	27.16
Diff. obs. and comp. ℜ	2.3%	0.2%	0.6%	0.4%	−1.0%	−0.2%	0.9%

	Θ=15°	20°	25°	30°	35°	40°	45°
				E=2105 kev			
ℜ from HKPP	0.993	2.098	4.95	10.54	19.98	29.1	35.0
Corrections	.601%	0.601%	0.601%	0.601%	0.601%	0.601%	0.601%
Final ℜ	.999	2.110	4.98	10.60	20.10	29.3	35.2
ℜ (K_0=46°)	.963	2.058	4.926	10.584	19.562	29.75	34.72
ℜ (K_0=47°)	.986	2.142	5.144	11.046	20.403	31.02	36.18
K_0 from ℜ		46.62°	46.25°	46.03°	46.64°	45.64°	46.40°
Mean K_0 from Θ=30°, 35°, 40°, 45°=46.18°							
ℜ (K_0=46.18°)	.967	2.073	4.965	10.637	19.714	29.98	34.98
Diff. obs. and comp. ℜ	3.3%	1.7%	0.3%	−0.6%	2.0%	−2.3%	0.9%

	Θ=15°	20°	25°	30°	35°	40°	45°
				E=2392 kev			
ℜ from HKPP	1.124	2.51	6.17	13.31	24.4	37.4	43.9
Corrections	0.604%	0.604%	0.604%	0.511%	0.511%	0.511%	0.604%
Final ℜ	1.131	2.52	6.21	13.38	24.5	37.6	43.2
ℜ (K_0=47°)	1.055	2.428	5.924	12.76	23.54	35.77	41.71
ℜ (K_0=48°)	1.083	2.524	6.173	13.29	24.51	37.21	43.37
K_0 from ℜ		47.96°	48.15°	48.17°	47.99°	48.27°	47.90°
Mean K_0 from Θ=30°, 35°, 40°, 45°=48.08°							
ℜ (K_0=48.08°)	1.085	2.532	6.193	13.33	24.59	37.33	43.50
Diff. obs. and comp. ℜ	4.2%	−0.47%	0.44%	0.37%	−0.37%	0.73%	−0.69%

corrections at this angle are greater than this amount and the evidence regarding higher phase shifts at these energies is thus unaffected. At 880 kev somewhat larger effects are produced. But even here they are practically negligible giving 0.3 percent at 20°, 0.17 percent at 25°, 0.06 percent at 30°. Inasmuch as one expects the effects of higher phase shifts to increase with energy, these effects at 880 kev have little interest. According to Table VI the values of the "Mean K_0" would increase by ~0.04° at 860 kev, ~0.08° at 1830 kev and ~0.10° at 2400 kev. Such changes will affect the magnitude of the interaction by ~0.01 Mev for a "square well" of depth 10.5 Mev or ~0.1 percent and will shorten the range of force by an amount corresponding to an increase of α in $Ae^{-\alpha r^2}$ by less than 0.2. The fit to the data by a fixed potential cannot be made consistently to this degree of precision and such a small effect in the range is of little interest. The difference between the values obtained by the "current time" and "air condenser" methods is seen to be insignificant and the values obtained by the latter will be disregarded from now on.

In Table XII the data of Heydenburg, Tuve and Hafstad are analyzed. The arrangement is similar to that used in Table XI. The table has three sections for 670, 776 and 867 kev, respectively. The observations of HHT have been made at scattering angles differing by 2.5° from Θ=20° to Θ=45°. The observed values of ℜ have been plotted by HHT on a large scale and smooth curves against scattering angle have been drawn by them. The numbers in the first row for each voltage in Table XII have been obtained from

these curves. These numbers are then increased by 0.43 percent so as to reduce the units to those used in Eq. (3.4). Since the acceleration of gravity is different in Washington from that in Madison the 0.43 percent takes into account this difference also. The value of the mean phase shift in Table XII was computed as the arithmetic mean of the values calculated from $\Theta=30°$, 35°, 40°, 42.5°, 45°. In other respects this table is just like Table XI. The percentage difference of observed and computed $\mathfrak{R}$ will be discussed after a consideration of the geometrical corrections.

Corrections due to geometry of apparatus.—It is seen that in all cases the experimental value of $\mathfrak{R}$ for $\Theta=15°$ is higher than the computed number by two percent or more. If the scattering yield into the infinitesimal angular range is $f(\Theta)d\Theta$ and if the actual spread is $\Delta\Theta$ then

$$\int_{\Theta_0-\Delta\Theta/2}^{\Theta_0+\Delta\Theta/2} f(\Theta)d\Theta/f(\Theta_0)\Delta\Theta \cong 1+(\Delta\Theta)^2 f''(\Theta_0)/24f(\Theta_0)$$

gives the ratio of the yield which should be observed to that which would be expected from the scattering at the average angle Θ_0 through the scattering range $\Delta\Theta$. If $f(\Theta)$ is approximated by const/Θ^5 we may expect the experimental values of $f(\Theta_0)$, omitting the correction for f'', to be too high by the factor

$$1+(5/4)(\Delta\Theta/\Theta)^2.$$

In order to account for the systematic deviations from expectation at $\Theta=15°$ without using higher phase shifts this factor must be 1.033 which calls for $\Delta\Theta=2.4°$. For a defining slit of the analyzing system 1.07 mm wide (slit A, Fig. 3 of paper by Herb, Kerst, Parkinson and Plain) placed 28.2 mm from the hole of the counter each point of the hole receives protons through an angular range of 2.2° which is of the correct order of magnitude to account for the observed effect. Since the average scattering angle is different for different points in the hole the correction may be expected to be larger than the above amount. On the other hand, some of the scattering angles responsible for the protons received have the same values for different points of the diaphragm.

The geometrical corrections have been worked out approximately on the assumption that the velocities of all the protons in the incident beam are parallel to each other and perpendicular to the edge of the slit of the analyzing system. This assumption does not correspond to fact com-

TABLE XII. *Phase shift analysis of data of Heydenburg, Hafstad and Tuve.*

	$\Theta=20°$	25°	30°	35°	40°	42.5°	45°
				$E=670$ kev			
$\mathfrak{R}$ from HHT	0.654	0.600	0.730	0.980	1.330	1.482	1.545
Corrections	.43%	.43%	.43%	.43%	0.43%	0.43%	0.43%
Final $\mathfrak{R}$	.657	.603	.733	.984	1.336	1.488	1.552
$\mathfrak{R}$ (K_0=24°)	.653	.600	.669	.899	1.223	1.347	1.393
$\mathfrak{R}$ (K_0=25°)	.652	.615	.721	1.010	1.406	1.555	1.611
K_0 from $\mathfrak{R}$		24.20°	25.21°	24.77°	24.62°	24.68°	24.73°
Mean K_0 from Θ=30°, 35°, 40°, 42.5°, 45°=24.80°							
$\mathfrak{R}$ (K_0=24.80°)	.652	0.612	0.711	0.988	1.369	1.513	1.567
Diff. obs. and comp. $\mathfrak{R}$	0.8%	−1.5%	+3.1%	−0.4%	−2.4%	−1.7%	−1.0%

	$\Theta=20°$	25°	30°	35°	40°	42.5°	45°
				$E=776$ kev			
$\mathfrak{R}$ from HHT	0.705	0.738	1.078	1.584	2.284	2.580	2.722
Corrections	.43%	.43%	0.43%	0.43%	0.43%	0.43%	0.43%
Final $\mathfrak{R}$	.708	.741	1.083	1.591	2.294	2.591	2.734
$\mathfrak{R}$ (K_0=27°)	.653	.698	0.976	1.550	2.275	2.542	2.641
$\mathfrak{R}$ (K_0=28°)	.657	.727	1.058	1.717	2.540	2.842	2.954
K_0 from $\mathfrak{R}$		28.44°	28.30°	27.25°	27.07°	27.16°	27.30°
Mean K_0 from Θ=30°, 35°, 40°, 42.5°, 45°=27.42°							
$\mathfrak{R}$(K_0=27.42°)	.651	0.710	1.010	1.620	2.386	2.668	2.773
Diff. obs. and comp. $\mathfrak{R}$	8.8%	4.4%	7.2%	−1.8%	−3.8%	−2.9%	−1.4%

	$\Theta=20°$	25°	30°	35°	40°	42.5°	45°
				$E=867$ kev			
$\mathfrak{R}$ from HHT	0.738	0.852	1.360	2.324	3.360	3.808	4.008
Corrections	.43%	.43%	0.43%	0.43%	0.43%	0.43%	0.43%
Final $\mathfrak{R}$	.741	.856	1.366	2.334	3.374	3.824	4.025
$\mathfrak{R}$ (K_0=29°)	.671	.816	1.300	2.209	3.315	3.717	3.866
$\mathfrak{R}$ (K_0=30°)	.680	.857	1.407	2.422	3.650	4.093	4.259
K_0 from $\mathfrak{R}$		29.98°	29.62°	29.59°	29.18°	29.40°	29.40°
Mean K_0 from Θ=30°, 35°, 40°, 42.5°, 45°=29.41°							
$\mathfrak{R}$ (K_0=29.41°)	.675	0.833	1.344	2.296	3.452	3.871	4.027
Diff. obs. and comp. $\mathfrak{R}$	9.8%	2.8%	1.6%	1.7%	−2.3%	−1.2%	0.05%

pletely but the divergence of the beam is difficult to estimate. The corrections for a very narrow proton beam will be considered first and the effect of the width of the beam will be taken into account later. In Fig. 1 the hole in front of the ionization chamber (hole c of paper by Herb *et al.*) is in the plane OXY. The plane OXZ is perpendicular to the slit face and goes midway between the slit edges. The Y axis is made parallel to the slit edges and the Z axis is made to intersect the beam. The element dS receives from the element dB

$$Nn\sigma(\Theta)R^{-2}\cos\chi dSdB = Nn\sigma(\Theta)\cos\chi dSd\Theta/R\sin\Theta \quad (7)$$

protons, where N is the number of protons that passed in the beam, n is the number of protons per unit volume in the scattering gas, $\sigma(\Theta)$ is the scattering cross section per unit solid angle, R is the distance between dS and dB and χ is the angle between the normal to dS and R. The $d\Theta$ is the change in Θ for fixed dS which corresponds to the change dB. The scattering angle for the point $P(B=0)$ is called Θ_0 and the distance $PO=R_0$. The slit width will be called $2b$. In the figure scattered protons pass just under the upper slit edge. One has

$$\begin{aligned}\cos\chi &= (R_0-B\cos\Theta_0)/R,\\ R^2 &= (R_0-B\cos\Theta_0)^2+y^2+(x-B\sin\Theta_0)^2,\\ R^2\sin^2\Theta &= (R_0\sin\Theta_0-x\cos\Theta_0)^2+y^2, \quad (7.1)\\ B &= R_0\cos\Theta_0+x\sin\Theta_0-(\cos\Theta/\sin\Theta)[(R_0\sin\Theta_0-x\cos\Theta_0)^2+y^2]^{\frac{1}{2}},\end{aligned}$$

where (x, y) are the coordinates of dS. The limits of integration for B are given by

$$\frac{x-B\sin\Theta_0}{R_0-B\cos\Theta_0}=\frac{x\mp b}{\mathfrak{h}}.$$

Letting

$$\xi=\Theta-\Theta_0, \quad \mathfrak{c}_0=\cos\Theta_0, \quad \mathfrak{s}_0=\sin\Theta_0$$

one finds the approximate expansions valid to second-order quantities in x, y, ξ

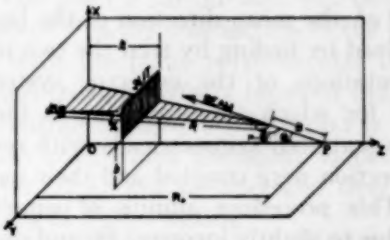

FIG. 1. Geometrical relations for the analyzing system. The slit is slit A of Fig. 3 of paper of HKPP. Element of area dS is in the plane of the round hole in front of ionization chamber. The direction of scattered protons is shown for special case of just missing the slit edge. Angle χ is formed by normal to dS and distance R.

$$B=\frac{x}{\mathfrak{s}_0}-\frac{y^2\mathfrak{c}_0}{2R_0\mathfrak{s}_0}+\xi\left(\frac{R_0}{\mathfrak{s}_0}-\frac{x\mathfrak{c}_0}{\mathfrak{s}_0^2}\right)-\xi^2\frac{R_0\mathfrak{c}_0}{\mathfrak{s}_0^2},$$

$$\frac{R_0-B\cos\Theta_0}{R^2\sin\Theta}=\frac{1}{R_0\mathfrak{s}_0}\left(1+\frac{x\mathfrak{c}_0}{R_0\mathfrak{s}_0}+\frac{x^2\mathfrak{c}_0^2}{R_0^2\mathfrak{s}_0^2}+\frac{\mathfrak{c}_0^2-2}{2R_0^2\mathfrak{s}_0^2}y^2-\frac{\xi^2}{2}\right),$$

and for the limits of ξ corresponding to the slit edges

$$\xi=\frac{-x\pm b}{\mathfrak{h}}+\frac{\mathfrak{c}_0y^2}{2R_0^2\mathfrak{s}_0}.$$

In these expansions, powers of ξ, x, y higher than the second are neglected. Expanding σ in powers of ξ and integrating over dS one obtains for the number of protons received

$$\begin{aligned}\frac{Nn}{R_0\mathfrak{s}}A\sigma(\Theta_0)\frac{2b}{\mathfrak{h}}\Bigg\{&1+\frac{\mathfrak{c}_0x_{Av}}{\mathfrak{s}_0R_0}+\frac{\mathfrak{c}_0^2(x^2)_{Av}}{\mathfrak{s}_0^2R_0^2}+\frac{\mathfrak{c}_0^2-2}{2R_0^2\mathfrak{s}_0^2}(y^2)_{Av}-\frac{b^2}{6\mathfrak{h}^2}+\frac{(x^2)_{Av}}{2\mathfrak{h}^2}\\&+\frac{\sigma'(\Theta_0)}{\sigma(\Theta_0)}\left[-\frac{x_{Av}}{\mathfrak{h}}+\frac{\mathfrak{c}_0(y^2)_{Av}}{2\mathfrak{s}_0R_0^2}-\frac{\mathfrak{c}_0(x^2)_{Av}}{\mathfrak{s}_0R_0\mathfrak{h}}\right]\\&+\frac{\sigma''(\Theta_0)}{\sigma(\Theta_0)}\left(\frac{b^2}{6\mathfrak{h}^2}+\frac{(x^2)_{Av}}{2\mathfrak{h}^2}\right)\Bigg\}. \quad (7.2)\end{aligned}$$

For a circular hole of radius a, $(x^2)_{Av}=(y^2)_{Av}=a^2/4$. The terms in x_{Av} can be eliminated by setting the counting system in symmetric positions with respect to the incident beam and using the mean of the counts so obtained. In the experiments of

Herb *et al.* the mean direction of the beam was determined by finding by trial the two positions or orientations of the collector system with $\Theta=15°$ for which the scattering is the same. Protons scattered symmetrically with respect to this direction were counted and their mean was used. This procedure admits of simultaneous errors due to slightly incorrect Θ_0 and due to the presence of x_{hw}. Since counts to both sides of the beam have been used the first-order effects of these errors disappear. If we write

$$\sigma(\Theta_0)\{1+\cdots\}=\sigma(\Theta_0)+f(\Theta_0)x_{hw}+g(\Theta_0)$$

the error ϵ in the determination of the beam direction for 15° scattering is found from

$$\sigma(\Theta_0+\epsilon)+f(\Theta_0+\epsilon)x_{hw}=\sigma(\Theta_0-\epsilon)-f(\Theta_0-\epsilon)x_{hw}.$$

Denoting the argument Θ_0 by subscript zero this gives sufficiently accurately

$$\epsilon=-x_{hw}f_0/\sigma_0',$$

where differentiation is denoted by the prime. For low Θ_0 Rutherford's formula can be used and one has approximately

$$\epsilon=(x_{hw}/\mathfrak{h})(1+\mathfrak{h}/4R_0),$$

so that with the dimensions of the apparatus used by Herb *et al.*, $\epsilon\leqq-0.23°$ for $x_{hw}=0.1$ mm. The mean of the counts for settings $\Theta_1\pm\epsilon$ is to within second-order quantities

$$\sigma_1+g_1+\tfrac{1}{2}\sigma_1''\epsilon^2+x_{hw}f_1\epsilon.$$

The fractional error introduced by x_{hw} and ϵ is thus

$$\delta=\frac{f_0^2}{\sigma_0'^2}x_{hw}^2\left[\frac{\sigma_1''}{2\sigma_1}-\frac{\sigma_0'f_1'}{\sigma_1f_0}\right]$$

with

$$f=\sigma\mathbf{c}/R_0\mathbf{s}-\sigma'/\mathfrak{h}.$$

Substituting this into the expression for δ one obtains

$$\delta=\frac{x_{hw}^2}{\mathfrak{h}^2}\left(\frac{\sigma_0\mathbf{c}_0\mathfrak{h}}{\sigma_0'\mathbf{s}_0R_0}-1\right)^2\left\{\frac{\sigma_1''}{2\sigma_1}-\left[\frac{\mathfrak{h}}{R_0}\left(\frac{\sigma_1'\mathbf{c}_1}{\sigma_1\mathbf{s}_1}-\frac{1}{\mathbf{s}_1^2}\right)-\frac{\sigma_1''}{\sigma_1}\right]\Big/\left(\frac{\sigma_0\mathbf{c}_0\mathfrak{h}}{\sigma_0'\mathbf{s}_0R_0}-1\right)\right\}. \quad (7.3)$$

The value used in the experiments is $\Theta_0=15°$. On account of the smallness of this angle the approximations $\sigma_0'/\sigma_0=-4/\Theta_0$, $\mathbf{c}_0/\mathbf{s}_0=1/\Theta_0$ are good enough. One then has

$$1-\sigma_0\mathbf{c}_0\mathfrak{h}/\sigma_0'\mathbf{s}_0R_0=1+\mathfrak{h}/4R_0.$$

If, in addition, the angle Θ_1 is also sufficiently small to make the scattering approximately Rutherfordian and to have $\mathbf{c}_1/\mathbf{s}_1=1/\Theta_1$, then one has

$$\delta=-10(x_{hw})^2\mathfrak{h}^{-2}(1+\mathfrak{h}/4R_0)^2\Theta_1^{-2}. \quad (7.4)$$

For $\Theta_1=15°$, $x_{hw}=1$ mm, $\mathfrak{h}=28.2$ mm this formula gives $\delta=-0.23$ percent. If x_{hw} is ~0.1 mm the experimental values must be raised, therefore, by about 0.2 percent and by about 0.1 percent at $\Theta_1=20°$ at the lower energies for which scattering at this angle is still roughly following Rutherford's formula. For angles close to 45° the scattering is approximately spherically symmetric and is very nearly so at higher energies. In this region the cross section can be approximated by

$$\sigma=K\mathbf{c},$$

where K is independent of the angle. With this approximation the general formula for δ gives for the large scattering angles

$$\delta=\frac{(x_{hw})^2}{\mathfrak{h}^2}\left(1+\frac{\mathfrak{h}}{4R_0}\right)^2\times\left\{-\frac{1}{2}+\left[1-\frac{\mathfrak{h}}{R_0}\left(1+\frac{1}{\mathbf{s}_1^2}\right)\right]\Big/\left(1+\frac{\mathfrak{h}}{4R_0}\right)\right\}. \quad (7.5)$$

For $\Theta_1=45°$, $x_{hw}=0.1$ mm one obtains on substitution the quite negligible error $-0.001(5)$ percent. This estimate is not very accurate because the approximation $\sigma=K\mathbf{c}$ is not very good for the calculation of σ''/σ. Graphs of σ as a function of Θ indicate that it is correct as to order of magnitude. Checks on the mechanical construction made by Herb *et al.* after the scattering measurements showed that $x_{hw}\sim0.01$ mm which decreases this error by 1/100.

Most of the quadratic terms in Eq. (7.2) have negligible values for the experimental arrangement. With $R_0=56$ mm, $\mathfrak{h}=28.2$ mm, $a=0.365$ mm, $b=0.536$ mm $\Theta_0=15°$ the values of the terms are in order of occurrence in Eq. (7.2)

$$\mathbf{c}_0^2a^2/4\mathbf{s}_0^2R_0^2=0.000148=0.015 \text{ percent};$$

$$a^2(\mathbf{c}_0^2-2)/8R_0^2\mathbf{s}_0^2=-0.008 \text{ percent};$$

$$-b^2/6\hbar^2=-0.006 \text{ percent};$$

$$-a^2/8\hbar^2=-0.002 \text{ percent}.$$

Approximating σ_0'/σ_0 by $-4/\Theta_0$ and σ_0''/σ_0 by $20/\Theta_0^2$ one has also

$$\frac{\sigma_0'\mathbf{c}_0}{\sigma_0\mathbf{s}_0}\left(\frac{a^2}{8R_0^2}-\frac{a^2}{4R_0\hbar}\right)=0.090 \text{ percent};$$

$$\frac{\sigma_0''}{\sigma_0}\left(\frac{b^2}{6\hbar^2}+\frac{a^2}{8\hbar^2}\right)=2.35 \text{ percent}.$$

The last correction is the largest. It represents the effect of the curvature of the plot of σ against Θ which was discussed qualitatively by means of the approximate formula

$$1+(5/4)(\Delta\Theta/\Theta)^2.$$

The sum of the above corrections is 2.4 percent. The observed scattering may be expected to be too high by this amount for the geometry used at $\Theta=15°$ if the incident proton beam is very narrow and if the correction δ due to a possible dissymmetry of the counter hole and counter slit is negligible. For small scattering angles at low energies this error is approximately proportional to the inverse square of the scattering angle. For high energies the scattering differs markedly from Rutherford's even at $\Theta=20°$ and the correction term $(\sigma_0''/\sigma_0)(b^2/6\hbar^2+a^2/8\hbar^2)$ is then much smaller than at $\Theta=15°$. If σ is plotted against Θ for $K_0=47.95°$ at 2392 kev, $K_0=43.92°$ at 1830 kev, $K_0=29.25°$ at 860 kev and σ''/σ is estimated graphically at $\Theta=20°$ the correction term $(\sigma_0''/\sigma_0)(b^2/6\hbar^2+a^2/8\hbar^2)$ is estimated to be at this angle 0.2 percent at 2392 kev, 0.6 percent at 1830 kev, 1.4 percent at 860 kev.

On account of the finite width of the beam there are additional corrections which will now be estimated. Fixed coordinates X, Y will be used in the plane of the hole with origin at the foot of the perpendicular from the center of the beam as shown in Fig. 2. The filaments in the beam will be specified by coordinates α, β with β parallel to Y and α in the direction shown in the figure. The distance from the hole to the center of the beam will be called $\bar{r}$. The distance from the point P to the hole will be called R_0. The point P is the intersection of the beam filament with the plane perpendicular to the slit face and passing midway between the slit jaws. The central filament of the beam is AB. The filament over which averaging is performed is PQ. Eq. (7.2) will be averaged over different positions of PQ by letting

$$x=X, \quad y=Y-\beta, \quad R_0=\bar{r}+\alpha/\sin\Theta_0.$$

The averaging will be carried out on the assumption that the center of the beam is in line with the center of the hole. The effect of lack of such alignment is partially taken care of in the discussion of δ. The cross section of the beam will be supposed to be circular of radius $\dot{\rho}$ and the proton density will be supposed to be uniform within this cross section. One has

$$(1/R_0)_{Av}=1/\bar{r}+(\alpha^2)_{Av}/(\bar{r}^3\sin^2\Theta_0)$$

$$=1/\bar{r}+\dot{\rho}^2/(4\bar{r}^3\sin^2\Theta_0).$$

This introduces the fractional error

$$\dot{\rho}^2/(4\bar{r}^2\sin^2\Theta_0).$$

For $\dot{\rho}=1.25$ mm, $\bar{r}=56$ mm at $\Theta_0=15°$ it is $0.00184=0.18$ percent but for $\dot{\rho}=2.50$ mm it is 0.72 percent. In addition corrections arise from an increase in the averaged $(y^2)_{Av}$. One has

$$(y^2)_{Av}=(Y^2)_{Av}+(\beta^2)_{Av}=(a^2+\dot{\rho}^2)/4.$$

On account of the extra term in $\dot{\rho}^2/4$ there is the additional fractional error

$$\frac{\mathbf{c}_0^2-2}{8r^2\mathbf{s}_0^2}\dot{\rho}^2+\frac{\sigma_0'\mathbf{c}_0\dot{\rho}^2}{8\sigma_0\mathbf{s}_0\bar{r}^2}.$$

With the above values of $\dot{\rho}$, $\bar{r}$, Θ_0 the first term is -0.10 percent for $\dot{\rho}=1.25$ mm, -0.40 percent for $\dot{\rho}=2.50$ mm; the second term using the approximation $\sigma_0'/\sigma_0=-4/\Theta_0$ is -0.4 percent for $\dot{\rho}=1.25$ mm and -1.4 percent for $\dot{\rho}=2.50$ mm. For the larger of these beam widths the total error at $\Theta_0=15°$ due to beam width is -0.90 percent and for the smaller beam width it is -0.28 percent. Since the beam width is not accurately known it is impossible to set close limits on this error.

The major part of the negative error caused by beam width is due to the term in σ_0'/σ_0. It is

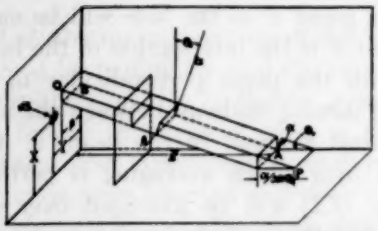

FIG. 2. Geometrical relations used for estimating effect of width of incident beam. Coordinate system α, β is used for designating different filaments of the beam. Coordinate system X, Y describes position of dS.

a result of the increase in the average scattering angle caused by the lateral extension of the proton stream. For high energies σ_0'/σ_0 at $\Theta_0=20°$ is much less than it would be on Rutherford's formula and this part of the error is correspondingly smaller. The value of σ_0'/σ_0 was estimated graphically. One obtains in this way the values given in Table XIII.

The numbers in the column under "sum" should be compared with values of $(\sigma_0''/\sigma_0) \times(b^2/6\mathfrak{h}^2+a^2/8\mathfrak{h}^2)$ which are 0.2 percent at 2392 kev, 0.6 percent at 1830 kev, 1.4 percent at 860 kev for $\Theta=20°$ and 2.3 percent for $\Theta=15°$. The net expected error due to the above causes may be thus expected to be between one percent and two percent for $\Theta=15°$.

The divergence of the incident proton beam also introduces an error the order of magnitude of which will now be estimated. The finiteness of the angular opening of the analyzing system will be neglected and the beam will be supposed to be very narrow. The angle made by the direction of protons which are being counted with the mean direction before scattering will be called Θ_0. The angle between the mean direction of the beam and the line of motion of the proton before scattering will be called θ. One finds discarding effects of higher order than the second in θ for an axially symmetric beam that

$$(\sigma/\mathbf{s})_{Av}=(\sigma_0/\mathbf{s}_0)+((\theta^2)_{Av}/4) \times[(\mathbf{c}_0/\mathbf{s}_0)(\sigma/\mathbf{s})_0'+(\sigma/\mathbf{s})''].$$

If the foil in front of the first hole of the collimating system acts as a source of protons then the chance of protons leaving an element of area in the foil and passing through an element of area of the last hole of the collimating system is nearly proportional to the product of these elements of area. Introducing rectangular coordinates $(x_1, y_1)(x_2, y_2)$ in the foil and in the last hole with origins on the axis of symmetry one has

$$\theta^2=[(x_1-x_2)^2+(y_1-y_2)^2]/L^2,$$

where L is the distance between the foil and the last hole. By averaging this expression over the two circles it is seen that

$$(\theta^2)_{Av}=(\theta_1^2+\theta_2^2)/2,$$

where

$$\theta_1=a_1/L, \quad \theta_2=a_2/L$$

with a_1, a_2 standing for the radii of first and last hole of the collimating system. The angle θ_1 is subtended by the radius of one hole at a point in the other hole. For small scattering angles one obtains thus approximating σ by const./Θ^4

$$(\sigma/\mathbf{s})_{Av}/(\sigma/\mathbf{s})_0=1+25(\theta_1^2+\theta_2^2)/8\Theta^2.$$

TABLE XIII. *Errors due to beam width.*

b	Θ_0	$\frac{b^2}{4r^2\mathbf{s}_0^2}$	$\frac{\mathbf{c}_0^2-2}{8r^2\mathbf{s}_0^2}b^2$	$\frac{\sigma_0'\mathbf{c}_0b^2}{8\sigma_0\mathbf{s}_0r^2}$	SUM	E (KEV)
1.25 mm	15°	0.18%	−0.10%	−0.36%	−0.28%	2392 1830 860
2.50 mm	15°	.72%	− .40%	−1.42%	−1.1%	2392 1830 860
1.25 mm	20°	.11%	− .06%	−0.02% − .05% − .17%	0.03% .00% − .12%	2392 1830 860
2.50 mm	20°	.42%	− .24%	− .09% − .20% − .69%	.09% − .02% − .51%	2392 1830 860

With $a_1=1.08$ mm, $a_2=1.40$ mm, $L=15$ cm, the measurements should be too high, because of the divergence of the beam, according to the above formula by 0.6(3) percent at $\Theta=15°$. It may be, however, that the original direction of the beam is partly preserved. If so, the above estimate is an upper limit to the error.

It should finally be mentioned that deviations of the incident beam from the plane of the scattering chamber may increase the scattering angle and decrease the yield. Professor Herb has estimated the magnitude of this error and finds it to be negligible.

It is a pleasure to acknowledge our indebtedness to Professor Herb for discussions concerning the construction and operation of the apparatus which have helped in the work of this section. Dr. S. S. Share has kindly checked the geometrical relations and other formulas.

Possible presence of p and d wave anomalies. Upper limits for their effect on K_0.—The geometrical corrections just discussed appear to be sufficiently large to account for the consistently too high values at $\Theta=15°$. For $K_1=-0.04=-2.29°$ one expects the following contributions to $\mathfrak{R}$ listed in Table XIV. The largest effects in $\mathfrak{R}$ are seen to be for $\Theta=30°$. It appears fair to claim that at 2392 kev the observations indicate a scattering agreeing within two percent with prediction in the vicinity of $\Theta=25°$ when only an s wave anomaly is used. This sets a provisional upper limit of $(0.123/1.03)2.29°=0.27°$ on $|K_1|$ at 2400 kev. At 1830 kev an upper limit of two percent in scattering at $\Theta=25°$ gives $(0.0772/0.87)2.29°=0.20°$ as the upper limit of $|K_1|$. At 860 kev it appears safer to claim three percent which gives $(0.0243/0.55)2.29°=0.10°$ for the upper limit. The data of HHT shown in Table XII indicate the possible presence of an excess of actual scattering from $\Theta=20°$ to $\Theta=30°$ over that expected for a pure s anomaly. The order of magnitude of the excess in $\mathfrak{R}$ at this angle at 800 kev is from Table XII, 0.050 which corresponds roughly to $K_1=-0.2°$. It appears to be premature, however, to conclude that this is a real effect because at $\Theta=40°$ the experimental values are below the values expected using only K_0. Since no such effect is apparent in the data of HKPP and since its theoretical explanation would require a somewhat complicated superposition of effects due to p and d waves it appears simplest at present to reserve judgment as to its origin. It is planned to analyze the data of HHT using observed counts rather than graphically interpolated values and to eliminate in this way personal judgment present in the above analysis. The geometrical effects are more difficult to estimate in the apparatus of HHT since settings at $\pm\Theta$ were not taken for each point so that first-order effects in x_M could remain. It should be noted that it is not easy to distinguish with the present experimental accuracy the effects of K_1 from those of K_2 and that the effects of K_2 can be very important for the final conclusions about the range of force if K_2 is large enough. In Table XV is shown the effect of K_2 at 2400 kev. In the first row (I) are listed the values of the change in the ratio to Mott $(\Delta\mathfrak{R})_2=(\Delta\mathbf{P})_2/\mathbf{P}_M$ due to $K_2=1°$ for $K_0=48°$. In the second row (II) are listed the values of $1+(\Delta\mathbf{P})_0/(\Delta\mathbf{P}_M)=\mathfrak{R}_0$ which would be the ratios to Mott if this K_2 were absent. The sum of the numbers in rows I and II is the expected ratio to Mott for $K_0=48°$, $K_2=1°$. The third row contains values of the ratio to Mott for $K_0=45.349°$, $K_2=0$. This value of K_0 was taken so as to give a value of $\mathfrak{R}$ for $\Theta=45°$ equal to that for $K_0=48°$, $K_2=1°$. The angular distribution of $\mathfrak{R}$ expected for $K_0=45.349°$ differs relatively little from that for $K_0=48°$, $K_2=1°$. The difference between the values of $\mathfrak{R}$ that would hold for $K_0=48°$, $K_2=1°$ and those for $K_0=45.349°$, $K_2=0$ is recorded in the last row of the table. Comparison of these numbers with those in the second row of Table XIV shows that deviations from the angular distribution expected for s scattering are rather similar for small K_1 and K_2. Allowing for a deviation of two percent from scattering expected for a pure s anomaly for $\Theta=25°$ at 2400 kev one would set an upper limit on $|K_2|$ of $(0.123/0.81)°=0.15°$ which according to line I of Table XV would

TABLE XIV. *Contributions to $\mathfrak{R}=\mathbf{P}/\mathbf{P}_M$ due to phase shift $K_1=-2.29°$.*

E (KEV)	$\Theta=15°$	20°	25°	30°	35°	40°	45°
2400	0.45	0.77	1.03	1.10	0.82	0.30	0
1830	0.39	0.65	0.87	0.92	0.69	0.25	0
800	0.25	0.41	0.53	0.55	0.41	0.15	0

limit the error in $1+(\Delta\mathfrak{R})_0$ at $\Theta=45°$ to $\pm0.6(7)$ or ±1.5 percent in scattering. According to Table VI the value of K_0 would be in error by $\pm0.4°$. Such an error would not affect seriously conclusions about the comparison of the proton-proton and proton-neutron interaction that are made below and it would only affect slightly conclusions about the range of force if this K_2 were present at 2400 kev but not at 860 kev. One expects K_2 to vary at least as fast as $E^{5/2}$. At 1000 kev the upper limit for $|K_2|$ is thus presumably $0.15°/(2.4)^{5/2}=0.017°$. At this energy $K_2=1°$ produces an effect of $-1.2(K_0=32°, K_2=1°)$ on the ratio to Mott at $\Theta=45°$ so that the expected error is $\sim\pm0.022$ in $\mathfrak{R}$ which $\sim\pm0.2$ percent in the scattering and causes a negligible error in this energy range.

In the above discussion Table XV was used. The effect of a finite change in $K_2(=1°)$ was computed for it. The changes in K_2 which have been considered for the discussion of experimental data are much smaller than 1°. The linear interpolation used may, therefore, be questioned. A calculation of

$$\left[\frac{\partial\mathfrak{R}}{\partial K_2}-\left(\frac{\partial\mathfrak{R}/\partial K_2}{\partial\mathfrak{R}/\partial K_0}\right)_{\Theta=45°}\frac{\partial\mathfrak{R}}{\partial K_0}\right]\delta K_2$$

shows that the last row of the table can be used for linear interpolation to obtain the effect of a very small K_2 to within a few percent. The last number (-4.41) in the first row is then taken place of by $(\partial\mathfrak{R}_0/\partial K_2)_{45°}/57.3=-4.53$ and is sufficiently accurate. At small scattering angles the above formula gives values about ten percent higher than the numbers in the first row. These, however, are not needed in the above discussion since the determination of K_0 relies on the scattering angles from 30° to 45°. Theoretical estimates of K_2 from the Gauss or exponential type of potential indicate that it is of the order of 0.01° at 2400 kev, i.e., roughly 0.1 of the value used above. If such estimates apply when constant potentials are used one may expect the effect on K_0 to be $\sim0.03°$ which is negligible in the applications made below.

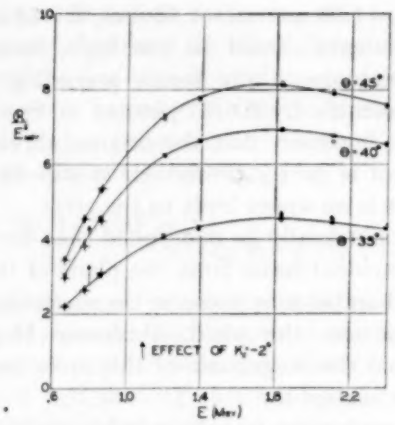

FIG. 3. Observed and computed scattering on assumption of pure s scattering anomaly for $\Theta=45°$, 40°, 35°. Ordinates give ratio to Mott divided by the square of the energy. Abscissae give the energy. Observations of HKPP are represented by circles; those of HHT by large upright crosses. The diagonal circles give values computed using the mean K_0 of Tables XI and XII. The effect of $K_2=-2°$ is roughly indicated by the length of the arrows.

In Figs. 3, 4 and 5 the agreement between expectation from a pure s scattering anomaly and observations can be seen in a different way. The curves are drawn for $\mathfrak{R}/E_{\text{Mev}}^2$ as ordinate and E_{Mev} as abscissae. The ordinate varies in nearly the same way with energy as the observed scattering. The curves are drawn through the diagonal crosses for which values of $\mathfrak{R}$ have been computed with the "mean K_0" derived from experiment and tabulated in the last column of Tables XI, XII. The circles represent the experimental points of Herb *et al.* and the upright large crosses are the experimental points of Tuve *et al.* There is a surprising absence of systematic deviations of the experimental points from the curves as one goes to higher energies indicating the probable correctness of the interpretation using a pure s scattering anomaly. In Fig. 3 the effect of $K_2=-2°$ is roughly indicated by the

TABLE XV. *Effect of K_2 at 2400 kev.*

K_0	K_2	$\Theta=15°$	20°	25°	30°	35°	40°	45°	
48°	1°	$(\Delta\mathfrak{R})_2=0.054$	0.165	0.148	−0.34	−1.63	−3.45	−4.41	I
48°	0	$\mathfrak{R}_0=1.085$	2.534	6.20	13.34	24.59	37.35	43.52	II
45.349°	0	$\mathfrak{R}_0=1.014$	2.279	5.54	11.94	22.06	33.56	39.11	III
		0.12	0.42	0.81	1.06	0.9	0.34	0.00	I+II−III

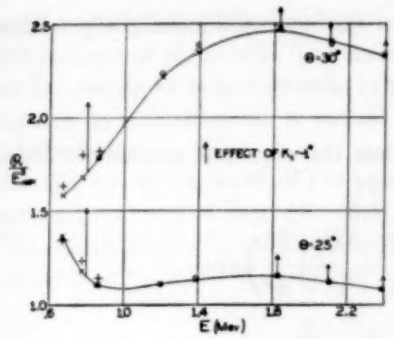

FIG. 4. Observed and computed scattering on assumption of pure s scattering anomaly for $\Theta=30°$, 25°. Notation is the same as in Fig. 3. The effect of $K_1=-1°$ is roughly indicated by the length of the arrows.

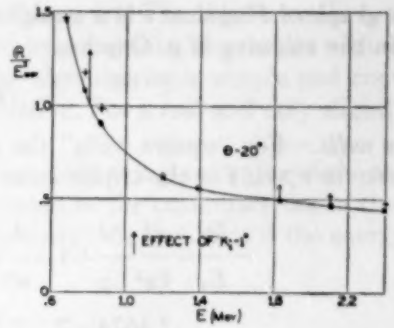

FIG. 5. Observed and computed scattering on assumption of pure s scattering anomaly for $\Theta=20°$. Notation is the same as in Fig. 3. The effect of $K_1=-1°$ is roughly indicated by the length of the arrows.

length of the arrow and in Figs. 4 and 5 the same is done for one-half of the effect of $K_1=-2°$ which is roughly the effect of $K_1=-1°$. The agreement between the two groups of experimenters is seen to be very good for the scattering angles 45°, 40°, 35° but at 30°, 25°, 20° the observations made in Washington give higher values than those in Madison. The practice of averaging observations made at $+\Theta$ and $-\Theta$ which was followed by Herb *et al.* is an argument for assigning more weight to their measurements at the smaller angles. This leads to the cancellation of first-order errors as has been discussed under "geometrical corrections." The origin of the discrepancy is not known, however, and it would be desirable to have further observations on this point. The apparent absence of K_1 at the higher energies will be discussed again in the "Concluding Remarks."

III. Calculation of the Potentials

1. The proton-neutron interaction

The scattering cross section of slow neutrons by protons determines the interaction potential for the antiparallel spin orientation (^1S state) when account is taken of the scattering in the ^3S condition. The experimental material is complicated by the effect of chemical binding of the protons to other atoms in hydrogen containing substances. The Fermi correction[16] for this binding has been discussed by several authors and will not be gone into critically here. Even though its complete quantitative justification is doubtful, there is some experimental evidence for its approximate validity through measurements of the scattering cross section for neutrons having several volts energy. Thus Carroll and Dunning[17] obtain 6.59×10^{-24} cm² as the lower limit for the collision cross section of neutrons having zero energy while unpublished measurements of V. W. Cohen and H. H. Goldsmith[17] indicate that the collision cross section for the Rh band neutrons is 20×10^{-24} cm² which would change Carroll and Dunning's figure to 80×10^{-24} cm² if Fermi's factor four were applicable. The difference between 65.9 and 80×10^{-24} cm² is not of primary importance for the determination of the ^1S interaction and allowance will be made for such variations in the experimental results.

The scattering cross section of a zero energy neutron having a statistical spin orientation with a free proton will be called σ_{np}. One has

$$4\sigma_{np}=12\pi a_3^2+4\pi a_1^2. \tag{8}$$

Here the quantity a is the intercept on the axis of r of the tangent to the graph of F against r, where r is the distance between proton and neutron. The tangent is taken at a sufficiently large distance to make the interaction negligible. The radial function is F/r and the a's will be positive if the tangent cuts the axis to the left of the origin. The values of a for triplet and singlet states, respectively, are $a_3<0$, $a_1>0$. For

[16] E. Fermi, Ricerca Scient. **7**, II, 13 (1936); H. A. Bethe, Rev. Mod. Phys. **9**, 71 (1937); N. Arley, Proc. Danish Academy **16**, 1 (1938). We are indebted to Prof. Wigner for discussions concerning these questions.

[17] H. Carroll and J. R. Dunning, Phys. Rev. **54**, 541 (1938); V. W. Cohen and H. H. Goldsmith, Phys. Rev. **55**, 597(A) (1939).

$r>r_0$ the graph of F against r is a straight line so that r can be increased indefinitely without ambiguity in the meaning of a. One has

$$(Fdr/dF)_{r_0}=a+r_0. \tag{8.1}$$

Square wells.—For "square wells" the potential energy has the constant amount $-D$ for $r<r_0$ and is zero for $r>r_0$. For the triplet state one obtains

$$\begin{aligned}-\frac{D_3}{E_3}&=\frac{\pi^2}{4\chi^2}+\frac{2}{\chi}+1-\frac{4}{\pi^2}+\left(\frac{32}{\pi^4}-\frac{8}{3\pi^2}\right)\chi+\left(-\frac{320}{\pi^6}+\frac{32}{\pi^4}\right)\chi^2+\cdots\\&=\frac{2.4674}{\chi^2}+\frac{2}{\chi}+0.59472+0.05832\chi-0.00434\chi^2+\cdots,\end{aligned} \tag{8.2}$$

where

$$\chi=(-ME_3/\hbar^2)^{\frac{1}{2}}r_0, \tag{8.3}$$

which gives with the fundamental constants chosen

$$\chi=0.3126(r_0mc^2/e^2)(-E_3/mc^2)^{\frac{1}{2}}=0.4370(r_0mc^2/e^2)(-E_3/\text{Mev})^{\frac{1}{2}}.$$

The energy of the deuteron is denoted by $E_3(=-2.17$ Mev). For this value $\chi=0.643_8\, r_0mc^2/e^2$. The series of Eq. (8.2) is sufficiently accurate for the calculation of D_3 with known E_3 and assumed r_0 for values of $r_0\sim 2.8\times10^{-13}$ cm. The intercept a_3 can be expressed as

$$a_3=-r_0[1+(\chi+c_2\chi^2+c_3\chi^3+\cdots)^{-1}]$$

with

$$c_2=\tfrac{1}{2},\quad c_3=\frac{2}{\pi^2}=0.20264,\quad c_4=-\frac{16}{\pi^4}+\frac{5}{2\pi^2}=0.08905;\quad c_5=0.0419.$$

This formula is good to about 0.2 percent for $r_0\sim e^2/mc^2$. One obtains

$$\begin{aligned}12\pi a_3^2&=12\pi(-\hbar^2/ME_3)[1+\chi+(3/4-2c_3)\chi^2+(c_3-2c_4)\chi^3+\cdots]\\&=3.058\times10^{-23}(-mc^2/E_3)[1+\chi+0.34472\chi^2+0.02454\chi^3-0.0117\chi^4+\cdots]\ \text{cm}^2.\end{aligned} \tag{8.4}$$

The first two terms in the brackets have been given by Wigner.[18] For $r_0=e^2/mc^2$ the last two terms give nine percent of the first two. The terms omitted in the above formula for $12\pi a_3^2$ decrease its value by about 0.1 percent for $r_0\sim e^2/mc^2$ as is found from exact solutions.

For the singlet state one has to determine the depth D_1 from a knowledge of a_1 which results from the experimental σ_s, and the computed $12\pi a_3^2$. With

$$\chi_1=r_0/(a_1+r_0) \tag{8.5}$$

one finds

$$z_1^2=\frac{M}{\hbar^2}D_1r_0^2=\frac{\pi^2}{4}-2\chi_1-\frac{4}{\pi^2}\chi_1^2+\left(\frac{8}{3\pi^2}-\frac{32}{\pi^4}\right)\chi_1^3+\left(-\frac{320}{\pi^6}+\frac{32}{\pi^4}\right)\chi_1^6+\cdots, \tag{8.6}$$

which becomes with the adopted choice of fundamental units

$$\begin{aligned}D_1&=5.233z_1^2(e^2/r_0mc^2)^2\ \text{Mev}\\&=5.233(2.4674-2\chi_1-0.40528\chi_1^2-0.05832\chi_1^3-0.00434\chi_1^4-\cdots)(e^2/r_0mc^2)^2\ \text{Mev}.\end{aligned} \tag{8.6'}$$

[18] E. Wigner, Zeits. f. Physik **83**, 253 (1933).

This series converges rapidly, the approximate value of χ_1 being 0.1. The third term in brackets is about 0.2 percent of the whole. The series has been checked by comparing the results with solutions obtained by means of trigonometric tables. The use of the above series is simple and convenient. The quantity χ_1 is positive for a virtual level since a_1 is positive. For a real and only slightly stable level χ_1 is negative.

The calculation of the depth of the square well which corresponds to a given value of the scattering cross section by means of Eqs. (8), (8.5), (8.6) is closely related to the customary use of the virtual level. The energy of the latter may be defined as a positive energy E_1 such that if the energy of the singlet state is $-E_1$ and if F is regular at $r=0$ then

$$dF/Fdr=(ME_1/\hbar^2)^{\frac{1}{2}};\quad (E=-E_1). \tag{8.7}$$

At zero energy (thermal neutrons) one has then approximately

$$dF/Fdr=(ME_1/\hbar^2)^{\frac{1}{2}}-Mr_0E_1/(2\hbar^2)=1/(a_1+r_0)$$

since $\partial/\partial E(\partial F/F\partial r)\sim -Mr_0/2\hbar^2$ when the phase at $r_0\sim\pi/2$. Hence

$$a_1\cong\hbar(ME_1)^{-\frac{1}{2}}-r_0/2$$

and

$$4\pi a_1^2=4\pi(\hbar^2/ME_1)[1-(ME_1/\hbar^2)^{\frac{1}{2}}r_0],$$

which is the customary formula for the scattering cross section in terms of E_1. It should be noted that in order to obtain this form it was necessary to assume that Eq. (8.7) holds at $E=-E_1$ and not at the energy of the virtual level.

The quantity χ_1 is related to E_1 in the present approximation by

$$\chi_1=r_0/(a_1+r_0)=r_0(ME_1)^{\frac{1}{2}}/\hbar-r_0^2ME_1/(2\hbar^2)$$

so that the depth D_1 is given by (see Eq. (8.6))

$$D_1=\frac{\pi^2\hbar^2}{4Mr_0^2}\left(1-\frac{8}{\pi^2}\chi_1+\cdots\right)=\frac{\pi^2\hbar^2}{4Mr_0^2}-\frac{4}{\pi}(E_1D_1)^{\frac{1}{2}}, \tag{8.8}$$

the latter form being directly obtainable[19] from the definition of E_1. Eq. (8.8), useful as it is for rapid estimates, is not quite accurate enough for the calculations needed here. On the other hand, Eq. (8.6′) is sufficiently accurate and avoids the introduction of a virtual level which is seen to be artificial when the range of force is of importance in the correction for range in the cross section.

Expansion for wells of any shape.—For the Gauss error potential the wave equation was solved by numerical integration. In order to have a check on the accuracy of the numerical work the values of the logarithmic derivative of the function needed in the determination of the proton-proton and proton-neutron potentials were checked against each other also by using a power series expansion. The method consists in obtaining a power series in $\kappa-\kappa_0$, $\lambda-\lambda_0$, $\mu-\mu_0$ for $dF/Fdx=y$ where F is the solution, regular at $x=0$, for

$$d^2F/dx^2+[\kappa+\lambda\varphi(x)+\mu\chi(x)]F=0. \tag{9}$$

Eliminating F one obtains the Riccati equation

$$dy/dx+y^2+\kappa+\lambda\varphi(x)+\mu\chi(x)=0.$$

[19] H. A. Bethe and R. F. Bacher, Rev. Mod. Phys. **8**, 82 (1936).

For fixed x the value of y is a function of κ, λ, μ. Partial differentiation with respect to these quantities will be designated by suffixes as follows

$$y_\lambda = \partial y/\partial\lambda, \quad y_{\lambda\mu} = \partial^2 y/\partial\lambda\partial\mu.$$

Differentiating the above differential equation successively one obtains ordinary differential equations for these derivatives:

$$dy_\kappa/dx + 2yy_\kappa + 1 = 0, \qquad dy_{\kappa\lambda}/dx + 2yy_{\kappa\lambda} + 2y_\kappa y_\lambda = 0,$$

$$dy_{\kappa\kappa}/dx + 2yy_{\kappa\kappa} + 2y_\kappa{}^2 = 0, \quad dy_{\kappa\lambda\mu}/dx + 2yy_{\kappa\lambda\mu} + 2y_\lambda y_{\mu\kappa} + 2y_\mu y_{\kappa\lambda} + 2y_\kappa y_{\lambda\mu} = 0.$$

For $x=0$ the function F should be a power series in x beginning with a term of power 1. Therefore,

$$y(0) = 1$$

independently of κ, λ, μ. Hence

$$y_\kappa(0) = y_\lambda(0) = \cdots = y_{\kappa\lambda\mu}(0) = 0.$$

The values of y_κ, etc. are, therefore, determined by the above linear differential equations and these boundary conditions. One obtains

$$y_\kappa = -F^{-2}\int_0^x F^2 dx\,; \quad y_\lambda = -F^{-2}\int_0^x F^2\varphi dx\,; \quad y_\mu = -F^{-2}\int_0^x F^2\chi dx\,;$$

$$y_{\kappa\kappa} = -2F^{-2}\int_0^x y_\kappa{}^2 F^2 dx\,; \quad y_{\kappa\lambda} = -2F^{-2}\int_0^x y_\kappa y_\lambda F^2 dx\,;$$

$$y_{\lambda\lambda\lambda} = -6F^{-2}\int_0^x y_\lambda y_{\lambda\lambda} F^2 dx\,; \quad y_{\lambda\lambda\mu} = -F^{-2}\int_0^x (4y_\lambda y_{\lambda\mu} + 2y_\lambda{}^2 y_\mu) F^2 dx\,; \tag{9.1}$$

$$y_{\kappa\lambda\mu} = -2F^{-2}\int_0^x (y_\kappa y_{\lambda\mu} + y_\lambda y_{\mu\kappa} + y_\mu y_{\kappa\lambda}) F^2 dx\,;$$

$$y_{\kappa\lambda\mu\nu} = -2F^{-2}\int_0^x (y_\kappa y_{\lambda\mu\nu} + y_\lambda y_{\mu\nu\kappa} + y_\mu y_{\nu\kappa\lambda} + y_\nu y_{\kappa\lambda\mu} + y_{\kappa\lambda} y_{\mu\nu} + y_{\kappa\mu} y_{\lambda\nu} + y_{\kappa\nu} y_{\lambda\mu}) F^2 dx.$$

The last formula applies to a differential equation including a fourth linear parameter ν. From the last formula one obtains the other derivatives of the fourth order by equating indices in $y_{\kappa\lambda\mu\nu}$. The $y_{\kappa\lambda}\ldots$ can be evaluated by means of the above formulas with numerical quadratures, and the needed values of F and y can be obtained from one numerical integration for F. The formulas for the first-order derivatives have apparently been given for the first time by BCP where they have been obtained by a slightly different method. In Wigner's Princeton lectures for 1936 the same formulas for first-order derivatives are obtained from Riccati's equation which suggested the extension to higher derivatives made here. An obvious extension to parameters entering nonlinearly can be made and is used for Eq. (12) below.

Formulas for neutron-proton potential for the Gauss error type interaction.—In the calculation of the proton-neutron potential use can be made of the simplication due to the fact that experiments are concerned with zero energy. The wave function is, therefore, practically a linear function of the distance beyond the region where the Gauss error function potential has an appreciable value. The effect on y of a change in the potential can be calculated for any distance greater than this and its effect on the collision cross section will be the same. It may be expected, therefore, that this distance can be eliminated from the calculations. In order to do this the distance will be made infinite. In

nuclear units the differential equation for the Gauss error potential and zero energy is

$$d^2F/dr^2+Ae^{-\alpha r^2}F=0. \tag{10}$$

Substituting $x=r\alpha^{\frac{1}{2}}$ one has

$$d^2F/dx^2+\lambda\varphi(x)F=0\,;\quad \varphi(x)=e^{-x^2}\,;\quad \lambda=A/\alpha, \tag{10.1}$$

which is of the form of Eq. (9). The intercept on the r axis is called a. It is connected with the collision cross section of neutrons with free protons by

$$\sigma=4\pi a^2$$

and with properties of F by $Fdr/dF=a+r$. In terms of x one has for any x beyond which φ is negligible

$$y=dF/Fdx=(x+a\alpha^{\frac{1}{2}})^{-1}. \tag{10.2}$$

It will be supposed that φ has been modified to be exactly zero beyond a certain distance. The limiting value of the result for an infinite value of this distance will be taken at the end of this calculation. To every λ there corresponds a definite value of the intercept and hence also of $a\alpha^{\frac{1}{2}}$ which by Eq. (10.2) determines y. One has thus asymptotically for large x:

$$y-y_0\sim(a_0\alpha_0^{\frac{1}{2}}-a\alpha^{\frac{1}{2}})x^{-2}, \tag{10.3}$$

where y, a correspond to λ, α and y_0, a_0 to λ_0, α_0. By the method explained for Eq. (9) one may expand $y-y_0$ as

$$y-y_0=(\lambda-\lambda_0)y_\lambda+\tfrac{1}{2}(\lambda-\lambda_0)^2y_{\lambda\lambda}+\tfrac{1}{6}(\lambda-\lambda_0)^3y_{\lambda\lambda\lambda}+\cdots,$$

where y_λ, $y_{\lambda\lambda}$, $y_{\lambda\lambda\lambda}$ are to be evaluated for $\lambda=\lambda_0$. This series can be calculated for a finite x and can be used directly in the above form as has been done in some of the calculations for interchecks between numerical integrations. The limiting form of the series will now be worked out for $x\to\infty$. For finite x outside the potential hole one has

$$y_\lambda=-I_1(x+a_0\alpha_0^{\frac{1}{2}})^{-2}\,;\quad I_1=\int_0^\infty F_0^2(x)\varphi(x)dx, \tag{10.4}$$

where $F_0(x)$ is the solution of Eq. (10) regular at $x=0$ evaluated for λ_0. The solution F_0 is normalized so as to have outside the potential hole:

$$F_0=x+a_0\alpha_0^{\frac{1}{2}}. \tag{10.5}$$

Similarly

$$y_{\lambda\lambda}=-2(x+a_0\alpha_0^{\frac{1}{2}})^{-2}\left[\int_0^{x_0}F_0^2y_\lambda^2dx+\int_{x_0}^{x}F_0^2I_1^2(x+a_0\alpha_0^{\frac{1}{2}})^{-4}dx\right].$$

Here $x_0<x$ and x_0 is also outside the potential hole. From Eq. (10.5) the last term can be integrated and gives

$$-I_1^2(x+a_0\alpha_0^{\frac{1}{2}})^{-1}+I_1^2(x_0+a_0\alpha_0^{\frac{1}{2}})^{-1}.$$

The sum

$$\int_0^{x_0}F_0^2y_\lambda^2dx+I_1^2(x_0+a_0\alpha_0^{\frac{1}{2}})^{-1}$$

must be independent of x_0 since $y_{\lambda\lambda}$ does not depend on it. One has thus

$$y_{\lambda\lambda}=-2(x+a_0\alpha_0^{\frac{1}{2}})^{-2}[I_2-I_1^2/(x+a_0\alpha_0^{\frac{1}{2}})],$$

where

$$I_2=\int_0^\infty F_0^2y_\lambda^2dx=\int_0^{x_0}F_0^2y_\lambda^2dx+I_1^2/(x_0+a_0\alpha_0^{\frac{1}{2}}). \tag{10.6}$$

The object of expressing I_2 as a sum is only that of having a form convenient for numerical evaluation. Proceeding similarly for $y_{\lambda\lambda\lambda}$ it is found that

$$y_{\lambda\lambda\lambda}=-6(x+a\alpha^{\frac{1}{2}})^{-2}[I_3-2I_1I_2(x+a_0\alpha_0^{\frac{1}{2}})^{-1}+I_1^3(x+a_0\alpha_0^{\frac{1}{2}})^{-2}],$$

where

$$I_3=\int_0^\infty F_0^2y_\lambda y_{\lambda\lambda}dx=\int_0^{x_0}F_0^2y_\lambda y_{\lambda\lambda}dx+2I_1I_2(x_0+a_0\alpha_0^{\frac{1}{2}})^{-1}-I_1^3(x_0+a_0\alpha_0^{\frac{1}{2}})^{-2}. \tag{10.7}$$

Substituting the values of y_λ, $y_{\lambda\lambda}$, $y_{\lambda\lambda\lambda}$ into the Taylor expansion and equating for large x the governing terms in x^{-2} one obtains with Eq. (10.3)

$$a\alpha^{\frac{1}{2}}-a_0\alpha_0^{\frac{1}{2}}=I_1(\lambda-\lambda_0)+I_2(\lambda-\lambda_0)^2+I_3(\lambda-\lambda_0)^3+\cdots, \tag{10.8}$$

which is convenient for the calculation of $a\alpha^{\frac{1}{2}}$ for different λ using a single numerical integration for λ_0. The above series can be inverted and gives them

$$\lambda-\lambda_0=(a\alpha^{\frac{1}{2}}-a_0\alpha_0^{\frac{1}{2}})I_1^{-1}-I_2I_1^{-3}(a\alpha^{\frac{1}{2}}-a_0\alpha_0^{\frac{1}{2}})^2+(2I_2^2-I_1I_3)I_1^{-5}(a\alpha^{\frac{1}{2}}-a_0\alpha_0^{\frac{1}{2}})^3+\cdots,$$

which determines λ through a and α. One obtains in this way for $\lambda_0=2.35$ evaluating the integrals at $x=3.5$ for the Gauss-error potential

$$A/\alpha=\lambda=2.35+0.037032(a\alpha^{\frac{1}{2}}-a_0\alpha_0^{\frac{1}{2}})-0.004102(a\alpha^{\frac{1}{2}}-a_0\alpha_0^{\frac{1}{2}})^2+0.000454(a\alpha^{\frac{1}{2}}-a_0\alpha_0^{\frac{1}{2}})^3-\cdots; \tag{10.9}$$

$$a_0\alpha_0^{\frac{1}{2}}=7.9535.$$

This formula becomes poor for large a but is convenient for the values indicated by present experimental material. The choice $\lambda_0=2.35$ was made so as to be able to start a corresponding expansion for proton-proton calculations.

It is also useful to have the following expansion for y as a power series in $\lambda-\lambda_0$ for $\lambda_0=2.35$, $x=3.5$,

$$y=0.08731-0.2059(\lambda-\lambda_0)-0.1303(\lambda-\lambda_0)^2-0.0847(\lambda-\lambda_0)^3\cdots \quad (\text{at } x=3.5),$$

which can be used with Eq. (10.2) for the calculation of a. This series has been checked against a direct numerical integration for $\lambda=2.25$ which gave $(dF/Fdx)_{x=3.5}=0.10668$. Exactly the same value is obtained by means of the series the successive terms contributing $0.08731+0.02059-0.00130+0.00008=0.10668$.

A slight error is made by extending the numerical integration to finite rather than infinite values of x. This error can be estimated using the formula for y_λ already explained. Using $x=\xi$ instead of $x=\infty$ in the calculations amounts to neglecting the part of φ in $\xi<x<\infty$. The first-order correction due to taking into account φ from ξ to η is

$$y(\eta)-y_0(\eta)=-\lambda(\eta+a_0\alpha_0^{\frac{1}{2}})^{-2}\int_\xi^\eta(x+a_0\alpha_0^{\frac{1}{2}})^2\varphi(x)dx,$$

where $a_0\alpha_0^{\frac{1}{2}}$ is the value obtained for $a\alpha^{\frac{1}{2}}$ by breaking the potential off at ξ, and $y_0(\eta)$ is the value of $y(\eta)$ obtained in the same way. On the other hand,

$$y(\eta)-y_0(\eta)=-(a\alpha^{\frac{1}{2}}-a_0\alpha_0^{\frac{1}{2}})/(\eta+a\alpha^{\frac{1}{2}})(\eta+a_0\alpha_0^{\frac{1}{2}}).$$

Comparing the two values of $y(\eta)-y_0(\eta)$ for infinite η one has the first-order correction

$$a\alpha^{\frac{1}{2}}-a_0\alpha_0^{\frac{1}{2}}=\lambda\int_\xi^\infty (x+a_0\alpha_0^{\frac{1}{2}})^2\varphi(x)dx.$$

For $\varphi(x)=e^{-x^3}$ this becomes approximately

$$a\alpha^{\frac{1}{2}}-a_0\alpha_0^{\frac{1}{2}}=(\lambda/2\xi)(\xi+a_0\alpha_0^{\frac{1}{2}})^2e^{-\xi^3}. \tag{10.91}$$

For $\lambda=2.35$, $\xi=3.5$, $a_0\alpha_0^{\frac{1}{2}}=7.95$ this estimate gives $(a\alpha^{\frac{1}{2}}-a_0\alpha_0^{\frac{1}{2}})/a_0\alpha_0^{\frac{1}{2}}=2.7\times10^{-4}$ which is negligible.

Intercomparison of numerical integrations.—In order to avoid unknown cumulative errors in numerical integrations the series solutions have been carried out in a few cases to $x=1$ and the cumulative effect of the term in δ^4F'' has been taken into account. The integration from $x=1$ to higher values has been carried out at intervals of 0.1 in x. For the numerical integrations used for proton-proton scattering the series solution usually stopped at $x\sim4$. An intercheck between the numerical integrations for proton-proton scattering for $\alpha=20$, $A=47.17$, $E=200$ kev, $r=2.00288$, $x=2.8000$ was made with the numerical integration used for proton-neutron scattering with $\lambda=2.35$. The differential equation for the proton-proton functions is

$$d^2\mathfrak{F}/dx^2+(\lambda e^{-x^3}-\beta/x+\gamma)\mathfrak{F}=0$$

and $\beta=0.06990$, $\gamma=0.009773$, $\lambda=2.3585$ have been used. With these values the direct numerical integration gave $d\mathfrak{F}/\mathfrak{F}dx=0.15250$. The first-order corrections are

$$y_\lambda\delta\lambda+y_\beta\delta_\beta+y_\gamma\delta\gamma=-0.00198+0.08258-0.01668=0.06392.$$

The second-order corrections are

$$\tfrac{1}{2}y_{\lambda\lambda}(\delta\lambda)^2+\tfrac{1}{2}y_{\beta\beta}(\delta\beta)^2+\tfrac{1}{2}y_{\gamma\gamma}(\delta\gamma)^2+y_{\lambda\beta}\delta\lambda\delta\beta+y_{\lambda\gamma}\delta\lambda\delta\gamma+y_{\beta\gamma}\delta\beta\delta\gamma=-0.000008-0.00764$$
$$-0.00020+0.00049-0.00007+0.00238=-0.00505.$$

The numbers are given in the same order as symbols. Most of the third-order corrections are negligible, only five being large enough to affect $y(x)$ in the fifth place. These are

$$\tfrac{1}{6}y_{\beta\beta\beta}(\delta\beta)^3+\tfrac{1}{2}y_{\beta\beta\gamma}(\delta\beta)^2\delta\gamma+\tfrac{1}{2}y_{\beta\beta\lambda}(\delta\beta)^2\delta\lambda+\tfrac{1}{2}y_{\beta\gamma\gamma}\delta\beta(\delta\gamma)^2+6y_{\beta\gamma\lambda}\delta\beta\delta\gamma\delta\lambda=0.00086-0.00014$$
$$-0.000045+0.000025+0.000025=0.00072.$$

Not all of the fourth-order corrections have been taken into account but the following give appreciable effects:

$$(1/24)y_{\beta\beta\beta\beta}(\delta\beta)^4+\tfrac{1}{6}y_{\beta\beta\beta\gamma}(\delta\beta)^3\delta\gamma+\tfrac{1}{6}y_{\beta\beta\beta\lambda}(\delta\beta)^3\delta\lambda=-0.000099-0.000019-0.000006=-0.00012.$$

The value of y for $\lambda=2.35$, $\beta=\gamma=0$ by numerical integration is 0.09315. The expected value of y for $\lambda=2.3585$, $\beta=0.06990$, $\gamma=0.009773$ is, therefore,

$$0.09315+0.06392-0.00505+0.00072-0.00012=0.15262.$$

This is to be compared with $y=0.15250$ obtained by numerical integration for these λ, β, γ. The

error in $xd\mathfrak{F}/\mathfrak{F}dx$ due to the remaining discrepancy is 0.00034. The corresponding error in K_0 is given by

$$\delta\left(\frac{xdF}{Fdx}\right)=-C_0^2\rho\Phi_0^2\left(\frac{xd\mathfrak{F}}{\mathfrak{F}dx}-\frac{\Phi_0^*}{\Phi_0}\right)^2\frac{\delta K_0}{\sin^2 K_0}.$$

In the present case it is $-2.6\delta K_0$. The error 0.00034 in $xd\mathfrak{F}/\mathfrak{F}dx$ produces therefore $\delta K_0=-0.00013=-0.007°$. At this energy such an error corresponds to roughly 0.2 percent error in scattering and is considerably below possible accuracy of an experiment. At higher energies the experimental accuracy is higher but here also an accuracy of 0.01° in K_0 is sufficient.

2. Coulomb effect for square wells

The depth of the square well inside of which the Coulomb repulsion between two protons is assumed to act must be somewhat greater than if this repulsion is supposed to exist only outside the well. It is necessary to take this effect into account because it amounts to about 0.8 Mev and affects, therefore, the comparison between proton-proton and proton-neutron interactions. In the work of BCP the effect of the Coulomb repulsion inside the potential hole was taken into account by two different methods. In the first method the wave functions inside the hole have been computed taking into account the Coulomb repulsion and using power series. This method is somewhat laborious. In the second method the first-order effects on the logarithmic derivative due to introducing the Coulomb repulsion and due to increasing the depth of the hole have been taken into account. This gave rise to the formula

$$\delta D=\frac{e^2z\int_0^z(\sin^2 z/z)dz}{r_0\int_0^z\sin^2 zdz}=\frac{e^2z[\ln 2z+0.5772\cdots-Ci(2z)]}{r_0(z-\sin z\cos z)},\quad Ci(x)=-\int_x^\infty\frac{\cos u}{u}du,$$
$$z=[2\mu h^{-2}(D+E')]^{\frac{1}{2}},\quad r_0=0.4371(r_0mc^2/e^2)(D+E')^{\frac{1}{2}}(\text{Mev})^{-\frac{1}{2}}. \tag{11}$$

The two methods agreed to within the accuracy desired then. The requirements for precision in the calculations are higher now on account of improvements and extensions in the experiments. The second method has been extended, therefore, so as to include second- and third-order effects. The differential equation is

$$\frac{d^2\mathfrak{F}}{dr^2}+\frac{2\mu}{h^2}\left(D+E'-\frac{e^2}{r}\right)\mathfrak{F}=0. \tag{11.1}$$

Here it is convenient to set

$$\beta_s=2\mu e^2/h^2,\quad y_s=d\mathfrak{F}/\mathfrak{F}dr. \tag{11.11}$$

For fixed r and E' the quantity y_s is a function of D, β_s. Using the formulas previously described in connection with the Gauss error potential one obtains

$$\frac{\partial y_s}{\partial\beta_s}=\frac{C+\ln 2z-Ci(2z)}{2\sin^2 z};\quad C=0.577216\cdots;$$
$$\frac{\partial y_s}{\partial D}=-\frac{\mu(z-\sin z\cos z)}{h^2\kappa_s\sin^2 z};\quad \kappa_s=(2\mu(E'+D)h^{-2})^{\frac{1}{2}}. \tag{11.12}$$

The values of these derivatives correspond to $\beta_s=0$. Similarly, letting

$$I_{DD}=\int_0^z(\sin z)^{-2}(z-\sin z\cos z)^2dz,$$

$$I_{\beta D}=\int_0^z(\sin z)^{-2}[C+\ln 2z-Ci(2z)](z-\sin z\cos z)dz, \tag{11.13}$$

$$I_{\beta\beta}=\int_0^z(\sin z)^{-2}[C+\ln 2z-Ci(2z)]^2dz,$$

one has

$$\frac{\partial^2 y_s}{\partial\beta_s^2}=-\frac{I_{\beta\beta}}{2\kappa_s\sin^2 z};\quad \frac{\partial^2 y_s}{\partial\beta_s\partial D}=\frac{\mu I_{\beta D}}{\hbar^2\kappa_s^2\sin^2 z};\quad \frac{\partial^2 y_s}{\partial D^2}=-\frac{2\mu^2 I_{DD}}{\hbar^4\kappa_s^3\sin^2 z}.$$

In the present approximation δD, the increase in the depth due to the Coulomb repulsion inside the potential well, is connected with β_s by

$$\frac{\partial y_s}{\partial\beta_s}\beta_s+\frac{\partial y_s}{\partial D}\delta D+\frac{\partial^2 y_s}{2\partial\beta_s^2}\beta_s^2+\frac{\partial^2 y_s}{\partial\beta_s\partial D}\beta_s\delta D+\frac{\partial^2 y_s}{2\partial D^2}(\delta D)^2=0,$$

so that sufficiently accurately

$$\delta D=\frac{e^2 z[\ln 2z+0.577216-Ci(2z)]}{r_0(z-\sin z\cos z)}f, \tag{11.2}$$

where

$$f=1+\frac{\partial^2 y_s/\partial\beta_s^2}{2\partial y_s/\partial\beta_s}\beta_s-\frac{\partial^2 y_s/\partial\beta_s\partial D}{\partial y_s/\partial D}\beta_s-\frac{\partial^2 y_s/\partial D^2}{2(\partial y_s/\partial D)^2}\frac{\partial y_s}{\partial\beta_s}\beta_s,$$

so that

$$f=1+\beta_s\epsilon/\kappa_s, \tag{11.3}$$

where

$$\frac{\beta_s}{\kappa_s}=\frac{e^2}{\hbar c}\left(\frac{Mc^2}{E'+D}\right)^{\frac{1}{2}}=\frac{0.223}{[(E'+D)/\mathrm{Mev}]^{\frac{1}{2}}}$$

and

$$\epsilon=-\frac{I_{\beta\beta}/2}{C+\ln 2z-Ci(2z)}+\frac{I_{\beta D}}{z-\sin z\cos z}-I_{DD}\frac{C+\ln 2z-Ci(2z)}{2(z-\sin z\cos z)^2}. \tag{11.4}$$

Some numerical values of ϵ and of the coefficient of e^2/r_0 in the first-order approximation for δD are given in Table XVI. The experimental values for nonvelocity dependent potentials lie close to $z=1.4$. The depth of the well is in this case 10.5 Mev so that $\beta_s/\kappa_s=0.069$ for low proton energies and is smaller than this at the higher energies. Hence $f=1-0.069\times 0.029=0.9980$. The second-order correction is thus -0.2 percent of the first-order correction. This extreme smallness of the second-order effect should not be interpreted as an indication of a similar ratio of third- and second-order terms in the series for δD because the three terms in $I_{\beta\beta}$, $I_{\beta D}$, I_{DD} approximately cancel each other. The three contributions for $z=1.2$ are $-0.257_7+0.393_9-0.159_6=-0.023$. Even though the third-order correc-

TABLE XVI. *Values of* $z[ln\ 2z+0.5772\cdots-Ci(2z)](z-\sin z\cos z)^{-1}$ *and of* ϵ.

$z=$	1.0	1.1	1.2	1.3	1.4	1.5	1.6	1.7
$z\frac{\ln 2z+0.5772-Ci(2z)}{z-\sin z\cos z}=$	1.554	1.566	1.580	1.596	1.613	1.633	1.655	1.679
$\epsilon=$	−0.019	−0.021	−0.023	−0.026	−0.029	−0.031	−0.034	−0.038

tion cannot be expected to be as small as 0.002 of the second there is no reason to expect it to be more than $(0.02)^2=0.0004$ of the first-order effect. The solution as used above can be thus expected to be good enough.

It will be noted that the first-order effect varies slowly with z. Since z itself varies slowly with E it also changes slowly with proton energy. As a good approximation, therefore, a range of force which fits experiment if the Coulomb effect is neglected inside the potential well fits it also if this effect is assumed to be present. The main change due to the Coulomb potential inside the potential hole is nearly a constant increase in the depth of the hole for a fixed range of force, energy and phase shift.

The accuracy of Eqs. (11.2), (11.3) and (11.4) for the computation of the correction to the depth of the square well due to the introduction of the Coulomb interaction inside of it has been tested using the third-order correction for the effect of the interaction on the wave function. Analogously to the formulas preceding Eq. (11.2) one obtains by the method of Eqs. (9.1) an expansion for y_s the first three terms of which give

$$\left(\frac{rd\mathfrak{F}}{\mathfrak{F}dr}\right)_{r_0}=r_0y_s=z\cot z+\frac{\beta_s[C+\ln 2z-Ci(2z)]}{2\kappa_s\sin^2 z}-\frac{\beta_s^2z}{4\kappa_s^2\sin^2 z}I_{\beta\beta}+\frac{\beta_s^3}{4\kappa_s^3\sin^2 z}I_{\beta\beta\beta}, \tag{11.5}$$

where

$$I_{\beta\beta\beta}=\int_0^z[C+\ln 2z-Ci(2z)](I_{\beta\beta}/\sin^2 z)dz. \tag{11.6}$$

Here z is the internal phase defined in Eq. (11), β_s is defined in Eq. (11.11), κ_s in Eq. (11.12), $I_{\beta\beta}$ in Eq. (11.13). The expansion in Eq. (11.5) is seen to be in powers of β_s/κ_s. It converges rapidly for radii $\sim e^2/mc^2$ in the energy range tried. The last term is slightly less than 0.0001 up to 2600 kev and can be neglected in most applications. The term in $I_{\beta\beta}$ is more important and is ~-0.002.

According to Eq. (11.2) a square well of depth $D^e=D+\delta D$ with Coulomb interaction acting inside of it gives nearly the same $rd\mathfrak{F}/\mathfrak{F}dr$ as a square well of depth D without the Coulomb interaction inside of it. For the latter $rd\mathfrak{F}/\mathfrak{F}dr$ can be evaluated as $z\cot z$ using z as in Eq. (11). At the same time $rd\mathfrak{F}/\mathfrak{F}dr$ for D^e with Coulomb potential can be computed using the more accurate method of Eq. (11.5). With $D=10.500$ Mev and $r_0=e^2/mc^2$ the two ways of computing $rd\mathfrak{F}/\mathfrak{F}dr$ agree to within 0.0001 for $E=200$ kev and 0.0002 for $E=2600$ kev. This accuracy is higher than any present requirement. Eq. (11.2) may be, therefore, considered as being sufficiently accurate for the calculation of the depth of a square well taking account of the Coulomb interaction down to $r=0$.

The value of δD depends slightly on the proton energy. For $D=10.500$ Mev one finds $\delta D=0.826$, 0.830, 0.834 Mev for $E=200$, 1400, 2600 kev, respectively. The variation in $D^e=D+\delta D=11.33$ Mev is less than 0.1 percent in the above range of energies. For most purposes, therefore, one can first calculate without taking into account the Coulomb interaction inside the well and then increasing the depth by the same amount δD throughout the present energy range.

The accuracy of this procedure has been tested directly as well. The phase shift was computed for $r_0=e^2/mc^2$, $D=10.500$ Mev and with no Coulomb potential inside r_0. It was then also computed for $r_0=e^2/mc^2$, $D^e=11.3302$ Mev, and with the Coulomb potential taken into account by means of Eq. (11.5). The value of K_0 for D^e

minus its value for D varies slightly with energy changing from 0.02° at $E=200$ kev to 0.06° at $E=2600$ kev. This change is invisible on the graphs for K_0 against E.

It is useful to have the numerical values of the functions of z that occur in the expansion of $rd\mathfrak{F}/\mathfrak{F}dr$ in Eq. (11.5). The necessary quantities are given in Table XVII.

3. Adjustment of range and values of interaction constants obtained from experiment

A "square well" potential of depth $D=10.5$ Mev (no Coulomb repulsion inside well) and radius e^2/mc^2 gives values of the phase shift which agree approximately with experiment. The comparison is shown in Figs. 6 and 7. In the first of these there are three curves for radius e^2/mc^2 and another set for a radius 1.25 e^2/mc^2. In the second of these figures graphs for a radius 0.75 e^2/mc^2 are used instead of for the radius 1.25 e^2/mc^2. In both cases experiment is seen to favor the range e^2/mc^2 in preference to the other two. The measurements of HKPP speak for a range slightly smaller than e^2/mc^2 indicating perhaps 0.95 e^2/mc^2 as the better value. Combined with experiments of HHT a better average fit is obtained for a slightly larger range. The graphs show that the range 0.75 e^2/mc^2 is too small and the range 1.25 e^2/mc^2 is too large if it is desired to represent the data as a whole. It is seen from

TABLE XVII. *Table of quantities for computation of logarithmic derivative of wave function for square well and Coulomb potential by means of Eq. (11.5). The second column gives the coefficient of $\beta_s/2\kappa_s$ in Eq. (11.5). The last two columns have been computed with Simpson's rule at intervals of 0.1 in z.*

z	$\frac{C+\ln 2z-Ci(2z)}{\sin^2 z}$	$\sin^2 z$	$I_{\beta\beta}$	$I_{\beta\beta\beta}$
0.4	1.027	0.1517	0.021	0.0022
.5	1.043	.2298	.042	.0053
.6	1.063	.3188	.072	.0112
.7	1.088	.4150	.114	.0212
.8	1.118	.5146	.171	.0368
.9	1.154	.6136	.244	.0602
1.0	1.197	.7081	.335	.094
1.1	1.247	.7943	.447	.142
1.2	1.307	.8687	.583	.207
1.3	1.378	.9285	.745	.296
1.4	1.463	.9711	.937	.415
1.5	1.564	.9950	1.162	.574
1.6	1.687	.9991	1.426	.783
1.7	1.836	.9834	1.733	1.061
1.8	2.020	.9484	2.091	
1.9	2.251	.8955	2.511	
2.0	2.545	.8268	3.004	

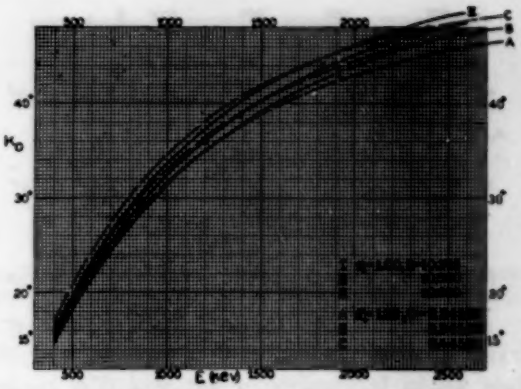

FIG. 6. Comparison of experimental and calculated phase shift for square wells of radii e^2/mc^2 and 1.25 e^2/mc^2. Circles represent observations of HKPP, upright crosses those of HHT. The depth of well is given in Mev. Coulomb interaction is supposed to take place outside the well only.

Figs. 6 and 7 that through the region 700–2400 kev a change of depth with fixed range produces a displacement of the curve by approximately a fixed amount. On the other hand, a change of range produces in addition a rotation. These relationships are only approximate but are helpful in forming an opinion regarding the range and depth of potential indicated by experiment. They are also true for the Gauss error potential which gives nearly the same shape of the (K_0, E) curve as the square well. The same percentage change in the range produces approximately the same amount of turning for the two types of potential. This relationship is true also for other potentials as long as the main part of the interaction occurs within a small distance. The effects of changes in depth and range are seen more clearly using a plot of $(\eta/C_0^2)\tan K_0$ against E. Such plots are shown in Figs. 8 and 9 the ranges for which correspond to Figs. 6, 7. The quantity plotted is chosen so as to give approximately horizontal curves through the present energy range as well as the region below 600 kev. The crowding of curves which occurs at low energies for the graphs of K_0 against E is seen to be absent for the plots of $(\eta/C_0^2)\tan K_0$. With either type of graph it is possible to adjust the two constants in the Gauss error type of potential so as to make K_0 have the desired values at two energies.

In view of the possibility of cumulative errors in the numerical integrations the range was adjusted also by means of formulas. This enables the calculation of corrections to A and α by

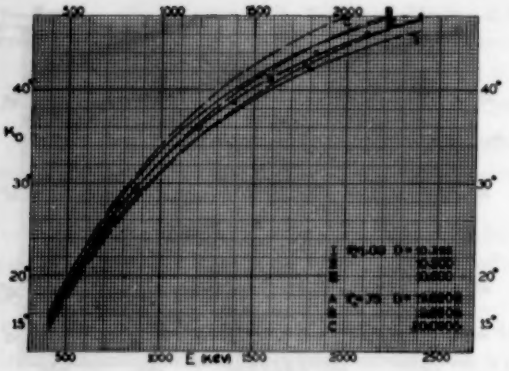

FIG. 7. Comparison of experimental and calculated phase shift for square wells of radii e^2/mc^2 and $0.75\ e^2/mc^2$. Notation and conventions are the same as for Fig. 6.

numerical integrations for values of these constants determined by rough inspection of the graphs. Several procedures have been found useful. In the first the range was fixed arbitrarily and the depth was determined at several energies so as to give the desired phase shift. If the range is too great the depth increases with energy. For small changes $\delta\alpha$, δA of depth and range the phase shift remains unchanged if

$$\frac{\delta\alpha}{\alpha}=\left[\int_0^\infty \mathfrak{F}^2e^{-x^2}dx \Big/ \int_0^\infty \mathfrak{F}^2x^2e^{-x^2}dx\right]\frac{\delta A}{A}. \quad (12)$$

The integrals in this formula having been determined by numerical integration at two or more energies, one knows the ratio of the percentage changes which must be made at two energies in order that the phase shift be unchanged. Hence one can determine the value of $\delta\alpha$ which is needed for obtaining the same A at the two energies. Roughly the same results can be obtained by noting how rapidly $\delta A/A$ decreases with an increase in α and extrapolating to 0. It is helpful to note that $\delta A/A$ varies approximately linearly with energy. This crudest method will be called the "percentage method." A third way involving numerical integrations for only one set of A and α is to use the approximate linear equations

$$\left[\delta\left(\frac{r\partial\mathfrak{F}}{\mathfrak{F}\partial r}\right)\right]_1=\left[\frac{\partial}{\partial\alpha}\left(\frac{r\partial\mathfrak{F}}{\mathfrak{F}\partial r}\right)\right]_1\delta\alpha+\left[\frac{\partial}{\partial A}\left(\frac{r\partial\mathfrak{F}}{\mathfrak{F}dr}\right)\right]_2\delta A, \quad (12.1)$$

$$\left[\delta\left(\frac{r\partial\mathfrak{F}}{\mathfrak{F}\partial r}\right)\right]_2=\left[\frac{\partial}{\partial\alpha}\left(\frac{r\partial\mathfrak{F}}{\mathfrak{F}\partial r}\right)\right]_2\delta\alpha+\left[\frac{\partial}{\partial A}\left(\frac{r\partial\mathfrak{F}}{\mathfrak{F}\partial r}\right)\right]_2\delta A, \quad (12.2)$$

where

$$\frac{\partial}{\partial\alpha}\left(\frac{r\partial\mathfrak{F}}{\mathfrak{F}\partial r}\right)=\frac{xA}{\alpha^2\mathfrak{F}^2}\int_0^x x^2e^{-x^2}\mathfrak{F}^2dx, \quad (12.3)$$

$$\frac{\partial}{\partial A}\left(\frac{r\partial\mathfrak{F}}{\mathfrak{F}\partial r}\right)=-\frac{x}{\alpha\mathfrak{F}^2}\int_0^x e^{-x^2}\mathfrak{F}^2dx, \quad (12.4)$$

and suffixes 1, 2 denote values of derivatives and changes for energies E_1, E_2 at which the adjustment is to be made. Evaluating the coefficients on the right side of (12.1), (12.2) by means of (12.3), (12.4) and computing the left sides by using the relation between K_0 and $r\partial\mathfrak{F}/\mathfrak{F}\partial r$, one obtains $\delta\alpha$ and δA.

Applying Eq. (12) to numerical integrations made for $\alpha=18$, $A=42.8$ and requiring a fit with the square well $r_0=e^2/mc^2$ at $E=200$ kev and $E=2000$ kev one obtains $\alpha=20.6$, $A=48.6$. The percentage method indicates using numerical integrations for $\alpha=16$ and $\alpha=18$ at 200, 800, 1400, 2600 kev that one must take $\alpha>18$ in order to obtain a fit with the square well for any pair of these voltages and that the approximate value of α is 20.

A set of accurate numerical integrations was made for $\alpha=20$, $A=47.17$. The Gauss error potential was broken off at the distance $3\ e^2/mc^2$ and the joining of internal to external wave functions was made at this distance. As expected this range is slightly too great (r_0 is too small) to fit the square well and is, therefore, definitely too great to fit experiment. The comparison is shown in Table XVIII.

The last figure is uncertain in this table but it is seen that $\alpha=20$ is too small. In the range 800–2600 kev the phase shift curve for this potential is turned by roughly the same amount under the curve for $D=10.5$, $r_0=e^2/mc^2$ as the experimental curve is turned above it.

From the accurate integrations for $A=47.17$, $\alpha=20$ the values of A, α needed to fit the square well $D=10.500$, $r_0=e^2/mc^2$ at 1400 kev and 2600 kev are found by means of Eqs. (12.1) and (12.2)

to be $A=51.55$, $\alpha=21.70$. By fitting the square well at 800 and 2600 kev one similarly finds $A=51.76$, $\alpha=21.78$ and fitting it at 200 kev and 1400 kev one obtains $A=51.85$, $\alpha=21.83$. It is seen that in the present energy region nearly constant values of A and α are needed to give results equivalent to a square well.

The sensitivity of the value of α to changes in K_0 can be computed using Eqs. (12.1) and (12.2) together with the relation of $r\partial\mathfrak{F}/\mathfrak{F}\partial r$ to K_0. One obtains in this way the values in Table XIX. In this table the first row is labeled E_1, E_2 and gives the values of the energies at which the adjustment of range is made. In the second row are listed the changes made in K_0 at the energies E_1, E_2. Here the entry (0, 0.4°) means that no change is made at the lower energy and that the phase shift is changed by 0.4° at the higher energy. The third row gives the resultant change in α, denoted by $\delta\alpha$. The last row gives the resultant α, which is obtained by adding $\delta\alpha$ to the value of α which corresponds to the pair E_1, E_2 and fitting the Gauss error potential to the square well of radius $r_0=e^2/mc^2$ and depth $D=10.500$ Mev. The lowest α obtained in Table XIX is 19.8. To make the value so low it was necessary to raise the phase shift by 0.4° at 800 kev from the value obtained for $r_0=e^2/mc^2$, $D=10.500$ Mev. Such an adjustment of range appears to be decidedly too low for α, since at 800 kev the 776 kev, 867 kev and 860 kev-experimental points lie practically on the curve for $r_0=e^2/mc^2$, $D=10.500$ Mev and since at 1830 kev, 2105 kev and 2392 kev the experimental points lie decidedly above

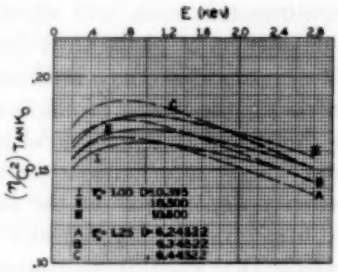

FIG. 8. Effect of change of range for square wells as shown by $(\eta/C_0^2)\tan K_0$ for the radii e^2/mc^2 and 1.25 e^2/mc^2 with depths in Mev. Note that change of range turns a curve and change of depth moves it up and down. These graphs are useful for interpolation eliminating the need for Coulomb functions at too many energies. The low energy point lies decidedly off the curve $r_0=1.00$, $D=10.500$ Mev when plotted in this way.

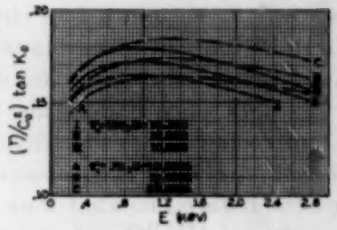

FIG. 9. Effect of change of range for square wells as shown by $(\eta/C_0^2)\tan K_0$ for the radii e^2/mc^2 and 0.75 e^2/mc^2.

this curve. It should be noted, on the other hand, that at 670 kev the experimental phase shift lies above the value expected for $r_0=e^2/mc^2$, $D=10.500$ Mev so that the correction of α towards smaller values appears to be called for from this point of view. It is probable, however, that such a correction is better represented by the last column in Table XIX where the phase shift is increased by 0.4° at 800 as well as 2400 kev. This adjustment requires according to the above calculation $\alpha=21.59$, $A=51.44$.

These values of A and α are in good agreement with the two ends of the experimental curve giving a good fit at 670 kev as well as at 1830, 2105 and 2392 kev. At intermediate voltages, however, the experimental phase shifts are consistently lower than the calculated, the larger deviations occurring at 1200 and 1390 kev where they are about 0.5°. The comparison of this curve with experiment is shown in Fig. 10. The theoretical curve is seen to be slightly bulged at intermediate voltages. The same tendency is noticed also for square wells with $r_0=e^2/mc^2$, $D=10.500$ and 10.520 Mev. It appears premature to conclude that these small deviations indicate an impossibility of representing the interaction by fixed potentials of the types discussed. It is remarkable, nevertheless, that the experimental points fall very beautifully on a smooth curve so that there appears to be some justification for requiring a better fit than has been attempted.

A better judgment regarding the validity of such conclusions can be obtained also from a direct comparison of observed and expected scattering shown in Fig. 11. This figure is to be compared with Fig. 8 of the paper of HKPP. In both of these figures the observed number of counts per microcoulomb is plotted against energy for fixed scattering angle. In Fig. 11 of the present paper the averages of the experi-

mental observations are plotted as circles from Table I of HKPP instead of results of different runs. Fig. 11 gives, therefore, an optimistic picture of the data since it does not show the scattering due to the errors in individual runs shown in Fig. 8 of HKPP. The observations of HHT have been reduced to what they would be in the apparatus of HKPP and are plotted as upright crosses. The diagonal crosses show the scattering that would be expected for a pure s anomaly with mean values of the phase shift obtained in Tables XI, XII from the experimental data. Such values are referred to here as "empirical." The empirical phase shift for Fig. 11 was obtained by plotting the experimental values of K_0 against E as in Fig. 10. There are shown besides in Fig. 11 three sets of theoretical curves. In order to avoid complicating the figure the empirical phase shift curve is not drawn. The full curves are for a square well with $r_0=e^2/mc^2$, $D=10.500$ Mev. The curve with short dashes is for a square well with $r_0=1.25$ e^2/mc^2, $D=6.34522$ Mev and the curve with long dashes is for the Gauss error potential $\alpha=21.59$, $A=51.44$. The conclusions arrived at in the comparison of computed and observed phase shift in Figs. 6, 7 and 10 are seen to be supported by Fig. 11. The comparison of Figs. 6 and 7 corresponds to the use of a mean of the curves for $\Theta=45°$, 40°, 35° and 30° and is somewhat more consistent in its indications concerning range than either of these curves. It is, nevertheless, seen also in the comparison with scattering that the range 1.25 e^2/mc^2 for a square well is decidedly too wide. The curves corresponding to it either cut across the region covered by experimental points or else they fit experiment at the lower energies but deviate from it markedly at the high energy end. The observations of HHT are seen to speak against the interpretation by $r_0=e^2/mc^2$, $D=10.500$ Mev and to favor rather $r_0=1.25\,e^2/mc^2$, $D=6.34522$ Mev or else $\alpha=21.59$, $A=51.44$. It is interesting to note that this indication is particularly marked for $\Theta=30°$. For this angle the scattering as a function of the energy should have a minimum at about 600 kev while the points of HHT lie too high and indicate that the minimum is at a lower energy. Inasmuch as the agreement of HHT and HKPP at $\Theta=25°$ is not as good as desirable and inasmuch as the agreement of the points of HHT with $r_0=e^2/mc^2$, $D=10.500$ Mev is fair at this angle a final conclusion regarding this question appears to be premature. At $\Theta=20°$ and 15°, the expected scattering is nearly independent of the potential assumed, the difference being too small in most of the region to show on the scale used. These curves have been drawn for $r_0=e^2/mc^2$, $D=10.500$ Mev. For $\Theta=15°$ the experimental points are consistently above the theoretical curve indicating the presence of geometrical corrections. This point has already been discussed in connection with Table XI.

TABLE XVIII. *Comparison of phase shift obtained for Gauss error potential $47.17e^{-\alpha r^2}$ with square well $D=10.500$, $r_0=e^2/mc^2$.*

$E=$	200	800	1400	2000	2600 kev
$K_0(D=10.5$ Mev$)=$	6.78°	27.90°	39.00°	45.10°	48.62°
$K_0(A=47.17, \alpha=20)=$	6.80°	27.83°	38.77°	44.71°	48.16°
Difference $=$	−0.02°	0.07°	0.23°	0.39°	0.46°

TABLE XIX. *Sensitivity of range to changes in phase shift.*

$(E_1, E_2)=$	(1400,2600)	(800,2600)	(800,2600)	(800,2600 kev)
$(\delta_1 K_0, \delta_2 K_0)=$	(0, 0.4°)	(0.4°, 0)	(0, 0.4°)	(0.4°, 0.4°)
$\delta\alpha=$	2.7	−2.0	1.8	−0.2
$\alpha=$	24.4	19.8	23.6	21.6

The adjustments for range that have been considered do not take into account the finer features of the experimental phase shift-energy curve. The three energies investigated in Washington when taken by themselves would give a definitely longer range than the phase shift curve taken as a whole. Similarly, the high energy part corresponds to a shorter range than the average values arrived at. It may be hoped that further experimental work will show whether such finer deviations of phase shift from theory are real. It appears that they indicate a possibility of inferring the shape of the potential as well as the range and that it may be possible to obtain from them information concerning a possible velocity dependence of the forces such as has been first proposed by Wheeler.

It is probable that the information concerning fits with phase shift curves corresponding to the simple potentials of fixed magnitude can be obtained by extending the experiments to higher as well as to lower energies. The possibilities for this will be discussed in the last section of the paper.

4. Comparison of the proton-proton and proton-neutron interactions

The comparison of the proton-proton and proton-neutron interactions made by BCP and by BS[14] indicated that in the ^1S state the proton-neutron attraction is slightly greater than the corresponding quantity for two protons. The experimental situation has improved considerably since then. The two types of scattering are known better and scattering experiments on neutrons in ortho- and parahydrogen indicate according to Teller and Schwinger and Teller[20] that the ^1S level of the deuteron must be virtual. The newer values support the previous view regarding the relative magnitude of the two interactions. In Table XX the comparison is shown for square wells.

The value 68.8×10^{-24} cm^2 corresponds to one of the possibilities in Table I of BS and has been used here so as to make it unnecessary to go into the effect of range. According to Carroll and Dunning 65.9×10^{-24} cm^2 is the probable lower limit for σ_{th} and according to Cohen and Goldsmith the probable value of σ_{th} is $(80\pm8)\times10^{-24}$ cm^2. There appears to be no doubt, therefore, that for the square well potential the proton-neutron attraction should be taken as the stronger. It should be noted that this conclusion is not sensitive to the range assumed as is seen in Table I of BS. It is also quite insensitive to the value used for the binding energy of the deuteron because with $E=-2.17$ Mev, $12\pi a_3^2=12.9\times10^{-24}$ cm^2 which is relatively small compared with σ_{th} [See Eq. (8)]. Since a_3^2 is approximately proportional to $1/E_3$ even a ten percent change in E_3 is of no importance as is seen from Table XX.

In Table XXI a similar comparison is made for the Gauss error potential. For this table the value of $12\pi a_3^2$ was redetermined using the Gauss error potential for the ^3S state. Since $12\pi a_3^2$ need not be known very accurately the value $\alpha=20$ was used. This gives $A(^3S)=85.5$ and $12\pi a_3^2=12.6\times10^{-24}$ cm^2. The difference between this and the corresponding value for the square well is seen to be practically immaterial.

According to Table XXI the relative values of the proton-proton and proton-neutron interactions are much the same for the Gauss error potential as for the square well. It appears, therefore, very probable that as long as the potentials are assumed to have fixed magnitude and the same range for the ^1S and ^3S interactions the proton-neutron potential should be taken as having a value roughly three percent higher than the proton-proton potential. The last row in Table XX shows that in order that this conclusion be materially affected by a change in the ^3S scattering cross section it is necessary to increase $12\pi a_3^2$ by roughly 30×10^{-24} cm^2 i.e., by more than twice the value expected on the simple views used here.

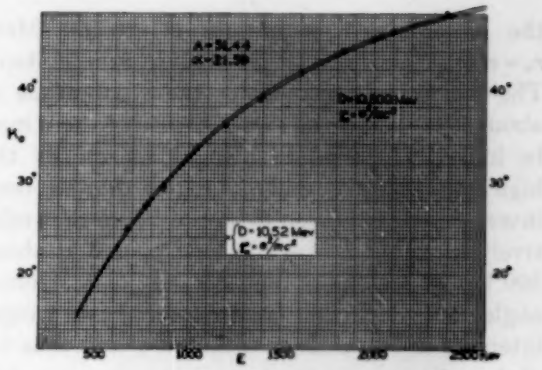

FIG. 10. The Gauss error potential with $A=51.44$, $\alpha=21.59$ compared with experiment and the square well potential $r_0=e^2/mc^2$, $D=10.500$ Mev. The effect of increasing the depth of the square well by 0.02 Mev is shown by the diagonal crosses. Circles give observations of HKPP, upright crosses those of HHT.

5. Possibilities at low and high energies and higher phase shifts

In Fig. 12 are shown graphs of a quantity proportional to the expected scattering in the region 200–600 kev. The quantity plotted is $4(\mathbf{c}/\mathbf{s})\mathfrak{M}\mathfrak{R}/E^2_{\text{Mev}}$. By means of Eq. (3.4) one can obtain from it the number of counts per microcoulomb per mm oil pressure in the standard design of apparatus. The graphs are plotted for

TABLE XX. *Comparison of proton-proton and proton-neutron interactions for the square well potential.*

σ_{th} IN 10^{-24} CM^2	D_{pp} IN MEV	D^c_{pp} IN MEV
80	11.75	11.35±0.03
68.8	11.65	" "
52	11.4	" "

[20] E. Teller, Phys. Rev. **49**, 420 (1936); J. Schwinger and E. Teller, Phys. Rev. **52**, 286 (1937).

the square well potentials $D=10.500$ Mev, $r_0=e^2/mc^2$ and $D=19.6905$ Mev, $r_0=3e^2/4mc^2$. The scattering expected for these potentials at about 2200 kev is the same. Either of them may be looked at as representing satisfactorily the high end of the experimental region that has been investigated. It is seen from the figure that relatively large differences can be expected at about 500 kev as well as around 350 kev at scattering angles near 45°. The curves for the two ranges intersect in the vicinity of 400 kev and thus for each scattering angle there is an energy region insensitive to the range of force. At 300 kev for 45° scattering one expects a relative difference between 25 percent and 20 percent for the shorter and longer range of force. At 450 kev the condition is even more favorable the scattering for the shorter range being roughly $\frac{1}{2}$ of that for the longer. The steepness of the curves at 250 kev and lower energies presumably introduces difficulties on account of the necessity of having an accurately defined energy of the incident protons. From this point of view measurements at 500 and 600 kev are more practical.

The first set of measurements published by Tuve, Heydenburg and Hafstad includes a point at 600 kev. Relatively good agreement was obtained with the expected angular distribution as is seen in Fig. 6 of BCP. The value of K_0 so obtained was fixed at the time between 21° and 22°. Even the higher of these values would speak for a shorter range than e^2/mc^2 for a square well as is seen in Figs. 6 and 7. It partly balances the new point of HHT at 670 kev which indicates a longer range. It will doubtless be of value to have more observations in this region. The counting difficulties at 45° caused by the low proton energy can be avoided by making measurements at smaller scattering angles. Measurements at 300 kev will have the obvious additional value of extending the phase shift curve over a wider energy region. The observations of Hafstad, Heydenburg and Tuve made in this region with a point counter were intended as a test of the attractive nature of the force and are hardly quantitative enough for the determination of the range of force. A comparison of the values obtained by Heydenburg, Hafstad and Tuve for the ratio of scattering at 45° to that at 25° is shown in Fig. 13. The values are obtained from their Table II. The high sensitivity of scattering to energy apparent in Fig. 12 must have introduced errors into these measurements in addition to those due to difficulties with the point counter. Only the point at 335 kev falls appreciably off

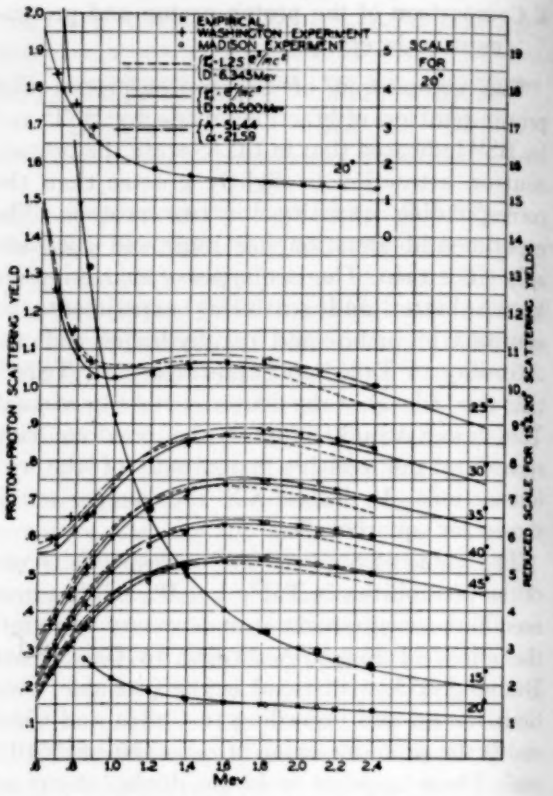

FIG. 11. Comparison of expected and observed scattering. This figure is to be compared with Fig. 8 of HKPP. Averages of their observations are plotted as circles. For scattering at 15° the observations are plotted as double circles. The upright crosses represent observations of HHT reduced to the scale of the apparatus of Herb *et al.* The diagonal crosses, designated as "empirical" are computed using the "mean K_0" of Tables XI, XII interpolating graphically for K_0, and assuming a pure s scattering anomaly. All the curves are theoretical assuming a pure s scattering anomaly. Note the definite effect of a 25 percent change in the range of force and the too high scattering expected for the Gauss potential ($A=51.44$, $\alpha=21.59$) around 1400 kev. The latter shows that the data contain more information than just about the range of force and depth of the interaction potential.

TABLE XXI. *Comparison of proton-proton and proton-neutron potentials for the Gauss error interaction.*

σ_{90} IN 10^{-24} CM^2	α	A_{np}	A_{pp}
80	20	48.9	47.2
80	22	54.0	52.4
65.9	20	48.3	47.2

the theoretical curves. The points appear to favor even a shorter range than e^2/mc^2 for a square well but such a conclusion from this energy region should obviously be postponed until more complete information is available.

In Fig. 14 are shown graphs for the scattering expected with the potentials $D=10.500$ Mev, $r_0=e^2/mc^2$ and $D=46.78$ Mev, $r_0=e^2/2mc^2$ on the assumption of pure s scattering. The curves are drawn for $\Theta=15°$, 25°, 35°, 45° and cover the energy range up to nine Mev. It is striking that the small angle scattering shows at the higher energies pronounced effects of range. This is to be expected since the scattering anomaly is spherically symmetric in the center of gravity system and since it becomes more important at high energies than the Coulomb scattering. To some extent this is a disadvantage because a check on the absolute values using small angle scattering becomes more difficult. Measurements in which the technique is tested around two Mev would be very valuable.

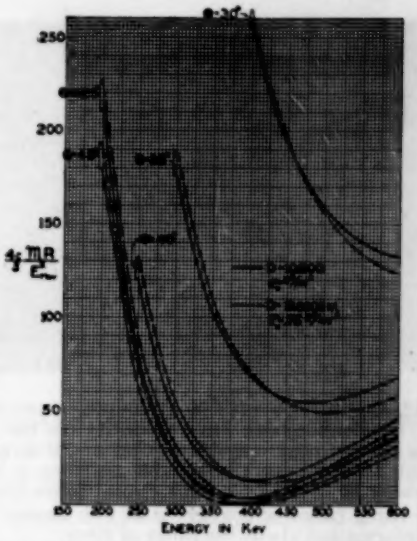

FIG. 12. The low energy region. The curves show how additional information may be obtained by observations at low energies. The quantity plotted may be used together with Eq. (3.4) to obtain proton counts per microcoulomb of incident protons.

The high energy region is expected to yield valuable information regarding higher phase shifts. The initial effect per $-1°$ for K_1 is given in Table XXII. The effect of K_1 is known to be simply additive to that of K_0 as is seen e.g., in Eq. (6.6) of BCP. The first row for each energy in the table gives the rate of change of the contribution to the ratio to Mott with respect to K_1 which is expressed in degrees. This rate of change is computed for very small K_1 and the effect tabulated is, therefore, the initial effect when K_1 just begins to make itself felt. In the second row for each energy the value in the first row is expressed as a percentage effect in the value expected for s scattering alone. The Mott ratio used in the denominator is that for $D=10.500$ Mev, $r_0=e^2/mc^2$ except for 1.83 Mev where the experimental values were used. For negative K_1, i.e., repulsive interaction, the effect of K_1 increases and remains positive as K_1 increases. For positive K_1, on the other hand, the initial effect of K_1 is negative, but as K_1 increases the effect becomes zero and then positive. This is analogous to the very small 45° scattering which is found at about 400 kev and represents a contest between the interference effect with the Coulomb scattering and the direct effect of the scattering anomaly represented by the term $108\eta^{-2}P_1^2\sin^2 K_1$ in Eq. (6.6) of BCP. One expects, therefore, a qualitative difference in the behavior for repulsive and attractive p waves which should show itself for rather small values of K_1. Thus at 2400 kev for $\Theta=20°$ one expects the compensation to occur at $K_1\sim10°$ and at $\Theta=30°$ for $K_1\sim5°$. At eight Mev the compensation is expected to occur for $\Theta=20°$ at $K_1\sim5°$ and for $\Theta=30°$ at $K_1\sim3°$. If the interaction is attractive it may therefore be missed at some angles. It does not seem probable that such compensations have already occurred using the somewhat old fashioned types of theory with exchange forces. But this possibility, nevertheless, exists and should be pointed out particularly since a form of mesotron theory has been proposed by Bethe[21] in which the direct contribution of the p wave anomaly is much larger than with exchange forces. This comes about on account of a strong dependence of the phase shift on the coupling between spin and orbital momentum, the phase shift being positive for $^3P_1$ and negative for $^3P_0$ and $^3P_2$.

The value of K_1 expected for potentials involving no spin-spin interactions can be obtained by substitution into formulas which express the

[21] H. A. Bethe, Fifth Washington conference on Theoretical Physics.

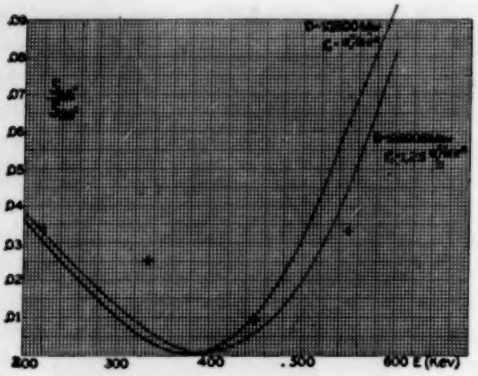

FIG. 13. Comparison with point counter experiment of Hafstad, Heydenburg and Tuve. Quantity plotted against energy is ratio of counts at 45° to that at 25° as given in their Table II. Note misprint in table assigning at 640 kev $S_{45°}/S_{20°}=0.038$ to $S_{45°}/S_{25°}$. The figure shows the possibility of using ratios of scattering at two angles for obtaining information about the range of force.

requirement of smooth joining of internal and external functions. For small phase shifts and for small effects on the wave function one can use Taylor's approximation[22] which in the present notation is

$$K_L \cong -\int (V/E')\mathfrak{F}_L^2 d\rho.$$

For the potential $Ae^{-\alpha r^2}$ this gives

$$|K_L| = \frac{|A|}{mc^2}\left(\frac{E'}{mc^2}\right)^{(2L+1)/2} \times C_L^2 \frac{\pi^{\frac{1}{2}}}{2}\frac{1}{2}\frac{3}{2}\cdots\frac{2L+1}{2}\alpha^{-(2L+3)/2}$$

and where the Coulomb function power series Φ_L is approximated by unity and the unit of length is $\hbar/(Mm)^{\frac{1}{2}}c$. For $A=38$, $\alpha=16$ calculations for 2400 kev using numerical integration and joining of wave functions gave $+0.47°$ for an attractive potential and $-0.33°$ for a repulsive one. The above approximation gives $|K_1|=0.41°$ which is just about the mean of the two values computed by numerical integration. The value of K_1 is sensitive to the extension of the potential towards the larger distances. Thus using a repulsive square well potential of absolute value 10.4 Mev through a distance e^2/mc^2 one obtains $K_1=-0.15°$. This value of K_1 is roughly $\frac{1}{3}$ of the value for the Gauss error potential while they give about the same phase shift for the s wave. For the potential $B\exp(-2r/b)$ used by Rarita and Present, Taylor's approximation is

$$K_L=(B/mc^2)C_L^2(E'/mc^2)^{(2L+1)/2} \times(2L+2)!/(2/b)^{2L+3},$$

the unit of length being again $\hbar/(Mm)^{\frac{1}{2}}c$. For $B=137\ mc^2$, $b=0.200$ this approximation gives $|K_1|=0.54°$. No attempt is made here to give exact values for the expected K_1 but it is intended to bring out the sensitivity of this quantity to the shape of the potential and the consequent difficulty of assigning to it a definite value.

According to Feenberg one expects from saturation inequalities the repulsive interaction in the ^3P state to be at least as great as $(1/3)72\ mc^2 e^{-16r^2}$ which leads one to expect $|K_1|>0.25°$ at 2400 kev. According to Table XXII one would expect an effect of about four percent at 15° and of about three percent at 20° for the total scattering. At 1830 kev the expected phase shift should be about 0.63 of 0.25° or 0.16°. One would expect then ~2.7 percent of total scattering at 15° and ~2.2 percent at 20° to be due to the p wave. Table XI shows no consistent evidence of the

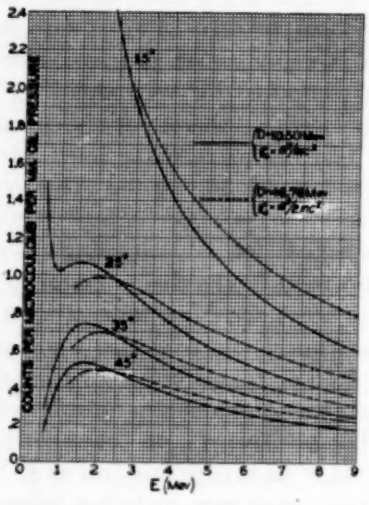

FIG. 14. High energy region. Quantity plotted against energy represents the number of counts per microcoulomb per mm oil pressure that would be expected for the scattering chamber of HKPP at energies up to nine Mev for an s scattering anomaly. Note the pronounced effect of the range of force. Also the definite divergence of the two theoretical curves at $\Theta=20°$ indicating the subordination of Rutherford scattering to the scattering anomaly.

[22] H. M. Taylor, Proc. Roy. Soc. **A134**, 103 (1931).

presence of such an effect. There is no indication of a systematic difference between 20° and 25° scattering which could be considered to be greater than the experimental error. On the other hand, the percentage of scattering expected due to the p wave at 25° should be about one-half of that at 20°. The data at 15° recorded in Table XI should be higher by a few percent than the expected values for a pure s scattering anomaly. There is thus no conclusive evidence from this scattering angle. The average percentage of the difference between observed and computed values taken for 2400, 2105, 1830 kev is 0.5 percent at 20°, 0.4 percent at 25°, 0.1 percent at 30°, 0.2 percent at 35°. From these numbers it appears surprising that the expected effect of ~2 percent at 20° did not appear and it may be that this should be taken as an indication against the customary saturation arguments with exchange forces. The evidence is not strong enough, however, to make a definite conclusion safe since the variations of the percentage differences at the separate energies are just about of the order of magnitude of the expected effects and since the expected effect of $|K_1|$ is sensitive to the shape and range of the potential. For $\alpha=20$ the minimum $|K_1|$ expected from saturation arguments corresponds to a repulsive potential $(85/3)e^{-20r^2}$. The effects expected for this potential are ~0.67 of those used above.

TABLE XXII. *Percentage effect on scattering per $K_1=-1°$. Quantity tabulated is $-100(\Delta\Re)_1/\Re\Delta K_1{}^c$. It represents the slope of $100(\Delta\Re)_1/\Re$ plotted against $-K_1$ which is expressed in degrees.*

$\theta=$	15°	20°	25°	30°	35°	E (MEV)
$-(\Delta\Re)_1/\Delta K_1{}^\circ=$	0.15	0.24	0.29	0.29	0.21	1.83
Percentage =	17	14	7.5	3.5	1.4%	1.83
$-(\Delta\Re)_1/\Delta K_1{}^\circ=$	.18	.27	.33	.33	.24	2.4
Percentage =	16	11	5.5	2.5	1.0%	2.4
$-(\Delta\Re)_1/\Delta K_1{}^\circ=$		.35	.43	.42	.30	4
Percentage =		6.9	3.4	1.5	.6%	4
$-(\Delta\Re)_1/\Delta K_1{}^\circ=$		.49	.61	.60	.43	8
Percentage =		4.5	2.2	1.0	.4%	8

IV. CONCLUDING REMARKS

It is seen from the above attempt to represent the experimental material that the range of force for the customary Gauss error type of potential cannot be taken as large as has been customary. The constant α in $Ae^{-\alpha r^2}$ cannot have the value 16 but must be taken to be about 21. This is approximately the change tried by Rarita and Present. In their work this change of range was indicated by the binding energy of H^3. Their calculations with the potential $Be^{-2r/b}$ in which a corresponding change of range was made give a too low value for the mass of He^4. Analogous but less accurate calculations made by them using the Gauss error potential give also a too low value for this mass. They pointed out that one cannot, therefore, fit the binding energies of H^3 and He^4 consistently using the simple exchange force theories. The degree to which this difficulty may be important has appeared in a different light in the calculations of Margenau and Warren and of Margenau and Tyrrell who have encountered relatively smaller difficulties in fitting the binding energy of H^3 with the Gauss error potential with $\alpha=16$. It is seen from the above analysis that such a fit, interesting as it is, cannot be made consistently with the scattering experiments. It appears likely from their results also that one will have difficulty in fitting the mass defects of both H^3 and He^4. Particularly for the latter a too low energy is expected. It is thus impossible to use fixed interaction potentials of the types assumed in these calculations. It may be that a solution of the problem will be given by a development of the mesotron theories of nuclear interactions.

It should be mentioned, however, that the behavior of phase shift with energy is sensitive to a velocity dependence of the potential. It has been pointed out by Wheller that exchange forces are special cases of a more general class of velocity dependence. It is also obvious from relativistic arguments that fixed exchange or ordinary potentials can only be a first approximation. By introducing a velocity dependence of the potential one can fit the experimental phase shift using a longer range of force. The approximate depths needed are seen in Table XXIII.

The table shows that one needs an approximately uniform increase of depth with energy and that the amount is relatively small. The adjustment is made so as to make the Gauss error potentials give the same phase shifts as the square well $r_0=e^2/mc^2$, $D=10.500$ Mev. The latter approximates the experimental phase shift

curve from 800 to 2400 kev. The increase in depth from 200 to 2600 kev is only 1.6 percent for $\alpha=16$ and 0.7 percent for $\alpha=18$. One can thus try to interpret the results using a range of 2.25×10^{-13} cm ($\alpha=16$) but with a progressive increase in depth of the well amounting to 1.6 percent per 1.2 Mev of the relative kinetic energy of the two protons. The change 1.2 Mev in the relative kinetic energy is ~10 percent of the kinetic energy which the two protons have inside the potential well. The velocity dependence suggested by the experiment is thus of the order of

$$\frac{1.6 \text{ percent}}{10 \text{ percent}} 100 \text{ percent} = 16 \text{ percent}$$

of the change in kinetic energy of relative motion. The depth of the square well potential 11.3 Mev would change on this basis to only roughly 9.5 Mev if the relative energy of the two protons is -10 Mev. If such a velocity dependence were speculatively supposed to show itself also in the ^3S interaction then it is imaginable that the degree of binding in such a nucleus as He^4 will be seriously affected. The sign of the effect does not appear to be immediately obvious since the distribution of relative momenta of the particles is important and this in turn depends on the structure of the nucleus which follows from the assumed interaction. The ^3S interaction may, however, be changing in a direction opposite to that of ^1S. A more careful analysis of this question would be helpful. It is clear, however, that even a relatively slow velocity dependence can affect quite fundamentally the conclusions from the binding energies of light nuclei.

If it is supposed that the ^1S interaction depends on velocity then the difference between the proton-neutron and proton-proton interactions becomes partly explicable. The relative kinetic energy of the two protons is smaller when they are close to each other on account of the Coulomb repulsion. At the boundary of a square well of radius e^2/mc^2 the difference in relative kinetic energy for a proton-neutron and a proton-proton collision of low energy is 0.51 Mev. Inside the square well the difference is larger on account of the increase in Coulomb energy. As a rough approximation one may estimate 0.83 Mev which is the correction for square well depth due to the Coulomb effect. The velocity dependence obtained from $\alpha=16$ would lead one to expect then a decrease of the interaction potential by 0.16×0.83 Mev$=0.13$ Mev. The difference to be accounted for is 0.4 Mev. The effect due to this velocity dependence appears to be too small. It may, nevertheless, be significant that it is of the right order of magnitude and in the right direction. Interactions emphasizing the effect of short distances would increase it.

TABLE XXIII. *Velocity dependence needed to account for the s phase shift.*

E	200	800	1400	2000	2600 KEV	a
A	36.8(7)	36.9(7)	37.1(8)	37.3(0)	37.4(5)	16
A	41.9(0)	41.9(7)	42.0(5)	42.1(3)	42.2(0)	18

The discrepancy between the scattering of fast and slow neutrons may also be connected with a velocity dependence of the forces of a slowly progressive type. An increase in interaction depth with velocity would decrease the scattering cross section for fast neutrons. At 2.8 Mev for incident neutrons the depth of the well could be expected to be increased by ~0.2 Mev which would produce only a very small effect in the right direction on the position of the ^3S level and hence on the scattering. The observed difference of ~17 percent needs presumably a different explanation along the lines of Schwinger's use of $(\boldsymbol{\sigma}_1\mathbf{r})(\boldsymbol{\sigma}_2\mathbf{r})$ types of coupling. These terms are now necessary in view of the experimentally established quadrupole moment of the deuteron and the proton-proton scattering experiments do not appear as yet to throw much light on interactions of this type on account of the predominance of the s wave anomaly.

The s wave anomaly is dissociated from the other phase shifts. The interactions of the $(\boldsymbol{\sigma}_1\mathbf{r})(\boldsymbol{\sigma}_2\mathbf{r})$ type do not couple the ^1S wave to other types of waves. This is a fortunate circumstance for the simplification of the analysis of experimental material but it also has made it impossible so far to relate the proton-proton experiments to the noncentral nature of nuclear forces.

With fixed interaction potentials it is possible in theory to distinguish between wells of different shapes. Shapes of potential wells having considerable extension to larger distances give a relatively small slope for the K_0, E curve at large energies. The curves have as a result a bulge in the central energy range (1400 kev) and cannot be fitted to this range if they are made to agree with experiment at 2400 kev and 800 kev. The relatively good agreement of the square well potential with experiment is presumably due, from this point of view, to the fact that it has no extensions to high energies. The mesotron type of potential appears hopeful in this connection. It will be reported on in another publication.

Summarizing the main results it has been found that: (*a*) There is no consistent evidence for p or d scattering above experimental error. The absence of the p wave is surprising from the point of view of Feenberg's lower limit for the ^3P repulsion but the experimental error is too large to make a definite conclusion safe. (*b*) The s phase shift depends on the energy so rapidly as to indicate a shorter range of force than has been customary to use in calculations with the Gauss error potential. This conclusion holds only if the potential is independent of velocity. A velocity dependence amounting to one-sixth of the change in relative kinetic energy would bring the range of force back to its old value. (*c*) The proton-proton interaction determined from the experiments is definitely smaller than the proton-neutron interaction in the ^1S state. The difference is approximately the same as that obtained by Breit, Condon and Present and by Breit and Stehn using the older observations of Tuve, Heydenburg and Hafstad. The difference is roughly three percent of the whole. This conclusion, however, is subject to modification in case the contribution due to ^3S scattering to the

Appendix

Table of Coulomb functions. The table gives the quantities needed for Eq. (7.8) of BCP.

E in kev	Φ_0^*/Φ_0	$\Phi_0\Theta_0$	$C\sigma^2\rho\Phi_0^2$	Φ_0^*/Φ_0	$\Phi_0\Theta_0$	$C\sigma^2\rho\Phi_0^2$	Φ_0^*/Φ_0	$\Phi_0\Theta_0$	$C\sigma^2\rho\Phi_0^2$	Φ_0^*/Φ_0	$\Phi_0\Theta_0$	$C\sigma^2\rho\Phi_0^2$
	$r=0.5e^2/mc^2$			$r=0.75e^2/mc^2$			$r=e^2/mc^2$			$r=1.25e^2/mc^2$		
200	1.0227	0.9034	0.01957	1.0327	0.8793	0.02997	1.0419	0.8606	0.0409	1.0502	0.8452	0.0522
400	1.0212	.9148	.04215	1.0292	.8946	.06453	1.0356	.8786	.0877	1.0403	.8649	.1115
600	1.0193	.9212	.06158	1.0259	.9017	.0940	1.0293	.8855	.1274	1.0307	.8702	.1614
800	1.0180	.9247	.07865	1.0221	.9053	.1199	1.0231	.8872	.1620	1.0209	.8690	.2045
1000	1.0164	.9269	.0940	1.0186	.9065	.1431	1.0168	.8861	.1927	1.0111	.8641	.2425
1200	1.0148	.9282	.1081	1.0150	.9063	.1642	1.0105	.8829	.2206	1.0012	.8567	.2765
1400	1.0133	.9288	.1211	1.0114	.9051	.1837	1.0040	.8787	.2461	0.9914	.8478	.3074
1600	1.0117	.9290	.13335	1.0080	.9031	.2017	0.9979	.8732	.2695	.9814	.8376	.3355
1800	1.0100	.9288	.1448	1.0044	.9007	.2187	.9914	.8672	.2914	.9714	.8267	.3614
2000	1.0086	.9282	.1557	1.0007	.8978	.2347	.9850	.8606	.3119	.9614	.8151	.3853
2200	1.0068	.9275	.1661	0.9972	.8945	.2497	.9787	.8534	.3309	.9513	.8030	.4074
2400	1.0054	.9265	.1759	.9937	.8909	.2640	.9724	.8459	.3489	.9413	.7904	.4280
2600	1.0037	.9255	.1853	.9900	.8871	.2777	.9659	.8381	.3659	.9312	.7777	.4472
2800	1.0022	.9242	.1944	.9864	.8831	.2907	.9595	.8299	.3820	.9210	.7646	.4652
	$r=1.5e^2/mc^2$			$r=2e^2/mc^2$			$r=2.5e^2/mc^2$			$r=3e^2/mc^2$		
200	1.0578	0.8323	0.0638	1.0702	0.8113	0.0883	1.0796	0.7942	0.1142	1.0858	0.7791	0.1412
400	1.0438	.8522	.1358	1.0456	.8283	.1859	1.0413	.8034	.2369	1.0307	.7757	.2881
600	1.0298	.8547	.1958	1.0207	.8212	.2651	1.0023	.7817	.3333	0.9742	.7350	.3984
800	1.0157	.8493	.2471	0.9956	.8032	.3308	0.9627	.7468	.4100	.9166	.6798	.4817
1000	1.0014	.8392	.2917	.9702	.7796	.3863	.9224	.7058	.4719	.8575	.6187	.5444
1200	0.9871	.8265	.3312	.9444	.7526	.4337	.8815	.6613	.5222	.7970	.5556	.5917
1400	.9728	.8117	.3666	.9184	.7237	.4748	.8405	.6156	.5626	.7352	.4931	.6259
1600	.9584	.7958	.3984	.8925	.6933	.5099	.7978	.5698	.5960	.6714	.4320	.6504
1800	.9440	.7786	.4271	.8659	.6626	.5406	.7550	.5240	.6223	.6066	.3731	.6661
2000	.9293	.7613	.4534	.8391	.6313	.5673	.7113	.4792	.6430	.5396	.3170	.6748
2200	.9146	.7433	.4774	.8121	.6004	.5903	.6667	.4355	.6589	.4712	.2638	.6774
2400	.8998	.7251	.4993	.7849	.5692	.6101	.6214	.3928	.6704	.4007	.2139	.6752
2600	.8849	.7065	.5194	.7574	.5386	.6273	.5755	.3518	.6780	.3280	.1673	.6688
2800	.8702	.6879	.5377	.7293	.5085	.6419	.5282	.3123	.6826	.2520	.1237	.6585

slow neutron scattering cross section is strongly affected by the interaction of ^3S with ^3D as has been pointed out by Schwinger. For a given range the data determine the proton-proton interaction probably to within better than 0.3 percent.

We would like to acknowledge our indebtedness to the two groups of experimenters for their whole hearted cooperation and to Messrs. Share, Hoisington and Kittel for occasional help. We are especially indebted to Professor Herb and Dr. Tuve for many discussions which have helped to clarify the interpretation. Grateful acknowledgment is made also of the financial assistance received from the Wisconsin Alumni Research Foundation, the Carnegie Institution of Washington and the WPA project in natural sciences at the University of Wisconsin.

Note in proof.—According to Lennart Simons [Phys. Rev. **55**, 792 (1939)] $\sigma_{pp}=14.8\times10^{-24}$ cm² so that $\sigma_{th}=59\times10^{-24}$ cm² and $D_{pp}=11.5(2)$ Mev. This differs by only 1.5 percent from $D_{pp}^{c}=11.35$ Mev. Potentials such as the meson potential which are more concentrated at small r may reduce this difference to zero.

JUNE 1, 1939 PHYSICAL REVIEW VOLUME 55

Reflectivities of Evaporated Metal Films in the Near and Far Ultraviolet

GEORGE B. SABINE*
Department of Physics, Cornell University, Ithaca, New York
(Received April 10, 1939)

The reflectivities of evaporated metal films from the visible to 450A have been determined for the following metals: Aluminum, antimony, beryllium, bismuth, cadmium, chromium, copper, gold, iron, lead, magnesium, manganese, molybdenum, nickel, palladium, platinum, silver, tellurium, titanium, zinc and zirconium. Photographic methods were used. From the visible to 2400A, a quartz mercury arc with calibrated wire screens and a quartz prism spectrograph were employed. From 2400A to 450A it was necessary to use a vacuum spectrograph with grating, a discharge tube, and oiled photographic film. The accuracy of the work in the near ultraviolet is of the order of three percent and in the far ultraviolet not better than five percent. Curves of reflectivity against wave-length for these metals are included.

1. INTRODUCTION

THE purpose of this paper is to extend the available information on the reflectivities of evaporated metal films. Most previous work has been confined to the determination of the reflectivities of metals in bulk or of sputtered and electrolytically deposited films. The reflectivities reported here are those which would normally be expected under ordinary laboratory conditions where the mirrors are exposed to air. They do not necessarily give the true reflectivity of the metallic surfaces before contamination by vapors and gases.

2. APPARATUS AND PROCEDURE

The method of evaporation and the equipment used are similar to that described by Williams and Sabine.[1] The metal to be evaporated was placed in a conical helix of fifteen-mil tungsten wire which could be heated by an electric current. In some cases, it was found to be advantageous to wrap two or three inches of the metal to be evaporated, if it were obtainable in wire form, around a short length of twenty-five-mil tungsten wire. This proved to be particularly useful in the case of metals which attack tungsten when molten or which evaporate only at very high temperatures.

The films were deposited on special scratch-free plate glass which had been washed with a strong solution of potassium hydroxide, then with hydrochloric acid, and finally dried in front of a fan with ethyl alcohol. Rubber gloves were worn on the hands and the glass was held

* Now at the Kodak Research Laboratories.

[1] R. C. Williams and G. B. Sabine, Astrophys. J. **77**, 316 (1933).

by a vacuum suction cup attached to a short length of brass rod. This avoided the possibility of getting grease from the fingers on the glass and made the handling of powerful reagents simpler. The cleaning of the glass is very important; it is useless even to attempt to coat a glass surface which water will not wet.

Pumping was continued for at least an hour and a half before evaporation in order to make certain that traces of water vapor and other volatile substances were removed so far as possible. The vacuum obtained was about 10^{-5} mm of mercury as read by a McLeod gauge. Filament currents of from fifteen to twenty-five amperes were used.

In the case of the mirrors prepared for this work, the thickness of the coating was regulated by continuing evaporation until the lighted filament was just visible through the film. Evaporated films will not reflect appreciably more light when made so thick as to be opaque; in fact, it is noticeable in some instances that the surface tends to crackle if the film is very thick. Except in the instances noted below, the mirrors reported on in this paper transmitted less than one percent of visible light as measured with a Weston Photronic cell.

The reflectivities were measured with different apparatus according to the region of the spectrum in which the measurement was to be made. For the region 2400–5000A the radiation from a quartz mercury arc was focused by a quartz-fluorite achromat upon the slit of a Hilger E3 quartz spectrograph and neutral screens (wire screens) of known transmission mounted near the lens were used to calibrate the photographic plate. The precautions pointed out by Harrison[2] in his discussion of near ultraviolet photometry were observed.

The arc was mounted on an arm which could be swung about a pivot to give any angle of incidence. (Approximately 18° was used.) The actual source was a small piece of plane quartz ground to a good diffusing surface on both sides and illuminated by the body of the arc. The enlarged image of this bit of quartz was focused on the slit of the spectrograph. The mirror holder ran in brass ways and was mounted at the hinge around which the arm holding the source rotated. Thus, the length of the light path from source to slit was the same for both the reflected and direct beams. The calibrated filters were inserted in the direct beam as close to the lens focusing light on the slit as possible. Eastman Commercial plates developed in D61a were used.

The plates were reduced in the standard manner on a Moll microphotometer. Characteristic curves were plotted for each wave-length at which the reflectivity was measured and each plate had its own calibration exposures. The accuracy of this work is difficult to estimate because some of the determinations necessarily had to be made on the underexposed heel of the characteristic curve. The error is considered to be of the order of three percent of the indicated reflectivity.

For measurements in the far ultraviolet, quite different apparatus was necessary. A vacuum grating spectrograph accommodating a 150-cm glass grating with 15,000 lines to the inch was used. The relative positions of plate holder and slit were the same as those described by O'Bryan.[3] The slit, the grating rulings, and the spectrum lines were horizontal and the dispersion of the grating was vertical so that the spectra were formed in narrow vertical strips. The film holder, which was semi-cylindrical in shape, could be moved independently of the mirror holder, thus providing for a large number of exposures. Both film and mirror holders could be moved from the outside by means of greased joints and their positions determined by means of pointers and scales.

The calibration exposures were made by swinging the mirror to such a position that its face lay along a plane perpendicularly bisecting the grating, thus permitting the beam from the grating to miss the mirror and be incident on the film. The reflected exposures were made by moving the mirror to the desired angle of incidence (about 18°) and moving the film into such a position that the reflected beam was incident upon it.

The source consisted of a semi-capillary water-jacketed end-on discharge tube. The electrodes

[2] G. R. Harrison, J. Opt. Soc. Am. **18**, 492 (1929).

[3] H. M. O'Bryan, Phys. Rev. **38**, 32 (1931).

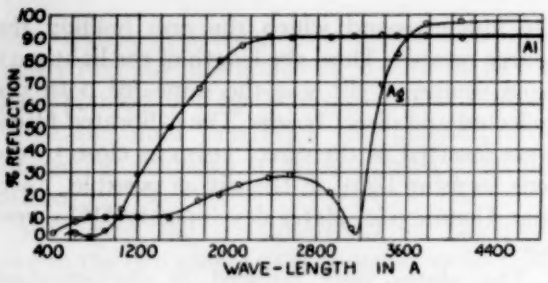

FIG. 1. Reflectivities of silver and aluminum.

were made of brass and were hollow so that they could be internally water cooled; each one was separately cooled with its own water circulating system. The central portion of the discharge tube, consisting of two concentric Pyrex glass tubes between which water was circulated for cooling, was waxed to the electrodes by means of ground joints. The gas used in the source was ordinary air admitted at reduced pressure through a controllable leak. This was found to furnish a satisfactory number of lines at all wave-lengths and to be steady in operation. The excitation was provided by a high potential transformer (about 35,000 volts) with a condenser of 0.005 microfarad capacity across the line and a commercial quenched spark gap in series with the tube.

The method of Harrison and Leighton[4] was followed in the calibration of the film. The constancy of slope of the H and D curves was found to extend to lower wave-lengths than those which they used. Eastman Superspeed film oiled with Cenco pump oil gave satisfactory photometric results. The film was mounted between glass plates and reduced by means of a Moll microphotometer. H and D curves were plotted for each wave-length at which reflectivities were measured and two calibration exposures were made for each exposure time. Two reflected exposures of different times were also made on each film.

The errors in this work may be considerable. The principal ones arise from irregularities of emulsion response because of variations in oil thickness and from fluctuations of intensity in the source. Since reflectivities determined from two different times of exposure differing by a factor of five were in good agreement, it is presumed that reciprocity law failure was not important. In general, it is expected that reflectivities in the wave-length region 2400A to 450A are not accurate to better than five percent of the indicated reflectivity and for reflectivities less than ten percent the error doubtless goes up very rapidly and may approach fifty percent.

The following metals were evaporated and their reflectivities measured in the near and far ultraviolet.

Aluminum

(Figure 1) This metal is easily evaporated and forms very brilliant films which are a gray-blue by transmitted light. The surfaces are rather soft but can be hardened by rubbing gently with absorbent cotton moistened with water. If deposited over chromium and hardened they are extremely resistant to scratching and can be cleaned if care is taken not to rub grit into the film. They do not suffer seriously by aging; indeed, mirrors remeasured after five months were found to retain their reflectivity substantially unimpaired.

The small hump shown in the reflectivity curve of aluminum near 650A is also reported in some unpublished work of H. M. O'Bryan. For wave-lengths shorter than 1200A, aluminum is exceeded as a reflector by several metals.

Silver

(Figure 1) The reflectivity curve shown here for silver is substantially the same in the near ultraviolet as that for chemically deposited films or for the metal in bulk. Silver is easy to evapo-

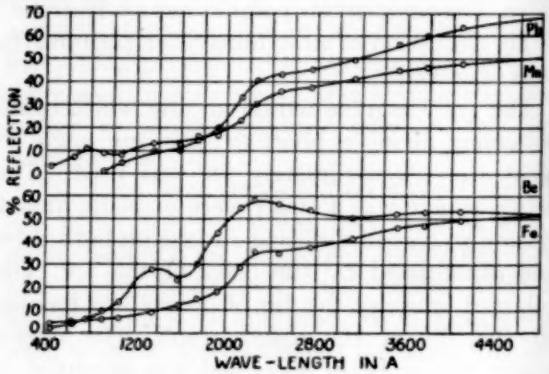

FIG. 2. Reflectivities of lead, manganese, beryllium and iron.

[4] G. R. Harrison and P. A. Leighton, J. Opt. Soc. Am. 20, 313 (1930).

rate and forms very brilliant films which are blue-gray by transmitted light and quite soft. The far ultraviolet reflectivity is definitely better than that for most metals. Unfortunately, it tends to tarnish rather badly.

Lead

(Figure 2) Very low filament temperatures are sufficient to evaporate lead. The deposit is extremely soft, and when first made is very bright. In the course of a week lead mirrors are completely destroyed by the formation of the oxide. When fresh they are brownish by transmitted light.

Manganese

(Figure 2) This metal forms hard bright films which are brownish by transmitted light and resemble chromium. It evaporates without serious difficulty.

Beryllium

(Figure 2) Next to aluminum, beryllium is perhaps the most satisfactory evaporated film. It does not evaporate readily, but with a little care, very good films can be prepared. The sharp minimum in reflectivity near 1600A corresponds roughly to a very deep minimum reported by Gleason[5] although his sputtered mirror was evidently much inferior to the evaporated film. Beryllium films do not tarnish noticeably with age.

Iron

(Figure 2) Iron was evaporated by wrapping a short length of wire around 25-mil tungsten wire. The films are surprisingly brilliant and quite hard. They resist tarnish and even when months old do not show signs of ordinary oxidation.

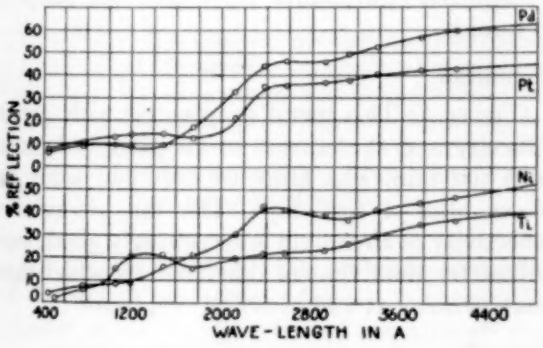

FIG. 3. Reflectivities of palladium, platinum, nickel and titanium.

[5] P. R. Gleason, Proc. Nat. Acad. Sci. **15**, 551 (1929.)

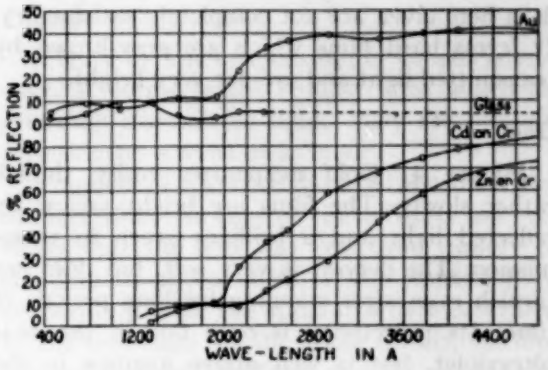

FIG. 4. Reflectivities of gold, glass, cadmium and zinc.

Palladium

(Figure 3) With the exception of platinum, palladium is the best far ultraviolet reflector so far investigated. It is evaporated in the same manner as iron and with this treatment forms very handsome durable films which are moderately hard.

Platinum

(Figure 3) For all work involving reflections at wave-lengths less than 1200A, platinum is the best mirror surface known. The extremely high melting point, however, makes it difficult to evaporate and materially increases the danger of contamination from the tungsten filament. The films are moderately hard, very resistant to tarnish, and quite bright. This film transmitted three percent of incident visible radiation. The reflectivity in the vacuum region is a little lower than that given in some unpublished work of H. M. O'Bryan. Gleason[5] reports a reflectivity at 600A for a sputtered platinum film nearly twice as great as that given here.

Nickel

(Figure 3) As in the case of iron, it is necessary to wrap nickel wire around a 25-mil tungsten filament because it dissolves tungsten very readily. The films are gray by transmitted light and very hard.

Titanium

(Figure 3) Evaporation of titanium is so difficult that it again is a metal for which the

data here given are not completely satisfactory. It forms hard films which are gray-brown by transmitted light and are not very bright.

Gold

(Figure 4) Gold evaporates easily though rather slowly. The films are bright yellow by reflected light and a brilliant green in transmission. The deposit is very soft, but does not tarnish even after standing for long periods of time. Its reflectivity is only fair in the near ultraviolet, but is well above average in the far ultraviolet. Qualitatively, this checks the results of Gleason's[5] work.

Glass

(Figure 4) The sample of glass whose reflectivity curve is shown in the far ultraviolet is ordinary plate glass of index of refraction 1.52. The dashed portion of the curve was taken from Nutting.[6]

Cadmium

(Figure 4) It was found necessary to evaporate cadmium over a previously evaporated film of chromium because it deposits in blotches on a glass surface. It is extremely soft and the mirrors appear brilliant, but have a bad tendency to form a bluish haze over the surface which is particularly noticeable by the light of a mercury arc. It is suspected that the very poor ultraviolet reflectivity of cadmium in the vacuum region is connected with the presence of this haze; zinc, which exhibits the same phenomenon, also has a very poor far ultraviolet reflectivity.

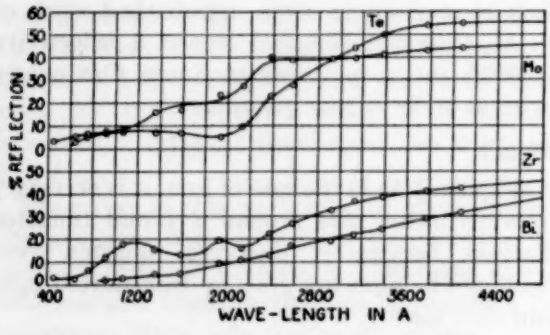

FIG. 5. Reflectivities of tellurium, molybdenum, zirconium and bismuth.

[6] P. G. Nutting, Phys. Rev. **16**, 129 (1903).

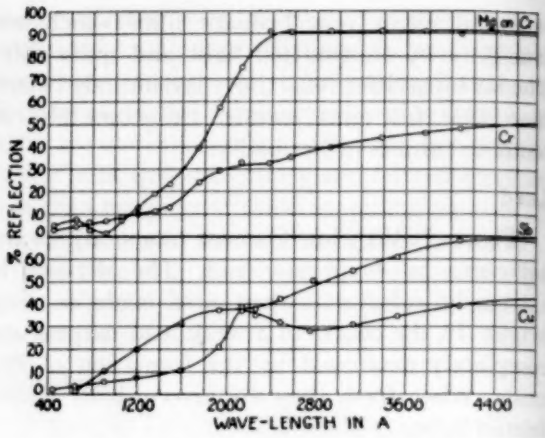

FIG. 6. Reflectivities of magnesium, chromium, antimony and copper.

Zinc

(Figure 4) Many of the remarks made about cadmium are equally true of zinc. It too must be evaporated over a film of chromium, and, as already mentioned, it gives trouble by the formation of a bluish haze sooner or later after it has been removed from the vacuum. Zinc is very soft and lasts well except for the formation of the haze.

Tellurium

(Figure 5) This metal evaporates with great ease. It forms soft bright films which are a brilliant red in transmission.

Molybdenum

(Figure 5) The data for molybdenum are not completely satisfactory because of the great difficulty in evaporating a sufficiently thick layer of the metal. The films are brownish by transmitted light, fairly hard, and not subject to tarnish.

Zirconium

(Figure 5) This metal evaporated with great difficulty and the mirrors so far produced have been too thin. The films are soft and went to pieces after a few days. The far ultraviolet reflectivity of zirconium is surprisingly good, but not better than that of other metals which are more permanent and easier to evaporate.

Bismuth

(Figure 5) Films of bismuth are readily produced, but have a very low reflectivity. The

deposit is pale yellow by reflected light and gray by transmitted light. It is exceedingly soft and loses in reflectivity rapidly when exposed to air.

Magnesium

(Figure 6) Like cadmium and zinc, magnesium must be deposited over a film of chromium. Fresh magnesium surfaces are extremely brilliant and have a very high reflectivity in the near ultraviolet. They tend to tarnish, however, and in the course of a month show definite signs of aging.

Chromium

(Figure 6) This metal forms extremely hard tenacious films which are brown by transmitted light. Its reflectivity is fairly high throughout the near and far ultraviolet. Although it has a tendency when molten to dissolve tungsten, it is not unduly difficult to evaporate.

Antimony

(Figure 6) Films of antimony are very easy to produce, but are exceedingly soft. It is grayish blue by transmitted light and is quite lasting. The reflectivity down to 1200A is fairly good.

Copper

(Figure 6) The evaporation of copper is very easy. It forms bright reddish films which are green by transmitted light. They are soft and tarnish after a week or so in air.

A number of other metals have been attempted unsuccessfully. In general, the difficulty has been either that the film was destroyed rapidly by standing in air, or that it was impossible to evaporate it with the apparatus here described. In the first class fall the alkali metals, calcium, gallium, indium, thallium, and tin, in addition to zinc and cadmium which have been discussed above. The other group consists of cobalt, columbium, iridium, rhodium, silicon, tantalum, uranium, and vanadium.

In conclusion, the author wishes to express his indebtedness to Professor R. C. Gibbs whose constant encouragement and friendly advice have made it possible to bring the work to a conclusion. He is also heavily indebted to Drs. J. E. Ruedy and R. C. Williams for advice in carrying out the evaporation work, and to Dr. H. M. O'Bryan for his generous aid in connection with designing the vacuum spectrograph for determining reflectivities in the far ultraviolet.

JUNE 1, 1939 PHYSICAL REVIEW VOLUME 55

The Magnetoresistance of Nickel in Large Fields

C. W. HEAPS
The Rice Institute, Houston, Texas
(Received April 13, 1939)

The magnetoresistance of a nickel foil has been measured in fields up to 24,000 gauss. A drop of the curves in large fields is found, in disagreement with Alocco's results on similar material, but in agreement with Gerlach's theory that a resistance decrease is produced proportional to the square of the increase of spontaneous magnetization. The constant of proportionality is shown to be dependent on the temperature. It is concluded that spontaneous magnetization may be increased by a magnetic field without saturation appearing, even up to fields of 200,000 gauss as produced by Kapitza.

A FERROMAGNETIC material, unmagnetized in the technical sense, is supposed to consist of randomly oriented domains all magnetized spontaneously to saturation. An external field changes the orientations of these domains and thereby alters the electrical resistance of the material. Furthermore, it appears to be a well established fact that if the spontaneous magnetization of the domains is increased the resistance is decreased. Two obvious ways of changing the spontaneous magnetization consist in (1) varying the temperature of the material,

and (2) varying the strength of a field which is always sufficiently large to maintain technical saturation, or complete alignment of domains.

There is considerable lack of agreement between the various experiments made at room temperature which use method (2) and attempt to detect resistance changes. Some of the earlier experiments[1] on longitudinal magnetoresistance in nickel show a definite maximum followed by a decrease in magnitude of the effect as the field is increased. The cause of this downward drop in the magnetoresistance curve was usually attributed to non-uniformity of field or to a transverse component of magnetization. Later measurements by G. Alocco[2] on thin square films of nickel do not show the drop of the curve. The data collected and shown graphically by McKeehan[3] give no evidence of this effect, perhaps because insufficiently strong fields were used. The results of Potter[4] and of Englert,[5] however, show a decided decrease of longitudinal magnetoresistance in nickel wires as the saturation field is increased.

Since a magnet capable of producing large uniform fields was available it seemed worth while to repeat the experiments with nickel in the form of a thin film as used by Alocco. This film was made by electrodeposition from a nickelous sulphate solution (containing ammonium chloride and boric acid) on to a stainless steel knife blade (kept in continuous rotation) after the manner of Bosworth.[6] A current density of 10 ma/sq. cm was used. The nickel film, about 2.4μ thick, was easily peeled off of the stainless steel with a razor blade. It was uniform and without holes. A section of dimensions 0.90×0.95 cm was cut out, mounted on a flat Bakelite plate, and provided with heavy copper terminals along opposite edges. These terminals were soldered on with Wood's metal.

The specimen was mounted on a holder similar to that used by Jones and Malam so that accurate adjustment of orientation could be made with respect to the magnetic field. For measuring the resistance change a special Wheatstone bridge with low resistances was constructed, and a galvanometer of low resistance and high sensitivity was used.

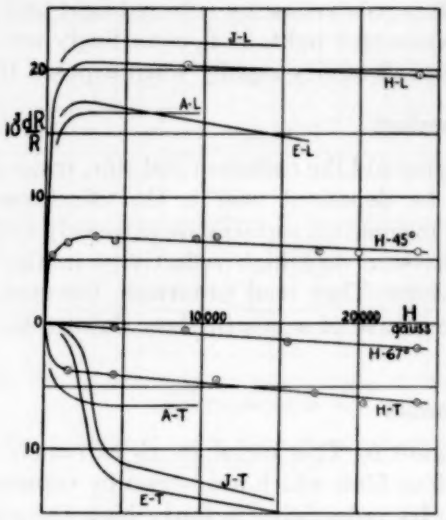

FIG. 1. Magnetoresistance of nickel as a function of magnetic field. Curves from various authors are indicated as follows: *J*, Jones and Malam; *H*, Heaps; *A*, Alocco; *E*, Englert. The letters *L* and *T* indicate longitudinal and transverse fields, respectively.

The magnetic field was supplied by a large water-cooled electromagnet, wound with copper tubing and having a current capacity of 600 amperes. The poles were 18.7 cm in diameter and 1.9 cm apart. For large fields there was approximately a 0.2 percent difference in field strengths between a point centered between the pole faces and a point halfway out along a radius of a pole. The field was therefore very uniform over the specimen which was placed at the central position.

In Fig. 1 are plotted the results obtained for various orientations of the specimen; also curves obtained by other experimenters are given. The two points on the down-sloping curve *H–L* were determined with considerable care, the specimen being oriented so as to produce a maximum value of dR/R. The second point was determined by making repeated measurements of the resistance change produced when the magnetic field was varied over the range between the two points.

It appears from the present experiments that for all orientations of the specimen there is produced approximately the same decrease of

[1] E. A. Owen, Phil. Mag. **21**, 122 (1911); C. W. Heaps, Phil. Mag. **22**, 900 (1911); W. Jones and J. E. Malam, Phil. Mag. **27**, 649 (1914).
[2] G. Alocco, N. Cimento **10**, 153 (1933).
[3] L. W. McKeehan, Phys. Rev. **36**, 948 (1930).
[4] H. H. Potter, Proc. Roy. Soc. **132**, 560 (1931).
[5] E. Englert, Ann. d. Physik **14**, 589 (1932).
[6] R. C. L. Bosworth, Trans. Faraday Soc. **30**, 549 (1934).

resistance by a given increase of the magnetic field beyond the saturation value. This conclusion is in general agreement with the results obtained by Englert, but Englert's data indicate a larger effect than is found in the present experiments. It is not clear why Alocco failed to find a drop in his curve for large fields; his curves are definitely at variance with those of other experimenters in this respect.

As regards the relative magnitudes of magnetoresistance found by different observers Fig. 1 indicates considerable diversity. It appears probable that polycrystalline material as used by different experimenters is widely different with respect to preferred orientations of crystallites. Kaya's results[7] on single crystals indicate, especially for the transverse effect, that magnetoresistance is decidedly sensitive to crystalline orientation.

It is interesting to note that the curve H–T of Fig. 1, if continued as a straight line up to fields of 200,000 gauss, gives the value of dR/R as found experimentally by Kapitza[8] in this field. Kapitza's results are not sufficiently accurate in themselves to detect a small slope such as that of H–T. Taken in conjunction with the curve H–T, however, Kapitza's data show that even in fields up to 200,000 gauss there is still no evidence of saturation of the spontaneous magnetization.

The work of Gerlach[9] and his collaborators, and of Potter, indicates that the change of resistance is proportional to the change in the square of the intensity of magnetization. Accordingly we may write $dR/R=aI^2$, where a is a constant and I is the specific intensity of spontaneous magnetization. From this equation we get $d(dR/R)/dH=ad(I^2)/dH$. The value of the left-hand side of this equation may be calculated from the drop of the H–L curve in Fig. 1. The work of Weiss and Forrer[10] on nickel gives $d(I^2)/dH=2.9\times10^{-3}$. Accordingly a is calculated to be -1.75×10^{-5}.

Suppose now that the spontaneous magnetization is reduced to zero by heating the nickel to a temperature above the Curie point. There will then be an increase of resistance given by the first of the above equations, this increase being superposed on any increase arising from the ordinary temperature coefficient. Gerlach and Schneiderhan[11] have determined the resistance-temperature curve of nickel through the Curie point, and find the resistance decrease (which arises from the disappearance of spontaneous magnetization of domains) to be accurately proportional to the square of the intensity of spontaneous magnetization. Their results give $a=-1.7\times10^{-4}$.

The discrepancy between these two values of a, obtained by the different methods, is large. A factor of 10 is not likely to be due to differences in the purity of the specimens used in the different experiments. If the constant a were independent of the temperature T we would have

$$\frac{d}{dT}\left[\frac{d}{dH}\left(\frac{dR}{R}\right)\right]=a\frac{d}{dT}\left[\frac{d(I^2)}{dH}\right].$$

From the work of Gerlach and Schneiderhan the value of the left-hand side of this equation may be calculated over the range 325° to 340°C. The data of Weiss and Forrer enable the value of the differential factor on the right-hand side to be calculated. As determined in this way a is found to decrease from -2.1×10^{-3} at 340° to -4.9×10^{-4} at 325°. Apparently, therefore, a depends upon the temperature, and the two methods used above for determining a cannot be expected to give the same result.

In summary it may be said that spontaneous magnetization is increased by an increase of a large magnetic field, and the resulting resistance decrease shows no saturation effect in the largest fields so far obtained in the laboratory. There is no satisfactory theory as to why the resistance decrease should be proportional to the square of the spontaneous magnetization. However, the constant of proportionality appears to be a function of the temperature, so that a given change of spontaneous magnetization, made at a high temperature, has a larger effect on the electrical resistance than the same change made at a lower temperature.

[7] S. Kaya, Science Reports Tohoku Imp. Univ. **17**, 1027 (1928).
[8] P. Kapitza, Proc. Roy. Soc. **123**, 334 (1929).
[9] W. Gerlach, Physik. Zeits. **33**, 953 (1932).
[10] P. Weiss and R. Forrer, Ann. de physique **5**, 153 (1926).
[11] W. Gerlach and K. Schneiderhan, Ann. d. Physik **6**, 772 (1930).

L_{III} Absorption of Iodine, Barium and Some Compounds of Barium*

EDWARD H. GREEN
Pupin Laboratories, Columbia University, New York, New York

(Received February 6, 1939)

The L_{III} absorption limits of solid I_2, metallic Ba, BaI_2, $Ba(OH)_2$, $BaBr_2$, BaH_2, $Ba(NO_3)_2$, BaO_2 and BaF_2 were examined with a two-crystal spectrometer. No secondary structure was detected in the I_2 limit. A very prominent absorption line was observed in the case of Ba and each of its compounds, and was in general more prominent in the compounds than in the pure element. In some of the compounds more or less pronounced secondary structure was observed, notably in the case of BaF_2. Pairs of curves were obtained showing the changes in this respect as the pure Ba absorbers were allowed to change in air to $Ba(OH)_2$. It is concluded that the L_{III} level of Ba is no wider than 4.06 volts. The ratio $r(III, M)$ is measured as 2.30 for Ba.

INTRODUCTION

THIS investigation was undertaken for the purpose of obtaining estimates of the L_{III}-level widths of some elements of intermediate atomic number. The two alternative methods of computing the level width from the observed variation of absorption coefficient with wavelength are justified as follows:

Richtmyer, Barnes and Ramberg[1] have presented the view that an observed x-ray absorption limit is the sum of a series of more or less evenly spaced absorption lines of uniform width and amplitude, the series terminating sharply at the center of the observed limit. The width of the energy level from which the electron was ejected would then equal the full width at half-maximum of any one of the absorption lines. In the case of an absorption limit whose contour is uncomplicated by the presence of secondary structures the *level width* is shown to be equal to the difference in abscissas of two points (A and B, Fig. 1) whose ordinates are $\frac{1}{4}$ and $\frac{3}{4}$, respectively, of the difference in ordinates between top and bottom of the curve (first method of measurement). Fig. 1 is patterned after the illustration offered by Richtmyer, Barnes and Ramberg. The dotted line is the sum of the continuum of absorption lines.

If, as shown in Fig. 1, there exists a narrow range of absorption lines of extreme prominence, there will be superimposed on the normal observed limit an "absorption white line" whose half-width may be taken to indicate at least the upper limit of the value of the level width. Such a result may be expected particularly in the case of an element like barium (56), because a new electron shell starts to be built up in the next element, lanthanum (57). Since the removal of the L_{III} electron of barium leaves the effective nuclear charge approximately 57 as far as the outer electrons are concerned, and since the most probable electron configuration in this case is that of lanthanum, there is evidently a strong probability that the ejected electron will occupy the completely empty $5d$ ($O_{IV, V}$) shell. Further, the transition is a permitted one. In emission it gives rise to the $L\beta_5$ line of La. The expected variation of absorption coefficient with wavelength in this case is represented by the full line in Fig. 1.

Richtmyer and Parratt[2] have reported measurements on this sort of absorption line superposed on the argon K limit.

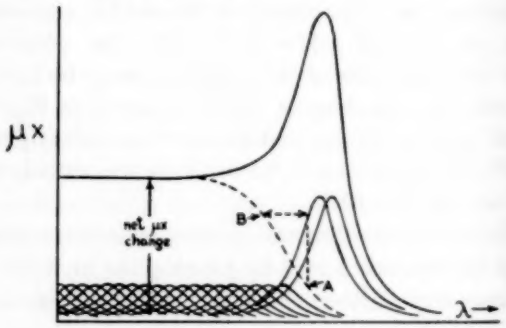

FIG. 1. X-ray absorption limit viewed as the sum of a series of absorption lines (after Richtmyer, Barnes and Ramberg).

* Publication assisted by the Ernest Kempton Adams Fund for Physical Research of Columbia University.

[1] F. K. Richtmyer, S. W. Barnes and E. G. Ramberg, Phys. Rev. **46**, 843 (1934).

[2] F. K. Richtmyer and L. G. Parratt, Phys. Rev. **53**, 678(A) (1938).

The observed absorption line, being the sum of several symmetrical curves and an asymmetrically disposed continuum of symmetrical curves, may be expected to be steeper on its long wave-length side. In the absence of independent information concerning the true shape of either the line or the edge, the measurement of the line's full width at half-maximum may be best approximated by measuring the half-maximum width of the steeper slope alone, and doubling this quantity. The smaller the difference in slope of the two sides, the greater will be the certainty of identification of the peak of the observed curve with the peak of the absorption line, and the smaller will be the error inherent in this second mode of measurement.

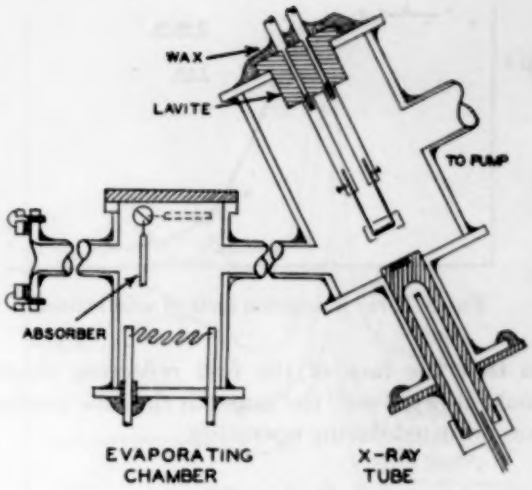

FIG. 2. Diagram of x-ray tube and evaporating chamber.

APPARATUS

The two-crystal spectrometer used in this investigation was of the "universal" form devised by Spencer.[3] The path of the x-ray beam was enclosed by gas-tight metal tubes and rubber diaphragms. Before each run the system was flushed out with hydrogen, and a continuous stream of the gas was maintained throughout the run. The entrance and exit windows of the hydrogen path were of thin Cellophane.

After reflection from the calcite crystals the beam of x-rays entered the Cellophane window of the ionization chamber and was absorbed in a 10-cm column of methyl bromide vapor. Immediately behind the entrance window was a sheet of very thin aluminum foil, maintained at the same potential as the chamber wall (45 volts), to prevent the diffusion of ions to the window. The ion current was detected by means of an FP-54 amplifier, operating at 2000 mm/volt sensitivity, with its control grid "floating." Because of the use of low filament current and potentials somewhat different from the manufacturer's recommended ones, the internal grid current was held to values so low that fluctuations in this quantity were negligible. The x-ray ionization current was usually between 15 and 30 times as great as the internal current.

The x-ray tube, Fig. 2, was made of brass sections, soldered together. It was fitted with a tungsten-button water-cooled target. Additional water cooling was required at the wall of the tube, for the protection of the soldered joints. The anode assembly was readily removable for cleaning the target. The filament consisted of a 1-cm long helix of 10-mil tungsten wire, mounted within a molybdenum focusing cup, and held in place by set-screws. The cathode system was insulated from the grounded tube and anode by means of a waxed-over plug of lavite. Filament power was drawn from the 60-cycle line by way of a Raytheon voltage regulator. The emission current was usually 200 milliamperes.

The voltage across the tube was maintained at less than 10 kv, to prevent the presence of a second-order spectrum at the first-order wavelengths under study. The tube was evacuated by means of a glass-oil vapor pump, backed by a Hyvac. A vapor freeze-out was inserted between pump and tube. Dry ice in alcohol was satisfactory as a refrigerant.

The exit window of the x-ray tube was of Cellophane, clamped between two brass rings, with a soft-rubber gasket so placed that it could force the Cellophane into intimate contact with the ring that was part of the x-ray tube. The distance from window to target was about 40 cm, to minimize failure of the Cellophane window from bombardment by electrons scattered from the target.

The pump, trap, tube and barium evaporating chamber were assembled as a rigid unit, and mounted on a cart resting on a circular track,

[3] R. C. Spencer, Phys. Rev. **38**, 618 (1931).

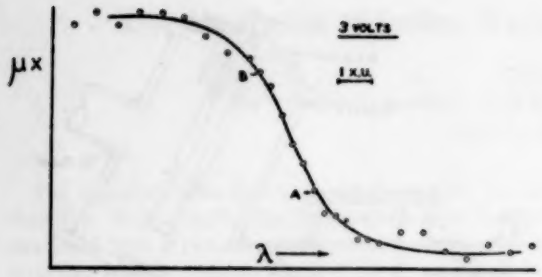

FIG. 3. X-ray absorption limit of solid iodine.

so that the face of the first reflecting crystal could always "see" the target as the tube position was adjusted during operation.

ABSORPTION SCREENS

Solid iodine screens were formed by spraying an ether solution of iodine toward a Cellophane sheet held about six inches away from the nozzle of the atomizer. The iodine landed in the form of small, damp particles. Another Cellophane sheet, backed by a rubber gasket, was clamped against this, so that an air-tight, wax-free, and metal-free space was formed for the confinement of the iodine and its vapor. Screens of this sort were oscillated in the x-ray beam near the ionization chamber. Seven different iodine screens were used.

Screens of BaO_2, $BaI_2 \cdot 2H_2O$, BaF_2 and $Ba(NO_3)_2$ were painted on cigarette paper from suspension in acetone. $BaBr_2 \cdot 2H_2O$ was applied from solution in water. $BaBr_2$ was produced by dehydrating the $BaBr_2 \cdot 2H_2O$ screen at 160°C and thereafter keeping it inside the x-ray tube, and manipulating it in the same manner as the barium described below.

Attempts to form metallic barium absorption screens sandwiched between protecting films of aluminum were abandoned because of the doubtful purity of the concealed barium after the "sandwich" had been exposed to air. An evaporating chamber was then mounted on the x-ray tube itself. In this, lumps of clean barium rested on a tungsten filament that had been cleaned electrolytically. A few fragments of dry ice, dropped into the chamber just before the insertion of the barium, formed a protecting atmosphere of CO_2, until the pump could remove the air from the system. The barium vapor was condensed on a sheet of glass 4 or 5 microns thick, mounted with wax on a ring which could be manipulated from outside, so that readings could be taken alternately, with and without the screen in place. A glass cover ground to fit the chamber permitted observation of the evaporating process.

Each run on barium metal required the formation of a new screen. Though completely opaque in the metal form, these evaporated sheets were thin enough so that the admission of a small amount of air would cause a sudden change to translucent whiteness, usually accompanied by more or less flaking of the screen away from its thin glass backing. After each run the pumps were shut down, and the slow leakage of air into the x-ray tube in the course of the ensuing hours would cause the formation of the white hydroxide, frequently without flaking.

A barium hydride screen was formed by the admission of dry hydrogen, to about 5 mm pressure, to a freshly formed barium screen. In this case the freeze-out was kept constantly replenished with dry ice to prevent the formation of a hydroxide screen. At the end of about four hours of slow change, the screen had become quite transparent (not white). The absorption curve was identical with that for metallic barium. After subsequent exposure to the "natural leakage" of the x-ray tube in the absence of the freeze-out, the screen became white, and the absorption curve changed to the usual $Ba(OH)_2$ curve. One other BaH_2 screen was formed, and a run was made with it, but all subsequent attempts failed because of flaking at some stage or other of the sequence.

It is to be noted that two of the pure-metal absorbers with which runs were made were transformed without mishap into $Ba(OH)_2$. Measurements were then made on them in this form. Similarly, one of the two successful BaH_2 screens was studied both before and after its transformation to $Ba(OH)_2$.

TABLE I. *Width of the L_{III} level of solid iodine.*

UNCORRECTED WIDTH	CORRECTED WIDTH
$W_0 = 3.0 \pm 0.1$ v $= 1.79 \pm 0.06$ x.u.	$W_T = W_0 - 0.20 - 0.04$ $= 2.8 \pm 0.1$ v $= 1.67 \pm 0.06$ x.u.

Results

Iodine

Seven runs, each on a different screen, were made with solid iodine (53). The observed limit shows (Fig. 3) no absorption lines. The width of the iodine L_{III} level is indicated in Fig. 3 as the difference in abscissas of the points A and B, corresponding to the points A and B of Fig. 1. Within the limits of the available precision, the

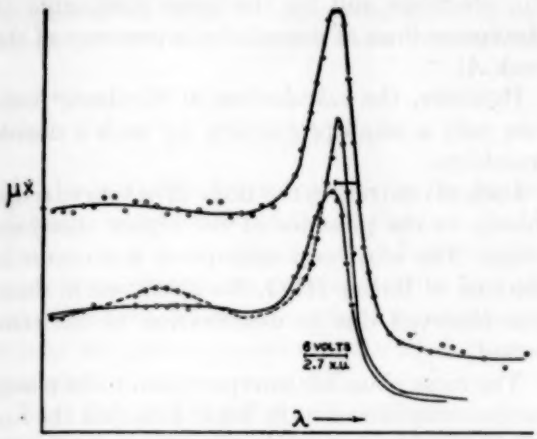

FIG. 4. X-ray absorption limit of metallic barium (full curves) and of barium hydroxide (partly dotted curve). To avoid confusion some of the observed points have been omitted. The two full curves differ in appearance only because of the different thicknesses of the respective metal films.

width measured in this way is the same as half the base of the right triangle whose hypotenuse is the tangent to the curve at its point of greatest slope and whose altitude is the net change of μx (Fig. 1).

The first column in Table I gives the mean uncorrected width of iodine L_{III}. The precision

TABLE II. *Barium L_{III} width of main absorption line.*

Substance	Uncorrected Width W_0 (Volts)	Uncorrected Width X.U.	Corrected Width $W_T = W_0 - 0.26 - 0.03$ (Volts)	Corrected Width X.U.
Ba	6.50±0.25	2.92±0.11	6.21±0.25	2.79±0.11
BaH_2	6.23±0.2	2.80±0.09	5.94±0.2	2.66±0.09
$Ba(OH)_2$	5.02±0.22	2.26±0.1	4.73±0.22	2.12±0.1
BaF_2	5.90±0.33	2.64±0.15	5.61±0.33	2.52±0.15
BaO_2	5.62±0.29	2.52±0.13	5.33±0.29	2.39±0.13
$Ba(NO_3)_2$	4.92±0.11	2.21±0.05	4.63±0.1	2.08±0.05
$BaBr_2 \cdot 2H_2O$	4.35±0.13	1.95±0.07	4.06±0.13	1.82±0.07
$BaI_2 \cdot 2H_2O$	5.10±0.2	2.29±0.09	4.81±0.2	2.16±0.09

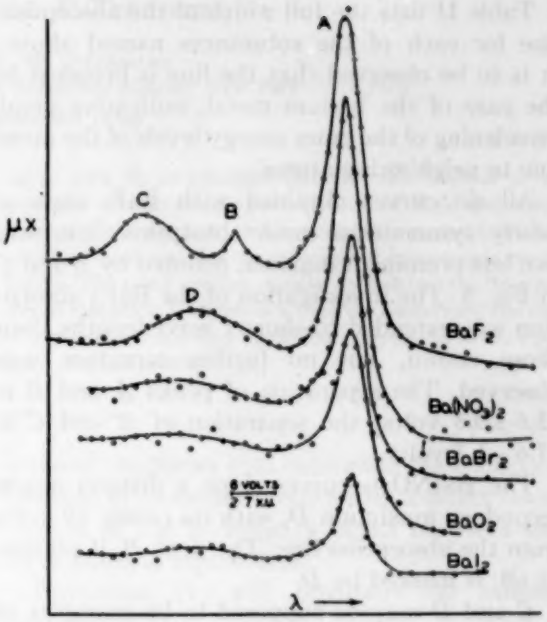

FIG. 5. Typical x-ray absorption curves for various barium compounds.

measure is calculated from the seven separate results in the usual way. The correction used for the (1, −1) rocking-curve width of 12 seconds is that suggested by Parratt.[4] It amounts to 0.2 volt. The correction for vertical divergence is also indicated.

Barium

Figure 4 (full curves) shows typical runs on solid barium. The measured half-width at half-maximum is indicated. Fig. 4 also shows the curve for the same screen that gave the lower of the barium metal curves after its transformation to $Ba(OH)_2$ (partly dotted curve). The two curves exhibit directly the effect of chemical combination. The two noteworthy facts are (1) the absorption line is considerably more prominent in the compound than in the pure metal, and (2) a smaller absorption maximum has made its appearance in the compound.

The same relative appearance was observed in the second Ba, $Ba(OH)_2$ combination, and in the BaH_2, $Ba(OH)_2$ combination.

Figure 5 shows typical curves for BaF_2, $BaBr_2$, $BaI_2 \cdot 2H_2O$, BaO_2 and $Ba(NO_3)_2$. BaH_2 is omitted from this group, as its absorption curve differs in no perceptible way from that of Ba.

Table II lists the full width of the absorption line for each of the substances named above. It is to be observed that the line is broadest in the case of the barium metal, indicating great broadening of the outer energy levels of the atom due to neighboring atoms.

All six curves obtained with BaF_2 show a nearly symmetrical main absorption line, and two less prominent maxima, denoted by B and C in Fig. 5. The investigation of the BaF_2 absorption was extended to shorter wave-lengths than those shown, but no further structure was observed. The separation of peaks A and B is 15.6 ± 0.5 volts; the separation of A and C is 27.6 ± 1.5 volts.

The $Ba(NO_3)_2$ curves show a distinct single secondary maximum D, with its center 19 volts from the absorption line. The peak B, if present at all, is masked by D.

C and D may be supposed to be examples of the secondary structure discussed by Kronig.[5] According to his theory, the separation of the secondary structure from the main edge is inversely proportional to the square of the lattice constant, in the case of similar crystal lattices. Now, both BaF_2 and $Ba(NO_3)_2$ form cubic crystals, the former with lattice constant $a=6.2$A, and the latter with $a=8.1$A. Qualitatively, it is readily seen in Fig. 5 that the larger separation occurs in the crystal of smaller lattice constant. Since the position of the main absorption *edge* is uncertain in these curves, quantitative comparison is not possible.

The peak B is possibly due to the following process: If the L_{III} electron is carried to the $O_{IV,V}$ shell (of lanthanum (57)) and simultaneously one of the six $O_{II,III}$ electrons is removed to infinity, another absorption line should appear, separated in voltage from the main one by an amount equal to the energy of binding of the $O_{II,III}$ electron. This is listed in Siegbahn's *Spektroskopie der Röntgenstrahlen* as $\nu/R=0.9$. The observed 15.6 volts corresponds to $\nu/R=1.15$. Since no considerable *absolute* accuracy is claimed for the spectroscopic difference-value of 0.9, this may be considered to be good agreement.

This explanation is further supported by the interesting observation that the peak B, in all six BaF_2 curves, is slightly steeper on its long wave-length side, and does not descend to as low a μx-value on its short wave-length side as on its long wave-length side. Its shape is determined by the energy distribution of the ionizing L_{III} electrons and by the same continuum of absorption lines as caused the asymmetry of the peak A.

However, the calculations of Pincherle[6] indicate only a small probability for such a double transition.

Lack of contrast in the $BaI_2\cdot 2H_2O$ curve is due merely to the presence of the highly absorbing iodine. The narrowest absorption line occurs in the case of $BaBr_2\cdot 2H_2O$. No alteration in shape was observed due to dehydration of the compound.

The most plausible interpretation to be placed on the array of widths in Table II is that the L_{III} level of barium is *no wider* than 4.06 ± 0.13 volts, and that the broadening of the $O_{IV,V}$ level due to neighboring atoms is *at least* $6.21-4.06=2.15\pm0.3$ volts in the case of metallic barium.

The ratio of μx at the short wave-length and long wave-length sides of the L_{III} edge is usually denoted by $r(\text{III}, M)$. It was given by Küstner[7] from data obtained by Nishina[8] as 3.06 for barium. Fifteen of the curves here discussed were suitable for a calculation of $r(\text{III}, M)$. The mean of these values is

$$r(\text{III}, M)=2.30\pm0.10.$$

This is about the same value as has been obtained by others for the heavier elements.[7, 9]

In conclusion, the author expresses his thanks to Professor Bergen Davis for his encouragement of this investigation.

[5] R. de L. Kronig, Zeits. f. Physik **70**, 317 (1931); **75**, 191 (1932).

[6] L. Pincherle, N. Cimento **14**, 185 (1937).

[7] Küstner, Physik. Zeits. **33**, 46 (1932).

[8] T. Nishina, Phil. Mag. **49**, 521 (1925).

[9] F. M. Uber and C. G. Patten, Phys. Rev. **42**, 229 (1932).

A New Proof of the *H* Theorem

O. HALPERN AND F. W. DOERMANN
Department of Physics, New York University, University Heights, New York, New York

(Received September 29, 1938)

Boltzmann's *H* theorem is here given a new proof based upon the properties of the probability coefficients that determine the transitions between different states of the total system or of any part of the system. The customary assumption is made that the frequency of these transitions is proportional to the population of the initial state, and the solutions of the equations determining statistical equilibrium are then fully discussed. These solutions either agree with those obtained directly with the aid of the principle of microscopic reversibility, or they divide into mutually independent and noncombining groups each of which in itself satisfies the principle of microscopic reversibility. The proof applies equally to Boltzmann, Bose and Fermi statistics. It involves a theorem concerning the rank of a matrix formed from coefficients appearing in the equations of equilibrium.

I. INTRODUCTION

IT IS our intention to present in the present paper a new proof of the *H* theorem, and to discuss, as well, certain aspects that arise in this connection. Before we proceed to this formulation, however, it seems in order for us to discuss briefly the present position of the *H* theorem in statistics.

For the maintenance of equilibrium in a statistical ensemble it is obviously necessary that the number of particles leaving a definite state per unit time shall be equal to the number of particles entering that state.[1] Thus in the simple case of a classical ideal gas one can write the conditions of equilibrium in the form:

$$\sum_{l,\,m}(A_{ik}{}^{lm}n_in_k-A_{lm}{}^{ik}n_ln_m)=0, \qquad (1)$$

where n_i denotes the average population of the ith state and $A_{ik}{}^{lm}$ is the probability coefficient that characterizes the transition from the initial states i, k to the final states l, m. In classical as well as in quantum statistics these coefficients obey the following relations:

$$A_{ik}{}^{lm}=A_{ki}{}^{lm}=A_{ik}{}^{ml}=A_{lm}{}^{ik}. \qquad (2)$$

Of these relations the first and second obviously follow from the identity of the molecules that constitute the gas. The third, on the other hand, which is of a special dynamical nature, holds true in classical statistics because of the properties of the forces that determine the transition, whereas in quantum physics it is a direct consequence of the hermiticity of all matrices that have physical significance.

Equations (1) will obviously be satisfied provided

$$n_in_k=n_ln_m; \qquad (3)$$

other solutions may, however, conceivably exist. If these relations (3) hold true, microscopic reversibility or detailed balancing is said to obtain; and it was these relations which Boltzmann was able to prove for the special type of interaction consisting of the collision of elastic hard spheres. Boltzmann's method of proof was to show that the well-known function

$$H=\Sigma n_i\log n_i$$

will be constant with the time only in case (3) hold, i.e., for microscopic reversibility. By an almost obvious adaptation of this line of reasoning Boltzmann's result was later so extended as to cover both the case of arbitrary $A_{ik}{}^{lm}$ (which, of course, still satisfy relations (2)) and the cases of Bose and Fermi statistics as well. These latter types of statistics can be described by an analogous formalism which involves only a slight alteration in the expression for the elementary transition probability. In place of $A_{ik}{}^{lm}n_in_k$ one has merely to write

$$A_{ik}{}^{l\cdot m}n_in_k(1\pm n_l)(1\pm n_m), \qquad (4)$$

where the upper and lower algebraic signs correspond to the Bose and Fermi statistics, respectively. Microscopic reversibility will then

[1] Here, as in the rest of the paper, we shall always talk about discrete states of unit weight. This means no restriction of generality, since the number of states can be assumed to be arbitrarily large, so as to include in the description classical as well as quantum statistics.

obtain provided, in place of (3),

$$n_i n_k(1\pm n_l)(1\pm n_m)=n_l n_m(1\pm n_i)(1\pm n_k). \quad (5)$$

From the point of view of a purely kinetic theory, however, this well established use of the H function to prove microscopic reversibility seems slightly artificial; for the H function (notwithstanding its extraordinary historical importance) appears to be somewhat of a relic of thermodynamical concepts. It is therefore highly interesting that—starting from the properties of the probability coefficients alone—we are able by purely mathematical reasoning to prove that relations (3) or (5) are unique provided the coefficients have not very exceptional values that are then immediately capable of a very simple *physical interpretation*. The results of the H theorem will in this way be given in a considerably generalized and detailed form.

II. Proof of the Extended H Theorem

In order that we may obtain a compact formulation of the extended theorem and our proof of it, we shall find it convenient to introduce the term "complex," by which we shall understand a special group of particles, which is able to undergo a transition from an initial to a final state. A complex may, for example, consist of two molecules, each in a specified state, which can by collision pass into other final states; or it may consist of the entire system which, because of the presence of internal forces, is able to pass from one state to another. These two cases constitute only illustrative examples for possible complexes. Our use here of the words "state" and "transition" will be discussed more fully at the end of this section.

Employing the previous assumptions, we can now easily write down the equations that determine the rate of change of the number of certain complexes. Discussing first the complex that consists of two molecules, we take for the rate at which complexes i, k pass over into complexes l, m the simple general expression

$$A_{ik}{}^{lm}n_i n_k(1+\alpha n_l)(1+\alpha n_m), \quad (6)$$

where α takes on the values $+1$, 0, -1 for Bose, Boltzmann and Fermi statistics, respectively. In order that equilibrium be maintained it is necessary for the complexes to reappear at the same rate at which they disappear, and this leads at once to the equations

$$\sum_{l,\,m}[A_{ik}{}^{lm}n_i n_k(1+\alpha n_l)(1+\alpha n_m) - A_{lm}{}^{ik}n_l n_m(1+\alpha n_i)(1+\alpha n_k)]=0. \quad (7)$$

In the second case, in which the complex consists of the entire system, Eq. (7) will appear considerably simplified, since we no longer have to distinguish between the different types of statistics. We now simply have[2]

$$\sum_s(A_r{}^s n_r - A_s{}^r n_s)=0. \quad (8)$$

Turning first to Eqs. (8), we observe that they constitute a system of linear homogeneous equations in the variables n_r which may be written in the conventional form

$$\sum_{s=1}^{N} a_{rs}n_s=0, \quad (9)$$

with

$$a_{rs}=(\sum_{t=1}^{N}A_r{}^t)\delta_{rs}-A_s{}^r \quad (10)$$

and with discrete states now enumerated from 1 to N. From (10) together with the properties of the probability coefficients $A_r{}^s$ it may at once be seen that the coefficients a_{rs} enjoy the remarkable properties:

$$a_{rr}>0; \quad a_{rs}=a_{sr}\leqq 0 \quad (r\neq s), \quad (11)$$

$$\sum_{s=1}^{N}a_{rs}=0. \quad (12)$$

We shall find it convenient to denote the Nth order square matrix of the a_{rs} by $\mathbf{A}^{(N)}$ and its determinant by $A^{(N)}$. That $A^{(N)}=0$ and that Eqs. (9) have as a solution

$$n_1=n_2=\cdots=n_N \quad (13)$$

is a trivial consequence of (12). This solution (13) will, however, then and only then be *unique* provided the matrix $\mathbf{A}^{(N)}$ is of rank $N-1$. The

[2] It will probably be understood without explicit mention that a single index stands in general for a group of as many indices as are necessary to give the complex unit weight.

possibility that $\mathbf{A}^{(N)}$ have a rank inferior to $N-1$ must therefore also be taken into account and this we shall do as soon as we have brought (7) into a form which allows an analogous treatment.

We first form the product

$$\Pi=\prod_{i=1}^{\nu}(1+\alpha n_i) \tag{14}$$

over the ν states that one molecule can occupy, and then divide through all Eqs. (7) by Π. (In the case of Boltzmann statistics $\alpha=0$ and this step is superfluous.) By a change of notation we may then write Eqs. (7) in the form

$$\sum_{i,\,m=1}^{\nu}(B_{ik}{}^{lm}p_{ik}-B_{lm}{}^{ik}p_{lm}), \tag{15}$$

where

$$p_{ik}=n_in_k/[(1+\alpha n_i)(1+\alpha n_k)] \tag{16}$$

and

$$B_{ik}{}^{lm}=A_{ik}{}^{lm}(1+\alpha n_i)(1+\alpha n_k)\times(1+\alpha n_l)(1+\alpha n_m)/\Pi. \tag{17}$$

Finally, by replacing the group of two indices by a single index which runs from 1 to $N=\nu^2$ and by introducing new coefficients defined in analogy with (10), we may write (15) in the form

$$\sum_{s=1}^{N}a_{rs}p_s=0. \tag{18}$$

Except in the case of Boltzmann statistics Eqs. (18) differ from Eqs. (9) in that the a_{rs} and the p_r are not now independent, since both depend upon the variables n_i. It might thus appear that Eqs. (18) would possess more solutions than if the a_{rs} were constant. That this is *not* the fact, so that we may always look upon (18) as a system of linear equations in the p_r, results essentially from the determinative circumstance that, despite their dependence on the n_i, the a_{rs} *still satisfy* relations (11) and (12). We shall for the present treat (18) as linear, postponing briefly the complete explanation.

As a direct result of (12) Eqs. (18) always have as a solution

$$p_1=p_2=\cdots=p_N, \tag{19}$$

which stands in direct analogy to (13) and leads at once to (3) or (5). Relations (13) and (19) already express, therefore, what may be called an ergodic theorem or the proof of microscopic reversibility. They inform us that all states of the entire system are equally populated or, similarly, that all complexes which can pass into each other are realized with equal frequency.

We must now complete our discussion of the possibility that (9) and (18) have other solutions than those given. For this purpose we once more turn to the matrix of the a_{rs}.

The properties of $\mathbf{A}^{(N)}$ expressed in (11) and (12) obviously remain invariant under the transformation of $\mathbf{A}^{(N)}$ by the *same* permutation of its rows and columns, i.e., by a re-enumeration of its diagonal elements. If, by such a re-enumeration, it be possible to bring $\mathbf{A}^{(N)}$ into the form:

$$\begin{pmatrix} \mathbf{A}_1{}^{(N_1)} & \mathbf{O} & \cdots & \mathbf{O} \\ \mathbf{O} & \mathbf{A}_2{}^{(N_2)} & \cdots & \mathbf{O} \\ \cdot & \cdot & & \cdot \\ \cdot & \cdot & & \cdot \\ \cdot & \cdot & & \cdot \\ \mathbf{O} & \mathbf{O} & \cdots & \mathbf{A}_M{}^{(N_M)} \end{pmatrix} \tag{20}$$

then clearly each of the submatrices $\mathbf{A}_k{}^{(N_k)}$ will of itself enjoy the corresponding properties (11) and (12). We may now formulate, for later proof,[3] the following.

Theorem:—A matrix $\mathbf{A}^{(N)}$ having properties (11) and (12) is either of rank $N-1$, or it may, by re-enumeration of its diagonal elements, be written in the form (20) in such a manner that each submatrix $\mathbf{A}_k{}^{(N_k)}$ is of rank N_k-1.

From this theorem we can immediately conclude that if (19) does not express the unique solution of Eqs. (18) (as it will provided the rank of $\mathbf{A}^{(N)}$ is $N-1$) then every other solution must be of the form

$$\left.\begin{aligned} p_1=p_2 &=\cdots=p_{N_1}, \\ p_{N_1+1}=p_{N_1+2} &=\cdots=p_{N_1+N_2}, \\ \cdot\quad\cdot\quad\cdot\quad\cdot\quad\cdot\quad\cdot\quad\cdot\quad\cdot\quad\cdot\quad\cdot\quad\cdot & \\ p_{N-N_M+1}=p_{N-N_M+2} &=\cdots=p_N, \end{aligned}\right\} \tag{21}$$

where the numbers $N_1, N_2, \cdots N_M$ are entirely *definite*. The physical meaning of all this is now very simple. In case the rank of $\mathbf{A}^{(N)}$ is $N-1$ we have microscopic reversibility. If, on the

[3] Section III is devoted entirely to the proof of this theorem.

other hand, $\mathbf{A}^{(N)}$ has rank less than $N-1$, then it will be expressible in the form (20) and this means that the system breaks up into groups of noncombining states. Obviously this can occur only for special (improbable) values of the coefficients a_{rs}. No statement can then, of course, be made about the relative populations of complexes that belong to different noncombining groups. Two such groups can coexist with arbitrary relative populations; the collisions will not lead to statistical equalization. Inside of each group, however, there is again only one solution possible and this is of the same type as previously described, so that microscopic reversibility obtains in the interior of this group.

We shall now interpolate a few words in proof of our statement that no extraneous solutions are introduced by the dependence of the a_{rs} on the n_i. We notice first that the particular form (20) assumed by $\mathbf{A}^{(N)}$ can depend only on the values of the $A_{ik}{}^{lm}$ and not on the n_i; for this form can be altered only by the vanishing (or the ceasing to vanish) of certain elements a_{rs} and such a change cannot, according to (17), be accomplished by changes in the values of the n_i. In particular the rank of $\mathbf{A}^{(N)}$ does not depend on the n_i. Suppose, at first, that this rank is $N-1$ and that in addition to solution (19) there should exist a distinct solution $p_i=p_i'$ (say for $n_i=n_i'$, $a_{rs}=a_{rs}'$). Then in addition to the relation

$$\sum_{s=1}^{N} a_{rs}'=0$$

there would hold among the columns of $\mathbf{A}^{(N)}$ the independent relation

$$\sum_{s=1}^{N} p_s' a_{rs}'=0;$$

but this is contrary to the supposition that the rank of $\mathbf{A}^{(N)}$ is $N-1$. The case of rank $R<N-1$ can be similarly treated.

The arguments which we have just set forth not only afford a proof of the H theorem, but also extend it to the case of arbitrary complexes and accidental degeneracy. We do not, however, claim to have proved anything equivalent to the ergodic hypothesis in the *strict sense* of the term. This is simply due to the fact that we started not from the exact equations for the average populations, but from what may be called *average* equations for the average populations. Quantum dynamics gives us directly equations not for the populations, but only for the probability amplitudes. Equations for the populations can be derived from these only by an averaging process over the phases, and this averaging process cannot be carried out without additional assumptions. Our equations are valid under the supposition that this averaging process has been carried out. And although there can be no doubt as to their physical correctness, they are not a direct consequence of quantum mechanics.

III. Proof of a Matrix Theorem

We shall find it necessary to consider the upper left corner square submatrices of $\mathbf{A}^{(N)}$; in conformity with our previous notation, we denote these by

$$\mathbf{A}^{(1)}=(a_{11}),\quad \mathbf{A}^{(2)}=\begin{pmatrix} a_{11} & a_{12} \\ a_{21} & a_{22} \end{pmatrix},\ \text{etc.},$$

and their respective determinants by $A^{(1)}$, $A^{(2)}$, $\cdots$. $\mathbf{A}^{(k)}$ has property (11), and in place of property (12):

$$s_r{}^{(k)} \equiv \sum_{s=1}^{k} a_{rs} \geqq 0 \quad (r=1, 2, \cdots k). \qquad (22)$$

If it should happen that $s_r{}^{(k)}=0$ $(r=1, 2\cdots k)$, i.e., that $\mathbf{A}^{(k)}$ should enjoy property (12), then, since (in conjunction with (12) for $\mathbf{A}^{(N)}$) this would involve $a_{r,\,k+1}=a_{r,\,k+2}=\cdots=a_{r,\,N}=0$, it is clear that $\mathbf{A}^{(N)}$ would have the form (20) with $M=2$, $N_1=k$, $\mathbf{A}_1{}^{(N_1)}=\mathbf{A}^{(k)}$. As for $\mathbf{A}_2{}^{(N_2)}$, it would also have both properties (11) and (12). Since, as we have seen, $A^{(N)}=0$ is a consequence of (12), so that the rank of $\mathbf{A}^{(N)}$ cannot be greater than $N-1$, it is now evident that our theorem of Section II follows immediately from the repeated application of the following.

Lemma:—If a matrix $\mathbf{A}^{(N)}$ having properties (11), (12) is of rank $R<N-1$, then it may, by re-enumeration of its diagonal elements, be written in such a form that its corner submatrix $\mathbf{A}^{(N_1)}$ of order N_1 enjoys property (12) and is of rank N_1-1.

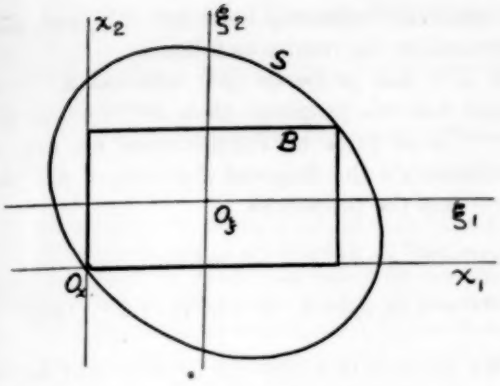

FIG. 1.

For this lemma we shall now given an entirely elementary proof. We denote by n the greatest integer such that

$$A^{(k)}>0 \quad (k=1, 2, \cdots n). \tag{23}$$

Since $A^{(1)}=a_{11}>0$ and $A^{(N-1)}=0$ because of the assumption $R<N-1$, clearly $1\leqq n<N-1$. According to a well-known theorem the quadratic form associated with $\mathbf{A}^{(n)}$, *viz.*

$$\sum_{r,\,s=1}^{n} a_{rs}x_r x_s,$$

is then *positive definite* as is also its inverse form of symmetric matrix $\mathbf{B}^{(n)}$, *viz.*

$$\left.\begin{aligned} Q(x_1, x_2, \cdots x_n) &\equiv \sum_{r,\,s=1}^{n} b_{rs}x_r x_s, \\ \mathbf{A}^{(n)}\mathbf{B}^{(n)} &= (\delta_{rs}). \end{aligned}\right\} \tag{24}$$

Two further properties of $\mathbf{A}^{(n)}$ and $\mathbf{B}^{(n)}$ can be deduced from (11) and (23). The first is important in that it shows property (23) to be invariant under a re-enumeration of the diagonal elements of $\mathbf{A}^{(n)}$; it states that if P is the value of *any* principal minor determinant of $\mathbf{A}^{(n)}$, then

$$P>0. \tag{25}$$

The second is that

$$b_{rs}\geqq 0 \quad (r, s=1, 2, \cdots n). \tag{26}$$

Relations (25) and (26) are seen by inspection to be true for $n=1$ and $n=2$; their validity for higher values of n follows by mathematical induction.

We now propose to investigate the consequences of the fact that $A^{(n+1)}\leqq 0$, and in particular to find out what it can tell us of the bordering elements

$$\left.\begin{aligned} a_{n+1,\,r}=a_{r,\,n+1} &\equiv -x_r \quad (r=1, 2, \cdots n), \\ a_{n+1,\,n+1} &\equiv y. \end{aligned}\right\} \tag{27}$$

If we develop $A^{(n+1)}$ as a bordered determinant and divide through by $A^{(n)}>0$, our investigation may be transferred to the relation

$$y-Q(x_1, x_2, \cdots x_n)\leqq 0, \tag{28}$$

which must be satisfied under the restrictions imposed by (11) and (22) for $k=n$, $n+1$; *viz.*

$$\left.\begin{aligned} &0\leqq x_r\leqq s_r^{(n)}\equiv s_r, \\ &x_r\neq 0 \text{ simultaneously for all } r, \\ &y=\sum_{s=1}^{n} x_s+\eta, \quad \eta\geqq 0. \end{aligned}\right\} \tag{29}$$

where the second relation follows from $y>0$ in combination with (28) itself.

We shall greatly clarify our problem by interpreting (29) (and subsequently (28)) graphically. To do so we employ the n dimensional space of the x's. Eq. (29) then states that the point $P\{x_1, x_2, \cdots x_n\}$ may not lie outside an $m(\leqq n)$ dimensional box B (Fig. 1), nor in one of its vertices, the origin O_x. We can bring the symmetry of the problem into more prominent relief by transforming it to parallel coordinates ξ_r having their origin O_ξ at the center of B:

$$x_r=\tfrac{1}{2}s_r+\xi_r \quad (r=1, 2, \cdots n). \tag{30}$$

In transforming (28) we observe that

$$\sum_s b_{rs}s_s=\sum_{s,\,t} b_{rs}a_{st}=\sum_t \delta_{rt}=1,$$

so that in particular

$$Q(\tfrac{1}{2}s_1, \tfrac{1}{2}s_2, \cdots \tfrac{1}{2}s_n)=\tfrac{1}{4}\sum s_r\equiv Q_0, \tag{31}$$

$$\sum_{r,\,s} b_{rs}s_r\xi_s=\sum_s \xi_s, \tag{32}$$

whence it is readily seen that (28) assumes the form

$$\eta+Q_0-Q(\xi_1, \xi_2, \cdots \xi_n)\leqq 0. \tag{33}$$

We now construct the central quadric surface S (Fig. 1):

$$Q(\xi_1, \xi_2, \cdots \xi_n) = Q_0, \tag{34}$$

which, according to (31) passes through O_x and its diametrically opposite vertex of B. Since Q is positive definite, S is an n dimensional non-degenerate hyperellipsoid having the property that $Q(\xi_1, \xi_2 \cdots \xi_n) \lesseqgtr Q_0$ according as $P\{\xi_1, \xi_2, \cdots \xi_n\}$ lies within or without it. Now the ξ coordinates of any vertex of B can, by re-enumeration of the diagonal elements of $\mathbf{A}^{(n)}$, be written in the form:

$$\tfrac{1}{2}s_1, \quad \tfrac{1}{2}s_2, \quad \cdots \tfrac{1}{2}s_l, \quad -\tfrac{1}{2}s_{l+1}(\neq 0),$$
$$-\tfrac{1}{2}s_{l+2}(\neq 0), \quad \cdots, \quad -\tfrac{1}{2}s_n(\neq 0). \tag{35}$$

and the value of Q for this vertex can be obtained from the function $Q(\frac{1}{2}s_1, \frac{1}{2}s_2, \cdots \frac{1}{2}s_n)$ by changing the sign of its last $n-l$ arguments. Since, however, according to (26) none of the coefficients of Q are negative, these changes of sign cannot result in increasing the value of Q above Q_0 (although they may leave it unaltered). Therefore no vertex of B can lie outside of S, so that no point within or on B can lie outside of S.

Returning now to relation (33) of which we seek a solution within or on B, we see at once that no solution of the inequality is possible ($A^{(n+1)} \lessdot 0$) and that the solution for the equality ($A^{(n+1)} = 0$) must correspond to some vertex (35) of B with, in addition, $\eta = 0$, i.e.,

$$y = \sum_{r=1}^{n} x_r. \tag{36}$$

Since the vertex (35) corresponds to the x coordinates

$$s_1, s_2, \cdots s_l, 0(\neq s_{l+1}), 0(\neq s_{l+2}), \cdots 0(\neq s_n), \tag{37}$$

we may, on referring back to (27) and (22), reformulate our results as follows:

If $\mathbf{A}^{(n)}$ has property (23) whereas $\mathbf{A}^{(n+1)}$ no longer has this property, then $A^{(n+1)} = 0$ so that $\mathbf{A}^{(n+1)}$ is of rank n. Furthermore we may so re-enumerate the diagonal elements of $\mathbf{A}^{(n)}$ that $\mathbf{A}^{(n+1)}$ has the properties

$$\left.\begin{aligned} &s_r^{(n+1)} = 0 \quad (r = 1, 2, \cdots l; n+1), \\ &s_r^{(n+1)} \neq 0, \; a_{r,\,n+1} = 0 \quad (r = l+1, l+2, \cdots n). \end{aligned}\right\} \tag{38}$$

We are now in a position to prove our lemma. If in (38) $l = n$ then $\mathbf{A}^{(n+1)}$ will have property (12) and be of rank n, so that it will serve as the matrix $\mathbf{A}^{(N_1)}$ of the lemma. Let us then suppose $l < n$. We denote by $\mathbf{A}'^{(n+1)}$ the matrix obtained from $\mathbf{A}^{(n+1)}$ by transposition of its last two rows and columns, so that we shall have for its last row:

$$\left.\begin{aligned} &a'_{n+1,\,r} = a_{n,\,r} \quad (r = 1, 2, \cdots n-1), \\ &a'_{n+1,\,n} = a_{n,\,n+1} = 0, \quad a'_{n+1,\,n+1} = a_{n,\,n}. \end{aligned}\right\} \tag{39}$$

Now $\mathbf{A}'^{(n-1)} = \mathbf{A}^{(n-1)}$ has property (23), so that $A'^{(n)} \gtreqless 0$. Let us first suppose $A'^{(n)} > 0$; then $\mathbf{A}'^{(n)}$ will also have property (23), so that (since $A'^{(n+1)} = A^{(n+1)} = 0$) $\mathbf{A}'^{(n+1)}$ will, by re-enumeration of $\mathbf{A}'^{(n)}$ alone ($s'_{n+1}{}^{(n+1)} = 0$ remaining thereby unaltered), assume properties analogous to (38). But according to (39) $s'_{n+1}{}^{(n+1)} = s_n{}^{(n+1)}$, and according to (38) $s_n{}^{(n+1)} \neq 0$ for $l < n$, so that our assumption $A'^{(n)} > 0$ is untenable and we have proved $A'^{(n)} = 0$. We have therefore obtained a submatrix $\mathbf{A}'^{(n'+1)} = \mathbf{A}'^{(n)}$ of rank $n' = n-1$ having the same properties as $\mathbf{A}^{(n+1)}$ but having a lesser order. If $l' < n'$ we may repeat the process described until we finally arrive at a matrix $\mathbf{A}''^{(n''+1)}$, for which $l'' = n''$. Since $l = 0$ is ruled out because of the exclusion of O_x, this must occur at least by the time $n'' = 1$.

On the Theory of Isotope Separation by Thermal Diffusion

W. H. FURRY, R. CLARK JONES, *Research Laboratory of Physics, Harvard University, Cambridge, Massachusetts*

AND

L. ONSAGER, *Department of Chemistry, Yale University, New Haven, Connecticut*

(Received April 6, 1939)

We here develop the theory of the processes in an apparatus with two concentric tubes, such as that used by Brewer and Bramley. In the first section we describe the process of thermal diffusion in general, and review the theoretical information on the subject. In Section II we set up the equations for the convection and diffusion processes, and obtain an expression for the net transport of a single isotope which is valid for arbitrary macroscopic properties of the gas. The assumption that the viscosity and heat conductivity of a gas are proportional to the absolute temperature is usually a good approximation; in this case the expression reduces to a simple form. In Section III we apply the transport equation to questions of separation factor and speed of operation. This is done both for the case of discontinuous operation, in which the approach to equilibrium is allowed to reach a certain stage and then the contents of an end-reservoir are removed, and for the case of operation with a continuous flow of gas through the tube. The advantages of the two methods are compared. In the last section we apply the formulas to a numerical example: the concentration of the C^{13} isotope by the use of methane, in an apparatus of moderate dimensions and power consumption.

I. INTRODUCTION

RECENTLY Clusius and Dickel,[1] and subsequently Brewer and Bramley,[2] have reported the results of experimental work on the separation of isotopes by thermal diffusion. Their results suggest that this may become an important method. In this paper we discuss theoretically the problem of applying the process of thermal diffusion to isotope separation.

The phenomenon of thermal diffusion consists in the fact that a temperature gradient in a mixture of two gases gives rise to a gradient of the relative concentration of the two constituents. If the mixture as a whole is at rest, the equilibrium concentration gradient is such that the effect of thermal diffusion is just matched by the opposing effect of ordinary diffusion. The effect is by no means small; in some cases the coefficient of thermal diffusion may be as much as half of the ordinary coefficient.[3] A similar phenomenon is known in the case of liquids, where it is known as the Soret effect;[4] the theoretical explanation of the Soret effect has been signally unsuccessful.[5]

No simple theory can give an account of thermal diffusion; neither its existence nor its sign can be derived from elementary considerations.[6] Its presence can be understood only by a detailed consideration of the equations of transport in a gas. The phenomenon was completely overlooked by the classic workers in kinetic theory; it was first discovered theoretically by Enskog[7] in 1911, and independently by Chapman[8] six years later, and first demonstrated experimentally by Chapman and Dootson[9] in 1917.

The theory was fully and elegantly developed by Enskog,[10] and Chapman.[8] The more accessible treatment of Chapman is, however, unfortunately invalid because of algebraic errors.[11] Chapman's corrected result[12] may be shown to be identical with the result of Enskog. It is the result obtained by Enskog in his doctoral dissertation that is given in the well-known textbook of Müller-Pouillets.[13]

[1] K. Clusius and G. Dickel, Naturwiss. **26**, 546 (1938).
[2] A. K. Brewer and A. Bramley, Phys. Rev. **55**, 590A. (1939).
[3] S. Chapman, Phil. Trans. **A217**, 184 (1917).
[4] Ludwig, Wien. Akad. Ber. **20**, 539 (1856); Soret, Ann. Chim. Phys. **22**, 293 (1881).
[5] Wereide, Ann. de physique **2**, 67 (1914); Porter, Trans. Faraday Soc. **23**, 314 (1927). Also see comment by Chapman, Phil. Mag. **7**, 1 (1929).
[6] S. Chapman, reference 5.
[7] D. Enskog, Physik. Zeits. **12**, 56 and 533 (1911).
[8] Reference 3, p. 115.
[9] S. Chapman and F. W. Dootson, Phil. Mag. **33**, 248 (1917); for a complete list of the experimental literature on thermal diffusion, see T. L. Ibbs, Physica **4**, 1133 (1937).
[10] D. Enskog, Doctoral Dissertation, Upsala, 1917, published by Almqvist and Wiksells.
[11] D. Enskog, Arkiv. f. Mat., Astron., o. Fysik **16**, No. 16 (1921).
[12] S. Chapman and W. Hainsworth, Phil. Mag. **48**, 593 (1924); the presentation of the value of D_T in this paper does not become complete until it is stated that the matrix a_{ij} is *symmetrical*.
[13] Müller-Pouillets, *Lehrbuch der Physik*, eleventh edition, Vol. 3, Part 2, p. 110.

The coefficient of thermal diffusion vanishes for Maxwellian molecules (molecules which interact with a force which varies as the inverse fifth power of the separation). For molecules such that the force varies as an inverse power of the separation which is greater than five, the direction of the diffusion is such that the lighter molecules move toward the warmer part of the gas, in general, while for an inverse power less than five, the lighter molecules accumulate in the colder part of the gas. A general result of the theory is that the coefficient vanishes when the mode of interaction, the radii, and the masses of the two sets of molecules, are all equal;[3] this fact is also obvious from symmetry.

Even to the first approximation (the result comes out as an infinite determinant), the coefficient of thermal diffusion can be stated in closed form only for the case of rigid elastic spheres, in which case the effect is greatest. The experiments show a coefficient which is in general something less than half of the value predicted for elastic spheres.

The equation of diffusion, with thermal diffusion included, is

$$c_1(\mathbf{v}_1-\mathbf{v}) = -D_{12}\ \text{grad.}\ c_1+(D_T/T)\ \text{grad.}\ T, \quad (1)$$

where c_1 is the relative *particle* density of the lighter constituent, with $c_1+c_2=1$; $\mathbf{v}_1$ is the *convection* velocity of the lighter constituent alone, while $\mathbf{v}$ is the convection velocity of the gas as a whole ($\mathbf{v}=c_1\mathbf{v}_1+c_2\mathbf{v}_2$); D_{12} is the coefficient of ordinary diffusion, which in the case of isotopes may be replaced by D, the coefficient of self-diffusion, and D_T is the previously mentioned coefficient of thermal diffusion; T is the absolute temperature. In the corresponding equation for c_2, the D_T term has the opposite sign.

It can be shown rigorously, for the case of hard spheres, that the ratio $D_T/D_{12}=k_T$ depends only on the relative concentrations and on microscopic quantities, but not on the pressure or temperature. It is reasonable to suppose that for actual molecules this ratio does not vary with pressure or temperature to any significant extent.

For the separation of isotopes, we are interested in the case when the two sets of molecules in question are chemically identical, and differ only in mass. In this case, the expression for k_T becomes greatly simplified, because the modes of interaction and the radii of the two constituent molecules are then the same, since these properties are completely determined by the electronic configuration. For this special case, Enskog's result reduces to[14]

$$D_T/D=k_T=\alpha c_1c_2, \quad (2)$$

where $\alpha=(105/118)(m_2-m_1)/(m_2+m_1)$, the m's being the relative masses of the two types of molecules. It is to be remembered that number 1 is the lighter species. This expression is the first approximation for the case of elastic spheres, in which furthermore we have retained only terms of the first order in $(m_2-m_1)/(m_2+m_1)$.

The experimental determinations of k_T for the case of *dissimilar* molecules yield values somewhat less than half of the theoretical result for elastic spheres.[9] Until experiment yields us values for k_T in the case of isotopes, therefore, we suggest that

$$\alpha=0.35(m_2-m_1)/(m_2+m_1) \quad (3)$$

be used as a provisional value in the design of apparatus. The exact value of the numerical coefficient will vary from molecule to molecule, because of the different modes of interaction.

When values for k_T in the case of isotopes are determined experimentally, they may lead to valuable conclusions about the nature of the intermolecular forces in the gas in question. Thermal diffusion should be an excellent way to obtain this information, because it is one of the few phenomena in a gas that depend essentially on the peculiar characteristics of the molecules.[15] The knowledge of k_T for the case of isotopes is particularly valuable, because in this case there is no mixing of the characteristics of two dissimilar molecules.

The use of thermal diffusion for separating isotopes was first suggested by Chapman.[16] Its use was discussed by Mulliken,[17] on the basis of Chapman's first treatment. Mulliken concluded that it could not compete with other methods,

[14] S. Chapman's earlier expression (reference 16) was

$$k_T=\frac{17}{3}\frac{m_2-m_1}{m_2+m_1}\frac{c_1c_2}{9.15-8.25\ c_1c_2}.$$

[15] S. Chapman, reference 3, p. 181; J. H. Jeans, *Dynamical Theory of Gases*, fourth edition (Cambridge, 1925), p. 325.

[16] S. Chapman, Phil. Mag. **38**, 182 (1919).

[17] R. S. Mulliken, J. Am. Chem. Soc. **44**, 1033 (1922).

but he did not consider the very effective method of fractionation employed by Clusius and Dickel.[1]

Clusius and Dickel ran a heated wire up the axis of a long vertical hollow tube, into which was put the gas whose isotopic constituents were to be separated. The combination of the effect of thermal diffusion and of the convection currents set up in the tube is such as to increase greatly the rather small separation caused directly by the radial temperature gradient. The light isotope collects at the top, while the heavier isotope goes to the bottom of the tube, as we shall discuss in detail in the next section.

The procedure of Brewer and Bramley[2] was very similar. They used two concentric tubes, of one and two centimeters diameter. The inner tube was heated.

In the following two sections we examine quantitatively what is occurring in this new method of separating isotopes. We find it possible to set up formulae showing the dependence of the performance characteristics on the dimensions of the apparatus, the temperature, the density, etc. These results should be useful in designing apparatus for isotope separation by this method.

II. The Convection Field and the Transport Equation

Description of apparatus and notation

The apparatus is supposed to consist of two concentric cylinders, the inner one heated and the outer one cooled, mounted in a vertical position, with reservoirs at the top and bottom communicating with the annular space between the cylinders, where convection and diffusion take place. The difference of the radii may be supposed small compared with either radius, so that we may proceed as if the convection were taking place in a thin flat slab, of breadth B equal to the mean circumference of the cylinders, thickness $2w$ equal to the difference of the radii, and length $2l$, the length of the tube.

In addition to the notation already introduced, we shall use the following: T_1, T_2 = absolute temperature of the outer, inner tube; $\Delta T = T_2 - T_1$; x = radial coordinate, $-w < x < w$; z = coordinate along the tube, $-l < z < l$; c = specific heat at constant pressure, in cal./gram-deg.; Q = heat flow, in cal./cm²-sec.; λ = thermal conductivity, in cal./cm-deg.-sec.; p = pressure; η = viscosity; ρ = density; g = acceleration of gravity; $\mathbf{J}_1$, $\mathbf{J}_2$ = flux of species 1, 2 in grams/cm²-sec.; τ = total upward transport, in grams/sec.; τ_1, τ_2 = upward transport of species 1, 2, in grams/sec. $\tau = \tau_1 + \tau_2$; c_1^0 = value of c_1 in the bottom reservoir; c_1^1 = value of c_1 in the top reservoir; κ_e = equilibrium value of c_1^1 with $\tau = 0$; κ_r = a specified value of c_1^1; m_t = mass of gas in the top reservoir; and t_r = relaxation time of the equilibrium. In all considerations subsequent to Eq. (29), the temperature dependent quantities are to be evaluated at the average temperature, $\frac{1}{2}(T_2 + T_1)$.

General treatment of the convection and diffusion field

Throughout this section and the next it will be assumed that it is the lighter isotope, species 1, which one is interested in concentrating. The considerations will be completely symmetrical in respect to the interchange of 1 and 2, however, if we understand that the vertical coordinate changes sign when we apply our equations to the concentration of a heavy isotope—that is, c_1^0 becomes the concentration c_2^0 in the top reservoir, while the small collecting reservoir would be at the bottom; and so on, in an obvious manner.

In the immediately following presentation, we shall develop a mathematical description of the convection and diffusion processes in the tube, and derive the fundamental relations which yield the transport of species 1 along the tube. Having obtained these relations, we then proceed in the next section to determine the behavior of the apparatus in the large: to find what separation factors can be obtained, and at what speed a mixture of given concentration may be produced.

We shall calculate the convection by using the temperature distribution as determined by conduction only. Near each end of the tube, where gas at a different temperature is entering, the temperature distribution is of course different. On the basis of the treatment of the convection problem given below, one finds that the length over which this difference remains appreciable is of the order of

$$l_r = (w^4 c g \rho^2 / 48 \eta \lambda)(T_2 - T_1)/(T_2 + T_1), \quad (4)$$

where here as in (5) the temperature dependent

quantities ρ, η, λ are evaluated at the average temperature $(T_2+T_1)/2$. Our neglect of these regions depends on the condition $2l_r \ll 2l$, which will usually be strongly satisfied in practice.

The treatment of the convection flow as lamellar is justified, since the Reynolds number may be shown to be roughly

$$(w^3g\rho^2/24\eta^2)(T_2-T_1)/(T_2+T_1), \tag{5}$$

which in practical cases will be very much smaller than the values at which turbulence occurs in flow through tubes or between plates.

In the region of the tube where the temperature gradient is determined by conduction alone, we have

$$\begin{aligned} Q&=\lambda dT/dx, \\ 2wQ&=\int_{T_1}^{T_2}\lambda dT, \\ \partial/\partial x&=(Q/\lambda)(\partial/\partial T). \end{aligned} \tag{6}$$

We shall neglect the dependence of λ on the concentration c_1 and also the dependence on c_1 of ρ, η, and D. These dependences are not large when the fractional difference of molecular weight is small. Moreover, only transverse differences have any significant effect on the performance, and the transverse difference of concentration is very small. Thus only the temperature dependences of the various quantities is of any importance.

The hydrodynamical equation of steady, viscous flow is

$$(\text{div. } \eta \text{ grad.})\mathbf{v}=\text{grad. } p-\rho\mathbf{g}. \tag{7}$$

We assume that the velocity is entirely in the vertical direction, and that it is independent of z; this is a very close approximation since the pressure variation within the tube is negligible. Then we have from (6) and (7)

$$(Q^2/\lambda)(d/dT)(\eta/\lambda)(dv/dT)=(dp/dz)+\rho g \tag{8}$$

with the boundary conditions

$$v(T_1)=v(T_2)=0. \tag{9}$$

By (1), the equation for the flux of species 1 is

$$\mathbf{J}_1=\rho[\mathbf{v}c_1+D(-\text{grad. } c_1+\alpha c_1c_2 \text{ grad. } \ln T)], \tag{10}$$

and a corresponding equation holds for $\mathbf{J}_2$.

We shall base our calculation of the transport of species 1 through the tube on the assumption that the time variation of the concentration c_1 at each point in the tube is negligible—that is, that the condition is either stationary or quasi-stationary. A stationary condition exists at final equilibrium in a closed apparatus, and also when there is a uniform output of the concentrated isotope. During the approach to equilibrium the condition will be essentially stationary provided each end-reservoir is sufficiently large. The volume of each reservoir must be larger than that of a length of tube in which the equilibrium concentration changes by a factor e.

Accordingly we proceed from the equations

$$\text{div. } \mathbf{J}_1=\text{div. } \mathbf{J}_2=0. \tag{11}$$

Eq. (10) then gives, on application of (6),

$$\begin{aligned} &(\partial/\partial T)(\rho D/\lambda)[(\partial c_1/\partial T)-(\alpha c_1c_2/T)] \\ &\quad=(\lambda\rho/Q^2)[v(\partial c_1/\partial z)-D(\partial^2 c_1/\partial z^2)]. \end{aligned} \tag{12}$$

The term containing $(\partial^2 c_1/\partial z^2)$ is the one that introduces the effect of longitudinal diffusion. The retention of this term would make it impossible to carry out the analysis in any simple manner. Since the effect of diffusion along the tube can be calculated separately quite accurately, we shall omit the term in question, and calculate from

$$\begin{aligned} &(\partial/\partial T)(\rho D/\lambda)[(\partial c_1/\partial T)-(\alpha c_1c_2/T)] \\ &\quad=(\lambda\rho/Q^2)v(\partial c_1/\partial z). \end{aligned} \tag{12'}$$

We now introduce a function $G(z, T)$ defined by

$$(\partial c_1/\partial z)G(z, T)=-(\lambda Q^3/\rho D)J_{1z} \tag{13a}$$

$$=Q^4[(\partial c_1/\partial T)-(\alpha c_1c_2/T)]. \tag{13b}$$

Then from (12′),

$$\begin{aligned} &(\partial/\partial T)(\rho D/\lambda)(\partial c_1/\partial z)G(z, T) \\ &\quad=\lambda\rho Q^2 v(\partial c_1/\partial z). \end{aligned} \tag{14}$$

From this point on we shall assume that the dependence of $\partial c_1/\partial z$ on T can be neglected. This is equivalent to assuming that $\partial c_1/\partial T$ is independent of z, which is physically reasonable for a quasi-stationary condition. We shall at once establish two important consequences of this assumption: First, the total transport τ through the tube is zero; second, G is a function of T only.

Since div. $\mathbf{J}_1$ is zero, the flow of species 1 must be constant along the tube—that is,

$$\tau_1 = B\int_{-w}^{w} \rho c_1 v dx = \text{constant},$$

$$\tau_1 = (B/Q)\int_{T_1}^{T_2} \lambda \rho c_1 v dT, \tag{15}$$

$$(d\tau_1/dz) = (\partial c_1/\partial z)(B/Q)\int_{T_1}^{T_2} \lambda \rho v dT$$
$$= (\partial c_1/\partial z)\cdot \tau = 0.$$

Then since $\partial c_1/\partial z$ is not identically zero, τ, the total transport, must vanish.

By (13a), we have

$$G(z, T_1) = G(z, T_2) = 0 \tag{16}$$

since J_{1z} must vanish at the walls. The factor $(\partial c_1/\partial z)$ on each side of (14) cancels, and since the only remaining quantity that can be a function of z is $G(z, T)$, one finds, on integrating (14) that $(\rho D/\lambda)G$ can depend on z only through an additive function of z. Then, since (16) hold identically in z, we have

$$G(z, T) = G(T). \tag{17}$$

We have now, canceling the $\partial c_1/\partial z$ in (14), and solving for v,

$$v(T) = (1/\lambda\rho Q^2)(d/dT)(\rho D G(T)/\lambda). \tag{18}$$

Then from (18) and (16),

$$G'(T_1) = G'(T_2) = 0. \tag{19}$$

If we now substitute (18) in (8), and differentiate with respect to T, we obtain as the differential equation for $G(T)$

$$\frac{d}{dT}\frac{1}{\lambda}\frac{d}{dT}\frac{\eta}{\lambda}\frac{d}{dT}\frac{1}{\lambda\rho}\frac{d}{dT}\left(\frac{\rho D}{\lambda}G(T)\right) = g\frac{d\rho}{dT} \tag{20}$$

with the boundary conditions

$$G(T_1) = G(T_2) = G'(T_1) = G'(T_2) = 0. \tag{21}$$

By the calculation of this single function one vas, by (18), a complete description of the convection process; and, within the limits of our approximations, one has, by (13), a description of the transverse diffusion, both thermal and ordinary. By the use of this same function we can proceed to obtain an expression for the transport of a single isotope along the tube.

According to (15) and (18) the net vertical transport of species 1 is

$$\tau_1 = (B/Q^2)\int_{T_1}^{T_2} \lambda c_1 c_2 (\rho D G(T)/\lambda) dT. \tag{22}$$

Partial integration and substitution from (13b) and (21) lead to the expression

$$\tau_1 = Hc_1c_2 - K\partial c_1/\partial z, \tag{23}$$

where H and K are positive constants defined by

$$H = -(B/Q^2)\int_{T_1}^{T_2} (\rho D\alpha/\lambda T) G(T) dT \tag{24}$$

and

$$K = (B/Q^2)\int_{T_1}^{T_2} (\rho D/\lambda)\{G(T)\}^2 dT. \tag{25}$$

We have removed c_1c_2 from under the integral sign of (24), because c_1c_2 varies only slightly with T. We could not consider c_1 as constant in (22), however, because it is only the slight variation of c_1 which prevents this integral from vanishing.

In Eq. (23) the term Hc_1c_2 gives the transport of species 1 caused by the existence, due to thermal diffusion, of a transverse flow of this isotope, which makes the concentration in the column of gas moving upward differ from that in the column moving downward. At the beginning of the process, when $\partial c_1/\partial z = 0$, this is the only cause of transport. After a longitudinal concentration gradient has been built up, the convection currents lead to a certain amount of remixing of the gas, represented by the term $-K\partial c_1/\partial z$. There is, however, another remixing effect which is not included in Eq. (23), because in replacing (12) by (12′) we omitted the term which corresponds to diffusion *along* the tube. Since the convection velocity will be small, however, the longitudinal diffusion will be practically independent of it. If we ignore the convection velocity, the transport of species 1 due to longitudinal diffusion is

$$\tau_{1d} = -K_d\,\partial c_1/\partial z,$$
$$K_d = (B/Q)\int_{T_1}^{T_2} \lambda \rho D dT. \tag{26}$$

The total transport of species 1 is obtained by adding τ_{1d} to the τ_1 given by (23).

Specialization to the Maxwellian case

The treatment so far has been general, in the sense that the quantities D, λ and η might have an arbitrary temperature dependence. If, however, the mean free path varies as the $(n-\frac{1}{2})$th power of the temperature and if α is independent of T, the following quantities should all be constant:

$$(\eta/T^n),\quad (\lambda/T^n),\quad (\rho D/T^n);\quad (\eta/\lambda),\quad (\rho D/\lambda).$$

Then (20) becomes

$$(d/dT)T^{1-n}(d^2/dT^2)T^{1-n}(dG/dT)$$
$$=-T^{-2}(\lambda^4\rho g)/(\eta D T^{2n-2}). \quad (27)$$

The general solution of (27) has been obtained, and there appears to be no bar to the explicit evaluation of H and K in this manner. The formulae would be awkward in practice, however, because of heavy cancellation of terms. The writers have worked out the cases of $n=\frac{1}{2}$ (hard spheres) and $n=1$ (Maxwellian molecules). Since the case $n=1$ is much simpler than any other, and corresponds fairly well to the temperature dependence of the properties of most gases, we suggest that the formulas for this case be used in practice. This simplification is particularly well justified because our knowledge of the all-important factor α itself is so inexact.

For $n=1$, integration of (27) and application of (21) gives

$$G(T)=-\{(\lambda^4 g\rho)/(24\eta D)\}\times(T_2-T)^2(T_1-T)^2/(T_2+T_1). \quad (28)$$

and (6) becomes

$$w=\lambda\Delta T/2Q, \quad (29)$$

where in this and all following formulae, ρ, D, λ, η and T are to be evaluated at $T=\frac{1}{2}(T_2+T_1)$. If (28) and (29) are used in (24), the result is

$$H=\{(w^2\rho^2\alpha g B)/(90\eta)\}(\Delta T/T)^2 f(\Delta T/T), \quad (30)$$

where

$$f(\Delta T/T)=30T^2(\Delta T)^{-4}\{(\Delta T)^2/6-T_1T_2+(T_1T_2)^2(T\Delta T)^{-1}\ln(T_2/T_1)\}$$
$$=15\textstyle\sum_k(\Delta T/2T)^{2k}/\{(2k+1)(2k+3)\times(2k+5)\}$$
$$=1+(15/3\cdot5\cdot7)(\Delta T/2T)^2+\cdots.$$

$f(\Delta T/T)$ has the value unity for $\Delta T=0$, and the value 5/4 for the extreme case $T_1/T_2=0$, and lies between these two values for intermediate cases. For $T_2=2T_1$, $f=1.016$, while for $T_2=3T_1$, $f=1.039$.

From (25) and (29), we have

$$A=H/2K=(63/4)\times\{(\alpha\eta D)/(\rho g w^4)\}f(\Delta T/T), \quad (31)$$

and (26) gives

$$K_d/K=1890(T_1^2+T_1T_2+T_2^2)\times\{D\eta/(w^3\rho g\Delta T)\}^2. \quad (32)$$

The corresponding relations for a gas consisting of hard spheres follow:

We introduce the abbreviations:

$$t=T^{\frac{1}{2}},\quad t_1=T_1^{\frac{1}{2}},\quad t_2=T_2^{\frac{1}{2}},$$
$$r=(t_2-t_1)/(t_2+t_1),$$
$$s(t)=(2t-t_2-t_1)/(t_2-t_1).$$

Then we find

$$G(t^2)=-\{(\lambda^4\rho g T)/(72\eta D)\}(t_2-t_1)^4\{1-(s(t))^2\}^2\times\{(6-2r^2)(3+rs(t))^2-(3+r^2)^2\}(3+r^2)^{-1}(5-r^2)^{-1},$$

$$w=\{\lambda/(3QT^{\frac{1}{2}})\}(t_2^3-t_1^3),$$

$$H=\{(4\alpha\lambda^3\rho^2 gT)/(3Q^3\eta)\}\times\{(t_2-t_1)^5/(t_2+t_1)(3+r^2)(5-r^2)\}\psi(r),$$

$$\psi(r)=1-r^2/5-(30+2r^2)\times\{r^2/(1\cdot3\cdot5\cdot7)+r^4/(3\cdot5\cdot7\cdot9)+\cdots\},$$

$$\psi(0)=1,\quad \psi(1)=4/9,$$

$$K=\{(10\lambda^7 g^2T^2\rho^3)/(63Q^7\eta^2D)\}\times\{(t_2-t_1)^9(t_2+t_1)/(3+r^2)^2(5-r^2)^2\}\varphi(r),$$

$$\varphi(r)=1-(692/825)r^2+(146/2475)r^4+(4/75)r^6+(13/7425)r^8,$$

$$\varphi(0)=1,\quad \varphi(1)=(2044/7425),$$

$$K_d=\{(\lambda\rho D)/(2QT)\}(t_2^4-t_1^4).$$

In some cases the ratio (32) will be quite small, so that (23) gives essentially the total transport. For example, with fixed dimensions of apparatus this will be true provided the pressure is sufficiently high ($(\rho/D)\propto$ (pressure)^2). For the sake of simplicity we shall proceed with most of

our considerations on the assumption that this condition $(K_d/K)\ll 1$, is satisfied. In cases where this is not true, it is only necessary to replace A in the following by

$$A_d = A/\{1+(K_d/K)\}. \quad (33)$$

III. Separation Factor and Speed of Operation

Discontinuous operation

We shall now apply the results we have just derived to the case of *discontinuous* operation, by which is meant that one waits until the upper reservoir has approached its equilibrium concentration, and then removes all of its contents, and starts over again. It is assumed that the reservoir is closed off from the tube during the removal of the gas; otherwise the mixing with gas drawn in from the tube would make it impossible to obtain the concentrations and amounts calculated here.

Our fundamental equation for these calculations is that for the total transport of species 1 up the tube. By (23) and (31) we have

$$\tau_1 = H\{c_1(1-c_1) - (2A)^{-1}(dc_1/dz)\}. \quad (34)$$

At the final equilibrium, when the concentration in the top reservoir has ceased to increase, $\tau_1 = 0$, and the solution of (34) is

$$c_1(z) = \tfrac{1}{2}\{1+\tanh A(z-z_0)\}, \quad (35)$$

where z_0 is determined by the condition that the total quantity of species 1 is conserved. If we set

$$c_1(-l) = c_1^0; \quad c_1(l) = \kappa_e, \quad (36)$$

we find for the equilibrium *separation factor:*

$$(\kappa_e/c_1^0)(1-c_1^0)/(1-\kappa_e) = e^{4Al}. \quad (37)$$

If κ_e is small with respect to unity, this becomes

$$(\kappa_e/c_1^0) \leqq e^{4Al}. \quad (38)$$

When τ_1 is not zero, but has some constant value—that is, before the final equilibrium has been established—the solution of (34) is

$$c_1(z) = \tfrac{1}{2}\{1+q\tanh qA(z-z_0)\}, \quad (39)$$

where $q = (1-4\tau_1/H)^{\frac{1}{2}}$.

Under the boundary conditions $c_1(-l) = c_1^0$, $c_1(l) = c_1^1$ we have now

$$c_1^1 = \tfrac{1}{2} - (q/2)\{q\tanh 2qAl - q_0\}/ \times\{q_0\tanh 2qAl - q\}, \quad (40)$$

where $q_0 = 1-2c_1^0$.

In practice, it will be advantageous to make the lower reservoir sufficiently large that c_1^0 does not drop appreciably during the separation, since if it should drop, one would not realize all of the separation factor. If the reservoir is sufficiently large, then, c_1^0 is also the initial concentration of species 1. The constancy of c_1^0 may often be secured more conveniently by maintaining a continuous flow through the bottom reservoir. The quantity q_0 is then constant and equal to the initial value of q, and the equation for the time rate of change of c_1^1 is

$$(dc_1^1/dt) = \tau_1/m_t. \quad (41)$$

Let $t(\kappa_r)$ be the time for the concentration of the top reservoir to rise from its initial value c_1^0 to some required value κ_r. The integral of (41) may then be expressed as

$$t(\kappa_r) = m_t\int_{c_1^0}^{\kappa_r} dc_1^1/\tau_1. \quad (42)$$

The integral must be done numerically or graphically, by calculating c_1^1 from (40) for several values of τ_1.

In many cases, however, a close approximation can be used, which eliminates the necessity of numerical integration. We note that

$$c_1(1-c_1) \equiv c_1(1-2c_1') + (c_1')^2 - (c_1-c_1')^2 \quad (43)$$

where c_1' is arbitrary. If κ_r differs from c_1^0 by only a small amount, say not more than 0.2 or 0.3, one can select a value of c_1' and a constant to replace the last term in (43) in such a way that the resulting linear expression is a good approximation to $c_1(1-c_1)$ throughout the range in question. If in (34) the quantity $c_1(1-c_1)$ is replaced by such a linear approximation, then (34) and (41) can be integrated explicitly, and the formula for c_1^1 so obtained represents a simple exponential approach to equilibrium, which can be characterized by a relaxation time. This gives us a useful way to describe the speed of operation for cases in which a linear approximation to (43) is valid. In the case that the

range of c_1 is larger than about 0.3, the approach to equilibrium is of a more complicated type, which can not be characterized even approximately by a relaxation time.

A suitable value for c_1' is the mean value of c_1^0 and κ_r. In the present case, the constant value inserted in place of $(c_1-c_1')^2$ will not appear in the relaxation time; then by the procedure outlined, we find a relaxation time (time for $c_1^1-c_1^0$ to rise to $1-e^{-1}$ of its equilibrium value):

$$t_r=(m_t/H)\{e^{4Al(1-2c_1')}-1\}/(1-2c_1'). \quad (44)$$

There are several special cases of (44) worth mentioning: If c_1 is always small compared to unity,

$$t_r\leqq(m_t/H)(e^{4Al}-1). \quad (45)$$

If the separation factor, which is e^{4Al} in this case, is much larger than one, we see that the relaxation time is directly proportional to the separation factor.

If, however, we are working in the middle region, where both c_1^0 and κ_r are approximately one-half,

$$t_r\leqq 4Alm_t/H; \quad (46)$$

while if c_1 is always close to unity,

$$t_r\leqq(m_t/H)(1-e^{-4Al}). \quad (47)$$

It may perhaps be possible in practice to reduce the equilibrium time to some extent by a suitable variation of the pressure during operation. From (30) and (31) we see that H and K vary, respectively, as the second and fourth powers of the pressure. According to (23) the transport of species 1 is determined essentially by H during the early part of the separation process, while $\partial c_1/\partial z$ is still small. Thus a high pressure at the beginning increases the transport. In order to reach a large concentration gradient finally, the pressure must be reduced again. By proper manipulation a considerable advantage might be obtained. Such a procedure, however, meets a considerable technical difficulty, since the volume of the upper reservoir would have to be varied along with the pressure in order to prevent the loss of a great deal of gas down the tube.

Continuous operation

So far we have been discussing operation with no total transport of gas through the tube. In such operation the concentrated material is obtained by waiting until the approach to equilibrium has reached a certain stage, and then removing the contents of the top reservoir. There is also available a continuous type of operation, in which a small steady flow of gas is removed from the top of the apparatus, so that there is a small total transport of gas along the tube.

The convection field with which we have been calculating, which is described by the function $G(T)$, provides no total transport along the tube. Because of the linearity of the hydrodynamical equation, however, we can superpose on the convection field an unidirectional velocity field corresponding to a very small additional pressure difference. Since the additional velocity field is unidirectional and c_1 varies only very slightly across the tube, we can omit all discussion of the details of the new field and the distribution of c_1 across the tube; we simply write for the transport of species 1 due to the new field the product of the mean value of c_1 at the given position along the tube and the total transport of gas. The *total* transport of species 1 is then

$$\begin{aligned}\tau_1' &= \tau_1+\tau c_1,\\ &= Hc_1c_2-K(dc_1/dz)+\tau c_1, \end{aligned} \quad (48)$$

where τ_1' is now constant along the tube. The quantities H and K may still be taken as defined by (30) and (31), since, with attainable speeds of operation, the velocities in the superposed unidirectional field will in practice be extremely small.

As before we introduce $A=H/2K$, and as a convenient dimensionless parameter,

$$n=\tau/H. \quad (49)$$

We shall treat only the equilibrium case, where c_1^1 has a constant value, κ_r. There is little value in treating the approach to the new equilibrium, because the apparatus presumably would be operated with $\tau=0$ until c_1^1 rose to the value intended for continuous operation. Then we have $\tau_1'/\tau=\kappa_r$ and therefore

$$\tau_1'=nH\kappa_r. \quad (50)$$

The differential equation for c_1 is now

$$\{-c_1^2+(1+n)c_1-n\kappa_\tau\}^{-1}dc_1=2Adz, \quad (51)$$

whose solution is

$$c_1(z)=\tfrac{1}{2}\{1+n+q' \tanh q'A(z-z_0)\}, \quad (52)$$

where

$$q'=\{(1+n)^2-4n\kappa_\tau\}^{\frac{1}{2}}.$$

Eliminating z_0 by the condition $c_1(-l)=c_1^0$, $c_1(l)=\kappa_\tau$ we find

$$\tanh 2q'Al=q'(\kappa_\tau-c_1^0)\{(1-n)\kappa_\tau +(1+n)c_1^0-2\kappa_\tau c_1^0\}^{-1}. \quad (53)$$

This rather formidable equation gives the important relation between τ and κ_τ. It must be solved in any given case by successive approximations. The procedure may usually be based on the assumption that n is small, since only for small values of n can a large separation factor be realized. If, for example, one replaces q' by unity in the left number, and by the linear approximation $1+n(1-2\kappa_\tau)$ in the right member, one obtains as a first approximation

$$n^{(1)}=\{(\kappa_\tau+c_1^0-2\kappa_\tau c_1^0)\tanh 2Al-(\kappa_\tau-c_1^0)\} \times(\kappa_\tau-c_1^0)^{-1}(1+\tanh 2Al-2\kappa_\tau)^{-1}. \quad (54)$$

The quantity q' can then be calculated with the value $n^{(1)}$ for n, and (53) can then be solved for the second approximation $n^{(2)}$, and so on. This particular procedure converges well if c_1^0 is small, but fails entirely if $c_1^0 \geqslant \frac{1}{2}$.

For cases in which the range of values of c_1 to be covered is small, one can simplify the analysis by replacing c_1c_2 in (48) by a linear expression in c_1, just as was done in obtaining Eqs. (44)–(47) for discontinuous operation. In the present case the resulting formula involves the parameters of the linear expression in a more complicated way than does (44). Simple formulas can be given, however, for each of the three special cases corresponding to (45)–(47). When c_1 remains fairly small throughout, we can replace c_1c_2 by c_1 in (48), and, remembering that n must be small, we obtain

$$(\kappa_\tau/c_1^0) \leqq (e^{-4Al}+n)^{-1}. \quad (55)$$

For cases in which c_1 is throughout in a range of values of perhaps 0.3 to 0.7, we can replace c_1c_2 by $\frac{1}{4}$, and find

$$(\kappa_\tau-c_1^0) \leqq (1-e^{-4nAl})/4n. \quad (56)$$

When $(1-c_1)$ remains fairly small, we can replace c_1c_2 by $1-c_1$ in (48), and obtain

$$(1-c_1^0)/(1-\kappa_\tau) \leqq (e^{4Al(1-n)}-n)/(1-n). \quad (57)$$

These three formulas correspond precisely to (45), (46) and (47), respectively, and involve just the same linear approximations.

Continuous operation is the only practical method if we wish to use several stages in series, and the use of multi-stage apparatus seems distinctly desirable if we wish to combine a large separation factor with large speed of production. We have seen that if c_1^0 is small, the quantity $n=\tau/H$ must be small compared to unity. Therefore, in any stage, the transport is effectively limited by the quantity $Hc_1^0(1-c_1^0)$, where c_1^0 is the concentration at the bottom of the stage in question. If, now, c_1^0 is small, we see that in order to obtain a transport equal to that of a later stage, H must be larger for the first stage. A large H, however, means either a large K, and then the separation will be small, or a large B. A compromise would probably be used in practice.

The multi-stage apparatus should therefore consist of a series of vertical tubes; the first tube should be of large size and will produce a small change of concentration; subsequent tubes should be made progressively smaller.

Comparison of the two types of operation in single-stage apparatus

In the case of small c_1, formulas (45) and (55) make possible a simple direct comparison of the separations obtained by the two methods at a given effective speed, provided that $4Al$ is large enough so that e^{-4Al} can be neglected compared to unity. Eq. (55) can be written

$$(\kappa_\tau/c_1^0) \leqq \{\theta/(1+\theta)\}e^{4Al}, \quad (58)$$

where

$$\theta=n^{-1}e^{-4Al}=(H/\tau)e^{-4Al} \quad (59)$$

is a parameter inversely proportional to the speed, and e^{4Al} is the equilibrium separation given by (38), which may also be obtained by

setting $n=0$, or $\theta\to\infty$. In *discontinuous* operation the quantity which corresponds to τ is m_t/t_0, where t_0 is the time allowed for the separation to approach equilibrium before the reservoir is emptied. Then if we put

$$\theta'=Ht_0/(m_te^{4Al}) \tag{59'}$$

equal values of θ and θ' correspond to equal effective speeds of production by the two methods. According to Eq. (45), the exponential approach to equilibrium now takes essentially the form

$$(\kappa_r/c_1^0)\leqq(1-e^{-\theta'})e^{4Al}. \tag{60}$$

The expressions (58) and (60) show that at a given effective speed a greater fraction of the equilibrium separation ratio can be obtained by using discontinuous operation.

In the case of c_1 near one-half, we can introduce the parameters

$$\varphi=(4Aln)^{-1};\qquad \varphi'=Ht_0/(4Alm_t), \tag{61}$$

equal values of which correspond to equal effective speeds. The equilibrium concentration difference, from (56) with $n=0$ is Al; and the realized concentration differences are, by (56) and (46),

$$(\kappa_r-c_1^0)\leqq\varphi(1-e^{-1/\varphi})\cdot Al \tag{62}$$

for continuous operation, and

$$(\kappa_r-c_1^0)\leqq(1-e^{-\varphi'})\cdot Al. \tag{63}$$

When less than a fraction $(1-e^{-1})$ of the equilibrium concentration difference is to be obtained, the continuous method works slightly better; otherwise, the discontinuous is better.

In the remaining case, c_1 nearly equal to one, it is not possible to introduce a single parameter characterizing the speed in such a way that a simple comparison of the two methods is possible. Rough computation from (47) and (57) shows that when large ratios $(1-c_1^0)/(1-\kappa_r)$ are required, continuous operation is decidedly faster.

General remarks on speed of operation

In the case of discontinuous operation, the quantity which characterizes the speed of operation in terms of the mass of the element with a given concentration, divided by the time required to produce it, is m_tf/t_r where f is the fraction of the molecular weight contributed by the element in question. This characteristic quantity varies as Hf. In the continuous case, the corresponding quantity is τf, which, for a given concentration, also varies as Hf. Thus in either case the variation of the speed, s, is given by

$$s\propto Hf\propto(w^3\rho^2\alpha Bf/\eta)(\Delta T/T)^2. \tag{64}$$

Since Al must have a given value, and since $D\propto\eta/\rho$, we see from (31) that w must vary as

$$w\propto(\alpha l)^{\frac{1}{3}}(\eta/\rho)^{\frac{1}{3}}. \tag{65}$$

If we accept (3), α varies as f, and we have the significant relation

$$s\propto f^{2.75}l^{0.75}(\rho\eta)^{\frac{1}{3}}B(\Delta T/T)^2. \tag{66}$$

To get a large speed at the specified concentration, it is evident that one should choose as light a molecule as possible, because of the strong dependence on f. The factor B can be increased by using a larger tube, or several tubes in parallel. Since under ordinary conditions ρ is proportional to the pressure, the speed varies as the square root of the pressure and as the three-fourths power of the length, *provided* that $2w$, the difference of the radii, is readjusted for changes of pressure and length in accordance with (65).

It is assumed in the argument leading to (66) that the ratio K_d/K is very small compared with unity, since otherwise we should not be justified in using (31), and should use instead the modified value (33).

The power expended because of conduction is by (29)

$$P_c=2lB(4.18Q)=4.18\lambda lB\Delta T/w \tag{67}$$

in watts, and, by (65), is proportional to $l^{\frac{1}{3}}\rho^{\frac{1}{3}}B\Delta T$; the viscosity and heat conductivity are independent of the pressure. Thus so far as conduction is concerned, the speed and power are just proportional to one another, as long as a fixed concentration difference is demanded, and a fixed temperature difference is used. The advantage of a rather large ΔT is evident; but there is little use in going to extreme temperatures, since it is the ratio of ΔT to the *mean* temperature that is involved, and also since the radiation loss will be large if T_2 is made very

high. The power consumption due to radiation between the walls is independent of w, and for nontransparent tubes is given by

$$P_r = 2lB(1-R_1)(1-R_2) \times (1-R_1R_2)^{-1}\sigma(T_2^4-T_1^4), \quad (68)$$

where R_1 and R_2 are the average reflection coefficients of the walls of the tubes, and $\sigma = 5.7 \times 10^{-12}$ watt/cm^2-deg.^{4}.

Effects of asymmetry; general constructional considerations

We shall here consider briefly the effect of asymmetry in the apparatus. Due to nonuniformity of heating or cooling of the tubes, it is possible that the temperature may vary around the tube. This will give rise to an additional convection, characterized by a slight upward flow at the hotter part of the annulus, and a corresponding downward flow at the colder part. For simplicity, we may suppose that the temperature field is still independent of z, but varies with the azimuthal angle, φ, in the simple manner:

$$T = f(r) + (\delta T/2)\cos\varphi. \quad (69)$$

One can then show that the essential effect is to introduce another contribution to the transport given by $-K_p dc_1/dz$, where

$$K_p/K = (315B^2/16\pi^2w^2)(\delta T/\Delta T)^2, \quad (70)$$

provided that $B \gg w$. Since K_p/K must be kept fairly small, Eq. (70) imposes rather strong conditions on the tolerable asymmetry of the temperature. In the apparatus to be discussed in the next section, K_p would become equal to K for $\delta T \leqq 5°$.

A lack of centering of the tubes would have a considerable direct effect on performance, because H and K depend on the third and seventh powers of w. The asymmetry in temperature brought about by the lack of centering would, if appreciable, be still more harmful. To minimize it, good conduction is essential. Thus metal tubes are to be preferred on several counts: for precision in construction, high conductivity, and large reflection coefficient to reduce radiation losses.

The importance of symmetry makes it evident that advantages in speed and concentration should be sought by increases in length rather than by the use of high pressures and small values of w. Also, both for accuracy of construction and because of the factor B^2 in (70), it is better to use several tubes in parallel rather than large tubes.

To avoid lack of symmetry in the temperature distribution, the water cooling must be efficient and the heating of the inner tube must be very uniform. Heating by condensation of a vapor rather than by resistance wire seems advisable.

IV. A Numerical Example: C^{13}

In order to illustrate the application of our formulas we shall apply them to the design of a single-stage apparatus for the concentration of C^{13}. Here we are concerned with the concentration of a *heavy* isotope at the *bottom* of the tube. Our equation for A and all our equations concerned with the speed of operation apply here with no change except the replacement of c_1 by c_2. A formal justification of this rule is provided by inspection of the fundamental equations (23) and (48). In these equations we must interchange c_1 and c_2; change the sign of the term in c_1c_2, since this term changes sign in rewriting (10) for species 2; and change the signs of the τ and τ_i' terms, because we are now concerned with transport *down* the tube. When this is done the equations are unchanged in form except for a change in sign of the term in $\partial/\partial z$. This is proper, since the concentration is now increasing downward instead of upward.

We take as the specifications of our apparatus: Length of tube, $2l = 800$ cm; $B = 2\pi l = 4\pi$; $T_1 = 300°$K; $T_2 = 600°$K; pressure, 1 atmosphere; and equilibrium concentration, $\kappa_e = 0.30$. Since the carbon isotope of mass 13 occurs with a natural abundance[18] of one part in about 92, and therefore $c_1^0 = 0.0108$, it follows at once from (37) that we must have $e^{4Al} = 39.3$, or $A = 0.0023$/cm.

The required value of the difference in radii, $2w$, and the speed of operation are now determinate, once we have selected the molecule which is to carry the carbon.

Our general discussion of the speed shows

[18] Vaughan, Williams and Tate, Phys. Rev. **46**, 327(A) (1934).

that one should use as light a molecule as possible (cf. Eq. (66)). Methane, CH_4, is therefore eminently suitable. Extrapolating to 450°K the data for CH_4 given in the *International Critical Tables*, we find

$$\begin{aligned} &\eta = 1.60\times10^{-4} \text{ poise},\\ &\rho = 0.433\times10^{-3} \text{ g/cm}^3,\\ &D \leqq 1.4\eta/\rho = 0.52 \text{ cm}^2/\text{sec.},\\ &\lambda = 1.20\times10^{-4} \text{ cal./cm-sec.-deg.}, \end{aligned} \tag{71}$$

and by (3)

$$\alpha = 0.0106.$$

The conditions on the relaxation length l_r (Eq. (4)), and the Reynolds number (5) are strongly satisfied, as we shall verify after $2w$ has been evaluated. In the case under consideration, however, it is not true that $K_d/K \ll 1$, so that the effect of longitudinal diffusion cannot be ignored. Thus we must equate not A, but A_d to the value 0.0023/cm.

Putting the values (71) in (31) and (32), we find

$$A = (3.3\times10^{-5})/w^4 \text{ and } K_d/K = (5.1\times10^{-4})/w^6.$$

Since A_d must have the value 0.0023, we have by (33),

$$w^6 - 1.45\times10^{-2}w^2 + 5.1\times10^{-4} = 0.$$

The larger of the two positive real roots gives the value $2w = 0.62$ cm. The ratio K_d/K is about 0.58, so that it certainly could not have been neglected.

In order to discuss the question of speed, we must know the value of H. We find by (30),

$$H = 2.3\times10^{-5} \text{ g/sec.}$$

The range of c_1 in question, 0.01 to 0.30, is just within the range of validity of the linear approximation (44). If we wait a length of time of the order of the relaxation time, we shall reach a concentration in the bottom reservoir of only about 0.194. In this case, we are concerned only with the range 0.01 to 0.19, and a suitable value of c_1' is 0.10. If we suppose the bottom reservoir contains 5.0 grams of gas—or approximately 10^4 cc—the relaxation time given by (44) is

$$\begin{aligned} t_r &= [5.0/(2.3\times10^{-5})]\times[(39.3)^{0.5}-1]/0.8\\ &= 4.9\times10^6 \text{ seconds} = 57 \text{ days}. \end{aligned}$$

The speed of production by the discontinuous method is thus 88 mg/day of methane, or about 66 mg/day of carbon, with a concentration of 19 percent C^{13}.

A rough idea of the speed obtainable in continuous operation may be obtained from Eqs. (58) and (60). These formulae really apply only in the approximation $c_1' = 0$, but should be fairly reliable for purposes of comparison when a more accurate value has already been found for one method. The use of the time t_r between removals in discontinuous operation corresponds to $\theta' = 1$ in (60). Putting $\theta = 1$ in (58), we see that continuous operation at a speed of 88 mg of methane per day will give a concentration of roughly $\frac{1}{2}\kappa_e$, or about 15 percent C^{13}. To obtain an estimate of the speed at concentration 19 percent, we put

$$\theta/(\theta+1) = 1 - e^{-1}$$

and obtain $\theta = 1.72$. Since θ is inversely proportional to the speed, continuous operation will give roughly $88/1.72 = 51$ mg/day of methane at 19 percent C^{13}.

The speed of production at 19 percent C^{13} can be calculated exactly from (53). The estimated value just obtained corresponds to $\tau = 5.9\times10^{-7}$ g/sec., or $n^{(1)} = \tau/H = 0.0259$. This can be used as a first approximation in solving (53). It gives $q' = 1.0161$, $\tanh 2q'Al = 0.95315$. The next approximation is now obtained by solving (53) for n as it occurs explicitly. The value obtained is $n^{(2)} = 0.0290$, and the value to which the approximations converge is $n = 0.0279$. This corresponds to a speed of 55 mg/day.

The power consumption due to conduction, by (66), is 2450 watts, while that due to radiation, by (67) would be 7000 watts if the tube walls were perfectly black ($R_1 = R_2 = 0$). If the walls were a polished metal, however, this value might well be cut down to less than 500 watts.

The Reynolds number, by (5), is of the order of 3. Since in the case of pure pressure flow through tubes or between plates this number must become of the order of several thousand before spontaneous turbulence occurs, it is difficult to believe that there could be any turbulence here.

By (4), the length of tube at each end in which the temperature gradient differs from

that determined by conduction is of the order of 0.4 cm, and thus may certainly be neglected.

The calculations given above for C^{13} are based on the value $\alpha=0.0106$ which is given by Eq. (3). This equation is, however, only a rough guess, albeit the best one possible. It may be found by experiment that the actual values of H and A for any given gas are distinctly different from those calculated from values of α given by (3), perhaps by as much as a factor 2. In practice, therefore, it will be necessary to do some preliminary work to find the actual value of α. It is suggested that this be done by running the apparatus at a fairly high pressure. For instance, in the example just discussed, the use of a pressure of two atmospheres instead of one will multiply H by 4, and divide A by approximately 4, so that the separation factor will be small, but so will also be the equilibrium time. If one now measures c_1^1 as a function of the time, one will obtain the values of both H and A. Either one will yield the value of α, by (30), or by (31), (32) and (33). We may now extrapolate A to the desired value by changing the pressure, since we know that H, A and K_d/K vary, respectively, as the second, inverse second, and inverse fourth power of the pressure.

Preliminary adjustments such as those just described will of course be necessary only in the first work on each gas. Once the correct value of α is known from experiment, our equations should make it possible to design apparatus which will perform in acceptable agreement with specifications.

One of us (L. O.) is indebted to Dr. G. Akerlof and Dr. G. W. King of the Chemistry Department, and to Dr. C. C. Furnas of the Chemical Engineering Department of Yale University for advice in regard to feasible construction and operation of apparatus on laboratory and industrial scale. The others (W. H. F. and R. C. J.) are grateful to Professor K. T. Bainbridge and Dr. R. Sherr of the Physics Department of Harvard University for interesting and helpful conversations.

JUNE 1, 1939 PHYSICAL REVIEW VOLUME 55

Calculation of the Second Virial Coefficient of Helium Gas for the Lowest Measured Temperature

LEON GROPPER
Department of Mathematics, Brooklyn College, Brooklyn, New York
(Received April 3, 1939)

IN RECENT articles[1] an explicit and calculable expression has been derived for the second virial coefficient of a monatomic gas. This is the B in the equation of state,

$$pV/RT=(1+B(T)/V+C(T)/V^2+\cdots)$$

and, assuming the Einstein-Bose statistics, is given by the formula,

$$B_{\text{E.B.}}=-\frac{N\pi^{\frac{3}{2}}\lambda^3}{2}-16N\pi^{\frac{3}{2}}\lambda^3\sum_{n,\text{ even }l}(l+\tfrac{1}{2})\times\exp\left[\lambda^2k_0^2(n,l)/a_0^2\right]-16\pi^{\frac{3}{2}}N\lambda^3\sum_{\text{even }l}(l+\tfrac{1}{2})\int_0^\infty dk_0\times\exp\left[-\lambda^2k_0^2/a_0^2\right](d\eta_l/dk_0). \quad (1)$$

Here, $\lambda^2=\hbar^2/mkT$, η_l is the phase found from the wave equation for the relative motion of two radially interacting molecules,

$$\frac{d^2v}{d\rho^2}+\left(k_0^2-\frac{m}{\hbar^2}a_0^2V-\frac{l(l+1)}{\rho^2}\right)v=0.$$

$k_0^2(\eta, l)$ are the discrete states for two such molecules, a_0 is the Bohr radius, and V is the interaction potential between the two molecules.

Extensive calculations have recently been made with formula (1) by Massey and Buckingham[2] on the inert gases, in particular, helium. These calculations are based on the use of the Slater-Kirkwood potential for the calculation of

[1] E. Beth and G. E. Uhlenbeck, Physica **4**, 915 (1937); L. Gropper, Phys. Rev. **51**, 1108 (1937).

[2] H. S. W. Massey, and R. A. Buckingham, Proc. Roy. Soc. **168**, 378 (1938).

TABLE I. *Comparison of analytical values of η_0 with those found by numerical integration.*

k_0	ANALYTICAL k_0	NUMERICAL η_0
$\frac{2}{3}$	−1.76	−1.8212
0.1	+1.66	+1.6480
0.02	+2.78	+2.7816
0	π	−

the phases for helium. In this paper we use the Slater-Margenau potential, which presumably takes into account all the more important Van der Waals' forces.

To compare (1) with the experimental values at low temperatures it is advisable to consider the case of helium because: 1. extensive low temperature measurements have been made with helium; 2. helium remains a monatomic gas down to the lowest temperatures ($T \leqq 4°$K); 3. the statistical wave-length of the helium molecule, $\lambda=(\hbar^2/mKT)^{\frac{1}{2}}$, is relatively large because the mass is so small, and the larger the wave-length the more pronounced should be the quantum effect; 4. the potential between two helium molecules has been theoretically calculated, so that, in principle at least, one should be able to deduce the experimental results solely from theory.

A comparison of (1) was made for the case of the lowest temperature for which B has been determined; namely, $T=3.708°$K. At this temperature the experimental value of B for a cubic centimeter of helium is, -4.17×10^{-3} cc [3] so that for a mole $B=-93.6$ cc.

The phases η_l were calculated by using the Slater-Margenau potential[4] in the region where V is presumed to be valid, and joining

$$V=\left\{7.7e^{-2.43\rho}-\left(\frac{0.68}{\rho^6}+\frac{5.37}{\rho^8}+\frac{28.4}{\rho^{10}}\right)\right\}\times10^{-10}\text{erg}$$

with an expression a/ρ^2-b for small values of ρ down to $\rho=0$. The reason for this choice of joining-on function is that it leads to Bessel functions for the solution of the wave equation, and these are tabulated. This joining on process could not appreciably alter the results, for the energies considered in the integral of (1) were very small, and over this region of small energies V and a/ρ^2-b practically coincided.

Before discussing the contribution to (1) from the $l=0$ term we shall investigate how many terms of the sum on l must be taken along at the lowest temperatures ($T\leqq4°$K). For sufficiently low temperatures the integrand in (1) will be appreciable only for very small k_0 say, $\lambda k_0/a_0\leq1$, because of the presence of the exponential. But for small k_0 and sufficiently large l the distance of closest approach will be well beyond the point where the potential is appreciably different from zero. Hence the phase shifts will be zero for such values of l. The question is what is meant by sufficiently large l? It was found that already for $l=4$, the distance of closest approach for an energy such that $\lambda k_0/a_0=1$ was $\rho=14.8$, far beyond the point where V is appreciably different from zero. For values of k_0 such that $\lambda k_0/a_0<1$ the distance of closest approach will be still farther out. And for values of k_0 such that $\lambda k_0/a_0>1$ the integrand in (1) rapidly diminishes because of the exponential. Hence the phases for $l=4$, 6, etc. at the low temperature $T=3.708°$K may be neglected.

On the other hand, the phases for $l=2$ are not negligible. This can be understood if one plots $(a_0^2mV/\hbar^2+l(l+1)/\rho^2)$ for $l=2$. One finds a very low broad maximum, 0.05. For all $k_0^2\geqq0.05$ the molecule will pass over the hump into the potential field, and one should expect considerable positive phase shift when one realizes that the depth of $a_0^2mV/\hbar^2$ is very large compared to this energy; namely, it is 0.36 as compared to $k_0^2=0.05$. Further, since values of k_0^2 considerably larger than 0.05 may be allowed before the exponential in (1) is negligible, one might then expect, qualitatively, that the contribution for $l=2$ is considerable. As a matter of fact it amounts to -91.3 at $T=3.708°$K. This result was obtained by first integrating (1) by parts. One gets for $l=2$

$$-40\pi^{\frac{1}{2}}\lambda^3N[\eta_2\exp(-\lambda^2k_0^2/a_0^2)]_0^\infty$$

$$-40\pi^{\frac{1}{2}}\lambda^3N\frac{2\lambda^2}{a_0^2}\int_0^\infty\exp(-\lambda^2k_0^2/a_0^2)k_0\eta_2dk_0.$$

Now $\eta_2(0)=0$ since there is no penetration as $k_0\to0$. Hence the integrated part of (1) vanishes. The remainder of (1) was evaluated by trape-

[3] Van Itterbeek, Leiden Comm., Supp. 70C (1932).
[4] H. Margenau, Phys. Rev. **38**, 742 (1931).

zoidal integration with the help of the following calculated phases

η_0	0	0.163	0.560	0.849	0.583	0.300
k_0	0	0.2	0.3	0.4	0.5	$\frac{2}{3}$

Since the integration was carried out with such a few phases, a partial test of the error made through trapezoidal integration was carried out by employing parabolic integration. There was only about one percent difference in the results.

We return to the contribution for $l=0$ and a discussion of the discrete states. It was found that the Slater-Margenau potential was just deep enough to accommodate one discrete level $(n=0, l=0)$ $k_0^2=0.0051$. This discrete contribution came to -148 cc.

For the continuous contribution with $l=0$, the phases were calculated analytically, as well as numerically, by passing a Morse potential very accurately through the Slater-Margenau potential. This analytic expression for the phases is rather complicated and is the form of an infinite series, which, however, is rapidly convergent for small k_0. In any case the numerical and analytic values were almost identical. The important range of values of k_0 was between zero and about two-thirds. Above that the factor $\exp(-\lambda^2 k_0^2/a_0^2)$ cuts out the contribution to the integral. In Table I some analytic values of η_0 are compared with those found by numerical integration. This table includes the extremes of the range. Enough values of η_0 were found to make the integration of (1) after first integrating by parts and noting that $\eta_0(0)=\pi$. This gave a contribution of $+125$. This together with the contributions from the $l=2$ term, the discrete term, and the pure Bose term, the net result for the second virial coefficient at $T=3.708°$K was found to be $B=-123$. Comparing this with the experimental result -93.6, one sees that there is about a thirty percent discrepancy. Since we estimate the numerical work to be within an error of 10 percent it is clear that the potential must be altered.

It is necessary to decrease either the depth or the range or both. This would have the double effect of raising towards zero the discrete energy and decreasing the positive phases. Both effects would contribute to making the virial coefficient less negative. While one cannot make quantitative statements about the potential one can, however, now set certain limitations on it. It must lie somewhere between the Slater-Kirkwood potential which gives a smaller well, and the Slater-Margenau potential. It cannot be smaller than the former, for the former does not take into account all the Van der Waals' forces. And it cannot be larger than the latter, since the latter already gives too large a negative virial coefficient.

Infra-Red Pleochroism and Fermi Resonance Associated with CH_2 Groups in Crystals

JOSEPH W. ELLIS AND JEAN BATH
University of California, Los Angeles, California
(Received May 2, 1939)

THERE are at least two crystalline materials containing methylene, CH_2, groups which are readily obtainable as single crystals and whose lattices have been worked out with considerable certainty by x-ray diffraction methods. These are the alcohol, pentaerythritol,[1] $C(CH_2OH)_4$, and diketopiperazine,[2] $(CH_2NHCO)_2$. In each of these crystals the CH_2 groups line up with respect to one another and with respect to the crystal axes in such a way that it is possible to transmit plane polarized infrared waves through thin sections and approximately keep the electric vector E of the light vibrating either parallel or perpendicular to the CH_2 symmetry axes. We wish to discuss the absorption bands near 1.7μ only and the pleochroism displayed by the dependence of these bands upon the azimuth of vibration of E.

The absorption by pentaerythritol in this region is shown in Fig. 1, which is a reproduction of the original recording spectrometer tracings. There are three bands: A, 1.703μ; B, 1.735μ; C, 1.763μ. Pentaerythritol is a tetragonal crystal in which the molecules are so aligned that the bisector lines of the CH_2 angles all parallel the c axis. Record I was obtained from a 0.88-mm specimen, so ground and oriented that the beam was parallel to the a_2 axis and E vibrated parallel to the c axis. Band A is strong and bands B and C are relatively weak. The resolving power is not large, since, because of the imperfect quality of the specimen and the loss of intensity introduced through polarizing, the slit width included a $\Delta\lambda$ of the order of magnitude 0.01μ. The calcite polarizing prism was of the Glan-Thompson type, which, because it transmits only the extraordinary wave, absorbs relatively little below 3μ.

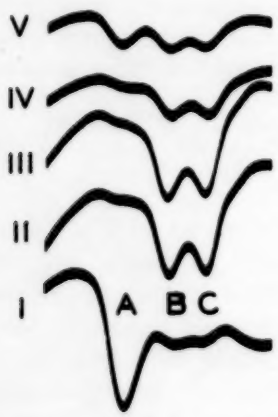

FIG. 1. Absorption of pentaerythritol.

In II and III, B and C are strong and A has almost vanished. These records were taken through a 0.98-mm specimen with the beam parallel to the c axis and with E inclined 10° to a_1 and 80° to a_2 in II and at right angles to this orientation in III. The choice of orientations was dictated by the predicted orientations of "hydrogen bonds," a subject to be dealt with more fully elsewhere. In IV the beam and E were parallel, respectively, to a_2 and a_1 in the 0.88-mm crystal. A thin cell of powdered crystal embedded in an appropriate mixture of CCl_4 and CS_2 and unpolarized light were used to obtain V. This record is useful to indicate the true relative intensities among A, B and C. The specimens were placed directly before the slit and it is probable that the departure from parallelism among the rays in the cone from the condenser mirror is responsible for the slight residual band A in those records, II, III, IV, in which it is expected to be absent. The five curves have different magnitudes of displacements from their base lines and hence the depths of bands cannot be compared among them. In particular the displacements in IV and V are low.

Since A appears when E is parallel to the symmetry axis in the CH_2 groups and disappears, or practically disappears, when E has no component parallel to this axis, it must be a π-type of vibration. We identify it as $2\nu_\pi$, the first harmonic of the symmetrical valence vibration in the triangular CH_2 "molecule." B and C are excited regardless of the direction of E, but with greater intensity when E is perpendicular to the axis.

[1] Llewellyn, Cox and Goodwin, J. Chem. Soc. 883 (1937).
[2] R. B. Corey, J. Am. Chem. Soc. **60**, 1598 (1938).

Moreover, they keep the same relative intensities. We interpret them as arising from the first harmonic of the asymmetrical valence vibration, $2\nu_a$, and the third harmonic of the bending vibration, $4\delta_s$. Because of the equality in intensities, regardless of the method of excitation, we assume that they represent Fermi resonance arising from the exact coincidence of two energy states. *B* and *C* are more efficiently excited through σ-type than through π-type of interaction. A comparison of intensities in II, III with I indicates, as is expected, that the CH_2 electric moment change associated with ν_a is greater than with ν_s. This seems reasonable when it is realized that the planes of two CH_2 groups are perpendicular to the other two, and hence in effect only two groups are functioning in II or III, whereas all four function in I.

The diketopiperazine story is similar to that just outlined. This is a monoclinic crystal with the planes of the flat ring molecules as well as the symmetry axes of the CH_2 groups parallel to the *b* axis and lying approximately in the (101) plane. Fig 2(I) was obtained with the beam and *E* parallel, respectively, to the *c* and *b* axes in a 0.60-mm specimen. II and III were secured with the beam parallel to *b* and with *E* vibrating respectively perpendicular and parallel to the (101) plane in a 0.78-mm section. Since the planes of the two CH_2 groups are parallel to each other and perpendicular to the (101) plane, greater σ-type excitation should occur in II than in III. In fact, it should be absent in III; we associate the residual *B* band in III with a failure to align perfectly the crystal and to the nonparallelism in the beam.

Our interpretations of *A* (1.703μ), *B* (1.745μ) and *C* (1.754μ) here are the same as with pentaerythritol, with this important exception. *B* and *C*, only partially resolved, alter their intensity ratio greatly, as I and II show. $2\nu_a$ and $4\delta_s$ do not exactly coincide and Fermi resonance is only slight. Therefore, *B* is essentially $2\nu_a$, and *C* is essentially $4\delta_s$. This cannot be said of the pentaerythritol bands.

FIG. 2. Absorption of diketopiperazine.

The band marked *X* in Fig. 2 we believe does not arise from CH_2 vibrations, but is associated with similar ones on the short wave side of *A*, the set belonging to what remains of the NH groups in the various resonating $(CH_2NHCO)_2$ structures assumed by Corey.[2]

Because of the results of Fox and Martin[3] on CH_2 groups it has not seemed necessary for us to defend the assignment of particular bands to these groups. It must be pointed out, however, that our assignments of frequencies to ν_s and ν_a reverses, at least in the two instances here involved, the order of assignment by Fox and Martin. We believe that the control of the direction of *E* vibration with respect to the symmetry axis of the CH_2 groups in our work establishes considerable confidence in our identifications.

[3] J. J. Fox and A. E. Martin, Proc. Roy. Soc. **167**, 257 (1938).

LETTERS TO THE EDITOR

Prompt publication of brief reports of important discoveries in physics may be secured by addressing them to this department. Closing dates for this department are, for the first issue of the month, the eighteenth of the preceding month, for the second issue, the third of the month. Because of the late closing dates for the section no proof can be shown to authors. The Board of Editors does not hold itself responsible for the opinions expressed by the correspondents.

Communications should not in general exceed 600 words in length.

Velocity of Radio Waves in Air

Colwell and Friend[1] report a determination of the velocity of radio waves in air between 50 and 80 percent the velocity of light. Vitter and Brieger[2] show a rather direct means of determining this velocity, and report a value which is within 2.5 percent of the velocity of light.

Several years ago, when first confronted with the problem of designing directional antennas for use with radio broadcast stations, the writer was concerned about this matter of velocity of radio waves in air. It is usually assumed that the waves from each of the elements making up the directive array leave the antenna and travel outward with a velocity equal to the velocity of light in free space; namely, 3×10^{10} cm/sec. If this assumption were not true, there would in some cases be a great discrepancy between the theoretical radiation diagram and the pattern obtained in practice. The writer has designed and adjusted several directional arrays, in which the final pattern obtained agreed very closely with the calculated diagram. One array in particular was of such dimensions that it very readily demonstrated the point in question. The spacing of the antennas, the current ratios, and the phase relations between antenna currents have been described elsewhere.[3] The electric field intensity, in millivolts per meter, for a power of 1000 watts is

$$F(\text{mv/m at one mile}) = 312.0[\cos(117^\circ\cos\phi) + 0.25\angle -90^\circ + 117^\circ\cos(\phi-30^\circ)], \quad (1)$$

where ϕ is measured counterclockwise from north in a horizontal plane. In deriving this equation, the velocity of propagation of the waves from each antenna was taken as the velocity of light in free space. The pattern resulting from Eq. (1) is shown in Fig. 1.

If we assume that the velocity of the waves leaving each antenna is 80 percent of the velocity of light, the equation for the horizontal pattern becomes

$$F(\text{mv/m at one mile}) = 312.0[\cos(146^\circ\cos\phi) + 0.25\angle -90^\circ + 146^\circ\cos(\phi-30^\circ)]. \quad (2)$$

The resulting pattern is shown in Fig. 2. In comparing Figs. 1 and 2, we see that the east and west lobes are not altered appreciably by the variation in velocity. This is due to the fact that the towers are distributed along the north and south line, so that the east and west lobes are formed by waves which leave each tower at approximately the same time. The towers are spread north and south over a half-wave-length so that the velocity effect is of great importance.

In adjusting a directive array, it is possible to determine the currents in each antenna, as well as the phase relations between the currents with great accuracy.[4] The undetermined quantity is then the velocity of propagation of the radio waves. The array in question, when placed in operation, yielded a measured pattern which was in very close agreement with Fig. 1, and not at all in agreement with Fig. 2. Among other measurements made on this array, several measurements of field intensity were taken at a number of points along a north radial, as indicated

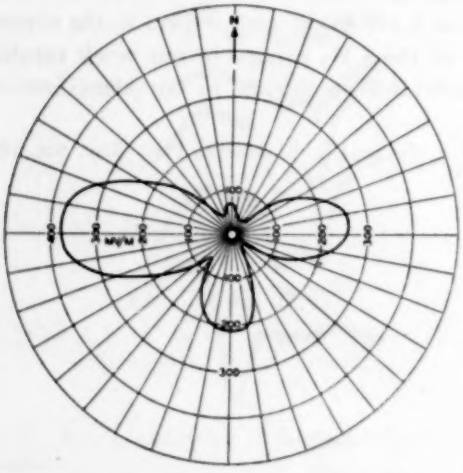

FIG. 1. Intensity pattern when the velocity is 80 percent of that of light.

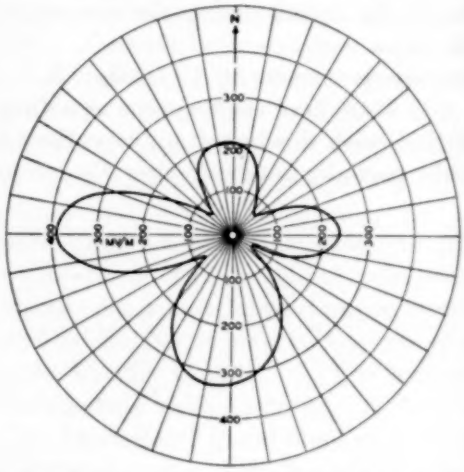

FIG. 2. Intensity pattern when velocity is the velocity of light.

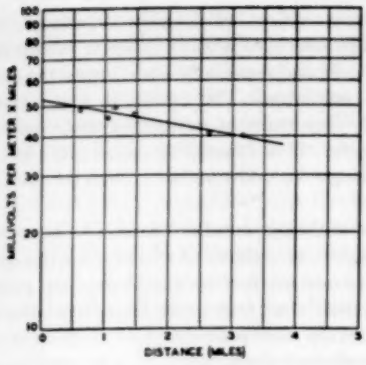

FIG. 3. Measured field intensities.

on Fig. 1. These values of field intensity were multiplied by the distance in miles to the measuring point to obtain the $F \cdot d$ curve shown in Fig. 3. This curve, when extrapolated to zero miles, yields the effective field intensity at one mile along this radial. Comparison of this value with Figs. 1 and 2 shows an excellent agreement with Fig. 1, which was based on a velocity of propagation of the radio waves equal to the velocity of light in free space.

GEORGE H. BROWN

RCA Manufacturing Co., Inc.,
Camden, New Jersey,
May 4, 1939.

[1] R. C. Colwell, A. W. Friend, N. I. Hall and L. R. Hill, Phys. Rev. **50**, 381 (1936); R. C. Colwell and A. W. Friend, Phys. Rev. **51**, 990 (1937).
[2] A. L. Vitter and L. C. Brieger, Phys. Rev. **55**, 416 (1939).
[3] George H. Brown, Proc. I. R. E. **25**, 101 (1937).
[4] George H. Brown and Gilbert Swift, Broadcast News, No. 28, 8 (1938).

Transmission of Slow Neutrons Through Crystals*

We have found a marked dependence of the slow neutron cross section upon the crystalline state of the material which the neutrons traverse.[1] Measurements of the transmission of slow neutrons through single crystals of iron, nickel, quartz and permalloy show that as compared with the polycrystalline state the materials are much more transparent when in the form of single crystals.

The cross section of single crystals may depend upon their thickness and the orientation of the crystalline axis relative to the neutron beam.[2] In quartz no such easily measurable effect was noticed with our highly collimated neutron beam.[3] Since the increase in transparency for single crystals is large and no easily measurable thickness effect was observable we conclude that under these conditions only a narrow band of the neutron wave-length spectrum is scattered by a single crystal orientation.

TABLE I. *Cross sections per atom or molecule for slow neutrons.*

	POLYCRYSTALLINE $\sigma \times 10^{24}$ CM^{-2}		SINGLE CRYSTAL $\sigma \times 10^{24}$ CM^{-2}	G/CM^3
Fe	12.0±0.2		7.0±1	1.6
			6.1±1	8.8
Ni	19.8±0.5		14.1±1.2	4.4
SiO_2	8.0±1	(fused)	4.5±0.6	3.7
	8.8±1	(sand)	4.1±0.6	1.3
	10.5	(additive)		
Permalloy				
(73% Ni−27% Fe)			10.2±1.3	6.2
(68% Ni−32% Fe)			10.2±1.3	6.2

TABLE II. *Cross sections of permalloy for slow electrons.*

	EXPERIMENTAL $\sigma \times 10^{24}$ CM^{-2}	COMPUTED FROM Ni−Fe CONTENT $\sigma \times 10^{24}$ CM^{-2}
78	12.5±0.7	18.2
45	16.0±0.8	15.8

In Table I the results of our measurements of the total cross section per atom or molecule are given.

In Table II are shown the cross sections of permalloy 78 and 45. In this case the material was in a polycrystalline state.

Previously[4] we have reported that the cross sections of compounds are not equal to the sum of the cross sections of the constituent elements. There one compared the cross section of compounds in polycrystalline states with the cross section of the elements which compose them. The constituent elements sometimes might be polycrystalline or even liquid. In this case, the effect is complicated by the different change of phase of the scattered wave[2] from the constituent elements which form the compound.

These phenomena are apparently connected with interference within crystal lattices.[5, 6] Some theoretical viewpoints for an understanding of the dependence of nuclear interaction upon crystal structure have been set forth.[1, 2, 7]

Because the slow neutron interaction is so dependent upon the crystalline state of the material the effective slow neutron cross section as usually measured must now be considered as characteristic of the state of the material and not immediately related to the true nuclear cross section per atom.

The permalloy and nickel crystals were obtained from the Bell Telephone Laboratory, through the courtesy of Dr. R. M. Bozorth. These crystals were grown by Mr. Boothby following a method described by Cioffi and Boothby.[8] Some of the quartz crystals were supplied by Professor Hubbard of Johns Hopkins University. We take pleasure in acknowledging the above cooperation.

MARTIN D. WHITAKER

New York University,
University Heights,
New York, New York,

HAROLD G. BEYER

Pupin Physics Laboratories,
Columbia University,
New York, New York,
May 15, 1939.

* Publication assisted by the Ernest Kempton Adams Fund for Physical Research of Columbia University.
[1] G. C. Wick, Physik. Zeits. **38**, 403–406 (1937).
[2] O. Halpern, M. Hamermesh and M. H. Johnson, Phys. Rev. **55**, 1125(A) (1939).
[3] Whitaker, Beyer and Dunning, Phys. Rev. **54**, 771 (1938).
[4] M. Whitaker and H. Beyer, Phys. Rev. **55**, 1124(A) (1939).
[5] H. v. Halban, and P. Preiswerk, Comptes rendus **203**, 73 (1936).
[6] D. P. Mitchell and P. N. Powers, Phys. Rev. **50**, 486 (1936).
[7] W. E. Lamb, Jr., Phys. Rev. **55**, 190 (1939).
[8] P. P. Cioffi and O. L. Boothby, Phys. Rev. **55**, 673(A) (1939).

A Prediction of the Remaining Course of the Present Sunspot Cycle

In a recent study,[1] the conventional periodic analysis of sunspot numbers was rejected in favor of a treatment which regards each rise and subsequent fall as an independent "outburst" and not as a superposition of steady periodic components. The usefulness was shown of the four-parameter family of curves

$$R = F(r-s)^a\, e^{-b(r-s)} \qquad (1)$$

for representing analytically the general course of each outburst (extending over roughly eleven years). Here R is the Wolf spot number at time r; and r starts from an initial value s, the time of the beginning of any particular outburst; while F, a and b are constants for the outburst. The form (1) matches the general course of spot numbers to an average accuracy of about ± 7 percent, when the observed *annual* numbers are fitted for the available 16 cycles completed since A.D. 1749.

Continuing this study the present authors are developing methods for fitting (1) to the smoothed run of *monthly* spot numbers. For the present, not yet completed, outburst, number 17, the tentative results in Table I are suggested.

The computed annual averages, R_C, are based on $s = 1933.46$, $a = 5.00$, $b = 1.13$ year^{-1}, $\log_{10} F = 1.0046$. These values require that maximum occur at time $v = 1937.9$ (November, 1937) at a height ("smoothed monthly number") of $V = 115$. In obtaining R_C, the small theoretical "overlap" from the preceding cycle, number 16, has been included for the years 1933–36 inclusive—to wit, 5, 3, 2, 1.

The Zurich determination of the maximum[2] from purely statistical considerations makes v 1937.4, and V 119.2. Max Waldmeier[3] on April 6, 1936, predicted 1937.7 and 124, and also the following approximate sunspot numbers for 1938–42 inclusive: 103, 76, 50, 30, 19. He had proposed the "outburst" hypothesis and fitted graphically two-parameter curves. Our adoption of form (1) leads to a more objective treatment.

The suggested curve of the present note matches within two or three percent the zero, first and second moments of the observed monthly numbers from June, 1933, to the end of 1938. Corrected numbers are not available for 1939. The Zurich height of maximum is computed closely enough, but it seems impossible to fit the date 1937.4 without making the computed spot numbers much too small during 1933 and early 1934.

Until this cycle has developed farther there will remain some uncertainty in the predictions. Superposed on the general trend which (1) approximately represents, sunspot numbers are subject to largish "random" variations; consequently tolerance always exists in fitting the parameters s, a, b, F; and especially when an outburst has barely passed its maximum. The resultant uncertainty in b is particularly important in estimating the remainder of the present cycle. This "damping constant" has averaged definitely larger for odd-numbered than for even-numbered cycles.

TABLE I. *Wolf numbers for spot cycle number 17.*

YEAR, r	COMPUTED R_C	OBSERVED R_0	YEAR, r	COMPUTED R_C
1933.5	7	5.7	1939.5	87
1934.5	7	8.7	1940.5	61
1935.5	37	36.1	1941.5	38
1936.5	84	79.7	1942.5	22
1937.5	111	114.4	1943.5	12
1938.5	109	109.6	1944.5	6

The next outburst, number 18, may be expected to commence, roughly, two-thirds of a year after the spot number has fallen to one-tenth of its maximum: say, early in 1944. A fraction more than four years after that—the summer of 1948—seems the most probable date of the next maximum; and any prediction of the course of spot numbers after cycle 18 ends is, we believe, highly speculative.

JOHN Q. STEWART
FORREST C. EGGLESTON

Princeton University Observatory,
Princeton, New Jersey,
May 12, 1939.

[1] John Q. Stewart and H. A. A. Panofsky, Ap. J. **88**, 385 (1938).
[2] Astronom. Mitteil. (Zurich) **137**, 392 (1939).
[3] Max Waldmeier, Astronom. Nachrichten **259**, 267 (1936).

On the Shape and Stability of Heavy Nuclei

On the basis of the drop model of the atomic nucleus, and from energy considerations only, Feenberg [1] has obtained a criterion for the stability of a spherical nucleus. This stability problem is very similar to one encountered in the biophysical theory of cell division and Feenberg's criterion is a special case of more general equations developed by Rashevsky and Young.

Rashevsky [2] considers a constant-volume infinitesimal deformation of the sphere, and evaluates the change in surface energy and the work done by diffusion drag forces set up by the cell metabolism. The latter derive from a potential c satisfying

$$\nabla^2 c = k \quad \text{inside the cell}$$
$$\nabla^2 c = 0 \quad \text{outside the cell}$$

and $k(c_2 - c_1) = D_1\, \partial c_1/\partial n = D_2\, \partial c_2/\partial n$ on boundary in which c becomes constant at infinity. The subscripts 1 and 2 refer to the two sides of the boundary. By putting $k = \infty$, $D_1 = D_2$, these formally become the equations satisfied by the Coulomb potential. Feenberg's considerations are thus a special case of Rashevsky's. It follows at once from the latter's equations that if a nucleus is stable under the particular (ellipsoidal) deformation studied by Feenberg, then it is stable under all infinitesimal deformations which leave it a figure of revolution. Thus, at least for axially symmetric deformations, Feenberg's criterion is *sufficient* as well as *necessary* for stability. This probably remains true when the restriction to axial symmetry is removed.

More information about the behavior of such systems can be obtained by studying the deformation which such surface and volume forces would produce. Some progress has been made with this problem in the biological case, though the work is still in an early stage of development.

By considering the cell to deform slowly against viscous drag[3, 4] and by making use of a mean-value theorem of

Betti,[4] it is possible to obtain the average rate at which the cell elongates in a specified direction under the action of the above-mentioned forces. The requirement that this average rate be < 0 for stability of a sphere slightly elongated in that direction gives another stability criterion. For the ellipsoidal case[5] this again reduces to that of Feenberg.

With these methods it is possible to go further and study finite deformations from the spherical shape. Slow deformation against viscosity is formally equivalent[4] to small deformation against elastic forces. Some of the work is applicable in an approximate way to a rather general class of convex shapes;[6, 7] while ellipsoidal shapes have been studied more exactly.[4, 5] It appears that once a cell becomes unstable it will continue to deform to a finite amount. This is the analog to the potential barrier for nuclear fission.

By sectioning the cell and applying Betti's theorem to each section, a beginning has been made in the study of the equatorial constriction which precedes the final division into two halves. In a rough way it can be shown[5] that as the cell elongates it will tend to pinch in at the equator and round up at the poles, so that it passes into a sort of dumbbell-shaped system.

Some aspects of rhythmic phenomena have also been considered,[7] without, however, trying to take into account the inertial terms in the hydrodynamic equations of motion. It would presumably be necessary to include these terms for application to the nuclear model.

GALE YOUNG

Ryerson Physical Laboratory,
University of Chicago,
Chicago, Illinois,
May 10, 1939.

[1] E. Feenberg, Phys. Rev. **55**, 504 (1939).
[2] N. Rashevsky, *Mathematical Biophysics* (1938), Chapters 8, 9.
[3] N. Rashevsky, *Mathematical Biophysics* (1938), Chapter 13, appendix.
[4] G. Young, Bull. Math. Biophys. **1**, 31 (1939).
[5] G. Young, reference 4, p. 75.
[6] N. Rashevsky, Bull. Math. Biophys. **1**, 23 (1939).
[7] N. Rashevsky, reference 6, p. 47.

The Approximate Equality of the Proton-Proton and Proton-Neutron Interactions for the Meson Potential

The comparisons of the proton-proton and proton-neutron potentials in ^1S states have indicated[1] that the attraction for the proton-neutron interaction is slightly stronger than that between two protons. The object of this letter is to call attention to the fact that the new measurements of L. Simon[2] on the scattering cross section of slow neutrons and protons combined with the new proton-proton scattering experiments of Herb, Kerst, Parkinson and Plain, and of Heydenburg, Hafstad and Tuve[3] speak in favor of a still closer equality of the two interactions and that this equality becomes practically perfect for the meson type of potential—$Ce^{-r/a}/(r/a)$. The relatively high values of minus the potential energy at small distances for this potential are responsible for the relative reduction of the difference between the two interactions in comparison with "square wells" and the Gauss error potential.

In Table I the ratio of the proton-neutron and proton-proton potentials is given for the "square well," the Gauss error potential and the meson potential. In all cases the Coulombian potential e^2/r is supposed to be superposed on the specific nuclear interaction for the protons.

TABLE I.

σ_{pp}	SQUARE	GAUSS	MESON
20×10^{-24} cm²	1.03(5)	1.03(6)	1.01(5)
14.8×10^{-24}	1.01(5)	1.0(15)	1.00(2)

The first row corresponds to the value of Cohen, Goldsmith and Schwinger[4] and the second to that of Simon.[2]

In computing the table the ranges of the interactions were chosen so as to fit the proton-proton scattering data. This gave for the contributions to the slow-neutron scattering cross section due to the triplet state $3.2(2)\times10^{-24}$ cm² for the "square well" and $3.1(5)\times10^{-24}$ cm² for the Gauss error well. For the latter $\alpha=20$ in Feenberg's notation was used. For the meson potential the contribution due to the triplet state was assumed to be the same as for the "square well." This assumption is perhaps one of the most speculative made above inasmuch as the effect of the triplet state should be computed by using spin-spin couplings derived from the meson theory. It is doubtful, however, that these effects can be computed with certainty on account of the necessity of cutting off the potentials to avoid divergence. We have been informed by Dr. Schwinger[5] and by Professor Bethe[6] that in their calculations with spin-spin terms the contribution of the triplet state to the slow neutron scattering cross section is practically the same as for "square wells." This result is reasonable since for other potentials this cross section is determined primarily by the binding energy of the deuteron and the approximate range of force. The effect of the shape of the potential energy curve, on the triplet cross section, is usually of the order of 10^{-25} cm² while the change due to Simon's value of the scattering cross section is $\sim5\times10^{-24}$ cm². There appears to be thus no special danger from this uncertainty.

It may be premature to claim an exact equality of the two interactions at this time. It is nevertheless fair to point out that the reasons for believing the proton-neutron attraction to be stronger[1] have disappeared through a combination of changes in experimental results and the introduction of the meson potential. It appears, therefore, more satisfactory than previously to use the same specific interaction in the ^1S state provided the interaction is concentrated at small distances as in the meson potential.

G. BREIT
L. E. HOISINGTON
S. S. SHARE
H. M. THAXTON

Department of Physics,
University of Wisconsin,
Madison, Wisconsin,
May 8, 1939.

[1] G. Breit, E. U. Condon and R. D. Present, Phys. Rev. **50**, 825 (1936); G. Breit and J. R. Stehn, Phys. Rev. **52**, 396 (1937); G. Breit, H. M. Thaxton and L. Eisenbud, Phys. Rev. **55**, 603(A) (1939) and p. 1018 of this issue.
[2] L. Simon, Phys. Rev. **55**, 792 (1939).
[3] R. G. Herb, D. W. Kerst, D. B. Parkinson and G. J. Plain, Phys. Rev. **55**, 603(A) (1939) and p. 998 of this issue. N. P. Heydenburg, L. R. Hafstad and M. A. Tuve, Phys. Rev. **55**, 603(A) (1939).
[4] V. W. Cohen, H. H. Goldsmith and J. Schwinger, Phys. Rev. **55**, 106 (1939).
[5] J. Schwinger, Phys. Rev. **55**, 235 (1939).
[6] H. A. Bethe, Washington meeting of American Physical Society, p. 1130 of this issue. Also private communication.

An Unsuccessful Search for Transuranic Elements

In 1934 Fermi[1] and his associates after bombarding uranium with neutrons found that the radioactive substances produced were not any of the elements between lead and uranium. They concluded that these bodies very probably were transuranic. This opinion was maintained also by subsequent investigators, especially by Hahn, Meitner and Strassmann, until the recent discovery[2] of the fission process in uranium presented some completely new viewpoints.

It has been recognized by Abelson[3] and others that some of the so-called transuranics are tellurium, iodine and other elements well below uranium. It remained to be proved whether there are any transuranics at all.

From a purely chemical standpoint this problem is obviously extremely difficult since one has to separate from *all* the elements some substances whose properties can only be guessed on the basis of the periodic system. A better line of approach is offered by the observation due to McMillan[4] that the activity produced in a very thin uranium layer by neutrons is of two types: recoiling, containing only fission products, and nonrecoiling containing a 23-minute period and a period of about two days. The cross sections for formation of these are about equal when the uranium is close to the neutron source, with paraffin behind it.

Since transuranics would certainly be found in the nonrecoiling fraction a detailed investigation of these two activities was made. The first is due to a well-known radioactive isotope of uranium, as was easily shown by chemical experiments. The second is not the daughter of the first as shown by a direct experiment in which the decay of the 23-minute activity was followed long enough to rule out the possibility of its tailing into the longer period. It was thought interesting, then, to establish the chemical nature of the second activity. Thin layers of ammonium uranate of a few millimeters air equivalent were irradiated with about 500μ amp. hours of 8 Mev D+Be neutrons close to the target of the Berkeley cyclotron. The nonrecoiling activity showed practically only two periods, the uranium mentioned above and a 2.3-day period due to a rare earth. This second chemical identification is shown by the fact that this activity does not precipitate with hydrogen sulfide in 6n or 0.3n hydrochloric acid or acetic acid solution using rhenium or lead as a carrier, that it is precipitated from acid solution by hydrofluoric acid or oxalic acid with lanthanum as a carrier, that it is precipitated quantitatively by potassium sulfate in neutral solution and by ammonia. Uranium can be easily separated from the 2.3-day activity by precipitating it in the presence of lanthanum with hydroxyquinoline in acetic acid solution; protoactinium can be separated by zirconium phosphate precipitation in 3n hydrochloric acid solution, thorium by an iodate precipitation in nitric acid solution and finally MsTh 2, an actinium isotope, is separated by fractional precipitation of the oxalates in normal nitric acid solution with lanthanum as a carrier.

In this last process the amount of oxalic acid was regulated in such a way as to precipitate about half of the lanthanum in the first fraction and the other fraction upon neutralization of the solution with ammonia. The first fraction contained most of the 2.3-day activity and the second half practically all the MsTh 2. This also shows that the rare earth is probably heavier than lanthanum.

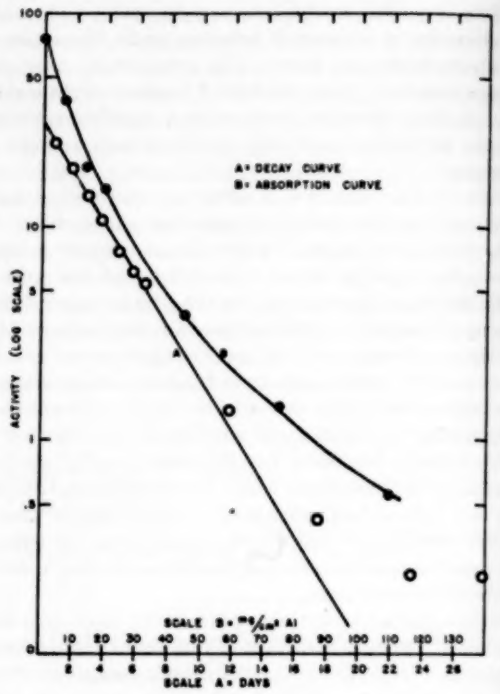

FIG. 1. Decay curve of the activity and the absorption curve of electrons in aluminum.

Figure 1 shows a decay curve of the activity and an absorption curve of the electrons in aluminum. The flattening out of the decay curve may be due to UX which has not been separated from this sample.

These experiments seem to show conclusively that no β-emitting transuranics have been so far observed, with the usual reservation of very short or very long periods.

The fact that a rare earth, which is necessarily a fission product of uranium is found among the nonrecoiling activities can perhaps be explained by the very rapid decrease of the range of the fission products when their mass increases.

On the other hand, the 23-minute uranium must decay into a substance with atomic number 93; hence a search was made for an alpha-emitter. An ionization chamber connected to a linear amplifier or a spherical ionization chamber in which the pressure could be varied[5] were used for this purpose. A sample showing a very strong β-activity due to the 23-minute period showed no alpha-activity above the natural thus ruling out the possibility of the 23-minute uranium decaying into a short life alpha-emitter.

In the hope of finding a long life emitter, U_3O_8 which had been kept intermittently for two years close to the target of the Berkeley cyclotron was used. We believe

that no other uranium sample today has had a stronger irradiation. The alpha-activity of this sample was examined and compared with the activity of U_3O_8 of the same source, but not irradiated. No difference could be detected. Two grams of the irradiated oxide were dissolved in 6*n* hydrochloric acid and rhenium added to the solution and precipitated as a sulphide. No activity was found in the rhenium. Similar experiments were performed also with a bombardment time favorable to the detection of a period of the order of magnitude of some days with negative results.[6]

The necessary conclusion seems to be that the 23-minute uranium decays into a very long-lived 93 and that *transuranic elements have not yet been observed.*

Thanks are due to Drs. E. McMillan and G. T. Seaborg for many discussions, to Professor E. O. Lawrence for his continued interest in this work and to the Research Corporation for financial assistance.

EMILIO SEGRÈ

Radiation Laboratory,
Department of Physics,
University of California,
Berkeley, California,
May 10, 1939.

[1] E. Fermi, E. Amaldi, O. D'Agostino, F. Rasetti and E. Segrè, Proc. Roy. Soc. **146**, 483 (1934).
[2] O. Hahn and F. Strassmann, Naturwiss. **27**, 11 (1939); L. Meitner and O. Frisch, Nature **143**, 239 (1939).
[3] P. Abelson, Phys. Rev. **55**, 413 (1939).
[4] E. McMillan, Phys. Rev. **55**, 510 (1939).
[5] H. Geiger and J. M. Nuttall, Phil. Mag (6) **22**, 613 (1911)
[6] See also P. Abelson, Phys. Rev. **53**, 211 (1938).

Concentrating the Uranium Isotope of Twenty-Three-Minute Half-Life*

The uranium isotope of twenty-three-minute half-life[1] can be concentrated with respect to U^{238} by the following procedure. Other products of the uranium bombardment are separated from the twenty-three-minute isotope in the process.

In an acid or neutral solution containing no oxidizing agent stronger than hydrogen ion, a highly excited uranium atom will probably settle down in the tetravalent state. The hydroxide corresponding to this state is a weaker base and less soluble than the corresponding uranyl compound. Consequently, hydrolysis is more complete and probably more rapid for salts of tetravalent uranium than for salts of hexavalent uranium. This results in an increase in the concentration of the tetravalent uranium in the first fraction of a hydrolytic precipitation from a mixture of the two salts. In these experiments, the twenty-three-minute uranium isotope, left in an excited state by the neutron capture and recoil gamma-ray emission, settles down in the tetravalent state and can be concentrated.

Ammonium uranyl acetate $[NH_4UO_2(CH_3COO)_3]$, was the salt used in these experiments. It can be prepared by dissolving ammonium pyrouranate in glacial acetic acid and crystallizing from a hot concentrated acetic acid solution.

Thirty to forty grams of this salt (15–20 g U) are dissolved in 100–150 cc of cold distilled water. The solution is placed in a 175 cc spherical soft glass flask surrounded by paraffin. In the center of the solution is placed the neutron source (110 mC Ra+Be). After a two-hour bombardment, the solution is poured into one liter of boiling water containing 10 g of ammonium acetate. A precipitate of a basic uranyl acetate appears within one to three minutes. To the suspension is added 0.1 g of decolorizing carbon (to aid filtering) and the solid removed by filtering with suction through a sintered glass funnel. The precipitate is dissolved and separated from the carbon by pouring a hot solution of 5 cc concentrated nitric acid and 20 cc glacial acetic acid into the funnel and applying suction. To the resulting solution is added 5 cc of an ammonium acetate solution (1 g/cc) and then a large excess of a hot concentrated solution of sodium acetate. The precipitate (1 to 2 g) of sodium uranyl acetate, $[NaUO_2(CH_3COO)_3]$, is filtered, washed first with cold glacial acetic acid, then with acetone and dried. Activity measurements on this sample are then made.

A modified Geiger-Müller counter with a 50μ mica window gives an observed activity from an activated sample of about 100 counts/minute per gram U. Measurements are started five minutes after the final precipitation and fifteen minutes after the cessation of bombardment. Blank runs on nonirradiated samples give observed activities of about 20 counts/minute/gram U five minutes after the final precipitation. When activated samples are measured without concentrating the twenty-three-minute uranium isotope, activities of 25 to 30 counts/minute/gram U are obtained. These measurements are made five minutes after the sodium uranyl acetate is precipitated and fifteen minutes after cessation of bombardment. This indicates that the procedure described increases the concentration of the twenty-three-minute uranium isotope with respect to U^{238} by a factor of the order of ten.

Decay curves of the activated samples show an initial decrease which changes gradually into an increase in activity. The increase is due to the build-up of the UX bodies. Elements other than uranium whose activities would interfere with the measurements are removed by the two precipitations.

Precipitation of rhenium sulphide from a concentrated sample of the twenty-three-minute uranium isotope should also precipitate the homologue of rhenium, element 93. Activity measurements on such precipitates gave negative results. From these results and from the activity measurements on the concentrated sample it can be concluded that element 93, if beta-active, has a half-life of less than one minute or greater than eleven hours.

Complete details of this work are being prepared for publication elsewhere.

JOHN W. IRVINE, JR.

Department of Chemistry,
Massachusetts Institute of Technology,
Cambridge, Massachusetts,
May 16, 1939.

* Contribution No. 73 from the Research Laboratory of Inorganic Chemistry of the Massachusetts Institute of Technology.
[1] Hahn, Meitner and Strassmann, Ber. **70**, 1374 (1937).

The Difference in Coulomb Energy of Light, Isobaric Nuclei

On the current[1] assumption of equal interaction between all pairs of elementary particles one can calculate for certain isobars the mass difference which is to be expected from Coulomb forces alone. These nuclei are of the type $(n-p)=\pm 1$, i.e., they contain an excess of one proton or one neutron. It is possible to assign the entire binding energy difference in these cases to the Coulomb repulsion alone, for it is assumed that the ground states of both members are symmetrical in the neutrons and protons, and therefore specifically nuclear forces will contribute equally to the binding of the isobars. Since the effect of the extra proton in the nucleus $(n-p)=-1$ is to increase the Coulomb repulsion, there will be a decrease in the binding energy and hence a tendency to emit positrons. The Coulomb energy may be calculated[2] on the assumption of a uniform distribution of charge throughout a nuclear volume which is proportional to the number of particles. Slight deviations from this approximation are to be expected when the $2p$ shell is completed at oxygen and again around neon when the $2s$ shell is filled.[3] If one assumes that the positron spectra are normal, it is possible to predict the half-life by using the fifth power dependence of the lifetime on the energy, a procedure which is justified by the calculations of Nordheim and Yost.[4]

By determining the upper limit of the positron spectrum we may directly measure the difference in binding energy of two isobars of the type mentioned above. This is just equal to the maximum energy of the emitted particles plus the energy required to change a hydrogen atom into a neutron, plus the mass of an electron, plus the mass of the emitted positron. Nuclei of this character may be formed in a number of ways, one of which is the endothermic (p,n) reaction. The threshold of this reaction is just the above binding energy difference, and we are thus able to have two independent means of making the comparison with theory. It is clear that they can give different results only if the emission of the positron leads to an excited state which subsequently makes a gamma-transition. In this case the reaction threshold is the most trustworthy method of investigation because it is difficult to determine the energy of the gamma-ray.

Comparison of theory with experiment is quite satisfactory from Be^{7} to F^{17}, but prior to the work being here reported there was a gap in the experimental data from Ne^{19} to Mg^{23}, and beyond this point there exist large discrepancies. For example, Si^{27} is reported to have a half-life of 6.7 min. where the theory would predict about 4 sec. Further the energy of the positrons is found to be 2.0 Mev and the expected energy is about 3.5 Mev. Al^{25} is also in contradiction, for the reported half-life is 20 min. instead of the expected 6 sec.

We have commenced a systematic study of these nuclei and have found that the reaction $F^{19}(p,n)Ne^{19}$ gives a radioactivity of approximately the expected half-life and upper limit. The measured half-life is 20 sec. and the absorption curve of the positrons indicates an upper limit of 2.5 Mev. According to the theory we expect an energy of 2.2 Mev and hence a half-life of about 40 sec. The theoretical half-life was computed by taking the average of the fifth power extrapolation from F^{17} and O^{15}. We are continuing the investigation of the positron spectrum in a cloud chamber since it is obvious that absorption measurements are, at best, rather rough. A preliminary determination of the threshold gives a value of 4.2 Mev, while using the theoretical energy difference we expect 4.0 Mev. On the other hand, using the actually observed positron upper limit leads to a better agreement between predicted and observed threshold energy.

The reaction $Na^{22}(p,n)Mg^{22}$ is of the type discussed above and should have a theoretical threshold of 4.8 Mev, a half-life of about 10 sec., and a positron upper limit of about 3.0 Mev. We have looked for this activity in NaCl using protons of 4.5 Mev, but only a weak, indeterminate activity of periods about 20 min. and something still longer was found. It seems reasonably certain that these activities may be ascribed to impurities in the rocksalt, and that they are not connected with the problem in hand. In view of the predicted threshold being higher than the available energy it is hardly surprising that the desired reaction was not found.

Still another reaction in this general group is $Ne^{21}(p,n)Na^{21}$ which should have a threshold of 4.4 Mev, a half-life of 15 sec., and a positron upper limit of about 2.6 Mev. Unfortunately Ne^{21} is present to only one part in 370 of normal neon, but nevertheless it should be possible to detect this reaction.

It is a pleasure to thank Professor Wigner for pointing out to us the interest in this problem.

J. G. Fox
E. C. Creutz
M. G. White
L. A. Delsasso

Palmer Physical Laboratory,
Princeton University,
Princeton, New Jersey,
May 3, 1939.

[1] M. A. Tuve, N. P. Heydenburg and L. R. Hafstad, Phys. Rev. **50**, 806 (1936); G. Breit, E. U. Condon and R. D. Present, Phys. Rev. **50**, 825 (1936).
[2] E. Wigner, Phys. Rev. **51**, 947 (1937); H. Bethe, Phys. Rev. **54**, 436 (1938); W. H. Barkas, Phys. Rev. **55**, 691 (1939).
[3] W. H. Barkas, reference 2.
[4] L. W. Nordheim and F. L. Yost, Phys. Rev. **51**, 942 (1937).

Simple Capture of Neutrons by Uranium*

It is known[1] that slow neutrons, besides producing fission, can also by simple capture give rise to a radioactive isotope of uranium (U^{239}) which emits beta-rays with a period of 23 minutes. We have attempted to ascertain the contribution of this process to the capture of thermal neutrons, in order to determine whether this absorption could account for the difference[2–5] between the total capture cross section and the cross section for fission. According to Meitner, Hahn and Strassmann, the simple capture of neutrons is a typical resonance process with a sharp absorption band at about 25 volts. They give 1200×10^{-24} cm^2 as the cross section at resonance, but they give no information as to the width of the absorption band and the capture cross section for thermal neutrons.

Our measurement was based on a determination of the number of disintegrations per second of the 23-minute period of uranium produced by thermal neutrons and of the number of thermal neutrons effective under the conditions of irradiation.

The procedure was as follows: (1) Purification of uranium from uranium X by dissolving uranyl nitrate in ether and shaking with a small amount of water. UX and other impurities remain in the water, while a large fraction of uranium remains in ether solution and a purified uranyl nitrate may be obtained by evaporating the ether. (2) Irradiation inside paraffin by means of the cyclotron with an indium foil as monitor placed elsewhere in a fixed position. (3) Second ether purification in order to separate the 23-minute life from all other activities which are not due to isotopes of uranium. (4) Measurement, by means of an ionization chamber, of the decay of the 23-minute life and the growth of the UX activity.

If the beta-rays of U^{239} and of UX (practically, only those of UX_2 are effective since the beta-rays of UX_1 are too soft to enter our chamber) had the same energy distribution, the ratio of initial activity of U^{239} reduced to infinite time of irradiation, to the saturation activity of UX would give the ratio of the number of disintegrations of U^{239} to the known number of disintegrations of UX_2, namely, 5×10^{-15} per atom per second. However, the absorption coefficients of the two beta-radiations are different. According to our measurements, the mass absorption coefficients in aluminum are 10 cm²/g for U^{239}, and 5.5 cm²/g for UX_2. We have therefore corrected our results for the absorption of beta-rays in the substance itself, in the container and in the window of the ionization chamber, and for the sensitivity of the chamber. The total correction factor was 3.4. Under our conditions of irradiation, the two activities so corrected were of the same order of magnitude.

(5) The activation was performed with and without Cd absorbers in order to isolate the contributions of thermal neutrons. (6) The number of thermal neutrons for a given indication of the monitor was obtained by comparing the activity induced in an indium foil when irradiated either in the uranium position with the cyclotron or in a paraffin arrangement of standard geometry (center of the surface of a cylinder of paraffin containing the source 3 cm below the surface) with a known Rn–Be source. The number of thermal neutrons per millicurie per cm² per second effective in activating the indium foil was taken[6] to be $7\sqrt{3}$.

In this way we found, in a first experiment, a cross section for the production of U^{239} by thermal neutrons of 1.0×10^{-24} cm².

In a second experiment, using the same method on a mixture of uranium and manganese, we determined simultaneously the capture cross sections for uranium and for manganese, and found 1.2×10^{-24} cm² and 10×10^{-24} cm², respectively. The good agreement of this last value with that obtained as the difference between the scattering plus capture cross section[7] 14.3×10^{-24} cm² and the scattering cross section[8] 2.1×10^{-24} cm² may be interpreted as a check on the accuracy of the method.

The width, Γ, of the resonance level at 25 volts may be calculated from the intensity of activation, and turns out to be of the order of one volt. This width and our value for the thermal neutron cross section for simple capture are not consistent with an interpretation in terms of the single-level formula of Breit-Wigner.

Summing the fission cross section of 2×10^{-24} cm² with the above cross section for simple capture of 1.2×10^{-24} cm² we find as the total absorption cross section for thermal neutrons 3.2×10^{-24} cm². Because of the large errors which can affect such measurements, this may not be inconsistent with the value 5×10^{-24} cm² previously reported[4] from absorption measurements, or with the value of 5.9×10^{-24} cm² reported by Michiels, Parry and Thomson.[5] If, instead, the total absorption is considerably larger, as reported by Whitaker *et al.*,[3] there must be some other process of absorption to account for the difference.

H. L. Anderson
E. Fermi

Pupin Physics Laboratories,
Columbia University,
New York, New York,
May 17, 1939.

* Publication assisted by the Ernest Kempton Adams Fund for Physical Research of Columbia University.

[1] Meitner, Hahn and Strassmann, Zeits. f. Physik **106**, 249 (1937).
[2] Anderson, Booth, Dunning, Fermi, Glasoe and Slack, Phys. Rev. **55**, 511 (1939).
[3] Whitaker, Barton, Bright and Murphy, Phys. Rev. **55**, 793 (1939).
[4] Anderson, Fermi and Hanstein, Phys. Rev. **55**, 797 (1939).
[5] Michiels, Parry and Thomson, Nature **143**, 760 (1939).
[6] E. Amaldi and E. Fermi, Phys. Rev. **50**, 899 (1936). The factor $\sqrt{3}$ appears in order to take into account the obliquity of the emerging neutrons.
[7] Dunning, Pegram, Fink and Mitchell, Phys. Rev. **48**, 265 (1935).
[8] M. Goldhaber and G. H. Briggs, Proc. Roy. Soc. **162**, 127 (1937).

Proceedings
of the
New York Section of the American Physical Society

MINUTES OF THE HAMILTON COLLEGE MEETING, APRIL 1, 1939

THE spring meeting of the New York State Section of the American Physical Society was held at Hamilton College, Saturday, April 1, 1939. At the business session a final revision of the Constitution and By-Laws was adopted. The following program of invited papers was enjoyed by approximately 130 members and visitors.

MORNING SESSION

Address of Welcome. President W. H. COWLEY, *Hamilton College*
Energy Production in Stars. H. A. BETHE, *Cornell University*
Ten Minute Papers on Laboratory and Demonstration Apparatus:
1. **A New Apparatus for Demonstrating Induced Currents.** HORACE A. SHERMAN, *The Manlius School*
2. **A Demonstration Board to Show the Fundamental Properties of Vacuum Tubes.** D. P. RANDALL, *Syracuse University*
3. **A Driving Head for Stationary Waves on Strings.** FRANK J. STUDER, *Union College*
4. **A New Type of Photographic Sensitometer.** WILLOUGHBY M. CADY, *Cornell University*
5. **Two Examples of Convincing Demonstrations.** PAUL F. GAEHR, *Wells College*

AFTERNOON SESSION

Nonreflecting Films. KATHERINE B. BLODGETT, *General Electric Company*
Some Physical Problems in Connection with the Design of Vacuum Tubes. H. E. MENDENHALL, *Bell Telephone Laboratories*
The Training of Science Teachers Under the Proposed Five-Year Plan. C. A. MOOSE, *State Teachers College, Albany*

PAUL R. GLEASON,
Secretary

Proceedings of the American Physical Society

Minutes of the Washington, D. C. Meeting, April 27–29, 1939

THE 227th regular meeting of the American Physical Society was held in Washington, D. C., at the National Bureau of Standards on Thursday and Friday, April 27 and 28, 1939, and at The Catholic University of America on Saturday, April 29, 1939. There were three parallel sessions for the reading of contributed papers on Thursday morning and afternoon, Friday morning and afternoon and on Saturday afternoon. On Saturday morning there were two parallel sessions. The presiding officers were Dean John T. Tate, President of the Society; Professor John Zeleny, Vice President; Dr. H. L. Curtis and Dr. Karl K. Darrow. The attendance at the meeting was over seven hundred.

On Friday evening the Society held its dinner at the Wardman Park Hotel. President Tate presided and called upon Professor R. T. Birge, Professor Nils Bohr, Dr. Lyman J. Briggs, Dr. Léon Brillouin, Dr. E. U. Condon, Professor H. D. Smyth and Professor John Zeleny to speak. There were two hundred and forty-seven members and their guests at the dinner.

Meeting of the Council

At its meeting held on Thursday, April 27, 1939 the death of one member (Kurt Ritzau) was reported. Two candidates were elected to fellowship and fifty-six candidates were elected to membership. *Elected to fellowship:* Paul M. Gross and Gleason W. Kenrick. *Elected to membership:* G. D. Adams, Jr., Charles L. Bartberger, France B. Berger, George A. Brueske, Georg Busch, Felix Cernuschi, Robert F. Christy, Howard S. Coleman, John G. Daunt, Leverett Davis, Lloyd T. DeVore, Werner R. Dubs, Walter P. Dyke, William N. English, Kenneth E. Fitzsimmons, Glyn W. A. Foster, John J. Gibbons, Piara S. Gill, Earle C. Gregg, Jr., Robert Q. Gregg, Berndt O. Grönblom, Howard C. Hardy, August C. Helmholz, Freeman K. Hill, Gilbert G. Hudson, Ivan Humphreys, Josef M. Jauch, Geoffrey Keller, Chihiro Kikuchi, Charles Kittel, R. S. Krishnan, Shuichi Kusaka, L. Jackson Laslett, Tom Lauritsen, Carl A. Ludeke, William B. McLean, C. W. McLenathan, John W. McNall, John M. Meek, Zen'emon Miduno, Lore C. Misch, James W. Moyer, Toshinosuke Mubo, Nathaniel B. Nichols, George Placzek, Foster F. Rieke, Robert W. Roop, Lynn H. Rumbaugh, Samuel J. Simmons, Massey Sitney, H. Hunter Smith, Harold A. Vagtborg, Samuel D. White, Zigmond W. Wilchinsky, Edwin F. Winkel and Walter Wrigley.

The regular scientific program of the Society consisted of one hundred and eighty-three contributed papers. The abstracts of these papers are given in the following pages. An author index will be found at the end.

W. L. Severinghaus
Secretary

Abstracts

1. University of Chicago Cyclotron. W. D. Harkins, H. W. Newson, R. J. Moon, A. H. Snell, L. A. Slotin, L. P. Borst, S. L. Simon, B. Carpenter and P. R. Bell. —A cyclotron built under the direction of the Chemistry Department of the University of Chicago has now been put into operation. The magnet frame is made of Armco steel and has a weight of about 60 tons; in addition there are 10.5 tons of copper in the exciting coils. The core diameter is 50 inches, having been designed to accommodate a projected accelerating chamber about 45 inches in diameter. The present accelerating chamber is 32.5 inches in diameter, and has a vacuum gap of 4.5 inches. The radiofrequency supply consists of two power triodes of the Sloan type, driven by a four-stage exciter with crystal control, and connected to the dee circuit through a short transmission line. With an operating frequency of 10.8 megacycles, deuterons are accelerated to a final energy of about 6.5 Mev.

2. The Massachusetts Institute of Technology Cyclotron. M. Stanley Livingston, John H. Buck and Robley D. Evans, *Massachusetts Institute of Technology.*—A 42-inch cyclotron is now under construction at Massachusetts Institute of Technology. This installation is to be the source of induced radioactive materials, to be used primarily in a cooperative medical research program supported by the John and Mary R. Markle Foundation. The cyclotron is housed in a new and specially designed laboratory building into which are built two baffle type water tank walls each two feet thick for protection of the operators. The magnet is constructed of Armco iron castings with General Electric exciting coils. Calibration data show the field to be exceptionally uniform and symmetrical. The "D's" are supported on the ends of coaxial quarter-wave resonant lines, eliminating insulators at points of high field. The oscillator unit uses shielded pair resonant lines for plate and grid circuits and Westinghouse 899 oscillator tubes. The cyclotron will be adjusted and operated by remote control from behind the protective walls. In the design of the cyclotron and the accompanying apparatus, an attempt has been made to combine the most satisfactory features of the various other installations. Slides will be shown illustrating the design features of the cyclotron and the laboratory.

3. The Purdue Cyclotron. W. J. Henderson, L. D. P. King and J. R. Risser, *Purdue University.*—The construction of the Purdue Cyclotron has been completed and it is now adjusted to produce deuterons of 8×10^6 electron volts energy or doubly charged helium ions of 16×10^6 electron volts energy. The magnetic field has been corrected by a ring shim of the type described by Rose.[1] In shimming the magnetic field to obtain maximum ion current it has been found that the slight bending of the $1\frac{1}{4}$" steel lid and floor of the vacuum chamber is an important factor in giving the correct magnetic field. Following a suggestion by Livingston[2] a low voltage arc source of ions has been adapted to the cyclotron. Using this type of source the ion beam passing through the deflector system is five to six times greater than with a filament source of the hot tungsten type. The ion currents that are obtained with the arc source are about three microamperes of deuterons and 1/30 microampere of helium ions. The helium ions are being used to investigate the production of artificial radioactivity in various elements. Several new nuclear reactions have been observed.

[1] M. E. Rose, Phys. Rev. **53**, 715 (1938).
[2] M. S. Livingston, M. G. Holloway and C. P. Baker, Rev. Sci. Inst. **10**, 63 (1939).

4. The Paths of Ions in the Cyclotron. L. H. Thomas, *Ohio State University.*—The author recently showed that in a cyclotron, the magnetic field of which varies suitably with position, the beam of ions may remain in resonance without being defocused, in spite of the relativity increase of mass with velocity, at least up to velocities at which terms in v^3/c^3 become important. The reasoning there used can be extended to give the required result to terms of all orders in v/c; the magnetic field required has then to be determined by numerical integration. The limitation to first-order variation of a central path, however, remains.

5. A New Type of Low Voltage, High Current Ion Tube for the Production of Neutrons. H. R. Crane and N. L. Oleson, *University of Michigan.*—An accelerating tube has been constructed which requires no difference of gas pressure to be maintained between the inside of the ion source and the high voltage accelerating gaps. The separation of the electrodes in the accelerating gaps is one mm. The ion source is a low voltage arc, employing a filament. It is easy to adjust the gas pressure to a value which is high enough so that a copious supply of ions is made in the source, but low enough so that no discharge takes place in the one-mm accelerating gaps. A large number of parallel holes pass through the accelerating electrodes and into the source, so that as many parallel ion beams are obtained. There is no limit to the number of parallel beams that can be used because there is no problem of the flow of gas from the source into the high voltage part of the tube. An experimental three-gap tube of over-all dimensions two inches diameter by 11 inches long produces a steady current of 1500 microamperes of deuterium ions at 35 kilovolts energy. Only a mechanical pump is used and a small leak of deuterium admitted. The only function of the pump and leak is to flush out other gases that form in the tube. If metal to glass seals were used, and the tube baked out, it could probably be sealed off. The purpose of the tube is to produce neutrons, by means of the *D–D* reaction.

6. Further Study of Cosmic Rays on the Pacific Ocean. Piara S. Gill, *University of Chicago.* (*Introduced by A. H. Compton.*)—Records of cosmic-ray intensity obtained on the R. M. S. Aorangi during 15 new voyages between

Vancouver and Sydney are discussed and compared with records taken during 11 voyages on the same route reported by Compton and Turner. The observed minimum of cosmic-ray intensity near the equator averages 10.3 percent less than the intensity at Vancouver, in good agreement with the value given by Compton and Turner. A correlation is found between the cosmic-ray intensity and the atmospheric temperature. An external temperature coefficient is found to be a function of latitude, with its highest numerical value of -0.25 percent per °C for latitudes higher than 40° (N and S). Using this variable temperature coefficient a latitude effect (about 8.5 percent) of magnetic origin alone is found. The mean latitude effect curve for 25 trips, corrected for external temperature, is flat beyond the critical latitudes (about 40°N and 38°S). The difference in cosmic-ray intensity between the Northern and Southern hemispheres beyond the critical latitudes after this temperature correction is found to be about 0 to 0.1 percent (probable error). This value is inconsistent with the galactic rotation effect predicted by Compton and Getting, but does not definitely rule out a more recent modification of their calculation.

7. Cosmic-Ray Bursts in Great Thicknesses of Lead. MARCEL SCHEIN AND PIARA S. GILL, *University of Chicago.*—Size-frequency distributions of bursts were obtained from analyses of records made by Carnegie model C cosmic-ray meters, shielded by 12 cm of lead, stationed at different locations. Energy distribution curves for the burst-producing radiation were made and compared with the depth-ionization curve obtained by Wilson. Because both curves, plotted on the same energy scale, have closely the same shape it was concluded that at least the greater part of the burst-producing radiation at sea level consists of penetrating ionizing rays, presumably mesotrons. The value of 10^{-4} was found for the creation probability of a burst by mesotrons of 2×10^{10} ev energy in a thickness of 12 cm of lead. This value leads to a cross section per nuclear particle (proton, neutron) of 2×10^{-30} cm², comparable to that estimated for nuclear explosions by Euler and Heisenberg. The ratio of the burst rates at Huancayo (3350 m above sea level) and Cheltenham (72 m) for different burst magnitudes was found to be constant, within the statistical errors, up to energies of about 1×10^{11} ev, and likewise for Teoloyucan (2285 m) and Cheltenham. For energies higher than 10^{11} ev the corresponding ratios of the burst rates increase rapidly with increasing energy of the incident particle. In order to account for this effect it is suggested that a part of the largest bursts is created by photons (electrons), a part which becomes predominant at higher elevations.

8. On the Production of the Hard Component of the Cosmic Radiation within the Atmosphere. L. W. NORDHEIM AND M. H. HEBB, *Duke University.*—The number of quanta or electrons of energy k times their range in unit lengths of radiation theory produced in matter by a primary electron of energy E is represented in excellent approximation by $N(k)dk=\alpha(E/k^2)dk$, where $\alpha=0.57$ for quanta and 0.44 for electrons. With this result and the available data on the energy distribution of the electrons coming from outside and on the distribution and absorption of the hard component (mesons) near sea level and underground, the hypothesis that the mesons are generated by the soft component within the atmosphere leads to the following consequences. The production efficiency by quanta or electrons of low energy (i.e. below 18 bev.) must be much smaller than by those of higher energy. The processes induced by the latter must be in the average of moderate multiplicity, the cross section being of the order 1/10 of that for the pair production by quanta. While in this way a reasonable account of the behavior of the hard component in the atmosphere can be given, considerable difficulties arise from the small absorption and the hardening of the cosmic radiation underground, as the required high cross sections for production of very energetic mesons would seem to necessitate similarly strong absorption by the inversion of the production processes.

9. New Evidence on the Nature of the Primary Cosmic Radiation. THOMAS H. JOHNSON, *Bartol Research Foundation of the Franklin Institute.*—Our recent directional measurements of the cosmic radiation at very high elevations near the equator have shown but a slight asymmetry of the order of 22 percent at the zenith angle 60°, the greater intensity being from the west. In comparing this with the relatively large latitude effect at the same elevation it is clear that only a small fraction, of the order of one-fifth, of the total field sensitive radiation can be produced by unbalanced positive primary rays. Since analysis of the latitude and directional effects at sea level shows that practically one hundred percent of the field sensitive mesotron component is produced by positive primary rays, we may conclude that the mesotrons are not secondary to the primary electrons of the soft component as often supposed. Arguments based upon fundamental properties of space (zero space charge at great distances from cosmic-ray sources, and a potential equilibrium at all points) show that any unbalanced component of the radiation must consist of rays of both signs but unequal masses. These neutralize each other in space since they travel with equal velocities but unequal energies. The more massive positive rays primary to the mesotrons are probably protons or some other more massive ion. The soft component primaries can be accounted for in the same picture if the initial rays emitted from the source are electrons which multiply by pair formation in the atmosphere of the source before they are decelerated in the retarding field surrounding the source.

10. The Contribution to the Soft Component of Cosmic Radiation by the Disintegration of Mesotrons. MARTIN A. POMERANTZ AND THOMAS H. JOHNSON, *The Bartol Research Foundation of the Franklin Institute.*—The contribution to the soft component of cosmic radiation arising from the disintegration of mesotrons has been investigated at an atmospheric depth of 20 meters water equivalent. A

quadruple coincidence counter train was mounted under a tower of lead in the basement of the Bartol Laboratory in such a manner that, when the apparatus was vertical, the net effective absorbing path traversed by coincidence-producing radiation was approximately two atmospheres. The absorption of the penetrating component which attained this depth was determined by interposing 20 cm of Pb in the system, and was checked against underground measurements by Auger and others.[1] When the apparatus was inclined toward a window at a zenith angle $\zeta = \sec.^{-1}(2)$ the amount of matter traversed by the coincidence-producing radiation remained the same, although the longer time required for the traversal of an equivalent mass of absorber resulted in a decrease in the intensity of the penetrating radiation, as has been previously reported.[2] Moreover, the absorption produced by 20 cm of Pb was much greater in this case, inasmuch as the disintegration of mesotrons had appreciably increased the soft component. From the absorption of the hard component determined by the vertical measurements, it was thus possible to arrive at a value of the ratio of the relative intensities of soft to hard component, $\kappa = 0.22$. The mean life of the mesotron has been calculated by applying this datum to Euler's relationship:[3]

$$\kappa = \frac{9}{4}\frac{x_0}{c\tau_0}\frac{\mu c^2}{2E_i} + \frac{1}{2}\frac{\mu c^2}{aT}.$$

With μ = one-tenth of the protonic mass, $\tau_0 = 2.8 \times 10^{-6}$ second, which is in good agreement with previous calculations.

[1] P. Auger, A. Rosenberg and F. Bertein, Comptes rendus **200**, 1022 (1935).
[2] T. H. Johnson and M. A. Pomerantz, Phys. Rev. **55**, 104 (1939).
[3] H. Euler and W. Heisenberg, Ergeb. d. Exakt. Naturwiss. (1938).

11. A Homogeneous Source of Protons for Use in Biological Investigations. G. W. Scott, Jr.* and C. P. Haskins, *Massachusetts Institute of Technology and Haskins Laboratory.*—A homogeneous source of high voltage protons for use in bombarding biological specimens is now under construction. The voltage supply is an electrostatic generator capable of producing voltages of the order of 600 kv, and with a current capacity of 750μA. The proton source is a modification of the focused electron beam type described by Scott.[1] Such a source is especially suited to this application because it permits easy control of beam intensity over a wide range as is demanded by the projected biological experiments. The significant features of this source will be discussed. The proton beam is to be accelerated in a multiple-section tube, mounted at 45 degrees to the horizontal as will be described. The tube will consist of a porcelain column six feet long and ten inches in diameter, held together with six textolite rods. A high resistance voltage divider rather than corona points will be used to distribute the potential among the accelerator sections, to ensure uniform distribution over a wide range of voltages. The beam will be analyzed and deflected through 45 degrees into the target chamber by a uniform magnetic field. There will be a brief discussion of the type of biological experiments to be performed with this apparatus.

* Haskins Laboratory Fellow.
[1] Phys. Rev. (in press).

12. Properties of the Hyperfine Structure of a Multiplet. Russell A. Fisher, *Northwestern University.*—Simple relations useful in the determination of nuclear magnetic moments from hyperfine structure data are available in many-electron atoms having well-defined multiplets. These relations, derived from the theory of hyperfine structure, are valid only if the relativistic corrections for the contributions of non-s electrons to the hyperfine splitting are negligible. With this assumption the following rules are derived: (1) In a multiplet having $S > L$ the sum of the several hyperfine interval factors within the multiplet depends only upon the contributions of the unbalanced s electrons of the configuration; (2) In a multiplet having $S < L$ the sum of the hyperfine interval factors within the multiplet depends only upon the contributions of non-s electrons. Several special cases of interest arise. If there is a single s electron in the configuration and $S > L$ the sum of the interval factors is $(L+\frac{1}{2})/Sa(s)$ where $a(s)$ is the coupling constant of the s electron. If there is no s electron in the configuration the sum of the interval factors is zero and in S states of such configurations there is no hyperfine splitting.

13. Intensities in the Hydrogen Secondary Spectrum. N. Ginsburg,* *Johns Hopkins University.*—In order to check on the analysis of the hydrogen molecular spectrum and to aid in the further analysis, a study of the relative intensities of about 600 lines in the region from 5600A to 8200A was made at various pressures and current densities. The region previously investigated by Kapuściński and Eymers[1] does not go further than 6442A and a number of very important bands lie in the near infra-red. The spectrograph used was of the Eagle type with a 15-foot, 15,000 lines/inch concave grating made stigmatic by means of a cylindrical lens. The photographic plates were calibrated by means of a step slit and a continuous source. This was a standardized tungsten band lamp; it gave the variation of the plate sensitivity with wave-length. The intensities in the molecular spectrum of hydrogen are very sensitive to the conditions in the discharge tube and the present investigation was made primarily to study these variations and to correlate them with the structure of the spectrum. Often this serves to fix the classification of lines in doubtful cases and it gives clues to the identity of unclassified lines.

* Johnston Scholar in Physics.
[1] W. Kapuściński and J. G. Eymers, Proc. Roy. Soc. **122**, 58 (1929).

14. A Recording Infra-Red Spectrophotometer. J. D. Hardy and A. I. Ryer, *Russell Sage Institute of Pathology, New York City.*—In an attempt to obtain quickly, quantitative data on the infra-red absorption spectra of biological materials an instrument of a semi-automatic recording type has been developed. Two light beams from the same Nernst filament are sent through a Wadsworth-Litrow

rocksalt prism spectrometer and brought to focus on two junctions of a thermopile. The junctions are connected in opposition and the intensity of one beam can be adjusted to follow any changes in intensity of the other. No loss in sensitivity is sustained by such an arrangement and the practical resolving power of the instrument is comparable with any but the best grating spectrometers. The precision of the instrument at present is ±3 percent in transmission. The spectral range from 0.4 μ to 15 μ can be plotted on a recording drum in 30 minutes. The curves so obtained are in terms of percent absorption and wave-length. The advantages of such an arrangement are: (1) curves can be obtained in less than 1/10 the time required to plot them by hand. (2) Many bands which are missed by hand plotting are discovered. (3) The data are plotted in percent absorption so that the band intensities can be studied.

15. Additional Band Systems of Silver Halide Vapors and a New Thermodynamical Calculation of Their Dissociation Energies. N. METROPOLIS AND H. BEUTLER, *University of Chicago.*—In connection with a study of the electronic states of the silver halides, some doubt was raised concerning the accepted value of the dissociation energy of AgI. Consequently a new thermodynamical calculation has been made, and a value of 2.93±0.10 ev has been obtained (previously accepted value 2.01 ev). However, in the case of AgBr it was not yet possible to get consistent values of the dissociation energy from the thermochemical data and the optical observations. By the investigation of the absorption spectrum of AgI at shorter wave-lengths, two new band systems have been found; their analyses have been reported.[1] A further investigation at longer wave-lengths has revealed another new band system extending from 4600–4170A where a continuum begins. This continuum and the unique arrangement of these bands can be understood by the consideration of the above new value of the dissociation energy. The band-heads are represented by the following formula

$$\nu_k = 23906 + 151.2(v' + \tfrac{1}{2}) - 206.1(v'' + \tfrac{1}{2}) + 0.41(v'' + \tfrac{1}{2})^2$$

based upon 45 band-heads, originating from $v'' = 0$–12 and $v' = 0$–4. The bands degrade to the red and are nearly equally spaced. In AgBr two new analogous band systems have been observed; one system lies in the region 2400A and the other at 4200A. Their formulae will be given.

[1] N. Metropolis, Phys. Rev. **55**, 636 (1939).

16. The Use of Polaroid in Depolarization Measurements on Raman Lines. FORREST F. CLEVELAND AND M. J. MURRAY, *Lynchburg College.*—Continuation of preliminary experiments[1] has resulted in the development of a method by which the depolarization factors of Raman lines can be accurately determined with comparatively short exposure times and with elimination of errors due to the polarization characteristics of the spectrograph. A Polaroid disk, so oriented that it passes light whose electric vector is horizontal, is placed between the Raman tube and the lens which condenses the scattered light on the slit of the spectrograph. Two exposures of equal duration are made, one with the arc below, the other with it at the side of, the Raman tube. The ratio of the intensities in the two exposures (depolarization factor) is determined by comparison with the lines of seven argon spectra produced by argon light of known intensity ratios. Results for the depolarization factors of Raman lines obtained from a mixture of benzene and carbon tetrachloride are given and comparison with previous data for these compounds is made. This paper covers part of a research program which has been aided by grants from the Virginia Academy of Science, Sigma Xi, and the American Association for the Advancement of Science.

[1] F. F. Cleveland and M. J. Murray, Phys. Rev. **53**, 330(A) (1938).

17. The Infra-Red Absorption Spectrum of Methylamine Vapor. A. P. CLEAVES, *Duke University,* AND E. K. PLYLER, *University of North Carolina.*—The infra-red absorption of methylamine vapor has been measured in the region from 2–10μ with cells of 18 and 38 cm length, using pressures from 3 cm to 50 cm. The most intense band at 9.57μ corresponds to the parallel vibration between the methyl and amino groups. Its overtone at 4.83μ has also been observed. The bending vibrations of the two groups give rise to several bands in the region from 6–7μ. This causes considerable overlapping which makes it difficult to locate band centers and band types. Three bands which originate from CH vibrations occur at 3.39, 3.46 and 3.54μ. The last two are of the parallel type. The bands due to the NH valence vibrations have also been found in the region of 2.7–3.0μ. A number of weaker bands due to combinations and overtones has been observed.

18. The Absorption of Methylamine Vapor in the Photographic Infra-Red.* L. G. BONNER, A. P. CLEAVES AND H. SPONER, *Duke University.*—The absorption spectrum of gaseous methylamine in the photographic infra-red has been studied in a stainless steel tube 105 feet in length with inside mirror polish. A three-m grating spectrograph was employed in the first order, and spectra have been taken covering the region from 6000–12,000A. Bands have been found at 10,330, 9940 and 7940A at five cm, 20 cm and 60 cm pressures, respectively. The band at 9940A is resolved. There is indication of two more weak continuous bands at 10,120 and beyond 11,800A. The first two bands have been recently reported by Thompson and Skinner.[1] In agreement with their conclusions we believe that there is no free rotation in the methylamine molecule and that the moments of inertia are about 8×10^{-40} and 40×10^{-40} g cm^2. It seems probable, however, that all strong bands must be associated with NH frequencies. The positions of the strong bands agree fairly well with measurements in liquid methylamine.[2]

* Supported in part by a grant-in-aid from the Penrose Fund of the American Philosophical Society.

[1] H. W. Thompson and H. A. Skinner, J. Chem. Phys. **6**, 775 (1938).
[2] M. Freymann and R. Freymann, Comptes rendus **202**, 1674 (1936); J. de phys. et rad. **7**, 476 (1936).

19. Raman Spectra of Gaseous Amines. J. S. KIRBY-SMITH AND L. G. BONNER, *Duke University. (Introduced by H. Sponer.)*—An investigation has been made of the Raman

spectra of a series of gaseous amines at pressures from two to three atmospheres. Results were obtained, using a high intensity apparatus built especially for the observation of the Raman effect in gases. Our measurements indicate Raman shifts as follows: Methylamine: 781 (2 *s*); 1042 (7 *s*); 1460 (3 *vb*); 2808 (6 *s*); 2889 (7 *b*); 2967 (10 *s*); 3368 (10 *s*); 3470 (2 *s*). Dimethylamine: 794 (2 *s*); 934 (7 *s*); 1448 (3 *vb*); 2792 (10 *s*); 2847 (7 *s*); 2965 (12 *vb*); 3384 (7 *s*). Trimethylamine: 271 (1); 363 (1); 422 (1); 830 (7 *s*); 1033 (2 *vb*); 1286 (5 *b*); 1457 (7 *vb*); 2741 (3 *s*); 2780 (10 *s*); 2829 (5 *s*); 2961 (10 *b*); 2990 (3 *vb*). A broad diffuse line without apparent structure lying at about 1450 cm^{-1}, and particularly intense in the case of trimethylamine, seems to be characteristic of these substances. This line is undoubtedly to be associated with the C−H bending frequency. The N−H valence frequencies which fall in the neighborhood of 3400 cm^{-1} appear as expected for the various compounds.

20. Excitation of O^{++} by Electron Impact. M. H. HEBB, *Duke University.*—The excitation of low states of certain atomic ions by impact of slow electrons is of considerable interest in the study of physical conditions in the nebulae. For this reason, at the suggestion of D. H. Menzel, a calculation was undertaken of the cross sections for transitions by electron impact between the lowest states of O^{++} which is a typical ion. The states considered were the ^3P, ^1D and ^1S states which arise from the ground configuration of the ion and lie within an interval of six volts. The method utilized was a modified Born approximation, using instead of plane waves the exact wave functions for an electron in a Coulomb field. Tables of the radial function in the Coulomb field were constructed and the radial integration of the integrals involved in the cross sections was carried out numerically. The $2p$ electrons of the ion were represented by an analytic approximation to the wave functions of Hartree for O^{++}. As a direct consequence of the Coulomb field, the cross sections in first approximation for electrons of low velocity vary inversely as the energy of the impinging electron and in order of magnitude range from 8×10^{-18} to 2×10^{-16} cm^2 for different transitions at ten volts.

21. Crystal Field Energy Levels in Pr Salts. CECIL B. ELLIS,* *Columbia University.*—In order that the rare earth crystal spectra may serve as a tool for determining the internal electric fields within crystals it is necessary that many of the patterns into which the crystal field splits the free-atom levels be experimentally determined. Hitherto in spite of the exhaustive low temperature wave-length lists of Spedding[1] and of Merz,[2] the crystal field lines could not be distinguished from the many vibrational lines usually present; so that no crystal field pattern has been completely identified except the ground state of Sm. By comparing the *raies ultime* in polarized light of thin crystals at room temperature (diluted with Ce) with the existing low temperature data, it is now possible to locate a few crystal field levels in two Pr salts: *Ethylsulfate:* $^3H_4=0$, 12, ···; $^1D_2=16708$, 16858, 16955; $^3P_0=20685$; $^3P_1=21275$, 21289; $^3P_2=22410$–22480 cm^{-1}. *Sulfate (Octahydrate):* $^3H_4=0$, 50, 110, 180, 230, 280, 320, 500; $^3P_0=20720$; $^3P_1=21158$, 21238, 21359 cm^{-1}. From comparison of Pr, Nd, Sm and Gd spectra it seems that sulfates and chlorides usually give the maximum possible number of almost equally spaced components, corresponding to crystal fields of low symmetry. In the ethylsulfates the number of components corresponds to a field of predominantly axial symmetry, which leaves M often a good quantum number—a point of great aid in analysis.

* Instructor at The College of the City of New York.
[1] F. H. Spedding *et al.*, J. Chem. Phys. **5**, 416 (1937).
[2] A. Merz, Ann. d. Physik **28**, 569 (1937).

22. Observations with a New Radiation Pyrometer. JOHN STRONG, *California Institute of Technology.*—Observations in the infra-red region of the spectrum were made with a new radiation pyrometer.[1] The monochromatic bands of radiation employed are isolated by means of the residual rays of apophyllite at 9.7μ, of quartz at 8.7μ, and of carborundum at 12μ. Solar observations on the strength of the Hartley ozone band and the Φ-band of water were made concurrently with the infra-red observations. Correlations between these observations have a bearing on the height and temperature of the ozone layer. The infra-red measurements at 8.7 and 12μ give the absorption of the atmosphere in this spectral region and they allow of a comparison between the heat radiation emitted by the sun and the Rayleigh-Jeans heat radiation from a laboratory blackbody.

[1] J. Strong, Phys. Rev. **54**, 242(A) (1938).

23. $L\alpha$ Satellites for Elements $41<Z<57$. L. G. PARRATT AND C. A. RANDALL, *Cornell University.*—The x-ray satellite lines accompanying the $L\alpha$-emission for elements $41<Z<57$ have been systematically studied with a two-crystal vacuum spectrometer. The qualitative relation between atomic number and the integrated intensities of the satellites relative to the $L\alpha_{1,2}$ lines agrees with the photographic measurements of Hirsh[1] and further confirms the Coster-Kronig interpretation of Auger production of the initial satellite state. Quantitatively, however, the present relative intensity measurements with the ionization method are lower than the photographic measurements[1] by a factor of about one-sixth. The observed satellite contour for each element has been resolved arbitrarily into the apparent constituent component lines. The wave-lengths and relative intensities of these components have been measured. A few satellite components, hitherto unreported, are found. Theory predicts[2] fifteen $L\alpha$ satellite components for Au(79), about twice as many as are included in the present analysis for the middle range of atomic numbers.

[1] F. R. Hirsh, Phys. Rev. **48**, 722 (1935).
[2] F. K. Richtmyer and E. G. Ramberg, Phys. Rev. **51**, 925 (1937).

24. Intensity Anomalies in Electron Scattering from ZnO. R. M. WHITMER AND H. J. YEARIAN, *Purdue University.*—Experimental electron scattering curves for ZnO have been obtained at temperatures of −183°C and at +350°C. There appears to be no appreciable variation of the anomalies observed at room temperature.[1, 2] Within

this range, the temperature does not appear to affect the rate of decrease of intensity with increasing $(\sin\theta)/\lambda$, which indicates that the characteristic temperature is considerably above the 355° estimated by Yearian.[2] Lark-Horovitz and Ehrhardt[3] have computed electron scattering curves from experimental x-ray data on ZnO, applying a temperature correction which was monotonic in $(\sin\theta)/\lambda$. This type of correction is given further support by the present work.

[1] H. J. Yearian and K. Lark-Horovitz, Phys. Rev. **42**, 405 (1932).
[2] H. J. Yearian, Phys. Rev. **48**, 631 (1935).
[3] K. Lark-Horovitz and C. H. Ehrhardt, Phys. Rev. **55**, 605(A) (1939).

25. X-Ray Diffraction by Liquid Ethyl Alcohol. G. G. HARVEY, *Massachusetts Institute of Technology.*—X-ray diffraction curves for liquid ethyl alcohol at a temperature of −75°C have been taken with monochromatic Mo $K\alpha$ radiation out to values of $(\sin\theta)/\lambda = 1.2$ and a Fourier analysis of these curves has been carried out. The weighted radial electron distribution function shows a number of well-defined peaks. The first of these, at about 1.5A, corresponds to the C−C (1.54A) and C−O (1.43A) distances in the molecule, the two being superposed. This composite peak is completely resolved from the remainder. A peak at about 2.4A may be interpreted as due to the other C−O distance within the molecule. These are the only definite distances, corresponding to permanent neighbors, that would be expected. A most interesting feature is the existence of a peak at about 2.9A corresponding to O−O intermolecular linkages, similar to the situation found in methyl alcohol.[1, 2] The area under this peak shows that each hydroxyl is linked to, roughly, two others, as was also found to be the case for methyl alcohol. Beyond this there are no very definite distances, the density curve rapidly approaching the average density.

[1] W. H. Zachariasen, J. Chem. Phys. **3**, 158 (1935).
[2] G. G. Harvey, J. Chem. Phys. **6**, 111 (1938).

26. Particle Size Determination with Side-Reflection X-Ray Cassette. C. NUSBAUM, *Case School of Applied Science.*—In 1926 von Laue published an article in which he developed an expression relating the particle size of a diffraction sample to the width of its diffraction line. This relationship was more general than that of Scherrer, previously published, as it holds not only for the cubic system, but also for particles whose three dimensions are different. It applies only to a divergent beam and necessitates the use of a Debye-Scherrer cassette. In many cases it is more convenient to use a Seemann-Bohlin (side reflection) cassette as in the case of thin metallic deposits. In this cassette the slit, sample and film are located on its circumference. By making the vertical divergence of the beam incident on the sample very small, sharp line definition is obtained. von Laue's expression then becomes

$$n = K\left[B\cos\theta - \frac{1}{B}\frac{\pi}{4}\left(\frac{h}{R}\right)^2\cos^2\theta\right],$$

where K is a constant, h half the vertical height of the beam, θ the Bragg angle, and B is defined by $B = B_0/R\sec\phi$ where B_0 is the width of the line at one-half maximum intensity, R the radius of the cassette, and ϕ the angle of incidence of the refracted beam at the film.

27. Crystal Structure of $LiOH\cdot H_2O$. RAYMOND PEPINSKY, *University of Chicago.*—$LiOH\cdot H_2O$ is monoclinic prismatic, with $a = 7.36$A, $b = 8.36$A, $c = 3.13$A, $\beta = 110.5°$. Space-group is $C_{2h}^3 - C2/m$, and density of 1.51 gives $Z = 4$ molecules per cell. Four oxygens are in reflection-planes, in hydroxyl groups, remaining four are in H_2O groups on twofold axes $(0,y,0)$. Lithiums are on twofold axes $(0,y,\frac{1}{2})$. Parameters are

O_{OH}: (104°, 0°, 160°);
O_{H_2O}: (0°, 75°, 0°);
Li: (0°, 125°, 180°),

with the remaining positions following from symmetry. Each lithium is at the center of an almost perfect oxygen tetrahedron, of edge 3.1A and with a Li–O distance of 1.99A. Two such tetrahedra share an edge parallel to the a axis in a reflection plane, and the paired tetrahedra then form unending chains in the z direction. The chains of paired tetrahedra are linked by hydroxyl bonding, the distance between bonded O's in adjacent chains being 2.7A. A more complete discussion of the structure will be published elsewhere.

28. The X-Ray K Absorption Limits of Iron, Nickel, Copper and Zinc. H. FRIEDMAN AND W. W. BEEMAN, *Johns Hopkins University.* (*Introduced by J. A. Bearden.*)—A double crystal spectrometer has been used to measure the mass absorption coefficients of Fe, Ni, Cu and Zn as a function of wave-length. Measurements have been made over a range of 50 volts at each K absorption limit. Intensities were measured with Geiger counters absorbing between 10 percent and 40 percent of the incident radiation. The I/I_0 ratios were repeatable to less than two percent at each point and wave-lengths were recorded to less than 0.02 x.u. employing the most recent data on emission lines to calibrate the instrument. Electroplated and rolled foils and metallic powders showed the same structure. For each metal definite structure has been found in the region lying within 20 volts of the high frequency side of the main edge, previously untested with the double-crystal spectrometer. The measurements also showed structure in the edges themselves in disagreement with some of the work of Barnes.[1] It is believed that this discrepancy is due partially to the higher resolving power of the crystals used and partially to the fact that the present work plots mass absorption coefficient. The shape of an I/I_0 curve is determined largely by the thickness of the absorber.

[1] A. H. Barnes, Phys. Rev. **44**, 141 (1933).

29. X-Ray Evidence on the Band Structure of Copper and Nickel. W. W. BEEMAN AND H. FRIEDMAN, *Johns Hopkins University.* (*Introduced by J. A. Bearden.*)—Calculations have recently been made of the band structure of Cu[1] and the results extrapolated to Ni.[2] Experimental evidence about the variation of density of states in these bands is furnished by the fine structure of the K absorption

edges and the shapes of the $K_{\beta_{2,5}}$ emission lines.[3] By a comparison of the wave-lengths of the K absorption limits and the $K_{\beta_{2,5}}$ lines, it can be shown that the latter must be due to transitions from the conduction levels and $3d$ bands to the empty K shell. Qualitative agreement is obtained in the case of Cu between the observed structure and the density of states in the conduction and d bands as calculated by Krutter. The structure for Ni is consistent with Slater's extrapolation of Krutter's work for Cu.

[1] H. M. Krutter, Phys. Rev. **48**, 664 (1935).
[2] J. C. Slater, Phys. Rev. **49**, 537 (1936).
[3] J. A. Bearden and C. H. Shaw, Phys. Rev. **48**, 18 (1935).

30. A High Vacuum X-Ray Spectrometer. J. H. MUNIER, *Johns Hopkins University.* (*Introduced by J. A. Bearden.*)—A double-crystal spectrometer has been developed for the study of long wave-length x-rays. The x-ray tube has been placed in the highly evacuated spectrometer chamber, permitting the use of an open window which greatly reduces the absorption in the path of the radiation. The detector is a Geiger-Mueller counter which has an aluminum window of 0.0001-inch thickness. This window will stand sufficient air pressure for satisfactory operation of the counter. The crystals used are the aquamarine form of beryl $Be_3Al_2(SiO_3)_6$ in which the 1010 planes have a grating constant of 8.08A. The physical resolving power of the pair used is 2000. The instrument has operated in a highly satisfactory manner in a study of the satellite structure and shape of the M series emission lines of tungsten. A study of the structure of the K absorption limit of aluminum and the L absorption limit of copper at 8A and 13A, respectively, is in progress.

31. The Diffraction of X-Rays by Liquid Tin and Liquid Chlorine. CARL GAMERTSFELDER, *University of Missouri.*—X-ray diffraction patterns of liquid tin at 250°C and 390°C and of liquid chlorine at 22°C under its own vapor pressure have been obtained. A diffraction camera with a 9.20-cm radius was used with Mo K_α radiation monochromatized by crystal reflection. In the case of tin, a flat sample 0.006 cm thick was used, it was heated electrically and its temperature was measured by means of a thermocouple placed near the sample. Liquid chlorine was contained in a thin-walled glass capillary 1.5 mm in diameter. The diffraction patterns of tin showed three peaks with a slight shelf on the main peak, while those for chlorine show three maxima. These intensity curves were corrected, fitted and analyzed in the usual manner, to obtain the atomic distribution curves. The distribution curve for liquid tin at 250°C has its first maximum at 3.38A, and the area under this peak indicates the presence of ten nearest neighbors. This agrees well with the distribution of atoms about a given atom in white tin. The distribution curve for tin at 390°C is similar to that for the 250°C except that the peaks appear less distinct. The distribution curve for chlorine at 22°C under its own vapor pressure shows that each atom has one discrete neighbor at 1.84A. This indicates that liquid chlorine is molecular with two atoms per molecule.

32. The Structure of Liquid Potassium. N. S. GINGRICH, *University of Missouri,* AND C. N. WALL, *North Central College.*—Analysis of x-ray diffraction patterns of liquid potassium has led to the determination of the atomic distribution in potassium at 70°C and at 395°C.[1] Information concerning the liquid state can be obtained from these atomic distribution curves by a method which has been used for liquid sodium.[2] It is assumed that the potential energy of a simple liquid has a pronounced minimum for a certain set of atomic configurations, and it is effectively infinite for all others. This set of configurations is characterized by assigning to each atom a small volume v within which it is free to move independently of other atoms without appreciably altering the condition of minimum potential energy for the entire assembly. The "free volume" v is obtained from the atomic distribution curve, the free energy is obtained from the free volume, and the entropy of the liquid is obtained from the free energy. With atomic distribution curves at different temperatures, a relation between the free volume and the temperature may be found, and hence, by extrapolation, the entropy of the liquid at the melting temperature and at the boiling temperature can be determined. Using the entropy of solid potassium[3] at the melting temperature, we calculate the latent heat of fusion as 2.06 kj/mol (experimental value 2.38 kj/mol).[4] Using the entropy of potassium vapor at the boiling temperature,[2] we calculate the latent heat of vaporization as 87.5 kj/mol (experimental value 84.9 kj/mol).[4]

[1] C. D. Thomas and N. S. Gingrich, J. Chem. Phys. **6**, 411 (1938).
[2] C. N. Wall, Phys. Rev. **54**, 1062 (1938).
[3] Simon and Zeidler, Zeits. f. physik. Chemie **123**, 383 (1926).
[4] *Int. Crit. Tables.*

33. The Mutual Absorption of the Rh and In Levels. J. H. MANLEY, *University of Illinois*; J. HORNBOSTEL, *New York University, Washington Square College,* AND H. H. GOLDSMITH, *Columbia University.*—We have employed the mutual absorption method,[1] applicable to case of overlapping levels, in order to obtain Γ_{In}, the width of the In level, and $|E_{In}-E_{Rh}|$, the spacing between the In and Rh levels. The four absorption curves (In abs − In det; In − Rh; Rh − Rh; Rh − In) obtained by using Rh detectors of 0.1 g/cm² and In detectors of 0.08 g/cm² and measuring the activity with a high pressure ionization chamber showed $\Gamma_{In} \leqq \Gamma_{Rh}$ and that $|E_{In}-E_{Rh}| \sim \Gamma_{Rh}$. To check this and to obtain quantitative results without excessive calculations, measurements were made with thinner detectors ($\delta_{Rh}=0.016$ g/cm² and $\delta_{In}=0.0076$ g/cm²), a G-M counter and a scale of eight arrangement. The values of the absorption coefficients are: (a) K(In − In) = 53 ± 4, (b) K(Rh − Rh) = 12 ± 0.8, (c) K(In − Rh) = 13 ± 3, and (d) K(Rh − In) = 5 ± 0.5. These yield $\Gamma_{In}=0.5\Gamma_{Rh}$ and $|E_{In}-E_{Rh}| = 1.1\Gamma_{Rh}$ in agreement with the results obtained with the thicker detectors. The value of $|E_{In}-E_{Rh}|$ is close to that obtained from the boron absorption method, and from an application of the Cd $1/v^3$ law. The value of K(In − In) is also in agreement with the In resonance cross section previously determined[2] from an analysis of the In − In curve obtained with thick detectors.

[1] H. A. Bethe, Rev. Mod. Phys. **9**, 71 (1937), ¶61, E.
[2] Manley, Goldsmith and Schwinger, Phys. Rev. **55**, 107 (1939).

34. On the Relation Between Neutron-Alpha and Alpha-Proton Scattering. H. PRIMAKOFF, *Polytechnic Institute of Brooklyn*, AND H. H. GOLDSMITH, *Columbia University*.—The assumption that the nuclear force between heavy particles is independent of charge leads to a simple relation between the proton and neutron elastic scattering cross sections for a given element.[1] A derivation of this relation has been found, independent of the details of the nuclear model and forces, and it has been employed in an attempted correlation of the experimental results of the scattering of neutrons from He,[2] and α-particles from hydrogen.[3] The resonance found in neutron-He collisions for a neutron energy $E_n \leqq 1$ Mev should appear in the proton-He case, for $E_p \leqq 2$ Mev or $E_\alpha \leqq 8$ Mev. Some evidence for the occurrence of such a resonance appears in the scattering of Th C' α-particles from hydrogen. Apart from the resonance, the magnitude and energy dependence of the neutron-α cross section is sufficient to account approximately for the observed deviations from the Rutherford-Coulomb scattering found for 2–6 Mev α-particles in hydrogen.

[1] H. Primakoff, Phys. Rev. **52**, 1000 (1937).
[2] H. Staub and W. E. Stephens, Phys. Rev. **55**, 131 (1939).
[3] Chadwick and Bieler, Phil. Mag. **42**, 923 (1921); Mohr and Pringle, Proc. Roy. Soc. **160**, 190 (1937).

35. Transmutation of Boron by Slow Neutrons with the Emission of α-Particles and Protons. J. B. FISK, *University of North Carolina*.—The transmutation of B^{10} by slow neutrons has been observed some 40,000 times by use of BCl_3 vapor in an ionization chamber coupled to a linear amplifier and recording oscillograph.[1] Evidence is obtained for the reaction $B^{10}(n, p)Be^{10}$ as well as for the well-known reaction $B^{10}(n, \alpha)Li^7$, the two being about equally probable. The (n, α) reaction is studied in detail. There are four or five energy groups, the most energetic corresponding to 2.90 Mev in good agreement with the 2.98 Mev available as calculated from nuclear masses. The groups may be interpreted in terms of excited states of Li^7 at 200, 410, 640 and 840 kev above the ground level. Alternatively, one may interpret the results of the experiment in terms of a level in Li^7 at 410 kev, together with a "multiplet" in B^{11} at 2.90, 2.70 and 2.06 Mev above the Li^7 ground state (i.e. the B^{11} excited level into which the slow neutron is captured is about 11.5 Mev above the ground level of B^{11}). This scheme is internally consistent and is unique. There are, however, severe theoretical difficulties with this scheme, as well as with the alternative interpretation.

[1] W. Maurer and J. B. Fisk, Zeits. f. Physik (in press).

36. The Disintegration of Boron by Slow Neutrons. M. GOLDHABER, R. D. HILL,* P. G. KRUGER AND F. W. STALLMANN, *University of Illinois*.—It has been shown recently by Lawrance, Burcham and Goldhaber[1] that the angular distribution of the disintegration tracks obtained in the disintegration of boron by a well-defined beam of slow neutrons ($B^{10}+n^1 \rightarrow Li^7+He^4$) is asymmetrical, the direction parallel to the neutron beam being favored. In their experiments a boron impregnated photographic emulsion was used. In order to distinguish between the direction of the He^4 and Li^7 recoils, which is not possible in a photographic emulsion, we have studied the boron disintegration in a Wilson chamber, containing targets of thin boron glass (about 1.5 mm stopping power). A beam of slow neutrons entered the chamber through an aluminum window. The rest of the chamber was shielded by Cd and B_4C. The angular distribution of 60 tracks has been measured by stereoscopic reprojection. The results are in qualitative agreement with those obtained with the photographic emulsion: More α-particles are found to be emitted forward than backward relative to the beam direction. Experiments in which the Al window of the chamber was covered by Cd show that about 90 percent of the observed disintegrations were due to C neutrons. The range of the α-particles from the boron disintegration has been measured for 80 tracks. In agreement with Bower, Bretscher and Gilbert[2] only one group of α-particles has been found. If a second group exists, it must be less than ten percent in intensity.

* 1851 Exhibition Scholar.
[1] A. M. Lawrance, W. E. Burcham and M. Goldhaber, Proc. Roy. Soc. Ser. **A** (in press).
[2] J. C. Bower, E. Bretscher and C. W. Gilbert, Proc. Camb. Phil. Soc. **34**, 290 (1938).

37. The Occurrence of Slow Mesotrons. C. G. MONTGOMERY, W. E. RAMSEY, D. B. COWIE AND D. D. MONTGOMERY, *Bartol Research Foundation*.—The explanation of the difference in the absorption of cosmic rays by equal masses of water and air postulates that mesotrons disintegrate spontaneously into electrons and neutrinos. To investigate this effect the following experiment was performed. A tray of counters, placed over a lead plate two centimeters thick, detected mesotrons entering the lead. Below the plate was another tray of counters for detecting the disintegration electrons. The recording circuit registered those counter discharges in the lower tray which followed, by a certain time interval, counter discharges in the upper tray. Observations were taken with the lead plate alternately present and absent. The difference in the counting rates represents the number of mesotrons which have stopped in the lead plate and subsequently disintegrated. Although a considerable number of disintegrations were expected, no appreciable number were observed. For example, in one series of observations, the time lag was 1.6 microseconds, and we expected about 40 disintegrations to be recorded per hour. The observed rate was 2.5 ± 3.4 per hour. Observations with other time lags gave similar results. This discrepancy suggests that some type of absorption process other than spontaneous disintegration is very effective in removing slow mesotrons from the cosmic radiation.

38. Studies with the Neutrons from *p-n* Reactions in Lithium and Beryllium. J. E. HILL, *University of Rochester*. (*Introduced by L. A. DuBridge.*)—The relative neutron yields, from lithium and beryllium, bombarded with 4.4-Mev deuterons and with 6.7-Mev protons, were obtained by measuring the induced radioactivity in silver produced by the neutrons after filtering them through 10 cm of paraffin. The results show the neutron yields at these energies for the four reactions Li-*d*, Be-*d*, Li-*p*, Be-*p*, to be in the ratio 1 : 1 : 1.8 : 1.9, with a probable error of 15 percent. The neutrons from the reaction[1, 2] $Li^7(p\text{-}n)Be^7$

have a sharp and controllable upper limit of energy equal to the difference between the proton bombarding energy and the energy threshold (2.0 Mev). They are therefore useful for determining thresholds for reactions of the type $(n\text{-}p)$ or $(n\text{-}\alpha)$. In this manner the threshold for the reaction $Al^{27}(n\text{-}p)Mg^{27}$ has been found at 2.6 Mev. This agrees with the value calculated by adding the maximum energy of the electrons from Mg^{27} (2.05 Mev)[3] to the energy of the gamma-rays (1.3 Mev) and subtracting the mass difference (n-H^1). Work is now in progress on other elements.

[1] L. A. DuBridge, Phys. Rev. **55**, 603(A) (1939).
[2] J. E. Hill and G. E. Valley, abstract 34, New York Meeting Feb. 24, 1939.
[3] M. C. Henderson, Phys. Rev. **48**, 885 (1935).

39. On the Temperature Dependence of the Scattering of Slow Neutrons in Ferromagnetics. F. BLOCH, *Stanford University.*—In the earlier derivation of the magnetic scattering we assumed that the neutron wave, scattered by magnetic interaction of the neutron moment and the atomic electrons, has an amplitude proportional to the saturation magnetization. It is shown that this result holds rigorously for the coherent scattering but that there is besides an incoherent scattering. This is small only because kTc (Tc=Curie temperature) is large compared to the initial and final energy of the neutron, considering in the latter a possible transfer of ferromagnetic energy into kinetic energy of the neutron. In the other extreme case of small Tc this incoherent scattering would be so big as to make the quadratic term in the magnetic cross-section temperature independent.

40. The Scattering of Neutrons by Helium Nuclei. W. E. SHOUPP, P. GERALD KRUGER, F. W. STALLMANN AND G. R. GAMERTSFELDER, *University of Illinois.*—The scattering of neutrons of mean energy of 2.6 Mev by helium nuclei has been studied by observing recoil helium nuclei in a cloud chamber filled with helium. Three thousand pictures yielded 940 tracks of which 475 had the proper momentum to have come directly from the source. As in other studies of this type[1,2] it was necessary to make corrections for random tracks and azimuthal angle. Within the limits of experimental error, the resultant angular distribution of recoil helium nuclei, in the center of mass system, indicates a deviation from spherically symmetrical scattering.

[1] Kruger, Shoupp and Stallmann, Phys. Rev. **52**, 678 (1937).
[2] Kruger, Shoupp, Watson and Stallmann, Phys. Rev. **53**, 1014 (1938).

41. The Production of Artificial Radioactivity by α-Particles. L. D. P. KING, W. J. HENDERSON AND J. R. RISSER, *Purdue University.*—The 16×10^6-volt doubly charged helium ions accelerated by the Purdue Cyclotron are being used to investigate the production of artificial radioactivity. The ion beam is about 1/30 microampere corresponding to 10^{11} particles per second. Pure graphite when bombarded becomes radioactive with a half-life of 2.1 minutes; the activity is undoubtedly O^{15} produced by $C^{12}(\alpha, n)O^{15}$. This reaction has not been reported with α-particle energies up to nine Mev. From the mass of O^{15} found from $O^{15}-N^{15}+e^+$ the above reaction becomes energetically possible at between eight and nine million volts. Silver becomes radioactive with a half-life of 26.8 minutes; the activity has been chemically identified as an isotope of indium and is assigned to In^{110} produced by $Ag^{107}(\alpha, n)In^{110}$. Rhodium exhibits strongly the 24.5-minute silver period reported by Pool.[1] When quartz is bombarded, a half-life characteristic of P^{32} is found.[2] This radioactive isotope is well known from other reactions. The process here is $Si^{29}(\alpha, p)P^{32}$. Other elements in which radioactivity has been observed are (with approximate half-lives): Selenium (6 hr., 1 hr., 1 to 2 min.); Gold (4 min., $3\frac{1}{2}$ hr.); Columbium (3 hr., 2 shorter periods); Sulphur (1.1 hr.); Molybdenum (85 to 90 min.). Accurate measurements of the half-lives and chemical identification of the radioactive isotopes are in progress.

[1] M. L. Pool, Phys. Rev. **53**, 116 (1938).
[2] Fahlenbach, Zeits. f. Physik **96**, 503.

42. Disintegration of the Isomers of Ag^{106}. T. ENNS, *University of Rochester.* (*Introduced by Charles V. Strain.*)—Palladium bombarded by high energy protons gives several radioactive periods of which two are the known isomers of Ag^{106} resulting from the reaction

$$Pd^{106}+p\rightarrow Ag^{106}+n.$$

One of the isomers decays to Pd^{106} by positron emission. The half-life is 25 minutes. The proton excitation curve shows a threshold of 3.8 Mev, which is in agreement with the positron energy limit obtained by M. L. Pool.[1] The other isomer decays to Pd^{106} by K-electron capture. The radiation consists chiefly of γ-rays. The half-life has previously been reported as 8 days.[1] The proton excitation curve gives a threshold of 3.9 Mev. X-ray absorption measurements indicate the presence of $K\alpha$-radiation. The energy level difference of 3.1 Mev between the Pd^{106} ground state and the Ag^{106} state giving the long period disintegration makes the existence of excited states of Pd^{106} possible.[2] The K-electron capture accompanied by the emission of a low energy neutrino leaves the Pd^{106} in an excited state. The ground level is reached by descent to successively lower energy states accompanied by γ-emission.

[1] M. L. Pool, Phys. Rev. **53**, 116 (1938).
[2] N. Feather and J. V. Dunworth, Proc. Roy. Soc. **A168**, 566–585 (1938).

43. Absence of New Exchange Forces in H_2 as Shown from Band Spectra. H. BEUTLER, *University of Chicago.*—M. Goldhaber suggested that scattering experiments could be quantitatively explained by the assumption of new forces between the protons giving an energy effect of about 80 cm^{-1} for protons at the distance apart equal to that in the ground state of H_2. If these forces be *spin-dependent*, the terms of para-H_2 should be found shifted with respect to those of ortho-H_2. The magnitude of that shift in any H_2-term should depend on its internuclear distance r. The transitions from $2p\sigma\,^1\Sigma_u$ ($v'=3$ and $v'=10$) to $1s\sigma\,^1\Sigma_g$ ($v''=0$ to 14) show conclusively that for $r=0.75$A to

$r=1.6$A no such shift larger than ± 3 cm^{-1} occurs. In addition, the positions of the ground levels of ortho- and para-H_2 have been determined relative to the dissociation level. There is no shift between the ortho- and para-H_2 larger than ± 10 cm^{-1}. If any new, *spin-independent* forces were active in H_2 they could be found (as M. Goldhaber suggested) by a comparison of the dissociation energies of H_2 and D_2. Spectrograms taken by the writer around 850A show that the energies of dissociation D_0 of H_2 and D_2 are 36116 ± 6 cm^{-1} and 36745 ± 25 cm^{-1}, respectively. With the usual extrapolation for the zero-point energy and the formulas for the isotope effect, the results for D_e are 38292 ± 8 cm^{-1} and 38290 ± 25 cm^{-1}, respectively. Although there is thus no evidence for the presence of new forces, it will be necessary to have a more rigorous theoretical treatment of the potential energy function of H_2 and D_2 around the minimum in order to exclude effects which may be hidden by the methods of calculation used.

44. The Infra-Red Absorption Spectrum of Methylamine. RALPH G. OWENS AND E. F. BARKER, *University of Michigan.*—The infra-red absorption spectrum of methylamine (CH_3NH_2) has been investigated for the gas between 2.9μ and 20μ with a grating spectrometer. For wave-lengths below 14μ a rocksalt fore prism was used, and for longer waves a prism of potassium bromide. Of the fourteen bands observed twelve are assigned to fundamental vibrations of the molecule. In appearance they resemble the parallel and perpendicular bands of a symmetrical molecule, indicating that the asymmetry is not great. As in the case of the methyl halides, there is an interaction between the levels ν_1 and $2\nu_4$. The CH_3 frequencies are of the same magnitude as those of methyl fluoride. The parallel band ν_3, due to mutual oscillation of the methyl and amino groups, is found at 1045.23 cm^{-1}, and is completely resolved. From its fine structure the average value of the two largest moments of inertia is found to be 37.6×10^{-40} g·cm^2. An unusual feature of this band is the enhancement of certain lines apparently due to superposition of a widely spaced set. If these should be interpreted as due to a nondegenerate perpendicular vibration, the indicated moment of inertia C with respect to the symmetry axis would be 7.2×10^{-40} g·cm^2. The frequencies observed in the gas agree very well with those reported by Kohlrausch for the Raman spectra of the liquid.

45. The Normal Electron Configuration of Singly Ionized Cerium. W. E. ALBERTSON AND G. R. HARRISON, *Massachusetts Institute of Technology.*—All levels from the configuration $4f^2(^3H)6s$ and $4f^2(^3H)6p$ have been discovered and identified with the aid of Zeeman effect data. The great intensities of the lines involved, their low temperature classes, and the near Lande "g" values for the levels indicate that in all probability the configuration $4f^26s$ is the lowest in Ce II. The lowest levels from $4f5d6s$ probably occur a few thousand wavenumbers above the ground state, combining with $4f^26s$ to give intense lines in the infra-red beyond 10,000A. More than 2700 Ce II lines have now been classified as arising from various transitions between 240 known energy levels.

46. The Lyman Lines of Hydrogen in Solar Emission. HENRY HEMMENDINGER, *Princeton University Observatory.* (*Introduced by Henry Norris Russell.*)—It has previously been shown[1] that there exist in the solar atmosphere regions of abnormally high excitation, characterized by an intensification of the helium and hydrogen lines in the chromosphere, and of the unidentified line λ5303 in the corona. A photometric study of the chromosphere on Harvard-MIT 1936 eclipse spectra reveals further details of the difference between "normal" and "excited" regions. The ratios of intensities of various metallic lines, for a given chromospheric level, remain substantially constant from one point to another, with the exceptions of λ4554 of Ba^+ and λ4226 of Ca. In excited regions the former of these is markedly weakened, the latter slightly weakened. The second ionization potential of Ba is two-tenths of a volt below Ly_α, that of Ca two-tenths below Ly_β; no other of the eleven metals with observed lines have first or second ionization potentials similarly placed with respect to early Lyman lines. An ultraviolet solar appendage has frequently been proposed to explain various phenomena, terrestrial and solar; present observations suggest the hypothesis that at least the variable part of the appendage does not consist of continuous radiation, but rather of line emission,[2] and specifically Lyman line emission. The lines of Ba^+ and Ca would thus be weakened in excited regions by a resonance process causing second ionization.

[1] G. G. Cillié and D. H. Menzel, Harvard Circular 410 (1935).
[2] M. N. Saha, Proc. Roy. Soc. London **A160**, 155 (1937).

47. The $L_{II}L_{III}$ Spin Doublet and the Value of the Fine Structure Constant. RAYMOND T. BIRGE, *University of California.*—Sommerfeld ("*Atombau*") assumed a value of the fine structure constant α, and found for the $L_{II}L_{III}$ interval, as determined from the $L\beta_1\alpha_3$ doublet only, that from $Z=41$ to 92 the screening constant s was apparently constant, aside from irregular fluctuations. Weighted average values of the $L_{II}L_{III}$ interval, for the elements $Z=29$ to 92, have now been obtained, after a critical study of all available x-ray data. As many as eight different measured doublets may be used, in some elements, for an evaluation of the interval. The resulting values of s, calculated with Sommerfeld's assumed $1/\alpha=137.17$, but with his original closed equation for the energy levels L_{II} and L_{III}, instead of the approximate expression actually employed by him in this work, are very definitely not constant. They do, however, form a well-defined curve, when plotted against Z. The values of s increase rapidly from about 3.33 at $Z=29$ to 3.45 at $Z=41$, then more slowly to a maximum of 3.52 at $Z=63$, and finally fall slowly to 3.46 at $Z=92$. By changing the assumed value of $1/\alpha$ to 136.70, one gets a simpler curve, in which the values of s rise from 3.37 at $Z=29$ to a final constant value of 3.63 holding for the range $Z=71$ to 92. Whether 136.70 is to be interpreted as a true or merely an apparent value of $1/\alpha$ can be decided only after a detailed study of the proper formula for the $L_{II}L_{III}$ interval, on the basis of modern quantum mechanics.

48. Relative Intensities of Singlet-Singlet and Singlet-Triplet Transitions. G. W. KING, *Yale University*, AND J. H. VAN VLECK, *Harvard University*.—The ratio of the intensities of singlet-triplet to singlet-singlet transitions can be calculated by means of Houston's[1] formulae in two ways: (a) from the deviations from the interval rule, and (b) from the distance of the singlet level from the center of gravity of the triplet levels. These calculations give the right order of magnitude, but the former gives results high, and the latter results low by a factor of about two. If Houston's formulae were strictly obeyed they would give, of course, the same value. The discrepancy indicates that the integral of the radial functions between the singlet and triplet differs from that for triplet with triplet, say by a factor λ. (On account of a zero in the matrix, the integral for the singlet with singlet does not occur.) The new parameter λ is evaluated ($\sim$0.75) from the positions of the four levels, and gives intensity ratios in good agreement with the observed.[2]

[1] Wm. V. Houston, Phys. Rev. **33**, 297 (1929) and Condon and Shortley, *Theory of Atomic Spectra*, p. 271.
[2] G. Wolfsohn, Zeits. f. Physik **83**, 246 (1933).

49. Experimental Study of Intensities in Benzene Vapor Absorption in the Region 2200–2600A. C. A. BECK AND W. F. RADLE, *Catholic University of America*.—Evidently, with temperature increase of a molecular system, intensities of ground state absorption bands decrease, while those starting in vibrational levels increase to an inversion temperature, then decrease. Comparison of intensity measurements of the most important bands agrees with the level assignments of Sponer, Nordheim, Sklar and Teller. Ground state bands decrease with temperature while the band at 37,482 cm^{-1} (B_0^0) shows an increase with temperature to a certain point as is expected from its assignment to 606 cm^{-1}. The temperature range is -30 to 250° C. These data are supported by calculations of state populations at various temperatures.

50. The Absorption of Thiocyanates in the 4.8μ Region. DUDLEY WILLIAMS, *University of Florida*.—Previous investigations of the infra-red spectra of organic isothiocyanates have revealed the presence of an intense absorption band near 4.8μ, while two Raman lines have been observed in the same frequency range. Thus further study of the broad infra-red band seemed desirable in order to detect possible complexities. The results of the present study indicate the existence of at least two absorption maxima near 4.8μ. Although the two bands could not be completely resolved, the frequencies of the oscillations giving rise to the band are shown to lie between 2100 cm^{-1} and 1950 cm^{-1}. These frequencies are somewhat lower than those of the observed Raman lines. Badger's explanation of the multiple frequencies of the mustard oils is discussed.

51. Band Spectra of Heavy Nitrogen and the Spectra of $N^{15}H$ and $N^{15}D$. R. W. WOOD AND G. H. DIEKE, *Johns Hopkins University*.—Spectra of the isotope N^{15} of nitrogen, $N^{15}H$ and $N^{15}D$ have been photographed in the second-order spectrum of a 21-foot aluminum grating ruled with 30,000 lines to the inch. The spin of N^{15} was determined by shielding the upper half of the spectrum band at 3580 (where the band head of N^{15} is uncontaminated by other bands) with a rotating disk provided with an open sector of adjustable width. Equality of intensity between the strong lines of the upper spectrum and the weak intermediate lines of the lower was obtained with an aperture of 120°, which gave the spin value $\frac{1}{2}$, corresponding to an intensity ratio of 3 : 1 for the strong and weak lines. The gas was prepared from ammonium chloride containing 70 percent of the heavy isotope, supplied by Professor Urey of Columbia University.

52. The Ultraviolet Absorption of Substituted Benzenes. A. L. SKLAR,* *The Catholic University of America*. (*Introduced by K. F. Herzfeld.*)—The weak benzene band at 2600A, which arises from the forbidden transition $A_{1g}-B_{2u}$, is greatly intensified by certain substitutions. Theoretically two effects are possible: a migration of a π electron (node in the plane of the ring) from the substitution into the ring, and the so-called induction effect which consists of a mixing of the levels. The latter effect turns out to be unimportant. A formula giving the effect of this migration upon the intensity of absorption has been developed. The strength of the 2600 band is proportional to that of the strong 2000 band with coefficients depending upon the extent of migration. These latter turn out to be large only if the wave functions of the ring and group overlap sufficiently and if the ionization energy of the group is sufficiently low. In those groups like NH_2 and OH which show strong intensification the low ionization energy must be due to the effect of the charge distribution in the NH and OH bond.

* This research was supported by a grant from the Penrose Fund o the American Philosophical Society.

53. Physical Factors Governing Biological Action of Radiation. F. S. BRACKETT AND ALEXANDER HOLLAENDER, *Division of Industrial Hygiene, National Institute of Health*.—A method is described for determining efficiency and relative absorption from action spectra obtained over a wide range of concentrations (number of organisms per cubic centimeter). Maximum efficiency of lethal action on bacteria is determined as a function of irradiation wave-length (2180–2950A) by establishing optimal concentrations for each wave-length. Optimal concentrations are shown to be a function of the gross absorptive power of the organism. Approximate effective absorption spectra are deduced from the action spectra at low concentration by correction for wave-length efficiency. Contributions to efficiency by screening action of less sensitive materials and quantum efficiency are discussed. Absorption spectra obtained directly are compared with those deduced from the action spectra and contributory uncertainties such as scattering discussed. It is pointed out that action spectra necessarily vary widely with concentration, and that most of the data in the literature cannot be strictly interpreted. In those cases where only

clearly thin cells or low concentrations have been used, both efficiency and absorption contribute, and the two factors cannot be separately evaluated.

54. Properties of Type II Photronic Cells Affecting Photometric Measurement. HAROLD S. STEWART, JR. AND BRIAN O'BRIEN, *Institute of Optics, University of Rochester.*—A 1-kw 115-volt projection tungsten lamp, maintained at 95.00 volts ±0.01 volt by a suitable regulator, and provided with cooled water filters, serves as light source. The desired spectral region is isolated by filters which, with a type II Photronic cell under test, are enclosed in a temperature-controlled force draft ventilated chamber. Current output of the cell through an external resistance which may be adjusted for any desired negative as well as positive value is recorded by a graphic potentiometer arrangement readable to about 1/40 percent. Short-period fatigue and dark recovery can be recorded to about this accuracy with a time resolving power of one second. Fatigue and recovery have been studied with a number of cells for several spectral regions including the near ultraviolet to determine circuit conditions yielding greatest constancy. Recovery can be reduced by applying an external direct potential while cell is dark, but performance is erratic. By application of suitable low frequency alternating potential during illumination, fatigue can be largely eliminated. Particularly striking is the great reduction of temperature coefficient by this means.

55. Optical and Photoelectric Properties of Potassium at Liquid-Air Temperatures.* DONALD M. PACKER,† *Institute of Optics, University of Rochester.*—For the first time, the same free surface of a metal has been investigated for its optical and photoelectric properties. Optical constants of opaque potassium films, formed in vacuum on optical flats cooled with liquid air, were determined visually, by using Drude's polarimetric method, at the principal mercury arc lines from 5780 to 3131A. Photo-current measurements were made at same time as optical observations with Pliotron amplifiers. Extinction coefficient and reflection curves dropped from high values in visible region to very low ones near 3500A. Refractive index curves were oppositely directed with values of 0.10 to 0.20 in visible region and rising to high values beyond the critical frequency. The latter occurred at 3250A, shifting to longer wavelengths with increasing age of surface. Maxima near 4300A, found in all the spectral photoelectron yield curves, shifted slightly toward the ultraviolet with aging surfaces. These maxima were also present in the spectral curves of photoemission per unit absorbed energy, shifting to higher frequencies, but not decreasing in relative magnitude as was expected from theory. These results were in general agreement with those reported by Ives and Briggs[1] after this work was completed.[2] All surfaces changed too rapidly, despite good vacuum conditions, for measurements to be repeated on any one surface.

* Read by title.
† Now at Washington University School of Medicine.
[1] H. Ives and H. B. Briggs, J. Opt. Soc. Am. **28**, 330 (1938).
[2] This work presented as partial fulfilment of requirements for Ph.D. degree, June, 1938, University of Rochester.

56. The Townsend Coefficients for Ionization by Collision in Pure and Contaminated Hydrogen as a Function of the Cathode Material. DONALD H. HALE, *University of California.* (*Introduced by Leonard B. Loeb.*)—The Townsend coefficients for ionization by collision were measured for mercury free hydrogen and hydrogen contaminated by sodium and NaH vapor. Cathodes of platinum and sodium and NaH-coated platinum were used. The values of α/p at the lower values of X/p are found to be smaller for pure hydrogen than for hydrogen contaminated with mercury vapor. The curves of β/α and γ for the platinum cathode plotted as functions of X/p show peaks at the lower values of X/p. The curves for the NaH cathode show a narrow and remarkably high peak at an X/p of 10. These peaks indicate a relatively large photo-emission effect $(\eta\theta g)/\alpha$ at the cathodes at the lower values of X/p. The values of β/α and γ for the platinum cathode show a general increase at the higher values of X/p because of secondary electron emission by positive ion bombardment. In the case of the sodium hydride surfaces the values of γ show little increase at the higher values of X/p. The values of γ as found in this work are used to calculate a sparking potential curve which is compared with the curve experimentally determined by Ehrenkrantz.[1]

[1] Florence Ehrenkrantz, Phys. Rev. **55**, 219 (1939).

57. The Definition of the Sparking Potential. LEONARD B. LOEB, *University of California.*—Analysis of static spark breakdown based on recent data indicates that the sparking criterion of Townsend taken from $i=i_0e^{\alpha x}/(1-\gamma(e^{\alpha x}-1))$ with $1-\gamma(e^{\alpha x}-1)=0$ is meaningless. The condition for *self-sustaining discharge*, that $\gamma e^{\alpha x}=1$, sets a *lower* limit or threshold for accumulation of space charges which *may* or *may not* lead to the discontinuous transient phenomenon with change of current called the spark. Above the threshold *only one* initiatory *electron* is *needed*. A spark will not occur unless that electron by a proper sequence of events blazes a conducting channel across the gap which generates a cathode mechanism leading to discharge. With potentials at which $\gamma e^{\alpha x}=1$ such sequences are extremely rare. Higher potentials are needed to ensure sufficient frequency of spark producing sequences for convenient observation. *Conventional*, experimentally observed, sparking potentials are values arbitrarily fixed by convenience of measurement, which may be well above the threshold determined by $\gamma e^{\alpha x}=1$. Dependent on the photo-currents used observed sparking potentials represent those at which about one in 10^8 photoelectrons succeeds in initiating a spark. Studies of the number of photoelectrons required to initiate a spark at different potentials are needed to give significance to sparking potential measurements.

58. Cloud Chamber Studies of Positive Point-to-Plane Discharge in Air at Atmospheric Pressure. STERLING GORRILL, *University of California.*—A study of positive point-to-plane discharge in air at atmospheric pressure was made with a Wilson cloud chamber for observation of the distribution of ions and chemical nuclei formed. Studies were made both of discharges from sharp points at high

voltages near the spark-over value, and of discharges from dull points at voltages very close to the onset value for corona discharge. For observation of the corona onset discharges, a mechanism was used by means of which the initiation of the discharge itself resulted in operation of the cloud chamber and the rapid cutting off of the high voltage on the gap. The study of the observed discharge streamers led to considerable detailed information concerning streamer characteristics. Experiments were performed to determine the characteristics of the large ion clouds observed in the region of the gap, and to investigate the mechanism by which they are produced. A mechanism is postulated explaining the formation of the clouds on the basis of diffuse photo-ionization throughout a considerable region, multiplication by collision of the ions thus produced, and subsequent movement of the ions in the existing fields to the positions in which they are observed.

59. Negative Point-to-Plane Corona Studies. ARTHUR F. KIP, *University of California.*—Investigations of the negative point-to-plane corona in air started by Trichel[1] have been continued. The linear relationship between current and frequency of current pulses is found to hold accurately only when pulses are periodic. For large points, pulses may be random and too far apart to provide a self-sustaining process. The positive ions necessary for starting these random pulses are produced by a hitherto unobserved discharge of much smaller magnitude than the pulse process above onset and presumably due to highly localized fields caused by dust, etc., on point surface. For a given voltage, the current is largest when pulses are periodic. Ultraviolet light produces two effects working in opposite directions; it tends to *increase* the current by insuring periodic pulses (caused by the constant photoelectron source at point), and it tends to *decrease* the current by the production of low mobility ions in air. Either effect may predominate, depending on size and surface condition of the point. Increasing the voltage does not materially increase the size of the active spot on the point. The maximum size of a single active spot is about 0.2 mm in diameter. Larger observed spots do not give single frequency of pulse, and are probably caused by several more or less separate spots, acting alternately.

[1] G. W. Trichel, Phys. Rev. **54**, 1078 (1938).

60. Offset and Breakdown Potentials in Point-to-Plane Corona Discharge in Air as a Function of Pressure up to 30 Atmospheres. G. G. HUDSON,* *Department of Physics, University of California, Berkeley. (Introduced by Leonard B. Loeb.)*—The breakdown and offset potentials for positive and negative point-to-plane coronas were studied in air at pressures up to 37 atmospheres with cylindrical hemispherically capped points of about 0.4 mm diameter as a function of pressure. The gaps were 3 mm for the negative points while they were 8 mm for the positive points in air. A sharp rise in breakdown potential with pressure was followed by a drop in potential to about half the value with a subsequent rise above 10 atmospheres in air for the positive point. The current-pressure curve roughly paralleled the potential curve while the onset potential showed a dip of about 10 percent. The breakdown potential for the negative point showed a dip of less than 10 percent at a pressure slightly above 10 atmospheres. The negative point current pressure curve was relatively little affected and the offset potential showed no change. Analogous results were reported by H. C. Pollock and F. S. Cooper,[1] and by Goldman and Weil,[2] at about 8 atmospheres. Data are insufficient to give an explanation for the nature of the sharp drop in air.

* Research Corporation Fellow at the University of California.
[1] H. C. Pollock and F. S. Cooper, Bull. Am. Phys. Soc. **13**, 7, Dec. (1938).
[2] Goldman and Weil, Zeits. f. Tech. Phys. of the U.S.S.R.

61. The Temperature Dependence of the Electrical Breakdown in Single Crystals. R. C. BUEHL AND A. VON HIPPEL, *Massachusetts Institute of Technology.*—Experimental difficulties had until now prevented the measurement of the breakdown strength of single crystals over a wide temperature range. This information on the other hand seems of decisive importance for the interpretation of the phenomena observed at room temperature. The authors therefore developed an apparatus, in which the breakdown strength can be measured between $-180°C$ and $+400°C$, and the current-voltage characteristic up to the breakdown point can be recorded. The first results of these experiments are presented, showing as the most interesting fact a steep decrease in the breakdown strength with falling temperature. This new effect can be explained by a decrease in scattering probability of the electrons with decreasing lattice vibrations.

62. The Atomphysical Interpretation of "Lichtenberg Figures" and Their Application for Studying Electric Discharge Phenomena. F. H. MERRILL AND A. VON HIPPEL, *Massachusetts Institute of Technology.*—The extremely fine, detailed drawing in Lichtenberg figures offers an unusually clear record of the early stages of discharge phenomena. The interpretation of these records in terms of electronic ionization, space charge, plasma formation and recombination is presented in this paper. After establishing the "normal" history of a gas discharge by a study of nitrogen between 5 mm and 30 atmospheres of pressure the admixture of CCl_4 shows the decisive influence of the electronic affinity of Cl on the development of the phenomena. A study of "Freon gas" follows clearing up the reasons for the usefulness of those new gases in suppressing corona discharges. Striking similarities exist between the surface discharges in the figures and space-charge discharges of thunderclouds. Finally figures in liquids link the field of gas discharges with that of the electrical breakdown of liquid insulators.

63. The Mechanism of the Lightning Discharge. J. M. MEEK, *University of California. (Introduced by Leonard B. Loeb.)*—A new physical picture of the observed leader/main stroke sequence of the lightning discharge is given by taking into consideration the change of resistance in the discharge

channel due to recombination of ions. The current in the pilot streamer is calculated to be of the order of 0.1 amp., the radius to be 0.3 cm. The observed speed of the pilot streamer is 2×10^7 cm/sec. so that the ion density in its tip may be calculated to be 10^{11} per cm^3; this explains the fact that the pilot streamer has not been photographed directly, as streamers of such ion densities are only weakly detectable in the laboratory. The ion density in the tip of the step leader, which can be photographed, is considered as 10^{14} per cm^3. Calculation of the resistance of the leader channel as a function of time shows that, with the current of 0.1 amp. which flows to the pilot streamer, the voltage gradient exceeds the breakdown value of 30 kv per cm at the cloud end of the channel when the time interval since the previous step is 50 microseconds, the average observed time interval between steps.[1] A further step leader then propagates down the partly ionized channel to reach the tip of the advancing pilot streamer. The high velocity of 10^9 cm per sec. for the step leader is accounted for, since the ion density ahead of its tip is of the order of 10^{10} per cm^3.

[1] B. F. J. Schonland, D. J. Malan and H. Collens, Proc. Roy. Soc. **A152**, 595 (1935).

64. Electrodisintegration of Beryllium. G. B. Collins, B. Waldman and W. Polye, *University of Notre Dame.*—The authors have previously[1] reported the disintegrations of beryllium by electrons. The experimental details of this investigation will be given. We have also obtained the threshold for the photodisintegration of beryllium induced by x-rays. The value obtained is about 1.63 Mev which is, within experimental error, identical with the threshold for electrodisintegration. This value also agrees well with the value 1.65 Mev obtained indirectly by Allison.[2] An excitation curve for the electrodisintegration of beryllium has been obtained which rises very rapidly. The shape of this curve is not inconsistent with what would be expected if the cross section for electrodisintegration were proportional to the square of the electron energy in excess of the threshold. If this relation is used to obtain the integrated effect of the electrons in the beryllium target, the cross section previously reported for 1.72 Mev electrons is increased to about 10^{-30} cm^2.

[1] G. B. Collins, B. Waldman and W. R. Polye, Phys. Rev. **55**, 412 (1939).
[2] S. K. Allison, E. R. Graves, L. S. Skaggs and N. M. Smith, Jr. Phys. Rev. **55**, 107 (1939).

65. Evidence for the Composite Character of the N^{13} β-Ray Spectrum. Ernest M. Lyman, *University of Illinois.*—Radioactive N^{13} decays with the emission of positrons and 280-kv γ-radiation. According to Richardson,[1] about 0.4 γ-rays are emitted per positron. The maximum energy of the positrons is 1.20 Mv. The presence of the 280-kv γ-rays naturally suggests that the positron energy spectrum is a composite one consisting of two superposed spectra, one with an endpoint at 1.20 Mv, the other with its endpoint at 0.92 Mv. The emission of a positron belonging to the latter spectrum is followed immediately by the emission of the 280-kv γ-ray; consequently either γ-β coincidences or γ-γ coincidences should be detected. The latter have been found by means of a coincidence counter arrangement which counted only γ-rays emitted from the source at an angle of less than 90° with respect to each other. The ratio of the number of 280-kv γ-rays to the total number of positrons is estimated to be 0.20 ± 0.15. In a similar experiment with C^{11} γ-rays, the coincidence rate was found to be negligible. Analysis of the shape of the N^{13} β-ray spectrum[2] shows that if it is resolved into two component spectra with endpoints at 1.20 Mv and 0.92 Mv, each approximately following the Fermi theory, then the ratio of the number of positrons from the 0.92-Mv spectrum to the total number is 0.25.

[1] J. R. Richardson, Phys. Rev. **55**, 609 (1939).
[2] E. M. Lyman, Phys. Rev. **55**, 234 (1939).

66. Further Experiments on the Recoil of the Nucleus in Beta-Disintegration. J. Halpern and H. R. Crane, *University of Michigan.*—Experiments[1] on the recoil of the nucleus in the disintegration of Cl^{38} have been continued. The fact (which we found as a result of our work last year) that momentum is not conserved in the system consisting only of the nucleus and the emitted electron has been confirmed. By measuring the momenta of the electron and nucleus we have been able to ascertain the direction of emission of the neutrino with respect to the direction of the electron in each case. Theoretical predictions according to both the Fermi and the K.U. theory are available. The experimental data agree slightly better with the Fermi than with the K.U. theory, but it is not safe to attach much significance to the results obtained so far, because of the possibilities for rather large experimental errors. An investigation into the manner in which droplets in the cloud chamber are produced by the recoil atom has been carried out. Evidence will be offered which indicates that the products resulting from dissociation of the gas molecules act as centers for condensation. This effect, in addition to ionization, accounts for the droplets observed.

[1] H. R. Crane and J. Halpern, Phys. Rev. **53**, 789 (1938).

67. Coincidences Between Beta-Rays and Gamma-Rays in Indium and Manganese.* Lawrence M. Langer, Allan C. G. Mitchell and P. W. McDaniel, *Indiana University.*—Using two reliable high speed counters in a coincidence circuit of resolving time, $t=3.4\times10^{-7}$ min., coincidences have been recorded between the beta- and gamma-radiation from radioactive indium (54 min.) and manganese (148 min.) produced by slow neutron bombardment with a 200-milligram radium-beryllium source. By interposing various thicknesses of aluminum between the source and the beta-ray counter, the ratio of beta-gamma coincidences to single beta-counts was observed as a function of the energy of the beta-rays. For indium, this ratio remains constant, whereas for manganese the ratio is dependent on the beta-ray energy. The results indicate that in both Mn and In there are gamma-rays time-correlated with the emission of beta-rays of all energies.[1] The results are also consistent with the idea that in In the beta-spectrum is simple, whereas in Mn the observed distribution is a composite of at least two modes of disintegration.[2]

Measurement of time-correlated gamma-gamma coincidences indicates that the average number of gamma-rays per beta-ray for In is more than one. No gamma-gamma coincidences could be detected for Mn.

* Supported by a grant from the Penrose Fund of the American Philosophical Society.
[1] A. C. G. Mitchell and L. M. Langer, Phys. Rev. **52**, 137 (1937).
[2] M. V. Brown and A. C. G. Mitchell, Phys. Rev. **50**, 593 (1936).

68. Fission of Uranium and Production of Delayed Emission by Slow Neutron Bombardment. E. T. Booth, J. R. Dunning and F. G. Slack, *Columbia University.*—The maximum range in air of the fission products of uranium has been determined by a differential ionization chamber and found to be 2.3[1] cm. The distribution in energies among the fission particles has been studied by measurement of the total ionizations produced by the individual fission particles in argon. Amplified ionization pulses were photographically recorded by means of an oscillograph, and compared with the amounts of ionization produced by uranium α-particles. Oscillograph records have also been made of the delayed neutron emission[2] from uranium after an exposure to a strong neutron source. The decay is found to have half-lives of about 3–14 seconds and 45 seconds. The cross section for delayed neutron emission produced by slow neutrons has been compared with the fission cross section for slow neutrons and found to be about 1/100 of the latter value, which our measurements indicate to be 2.5 to 3×10^{-24} cm^2.

[1] Anderson, Booth, Dunning, Fermi, Glasoe and Slack, Phys. Rev. **55**, 511 (1939).
[2] Roberts and Wang, Phys. Rev. **55**, 510 (1939).

69. Scattering of Slow Neutrons by Uranium. H. H. Goldsmith, V. W. Cohen and J. R. Dunning, *Columbia University.*—The total cross section (scattering+capture) of U for thermal neutrons has been redetermined[1] by using a Rn-Be "howitzer" source, a highly collimated neutron beam, analyzed samples of U_3O_8 containing less than 0.05 percent H_2O and a BF_3 detecting chamber. We obtain a value for the total cross section of $20\pm2\times10^{-24}$ cm^2, neglecting possible non-additive effects in the molecule.[2] The scattering cross section may be estimated to be about 15×10^{-24} cm^2 from the value of $2\text{–}3\times10^{-24}$ cm^2 for the fission cross section,[3] a value for the radiative capture cross section of $\sim3\times10^{-24}$ cm^2 obtained by assuming a reasonable width of the 25-volt resonance.[4] To obtain an independent determination of the scattering cross section use is made of the fact that the absorption processes (fission +radiative capture) exhibit a $1/v$ type of variation whereas the scattering process is independent of the velocity for slow neutrons. This means that in the region of 1 ev the total cross section is almost entirely due to scattering and therefore the cross section for D neutrons should be slightly less than 20×10^{-24} cm^2. Preliminary measurements confirm this.

[1] Dunning, Pegram, Fink and Mitchell, Phys. Rev. **48**, 265 (1935).
[2] Whitaker and Beyer (see abstract 72, this meeting).
[3] Anderson, Booth, Dunning, Fermi, Glasoe and Slack, Phys. Rev. **55**, 511 (1939).
[4] Meitner, Hahn and Strassmann, Zeits. f. Physik **106**, 249 (1937).

70. The Radioactivity of the Fission Products from Uranium Bombarded with Slow Neutrons. G. N. Glasoe and J. Steigman, *Columbia University.*—An experiment, suggested by Fermi and independently by Joliot and by Meitner and Frisch,[1] was performed to observe the radioactivity of the fission products from uranium. These products were collected in a Cellophane foil and the activity measured by placing the foil around a G-M counter. The uranium, in the form of uranium oxide electrolytically deposited on thin copper sheet, and the Cellophane were mounted with a separation of about 2 cm in an evacuated aluminum cylinder placed in paraffin near the cyclotron. Neither irradiation of the chamber containing no uranium nor leaving it evacuated for several days with no neutron bombardment showed any activity in the Cellophane. Two minutes after the end of a 30-minute irradiation several thousand counts per minute were observed. The decay was followed for four days and showed a long half-life of about 40 hours. A preliminary analysis of this decay showed other periods of about 6 hours, 80 minutes, 20 minutes and 10 minutes with the possibility of several shorter periods. Volatile products from irradiation of uranium in solution were collected in a vessel cooled with liquid nitrogen and showed periods of the order of 80 minutes and 10 minutes.

[1] L. Meitner and R. Frisch, Nature **143**, 471 (1939).

71. Mechanism of Nuclear Fission. N. Bohr, *Institute for Advanced Study,* and John A. Wheeler, *Princeton University.*—An estimation of the energy required to separate the nuclei of thorium and uranium into two or more parts of comparable mass and charge shows conclusively that the fission process cannot be attributed to a quantum mechanical effect analogous to alpha-particle emission from the ground state of a heavy nucleus but that we have to do with an essentially classical effect arising from the possibility of comparatively large deformations of the excited compound nucleus.* The electrostatic repulsion of the nuclear particles will, in fact, for the heaviest nuclei nearly compensate the effect of the short range forces in opposing such deformation and a simple calculation shows that the energy required for a critical deformation is of the same order as the neutron binding energy. From the arguments familiar from the theory of monomolecular reactions, the disintegration constant for the system when excited with the energy E is given by $N^*(E-E_c)/h\rho(E)$, where ρ is the density of energy levels in the original state of the excited nucleus, E_c is the potential energy of deformation in the critical state, and $N^*(E^*)$ is the number of energy levels in that state with energy less than E^*. On these lines the dependence of fission probability on energy, and the statistical distribution in size and mass of the fragments and their initial excitations, are estimated.

* L. Meitner and R. Frisch, Nature **143**, 239 (1939). See also N. Bohr, Nature **143**, 330 (1939) and Phys. Rev. **55**, 418 (1939).

72. An Experimental Study of the Additivity of Slow Neutron Cross Sections. Martin D. Whitaker, *New York University,* and Harold G. Beyer, *Columbia University.*—The results of our recent experiments[1] on the transmission of slow neutrons through paramagnetic salts

showed such unexpectedly large differences in the cross sections of the salt and the additive cross sections of the constituent elements that we have extended our original investigation to include other combinations of elements. The results to date are shown in Table I. The cross section measurements for the elements and the compounds studied were made under essentially the same conditions with careful consideration of purity of samples and their water content. It is interesting to note that the difference between the observed cross section and the additive cross section is sometimes positive and sometimes negative. The sulfide of zinc (ZnS) shows a larger cross section than zinc oxide although the oxygen cross section is twice that of sulfur.

TABLE I. *Total neutron cross sections for scattering + capture.*

MATERIAL	MEASURED $\times 10^{24}$ cm^{-2}	ADDITIVE $\times 10^{24}$ cm^{-2}	DIFFERENCE
Ni	20.0	—	—
Cu	10.5	—	—
S	2.0	—	—
O[2] (Gas)	4.1	—	—
Zn	4.5	—	—
Fe	12.0	—	—
CuO	16.2	14.5	1.7
Cu_2O	29.5	25.0	4.5
CuS	16.5	12.6	3.9
Cu_2S	27.7	23.1	4.6
ZnO	7.7	8.5	−0.8
ZnS	9.7	6.5	3.2
Permalloy (Ni (78) Fe (22))	12.8	18.2	−5.4

Permalloy gives the most striking result yet obtained. As a matter of fact the measured cross section for 78 permalloy is smaller than is to be expected from the nickel content alone. Some data on the transmission of slow neutrons by large crystals will be presented.

[1] M. Whitaker, H. Beyer and J. Dunning, Phys. Rev. **54**, 771 (1938).
[2] H. Carroll and J. Dunning, Phys. Rev. **54**, 541 (1938).

73. On Neutron Scattering in Crystals and Alloys. OTTO HALPERN, M. HAMERMESH AND M. H. JOHNSON, *New York University.*—The customary assumption of additivity of nuclear scattering cross sections[1] has to be modified if the scattering is coherent and has Laue maxima in addition to the trivial diffraction in the forward direction. Specially marked deviations are to be expected in the case of chemical compounds or real mixed crystals if the nuclei of the constituents form *one* lattice and happen to scatter with opposite phases. Apart from the influence of the change in lattice distance and the appearance of sublattices these effects would always lead to a diminution of the cross section for coherent scattering. Thermal motion of the lattice which produces an incoherent background can give rise to deviations from the additivity in both directions. The influence of nuclear spins, isotopes and preferred orientations is also discussed. Characteristic differences are expected to appear if because of a change in composition or differences in the method of preparation, the constituents group themselves in separate microcrystals. Experiments in this field promise to give information about the relative phases of the nuclearly scattered waves as well as about the physical constitution of the solid state. Values for nuclear cross sections require redetermination as a consequence of these calculations. The arguments presented here are also of importance for the interpretation of experiments in the field of magnetic scattering and particularly of polarization phenomena in ferromagnets.

[1] See the preceding experimental paper by M. Whitaker and H. Beyer.

74. Hyperfine Structure in the Spectrum of Indium III. J. S. CAMPBELL AND J. R. DAVIS, *Institute of Optics, University of Rochester.*—Vacuum spectrograms made with a five-meter 15,000-line/inch grating and a hot spark source resolve the In III lines λ1748.77 $5s\,^3S_1 - 5p\,^3P_1$ and λ1625.26 $5s\,^3S_1 - 5p\,^3P_2$ as hyperfine doublets having the separations 3.78 cm^{-1} and 3.55 cm^{-1}, respectively. Using the nuclear moment (9/2) of indium, and the theoretical ratio between the splitting factors of the two P states, these line separations give the separation of the S levels as 3.66 cm^{-1} and that of the P_1 levels as 0.35 cm^{-1}. The splitting factor for the 5s electron is 0.73, in fair agreement with the value 0.707 obtained by applying the Goudsmit-Bacher relations to the total splitting factors of the $5s \cdot ns$ terms of In II.[1]

[1] F. Paschen and J. S. Campbell, Ann. d. Physik **31**, 29 (1938).

75. The Absorption Coefficient of Gases for Light of Wave-Length 1215.7A. WILLIAM M. PRESTON, *Harvard University.*—It is well known that air is relatively transparent to light in the region between 1200 and 1350A. Because of the abundance of hydrogen in the chromosphere and in solar prominences, it is possible that the earth may receive an intensity at 1215.7A (first line of the Lyman series) far greater than at neighboring wave-lengths, which might penetrate far enough to influence the lower layers of the ionosphere. An apparatus, built for another purpose, has been used to measure accurately the absorption coefficients of the constituents of air at this wave-length. The source was a hydrogen discharge; the absorption cell had LiF windows; the light was analyzed by a one-meter grating and the intensity measured by a photoelectric cell. The results were, for the absorption coefficient per centimeter path reduced to normal temperature and pressure: air (dry, CO_2 free) 0.063; oxygen 0.28; nitrogen 0.005; carbon dioxide 2.01; water vapor 395. The absorption coefficient of air appears to increase with the pressure. At low pressures, a column of dry, CO_2 free air equivalent to 16 cm at NTP will reduce the intensity by a factor $1/e$.

76. Zeeman Effect at Fields of 100,000 Gauss. GEORGE R. HARRISON AND FRANCIS BITTER, *Massachusetts Institute of Technology.*—A new electromagnet of the type recently described[1] has been used to obtain Zeeman resolution of spectral lines at fields up to 99,830 gauss. Though power consumption at highest fields is 1800 kilowatts, current through the magnet can be held constant to within 0.1 percent over several hours. The field is uniform to one percent throughout a volume of 25 cc. An arc has been constructed to operate with arc stream parallel to the lines of force, and light can be removed transversely. Use of rare earth and other oxide powders in a horizontal arc is made possible by electrodes compressed with silver powder by Professor John Wulff. Excitation temperatures in the

arc are apparently increased by the presence of the field. The arc is dimmed slightly in intensity when the field is applied, apparently because a shorter gap must be used. Photographs of strong lines can be obtained in five minutes with a 35-foot concave grating. Typical patterns of cerium and europium will be shown.

[1] F. Bitter, Rev. Sci. Inst. **7**, 482 (1936).

77. Analysis of a Queer Zeeman Effect Pattern in Tungsten. J. H. ROBERSON AND J. E. MACK, *University of Wisconsin.*—Although the tungsten arc line λ4659 (transition between the level 21453, $J=1$, and the normal level, $J=0$) has previously been reported as an ordinary simple triplet, investigation in magnetic fields up to $4.28\cdot10^4$ c.g.s. shows that, while the pattern remains approximately symmetric, the line wanders bodily toward higher frequencies, verifying the equation given by J. E. Mack and O. Laporte.[1] The constant K for the interaction of levels 21448_2 and 21453_1 is tentatively evaluated at $6\cdot10^{-2}$.

[1] J. E. Mack and O. Laporte, Phys. Rev. **51**, 291 (1937)

78. Theory of the Paschen-Back Effect for Intermediate Coupling. J. B. GREEN AND J. F. EICHELBERGER, *Ohio State University.*—General spectroscopic theory has been applied to the Paschen-Back effect and simplified methods developed for determining the positions of the energy levels and intensities of lines for cases of intermediate coupling. They are expressed in terms of *LS*-coupling as the zero-order functions. The description of the results in words is then very simply and easily stated in terms of the *LS*-coupling designations and the transformation coefficients.

79. Sensitized Fluorescence of Lead. J. GIBSON WINANS, FRANCIS J. DAVIS AND VICTOR A. LEITZKE, *University of Wisconsin.*—The sensitized fluorescence of lead in mercury vapor was observed with simplified apparatus[1] using 2536 or 1854 for excitation. With five to ten-minute exposures, twelve lead lines were obtained including the five observed by Kopferman.[2] With a seven-millimeter nitrogen atmosphere, the higher energy lead lines 2613, 2873, 2802, 2663 were stronger with respect to the lower energy lines 2833, 3683, 3639, 4058 for 2536 excitation as well as for 1854 excitation. Additional lead lines observed were 3739, 3572, 2823, 3260? and 2577. 3260 may be due to cadmium. Impurity lines from thallium were also present. A Tesla discharge through the mercury lead mixture showed a narrow continuous type band with short wave edge at the lead line 2833. This band is analogous to one observed at 2768 for thallium and it is probably due to Pb_2. A drop of liquid mercury was found to produce strong evaporation of lead or thallium from a hot drop of the metal. The evaporated lead or thallium forms black clouds of condensed metal.

[1] J. G. Winans and R. M. Williams, Phys. Rev. **52**, 930 (1937).
[2] H. Kopferman, Zeits. f. Physik **21**, 316 (1924).

80. The Response of Several Fluorescent Materials to Short Wave-Length Ultraviolet Radiations. N. C. BEESE, *Westinghouse Electric & Manufacturing Company.*—A quartz monochromator has been used to measure the relative response of several synthetic phosphors in the region of 2200A to 3150A. The deactivating effect of copper and nickel on certain substances is represented graphically. With a vacuum grating spectrograph the response characteristics of zinc silicate and calcium tungstate have been extended to the Schumann ultraviolet region.

81. Energy Distribution of OH Molecules in Sensitized Fluorescence. ELISABETH REED LYMAN, *University of California. (Introduced by F. A. Jenkins.)*—Photometric intensity measurements were made of the OH spectrum excited by sensitized fluorescence. Mixtures of gases in the fluorescence tube which were used were $Hg+H_2O$, $Hg+H_2O+N_2$, $Hg+H_2O+He$. Metastable $^3P_0$ Hg atoms impart their energy by collisions of the second kind to the OH molecules first formed with little if any rotation. Thermal distribution of rotational energies was not obtained in any fluorescence spectrum of OH. Too large energies in the high rotational states were found probably arising, as in the case of HgH,[1] in the excitation process and in collisions during the lifetime of the excited molecule. In the (0,0) λ3064 and the (1,0) λ2811 bands there is a sudden drop of intensity to zero above the rotational level $J'=17\frac{1}{2}$ for the (0,0) band and $J'=11\frac{1}{2}$ for the (1,0) band. The energies for $J'_{(0,\,0)}=17\frac{1}{2}$, 37444 cm^{-1}, and $J'_{(1,\,0)}=11\frac{1}{2}$, 37501 cm^{-1} agree with the energy for $^3P_0$ Hg atoms, 37642 cm^{-1}. The intensities of lines from $J'_{(0,\,0)}=16\frac{1}{2}$, $17\frac{1}{2}$ and $J'_{(1,\,0)}=10\frac{1}{2}$, $11\frac{1}{2}$ are slightly enhanced. The enhancement may be explained as due to the large cross section for energy transfer by collision for states of nearly the same energy as $^3P_0$. Measurements of the (0,0) and (1,0) bands for molecules undergoing collisions with N_2 indicate a transfer of molecules from the vibrational level $v'=1$ to high rotational levels of $v'=0$ with increasing pressures of N_2, as well as some reduction of rotational energy towards thermal values. Collisions with helium appear much less efficient than collisions with N_2 in removing vibrational, rotational, or kinetic energy from the OH molecules.

[1] F. F. Rieke, J. Chem. Phys. **4**, 513 (1936).

82. Quenching and Depolarization of Mercury Resonance Radiation by Foreign Gases. LEONARD O. OLSEN, *Case School of Applied Science.*†—The polarization of mercury resonance radiation excited by the plane-polarized light from a water-cooled mercury arc is affected by a foreign gas in the resonance bulb and by an external magnetic field. Experimental results have been secured for the gases, nitrogen, deuterium, carbon dioxide and helium, their effects on the polarization having been studied as a function of gas pressure in zero applied field and as a function of applied field intensity at fixed gas pressures. The rotation of the plane of polarization produced by magnetic fields has also been observed for fixed gas pressures. These results have been used to calculate quenching and depolarization cross sections. The cross sections so determined agree well with the percentage polarization as a function of gas pressure data. The agreement with the magnetic field data is not as good. The indication is that there is a dependence of effective mean life on the intensity of the applied magnetic field.

† Experimental work performed at the University of Iowa Physical Laboratory.

83. A Variable Oscillator for Ultra-High Frequency Measurements. RONOLD KING, *Harvard University.*—A fundamental theorem regarding coupled ultra-high frequency circuits is explained together with its experimental verification. The importance of the theorem in the measurement of current and voltage is discussed. The conditions of the theorem are applied to determine the design of a variable oscillator for use in the ultra-high frequency measurement of current, voltage, resistance, reactance, dielectric constant, permeability, etc. in the range from 50 to 300 megacycles. The circuit, construction, and frequency characteristics of the oscillator are described. Its usefulness for purposes of measurement and demonstration is outlined.

84. Supersonics and the Effect of Water Vapor on Molecular Vibrations in CO_2. W. H. PIELEMEIER AND D. TELFAIR, *The Pennsylvania State College.*—Acoustic interferometer measurements were made at approximately 28°C and atmospheric pressure from which the wave velocity and the absorption in CO_2 were computed. About twenty H_2O concentrations were used with each of ten frequencies ranging from 284 to 1595 kc/sec. At each frequency, μ (the absorption per wave-length) rises with increasing humidity to a maximum of approximately 0.27 and then drops slowly, but at the lower frequencies it also passes through a *minor* peak before saturation is reached. As the major absorption peak is approached and passed the *velocity* drops nearly ten meters/sec. and a one-meter/sec. drop occurs near the minor peak. As the frequency f is increased the critical (major peak producing) H_2O concentration h increases also; i.e. $f_m=[60+8(10)^4h]$ kc/sec. For the minor peaks $f_{m'}=[54+2(10)^4h]$ kc/sec. These relationships show that there are at least two types of vibration within the CO_2 molecule differing widely in the manner that water vapor effects their rate of adjustment to the periodic temperature changes associated with supersonic waves. Previously only *one* adjustment rate for a given humidity had been found although Eucken[1] and others have searched for more.

[1] A. Eucken and E. Nümann, Zeits. f. physik. Chemie **B36**, 163 (1937).

85. Effect of Temperature on Supersonic Velocity in CO_2. C. J. OVERBECK AND E. WILER, *Northwestern University.*—Reports on experimental work in supersonics, relating to the anomalous absorption and dispersion in gases, CO_2 in particular, show conflicting results. There is support for both the resonance theory[1] and the collision theory[2] as the explanation of the anomalous effect. This led the authors to the task of attempting to find the reasons for the experimental discrepancies. Apparatus was built quite similar to that used in the earlier work and tests were conducted as changes were instituted. The probable cause of the conflicting experimental evidence has been located as a gas contamination, namely gases released from the Bakelite, rubber and cork elements used in the earlier gas chambers, and possibly also to a trace of water vapor from the CO_2 supply. Data will be presented giving the velocity values in CO_2 at 90 kc for a temperature range from 20°C to 418°C, obtained using a complete metal and glass chamber with special precautions to reduce the water vapor content. The experimental evidence supports the collision theory; the slope of the curve, however, is considerably less than that reported earlier.

[1] See H. L. Penman, Proc. Phys. Soc. **47**, 543 (1935).
[2] See G. W. Warner, J. Acous. Soc. Am. **9**, 30 (1937).

86. Theory of Secondary Peak for Sound Absorption in CO_2. HAROLD L. SAXTON, *Pennsylvania State College.*—Use of approximate formulas for absorption of supersonic waves in CO_2 has previously yielded surprisingly good results over a limited range of frequency. The error introduced by such approximations will be discussed. The data obtained by Pielemeier and his co-workers by varying the water vapor content of a gas cover a much greater range of the ratio of period to "mean lifetime of a quantum" and display a secondary peak not as yet observed by others, and not predicted by the simplest theory. This peak is explained by treating the gas as "3-state" in the δ mode and "2-state" in the valence mode of vibration. Characteristic curves of this theory will be presented and the check with experimental results will be demonstrated.

87. Transmission of Sound Through Plates at Oblique Incidence. F. H. SANDERS, *National Research Council, Ottawa, Canada.*—The transmission of high frequency sound through plates of brass and nickel has been studied for angles of incidence ranging from 0 to 70 degrees. Effective plate thicknesses varied from one-twentieth of a wave-length to around one wave-length. In addition to strong transmissions in the region below the normal critical angle very sharp and intense transmission maxima have been observed at angles of incidence greatly in excess of the critical angle. These transmission maxima fall within three clearly defined angular regions: (1) angles between zero and the critical angle for longitudinal waves; (2) angles between the critical angle for longitudinal waves and the critical angle for transverse waves; and (3) angles above the critical angle for transverse waves. In regions (1) and (2) the observed data are in satisfactory agreement with a recent theory due to Reissner[1] and good values of the elastic constants are obtained. By an extension of Lamb's[2] theory for flexural vibrations in bars the results in region (3) can be interpreted.

[1] Reissner, Helv. Phys. Acta **XI**, 140–155.
[2] Lamb, *Dynamical Theory of Sound*, second edition, Section 45, p. 122.

88. Recording of Critical Frequencies of the Ionosphere. OLOF RYDBECK, *Harvard University.* (*Introduced by H. R. Mimno.*)—A double-detection sweep-frequency receiver and recording amplifier has been designed for recording the signals from the laboratory's variable-frequency transmitter. The receiver is flexibly built, with easily exchangeable cam disks and plug-in coils. The mechanical tuning has no back-lash and mechanical synchronization is easily obtained with a friction drive on the motor shaft. No ground wave is necessary for synchronization and the receiver is therefore especially suited for long base recording.The

radiofrequency gain is approximately constant over the tuning range, its average value being 10^6. The audiofrequency system is of unusual design. The strongest pulses received are recorded with a minimum of distortion and transients. The circuit elements are determined not only by the frequency range desired but also by the maximum amplitudes handled. Various records obtained with the equipment will be discussed. Unusual echoes, probably arriving from very distant sunrise regions in the ionosphere, have been recorded over the frequency range.

89. The Apparent Motion of Clouds of Abnormal *E* Region Ionization. J. A. PIERCE AND H. R. MIMNO, *Harvard University.*—Previous researches have indicated that abnormal *E* region ionization appears in patches which may be very small or may have lateral dimensions of hundreds of kilometers, and which may or may not appear fixed with respect to the earth. Occasionally radio echoes are returned from such clouds even when they are not directly overhead. It is possible, in some of these cases, to estimate the vertical thickness of the clouds and to measure the lateral distance to the reflecting surface as a function of time. These measurements indicate that a typical ionized region of this sort is not more than a few kilometers thick and passes the observer with a speed which may be as great as 500 kilometers per hour. It is suggested that this apparent motion may be the result of an ionizing beam which sweeps across the atmosphere liberating electrons which disappear quickly after the passage of the beam.

90. Velocity of Light Apparatus.* WILMER C. ANDERSON, *Harvard University.*—A number of improvements and changes in the velocity of light apparatus[1] utilizing radiofrequency interferometry have been made recently. Principal changes have been made in the method of modulation of the light beam, the control of the modulation frequency, the receiving system, the substitution of a recording system for visual observation, and the use of a new optical system to lessen end-point errors. Preliminary records and pictures of the apparatus are shown.

* Partly financed by Carnegie Corporation of New York.
[1] W. C. Anderson, Rev. Sci. Inst. **8**, 239 (1937).

91. Scattering of Light by Water as a Function of Angle. L. H. DAWSON AND E. O. HULBURT, *Naval Research Laboratory.*—According to theory of scattering of light by isotropic particles that are small with respect to the wave-length of light, the scattered intensity at angle θ to the direction of propagation varies as $1+\cos^2\theta$. Measurements of the scattered intensity for pure water were made at $\theta=45°$, 90° and 135° for wave-lengths from about 3660 to 7000A. An excess forward scattering was observed in three ways, visually, photographically and with photoelectric counter. The intensity at 135° was about 60 percent greater than at 45°; theory would put the intensities equal for the two angles. It appears difficult to determine whether the difference was a property of pure water, and related to polarization defect, due to anisotrophy of the scattering centers, or was caused by slight optical impurities in the water.

92. Multilayer Films of High Reflecting Power. C. HAWLEY CARTWRIGHT AND A. FRANCIS TURNER, *Massachusetts Institute of Technology.*—By alternately depositing films of high and low indices of refraction on glass such that each film has an optical thickness $nd=\lambda_0/4$, the reflecting power for any pre-selected wave-length, λ_0, can be increased to over 80 percent. A monochromator is formed by reflecting white light from two or more such filters and the wave-length of the reflected light can be varied somewhat by changing the angle of reflection. By suitably choosing the film thicknesses, a color separation filter was made which reflected 85 percent in the green and transmitted 90 percent in the red. Films of titanium dioxide ($n=3.0$) separated by films of cryolite ($n=1.3$) were found to be quite rugged. The films of TiO_2 were deposited either by evaporating TiO_2 in a high vacuum or by converting hot $TiCl_4$ vapor in air to a TiO_2 film. The cryolite films were deposited by evaporation in a high vacuum. However, it seems possible to replace the cryolite by SiO_2 deposited in air from $SiCl_4$ vapor.

93. Integrating Meters for Ultraviolet Radiation. J. B. H. KUPER, *Washington Biophysical Institute,* AND F. S. BRACKETT, *Division of Industrial Hygiene, National Institute of Health.*—Integrating meters for recording the amount of solar ultraviolet received have been developed in cooperation with Dr. H. C. Rentschler and used for over a year in connection with a study of the influence of climate on epidemiology. The meters consist of photo-cells with pure titanium cathodes (threshold about 3200A) in connection with fixed condensers and cold-cathode gas-filled tubes ("trigger tubes"). These are sealed in evacuated extensions of the photo-cell envelopes for protection against moisture. Each discharge of a trigger tube is recorded on a telephone message register which may be located a considerable distance from the cell. The circuit used was chosen to give the greatest possible reliability without overloading batteries or tubes, and the meters operate with no skilled attention except for routine calibration checks every few months. An unskilled observer reads the message register daily, but automatic photographic registration could be used instead, if desired. The spectral response of the photo-cells is chosen to give a good approximation to the erythemal curve. Geometric factors in the photo-cell response, and reliability of the calibration will be discussed and some preliminary data on seasonal variations in solar ultraviolet will be presented.

94. Binding Energy of Li^7. K. G. CARROLL, *Yale University.*—Calculations have been made on the stability of the Li^7 nucleus in its ground state by employing the symmetric interaction in its usual form: $V_{ij}=-Ae^{-r_{ij}^2/a^2}\times[w+mP_{ij}+bQ_{ij}+hP_{ij}Q_{ij}]$. Similar to results for Li^6,[1] the simple Hartree approximation yields less than a third of the observed binding (39 Mev). With two variation parameters (corresponding to pre-formed "shells") this may be considerably improved, but still remains far from the true value. By means of a second-order perturbation

calculation the effect of improving the ground state function with higher members of a complete set of oscillator functions is calculated. Convergence is found to be more rapid than for Li^6. An upper bound to the second-order perturbation including all members of the set is obtained. Convergence is estimated by means of a third-order calculation. For the most favorable choice of nuclear parameters, the binding energy of the ground state appears to fall short of the experimental value by at least 25 percent. The use of parameters recently suggested by Breit[2] increases the discrepancy. The results agree with those for He^{3} [3] and Li^6 in indicating a systematic failure of the present interaction for nuclei beyond He^4.

[1] H. Margenau and K. G. Carroll, Phys. Rev. **54**, 705 (1938).
[2] G. Breit, Phys. Rev. **55**, 603 (1939).
[3] W. A. Tyrrell, New York Meeting, Feb. 23–25, 1939.

95. Nuclear Excitation of Indium by X-Rays. B. Waldman, G. B. Collins, E. M. Stubblefield, *University of Notre Dame*, and M. Goldhaber, *University of Illinois*.—It has been shown recently that the stable nucleus In^{115}, when excited by x-rays, may be left in a metastable excited state, designated by In^{115*}, from which it decays, emitting negative electrons, with a half-life time of approximately four hours.[1, 2] As the transition from the ground state of In^{115} directly to In^{115*} is highly forbidden, the process can be described as an excitation from the ground state to a higher level ("activation" level) and the subsequent return to the metastable state, In^{115*}. We have obtained a yield curve by measuring the activity of indium as a function of the energy of the electrons producing the x-rays. This curve shows a threshold at 1.2 ± 0.1 Mev and an abrupt change of slope at 1.55 ± 0.1 Mev, indicating the existence of two "activation" levels.

[1] Pontecorvo and Lazard, Comptes rendus **208**, 99 (1939).
[2] Collins, Waldman, Stubblefield and Goldhaber, Phys. Rev. **55**, 507 (1939).

96. Nuclear Energy Levels in B^{10}. P. Gerald Kruger, F. W. Stallmann and W. E. Shoupp, *University of Illinois*.—A previous[1] examination of the gamma-rays from Be^9 bombarded with one-Mev deuterons revealed six gamma-ray lines. Two thousand new cloud-chamber pictures taken with a stereoscopic camera give data which show twenty-seven γ-ray lines between 0.29 Mev and 4.71 Mev. Twenty-six lines are observed by Compton recoil electrons from a thin mica foil. Seventeen lines are confirmed by the measurement of thirty-three $\pm$ pairs which were formed in the gas in the cloud chamber. In all cases where $\pm$ pair energies are available the gamma-ray energies from those measurements are considered more reliable than those from the Compton recoil electron groups, though in most instances the two values agree to ±0.04 Mev. From these lines it appears that nine levels in the B^{10} nucleus have been established. By using the calculations of Feenberg and Wigner[2] one obtains the following classification of the levels: $^3S_1$ as the ground state (relative energy zero); $^3D_{123}$ at 0.29 Mev, 0.44 Mev and 0.57 Mev; $^1S_0$ at 1.45 Mev; $^1D_2$ at 1.98 Mev; $^3F_{234}$ at 2.89 Mev; $^3D_{123}$ at 3.65 Mev; $^1D_2$ at 4.71 Mev.

[1] P. G. Kruger and G. K. Green, Phys. Rev. **52**, 773 (1937).
[2] E. Feenberg and E. Wigner, Phys. Rev. **51**, 95 (1937).

97. Distribution in Angle of Protons from the Deuteron-Deuteron Reaction. A. Ellett, J. A. Van Allen and D. S. Bayley, *University of Iowa*.—The fore and aft asymmetry reported earlier[1] has been found to be due to low energy deuterons in the incident beam arising from grazing collisions with the walls of the capillary tube through which the beam entered the gas target chamber. Substitution of a series of thin diaphragms eliminates this scattering and the consequent asymmetry. We find that the distribution in angle reduced to the center of mass reference system may be represented by $I(\theta)=1+A\cos^2\theta$ and that the value of A depends upon the bombarding energy as in the table below:

Bombarding energy kev	330	250	200	133
A	1.45	1.2	1.05	0.9

[1] A. Ellett and R. D. Huntoon, Phys. Rev. **54**, 87 (1938).

98. On the Photoelectric Effect of the Deuteron. L. Eisenbud, *Princeton University*.—The experiment of von Halban[1] indicates that the ratio of the intensities of the photo-neutrons from deuterium in the direction of the incident thorium C'' γ-rays and at right angles to this direction is in contradiction with the ordinary theory of the deuteron. Theory gives the value 0.25 for the ratio of the intensity of the ^1S wave (arising in the photomagnetic dipole transition) in the direction of the γ-ray, to the intensity of the ^3P wave (produced by the photoelectric dipole transition) at right angles to the γ-ray beam. This number is to be compared with the ratio obtained by experiment which is between 0.01 and 0.13. In an effort to understand the discrepancy the effect of the introduction of a neutron-proton interaction, which contains, in addition to the usual terms, a vector-vector and a tensor-tensor interaction, has been investigated. This leads to a coupling of waves of different orbital angular momenta, and also to coupling between triplet and singlet waves. In particular the ground state of the deuteron will contain both ^3S and ^3D waves. On these assumptions there is a possibility of explaining von Halban's results in two ways. (1) Electric dipole transitions from the ^3S wave of the ground state lead to a ^1P wave through the coupling of this wave with ^3P. The ^1P wave can interfere in the forward direction with the ^1S wave which comes from the ^3S in the ground state by magnetic dipole transition. (2) Electric dipole transitions from the ^3D wave in the ground state to ^3P can increase the neutron intensity at right angles to the γ-ray beam. The conclusions which can be derived without detailed information on the exact forms of the interactions will be discussed.

[1] H. von Halban, Nature **141**, 644 (1938).

99. Search for Excited State of C^{13}. J. Reginald Richardson, *University of Illinois*.—An excited state of C^{13} at about 270 kv is suggested by the gamma-radiation[1] from N^{13}. It would seem possible for the product nucleus to be left in this excited state in the reaction $C^{12}(d,p)C^{13}$, provided there is no selection rule forbidding the transition. The existence of the excited state would be indicated in the energy distribution of the emitted protons.[2] A more detailed search was made for group structure in

these protons, as produced by the bombardment of a thin target of carbon by 900-kv deuterons from the cyclotron. No evidence of group structure was found. The results indicate that the probability that the C^{13} nucleus be left in such an excited state compared with the probability that it be left in the ground state is less than five percent, provided the energy of the excited state is 180 kv above ground, or greater. Efforts are being made to decrease these limits.

[1] J. R. Richardson, Phys. Rev. **55**, 609 (1939).
[2] J. D. Cockcroft and W. B. Lewis, Proc. Roy. Soc. **A154**, 261 (1936).

100. The Meson Theory of Nuclear Forces and the Quadrupole Moment of the Deuteron. H. A. BETHE, *Cornell University.*—Kemmer[1] has proposed a theory of nuclear forces based upon the emission and reabsorption of neutral and charged mesons, the theory being symmetrical in all these types of mesons (S-theory). An alternative theory is possible which involves only neutral mesons (N-theory). To explain the saturation of nuclear forces and the attraction between nuclear particles in the singlet state, the forces must be spin-dependent. It is simplest to assume spin-dependent forces only. The theory diverges at small distances and requires "cutting off." The interaction makes the ground state of the deuteron a mixture of a ^3S and a $^3D_1$ state, and thus predicts an electric quadrupole in the N-theory moment of the deuteron. The sign of this quadrupole is in agreement with the observations of Kellogg, Rabi, Ramsey and Zacharias[2] ("cigar shape"), in the S-theory it is opposite. The cutting-off radius r_0 and the value of the quadrupole moment Q can be determined from the requirement that the energies of both the singlet and the triplet state of the deuteron be given correctly. This gives $Q=1.27\cdot10^{-27}$ cm^2 on the N-theory and $\sim-4\cdot10^{-27}$ cm^2 on the S-theory, as compared with about $2\cdot10^{-27}$ observed. Q is insensitive to the way in which the potential V is cut off.

[1] N. Kemmer, Proc. Cambr. Phil. Soc. **34**, 354 (1938).
[2] Kellogg, Rabi, Ramsey and Zacharias, Phys. Rev. **55**, 318 (1939)

101. β-Decay and Spin of N^{13}. B. O. GRÖNBLOM, *Cornell University.* (*Introduced by H. A. Bethe.*)—Richardson[1] has shown that the β-decay of N^{13} leads to two states of C^{13} with an energy difference of 285 ± 20 kv, about 80 percent of all transitions leading to the excited state. Similar conclusions were reached theoretically by Bethe, Hoyle and Peierls.[2] Assuming that the C^{13} states are components of a ^2P level,[3] and that N^{13} behaves analogously, the original Fermi theory would predict a transition to only one of the C^{13} states. We must use instead the spin-dependent modification of the Fermi theory proposed by Gamow and Teller,[4] which is also required[5] by the large probability of the β-transition $He^6\rightarrow Li^6+\beta+n^0$ (probably a $^1S-{}^3S$ transition). From the ratio of the transition probabilities the spins of the various states of C^{13} and N^{13} can be deduced using the Gamow-Teller theory. If both nuclei have a $^2P_{\frac{1}{2}}$ ground state[3] 75 percent should lead to the excited state of C^{13} in good agreement with the experiment. All other assumptions lead to disagreement, e.g. if both ground states are $^2P_{\frac{3}{2}}$, the figure should be 23 percent. The conclusion is in agreement with the calculations of Bethe and Rose. From the observed lifetime of N^{13} we obtain for the β-decay constant $\tau_0=0,\ 5\cdot10^4$ sec. (previous value 1, $1\cdot10^4$ sec.[6]).

[1] J. R. Richardson, Phys. Rev. **53**, 610 (1936).
[2] H. A. Bethe, F. Hoyle and R. Peierls, Nature **143**, 200 (1939).
[3] M. E. Rose, H. A. Bethe, Phys. Rev. **51**, 205 (1937).
[4] G. Gamow and E. Teller, Phys. Rev. **49**, 895 (1936).
[5] M. Goldhaber, unpublished.
[6] H. A. Bethe and C. L. Critchfield, Phys. Rev. **54**, 248 (1938).

102. Slowing Down of Neutrons by Heavy Nuclei. G. PLACZEK, *Cornell University.* (*Introduced by H. A. Bethe.*)—A rigorous solution of the integral equation for the slowing down process by collisions with nuclei of masses higher than the neutron mass has been obtained. In particular, for neutron energies E small compared to the original energy, the solution assumes the form:

$$\rho(E)dE=\frac{ql\left(\frac{m}{2}\right)^{\frac{1}{2}}(1-p)}{1-p(1-\log p)}E^{-\frac{1}{2}}dE.$$

(ρ neutron density, q number of neutrons produced per second, l mean free path, $p=(M-m/M+m)^2$.) The results are applied to the discussion of experiments studying nuclear energy levels with neutrons slowed down in heavy substances. Furthermore, the possibility of detecting small capture cross sections by slowing down experiments is discussed.

103. The Exponential and Meson Potentials. S. SHARE, L. E. HOISINGTON AND G. BREIT, *University of Wisconsin.*—Recent experiments[1] on the scattering of protons by protons permit the determination of the range of force acting between two protons on the supposition that the potential is not velocity dependent.[2] They also allow the elimination of fixed potentials with certain shapes. The exponential potential used in the calculations of Rarita and Present on H^3 and He^4 has a correct average range but a wrong shape. For it the phase shift increases relatively too rapidly at low and too slowly at high energies. This is due to too much interaction at large distances. The meson potential $Ce^{-r/a}/(r/a)$ can be made to fit experiment nicely using $a=.42e^2/mc^2$, $C=-89.6mc^2$. The range corresponds to the mass of the heavy electron of 330 m. Such a determination of mass is affected by a possible velocity dependence.

[1] R. G. Herb, D. W. Kerst, D. B. Parkinson and G. J. Plain, **55**, 603(A) (1939); N. P. Heydenburg, L. R. Hafstad and M. A. Tuve, **55**, 603(A) (1939).
[2] The *a priori* possibility of velocity dependent potentials for nuclear particles has been pointed out by J. A. Wheeler.

104. The Vibration-Rotation Energies of Tetrahedrally Symmetrical Molecules. W. H. SHAFFER, H. H. NIELSEN AND L. H. THOMAS, *Ohio State University.*—The complete quantum mechanical Hamiltonian for the oscillating and rotating xy_4 type molecule has been derived perfectly generally to second approximation. It is convenient to transform $H=H_0+H_1+H_2$ by a contact transformation THT^{-1} into $H_0+H_1'+H_2'$ so that H_1' contains to second

approximation only the coriolis interaction terms arising from the degenerate oscillations. Linear combinations of the zeroth-order eigenfunctions may always be found such that the matrix H_1' will have elements only along the principal diagonal. These functions have been found for the ground state and for the states ν_1, ν_2, ν_3, ν_4, $2\nu_3$, $2\nu_4$, $\nu_1+\nu_3$, $\nu_1+\nu_4$, $\nu_2+\nu_3$, $\nu_2+\nu_4$, $\nu_3+\nu_4$. Our results in first approximation are in agreement with those of earlier investigators except for the state $\nu_3+\nu_4$ which splits up into nine component levels in general where $\zeta_3 \neq 0$ and $\zeta_4 \neq 0$, ζ_3 and ζ_4 being the moduli of the angular momentum vectors due to the degenerate oscillations ν_3 and ν_4. Using the above eigenfunctions the vibration-rotation energies are evaluated in terms of the potential energy constants for these states to second approximation from H_2'. Our results show that in general the second-order energies depend also upon the quantum number K, an effect which becomes important not only for the state ν_4, as Jahn has shown, but also for all harmonic and combination bands of ν_4. Selection rules and quantum amplitudes of the dipole moments have also been determined.

105. Viscosity in Two-Dimensional Systems. EDWARD BOYD AND WILLIAM D. HARKINS, *University of Chicago.*—Interesting relations are exhibited in the viscosity of monolayers, such as those of acids and alcohols on aqueous subsolutions. For liquid monolayers: (1) The relation between viscosity (σ) and pressure (f) is

$$\log \sigma = \log \sigma_0 + Kf. \qquad (1)$$

(2) If the molecules are oriented perpendicular to the surface, the viscosity rises rapidly with the length of the molecule. Increase of lateral pressure may cause a change to a "plastic-solid" state in which: (3) The viscosity is almost independent of pressure, and (4) Decreases rapidly as the length of the chain increases. Thus: (5) The increase of viscosity near the transition pressure is very great for short, and very small for long molecules. (6) The viscosity increases rapidly with the closeness of molecular packing. Thus with the same number of carbon atoms an alcohol of area 21.8 has about 30 times the viscosity of an acid of area 24.4 sq. A per molecule. Our Eq. (1) is analogous to Eq. (3) of Moore and Eyring

$$\log \sigma = \log \frac{h}{a} + \frac{\Delta F^{\ddagger}}{k'T},$$

from which it can be shown that our K has a calculated value 0.058 in absolute units while the experimental values for the 14 to 20 C atom acids range from 0.022 to 0.076.

106. On the Electromagnetic Field Produced by an Electron. V. F. WEISSKOPF, *University of Rochester.*—An analysis of the electric and magnetic field in the immediate neighborhood of an electron has been made by computing the electric field energy $U_{el} = 1/8\pi \int E^2 dv$ and the magnetic energy $U_{mag} = 1/8\pi \int H^2 dv$. The evaluation of these expressions for a single electron gives

$$U_{mag} \leqq \lim_{a=0} e^2 \frac{(h/mc)^2}{a^3},$$

where a is the critical electron radius. U_{mag} is equal to the energy of the field of a magnetic dipole density concentrated in a volume of linear dimensions a, so that we can identify U_{mag} as the energy of the field of the spin. U_{el} contains, apart from the electrostatic field of the charge, another term U_{el}' which is the energy of an alternating solenoidal field. This latter field is produced by the well-known fluctuating rotatory motion of the electron, which is responsible for the spin. The calculation gives $U_{el}' = U_{mag}$, so that the total contribution $1/8\pi \int (E^2 - H^2) dv$ of the spin to the self energy vanishes. The theory of the positron leads to different results: one gets $U_{mag} \leqq e^2(h/mc)/a^2$, which can be shown to be the field energy of a dipole density spread over a finite region in the same way as the charge of an electron in positron theory.[1] A direct proof of this spread of the magnetic polarization M can be given by calculating $M(r-\xi/2)M(r+\xi/2)$, which is finite for $\xi \neq 0$ and is proportional to the charge distribution $\rho(r-\xi/2)\rho(r+\xi/2)$. The electric field energy U_{el} is negative in positron theory: $U_{el} = -U_{mag}$. This is explained by the fact that the fluctuating oscillatory motion of the electron is according to the exclusion principle in opposite phase to the fluctuating motion of the vacuum electrons. The presence of the electron decreases the electric field energy of the vacuum electrons by destructive interference. The contribution of the spin to the self energy does not vanish in positron theory. It leads, together with the energy of the oscillations produced by fluctuations of the radiation field, to a logarithmically divergent term.

[1] See abstract of a paper given at the meeting of the A. P. S. in New York, Feb. 23–25, 1939.

107. A Modification of Special Relativity. CHESTER H. PAGE, *Lafayette College.*—Time observations in a laboratory are made by using clocks which have been synchronized while at rest beside each other, and then transported to observation points. Such observed times, and velocities based thereon, have the subscript 0 to distinguish them from "basic" times and velocities. "Basic" times are those indicated by clocks transported infinitely slowly. We postulate: (1) Position measurements are independent of clock transport velocity. (2) $c_0^2 = c^2 + w_0^2$, where c_0 is the observed velocity of light, w_0 is the observed clock transport velocity, and c is the basic velocity of light. From these postulates we immediately derive the slowing down of a clock in motion:

$$T_0 = T\left(1+\frac{w_0^2}{c^2}\right)^{-\frac{1}{2}} = T\left(1-\frac{w^2}{c^2}\right)^{\frac{1}{2}},$$

where w is the basic velocity of transport. By considering the setting back of a clock while being transported to the position of an event, we find that the positions and basic times of an event referred to laboratories (reference systems) having a basic relative velocity V are interrelated by the Lorentz-Einstein transformations, although positions and observed times are not. With available transport velocities, the difference is experimentally indistinguishable.

108. Nuclear Spins and Magnetic Moments by the Alpha-Particle Model. R. G. SACHS, *Johns Hopkins University.*—Some properties of the light nuclei of the type

$\pi\alpha\pm1$ have been calculated[1] on the basis of the α-particle model. By means of this description, spins and magnetic moments of the same nuclei are calculated. The results for the magnetic moments of many of the nuclei are undetermined within a certain range of possible values since the relative order of magnitude of the spin-orbit coupling and the separation of rotational levels is unknown. This ambiguity does not appear in the Hartree model,[2] so that the magnetic moments as calculated by the two models are somewhat different. The most notable difference occurs for the spins of C^{13}, N^{13}, which have not yet been measured; the Hartree model predicts a spin of $\frac{1}{2}$ for them, but the α-model yields a spin of $\frac{3}{2}$. The α-model appears to give slightly better agreement for those magnetic moments that have been measured.[3]

[1] L. R. Hafstad and E. Teller, Phys. Rev. **54**, 681 (1938).
[2] M. E. Rose and H. A. Bethe, Phys. Rev. **51**, 205 (1937).
[3] H. A. Bethe, Phys. Rev. **53**, 842 (1938).

109. Groups of Quantum-Mechanical Contact-Transformations and the Degeneracy of Energy-Levels. J. M. JAUCH,* *University of Minnesota.* (*Introduced by E. L. Hill.*)—It is well known that the invariance of the Schrödinger equation under the three-dimensional rotation group is not sufficient to give an explanation of the degeneracy of the energy-levels in the hydrogen atom. The "accidental" degeneracy with respect to the quantum number l remains unexplained. It is now possible to set up a continuous group of quantum-mechanical contact-transformations such that under this group the space of an energy-level transforms according to an irreducible representation of this group. For the hydrogen atom this group is isomorphic to the four-dimensional rotation group, a result already stated by Fock[1] and Bargmann.[2] The group has been determined in the case of the two-dimensional hydrogen atom and the two- and three-dimensional oscillator. The transformations have an analogy in classical mechanics and represent there transformations of one orbit in phase space into another orbit of the same energy.

* Swiss Exchange Fellow of the Institute of International Education.
[1] V. Fock, Zeits. f. Physik **98**, 145 (1936).
[2] V. Bargmann, Zeits. f. Physik **99**, 576 (1936).

110. Born's Reciprocity and Mie's Theory of Field and Matter. ALFRED LANDÉ, *Ohio State University.*—Born's theory of reciprocity concerning an upper limit to the corpuscular momentum is transferred to the electromagnetic field. The classical Mie theory of field and matter points to a normalization and then to a limitation of the vector potential which leads to a quantum theory of the field including charge and current. Its first application is the quantization of the charge itself ($C=ne$) replacing the explanation by means of a spherical model in a modified Maxwell field. The principal objection to Born's reciprocity was that "nobody would be able to move" if there were such a small upper limit to the momentum as is Born's b. This objection is removed by the result that there is an upper limit to the velocity ($0.999992\cdot c$) for all masses rather than a common upper limit to the momentum.

111. Parameters More Fundamental Than the Space-Time Coordinates. ENOS E. WITMER, *University of Pennsylvania.*—It is well known that the true quantities belonging to the Lorentz group are spinors, of which tensors form only a special class. This leads to the idea that it might be possible and advantageous to express physical quantities as functions of fundamental spinors instead of the fundamental vector x, y, z, ct. Let[1]

$$x=(\xi^1\bar{\xi}^2+\xi^2\bar{\xi}^1)-(\bar{\eta}_1\eta_2+\bar{\eta}_2\eta_1),$$
$$y=-i(\xi^2\bar{\xi}^1-\xi^1\bar{\xi}^2)+i(\bar{\eta}_2\eta_1-\bar{\eta}_1\eta_2), \text{ etc.}$$

Here ξ^1, ξ^2, $\bar{\eta}_1$, $\bar{\eta}_2$ are the fundamental spinors. In terms of these parameters the operators $\partial_{r\bar{s}}$ of spinor analysis become very symmetrical expressions. Thus

$$\partial_{1\bar{1}}=\frac{2}{S}\begin{vmatrix}\dfrac{\partial}{\partial\bar{\xi}^1} & \dfrac{\partial}{\partial\bar{\eta}^1}\\ \xi_1 & \eta_1\end{vmatrix},$$

where

$$S=2\begin{vmatrix}\xi^1 & \eta^1\\ \xi_1 & \eta_1\end{vmatrix}.$$

S is the "complex interval." The use of these parameters might be a step forward in dealing with the basic problems in physics today. It seems improbable that our present concept of space-time will be forever satisfactory. Therefore, even if these particular parameters do not represent an advance, the idea that physics may some day require the use of more basic independent variables than the ones now in use should not be abandoned. This is in accord with the general idea that even our most basic concepts may be replaced by others still more fundamental.

[1] G. Rumer, Physik. Zeits. **32**, 619 (1931).

112. Devitrification Temperatures of Aqueous Solutions.* BASILE J. LUYET, *Saint Louis University.*—Using the method of immersion in liquid air in thin layers I could vitrify solutions of inorganic substances: chlorides, sulfates, nitrates, hydrates, etc. and of organic compounds such as formaldehyde, ethylene glycol, glycerol, glucose, sucrose, dextrin, gums, agar, amino-acids, gelatin, albumin, etc. These solutions devitrify, i.e. crystallize and become opaque when their temperature is raised. Contrary to what is usually thought, the curves of the devitrification temperatures in terms of time turn parallel to the time axis within a narrow range of temperatures. This contradicts the view that any glass should finally crystallize if enough time is allowed. The solutions investigated have devitrification temperatures which range in increasing order when the substances dissolved are arranged in the order of increasing molecular complexity. At very high concentrations there is no devitrification at any temperature (a property of interest for the study of bound water); at an intermediate range of concentrations (for example, 2.4 M for sucrose) devitrification occurs according to a certain pattern and at certain temperatures; at a lower range (1 to 2 M for sucrose) the devitrification pattern is different and the temperatures are considerably higher. Within such a range (from 1 M to 2 M for sucrose) a large increase in concentration causes little lowering of the devitrification temperatures.

* Read by title.

113. Experimental Test of the Statistical Theory of Scaling Circuits. HAROLD LIFSCHUTZ AND O. S. DUFFENDACK, *University of Michigan.*—Extending previous work on the statistical theory of counting losses in Geiger-Müller counters and recorders, the parallel method[1] was used to determine the losses in a Cenco counter fed by a vacuum tube scale-of-eight. The Cenco counter was compared against a vacuum tube frequency meter. The experimental efficiency curve thus obtained was checked against the theory of Aloaglu and Smith. To do this the resolving times, σ and τ, of the G-M circuit and Cenco counter were found by observing the maximum *random* rate from the G-M tube and the maximum *periodic* rate of counting of the Cenco counter. These maxima were 400,000 and 4080 counts per minute, respectively. The theoretical curve thus obtained agreed well with the experimental curve up to input rates to the system of 38,000 counts a minute where the Cenco counter exhibited losses of 65 percent. At still higher counting rates the experimental curve appears to show a somewhat more rapid choking of the counter than predicted by the (idealized) theory. The Cenco counter shows negligible counting losses up to 17,000 counts a minute for the above values of σ and τ. Its useful speed is thus increased by a factor 400 over its speed when employed in a scale-of-one, in agreement with the theoretical prediction.

[1] H. Lifschutz and O. S. Duffendack, Phys. Rev. **54**, 714 (1938).

114. The High Frequency Modulation of Geiger Counters. J. N. SHIVE, *Johns Hopkins University.* (*Introduced by J. A. Bearden.*)—From a study of the current theories of the Geiger-Müller counter breakdown it seems plausible to expect that if an a.c. voltage is superimposed on the d.c. threshold of a counter, an ionizing particle arriving during the positive half-cycle will produce a complete breakdown, while for a particle arriving during the reverse half-cycle the discharge can proceed no further than the first Townsend avalanche. The consequent halving of the normal plateau counting rate under these conditions has been looked for in a number of variously constructed counters, and has been observed in some counters for modulation frequencies up to three mc. Experiments with a modulated x-ray source have shown that with source and counter in phase opposition, the counting rate is in these cases substantially one-half the normal background rate up to modulation frequencies of 300 kc. This investigation was undertaken in an attempt to establish a workable method for measuring speeds of neutrons in homogeneous groups of high energy. With a counter and neutron source modulated at 300 kc, having a separation of one meter, it should be possible to measure the velocities of neutrons of 10,000 v energy.

115. The Detection of Single Positive Ions, Electrons and Photons by a Secondary-Electron Multiplier. JAMES S. ALLEN, *University of Minnesota.*—A secondary-electron multiplier tube has been developed and used successfully for counting single positive ions, electrons and photons. This tube has 12 electrodes covered with a thin layer of beryllium. Tests have shown that with 300 volts per stage this tube will multiply the primary ion current by a factor of 10^5. The use of guard ring insulation and electrostatic shielding for the final collecting electrode has reduced the background current to an extremely low value. The last electrode was connected to the grid of the first tube in a linear amplifier. In order to count single positive ions the tube was waxed to the end of a simple mass-spectrograph. A few microamperes of electron current in the ion source were sufficient to produce large numbers of positive ions. The pulses produced were so large that only a few of the stages of the thermionic amplifier were necessary to amplify them sufficiently to be seen on the screen of a cathode-ray oscillograph. The multiplier tube has an extremely low background counting rate. Ions having energies from 50 to 20,000 volts and masses from one to 32 were detected. By increasing the gain of the thermionic amplifier, electrons could be counted. With still more gain single photons were counted. The height of the pulses due to electrons was about one-seventh that of the positive ion pulses, while the photon pulses were much smaller.

116. An Automatically Recording Geiger-Müller Counter Circuit. LYNN J. BRADY, *The Pennsylvania State College.* (*Introduced by Wheeler P. Davey.*)—A circuit has been developed by which the intensity of x-rays as registered by a quantum counter may be recorded automatically on a moving roll of paper. This circuit, which has been considerably modified from that of Gingrich, Evans and Edgerton, automatically corrects for changes in x-ray intensity due to any reasonable variation in x-ray tube current, and records the rate of arrival of impulses from the quantum counter in the form of the customary Intensity *vs.* Angle curves. Statistical fluctuations are nearly ironed out without loss of resolution. Easy adjustment of sensitivity and of location of zero is provided. The whole circuit is a.c. operated.

117. Discharge Counters of Unconventional Geometry. SANBORN C. BROWN AND ROBLEY D. EVANS, *Massachusetts Institute of Technology.*—This paper reports a successful general method for removing the geometrical restrictions from discharge counter design. In a previous paper[1] we discussed the operation of the coaxial cylinder discharge counter using a modification of the parallel circuit introduced by Neher and Harper[2] to quench the discharge from outside the counter. This method has now been extended to the cases of counters with parallel plate, parallel ring, parallel wire and concentric sphere electrodes. These geometries all function as true discharge counters as do Geiger-Müller tube counters, and are therefore sensitive to gamma-rays and beta-rays as well as the heavily ionizing particles. The general electrical characteristics of all the different geometrical types are similar. The counting rate is dependent on the applied voltage in the operating range, but this does not prove to be a serious disadvantage if an efficient potential stabilizer is used. The counters operate satisfactorily at voltages between 500 and 1500 when filled with dry air at pressures between 0.5 and 3.0 cm of Hg. The performance is independent of the material of which the electrodes are made. The removal of geometrical re-

strictions for discharge counters means that it is no longer necessary to design an experiment to suit the conventional tubular Geiger-Müller geometry, but the discharge counters can be given a geometry which is optimum for the particular detection problem at hand.

[1] Brown and Evans, Phys. Rev. **53**, 914(A) (1938).
[2] Neher and Harper, Rev. Sci. Inst. **7**, 441 (1936).

118. Improvements in the Counting Rate Meter. ROBLEY D. EVANS AND ROBERT L. ALDER, *Massachusetts Institute of Technology.*—The counting rate meter as originally described[1] had the defect of nonlinearity which was particularly severe at high counting rates. Without modifying the general principles involved, several changes have been made in the original circuit which make it adaptable to high speed counting. These changes involve (a) use of the Neher-Pickering[2] circuit adapted for a reasonable drain on the neon stabilized high voltage supply by the use of 10^7-ohm resistors in the grid and cathode circuits, (b) the multi-vibrator stage is inverted to receive a positive pulse, and its time constant greatly reduced by lower values of its resistors and capacitors, and (c) the tank circuit pulses, which now are of much shorter duration, retain their former high microcoulomb values through the use of an output tube having a high mutual conductance, such as the 6L6 or 1852.

[1] Gingrich, Evans and Edgerton, Rev. Sci. Inst. **7**, 450–456 (1936).
[2] H. V. Neher and W. H. Pickering, Phys. Rev. **53**, 316 (1938).

119. A Simple Circuit of Short Resolving Time for Coincidences. LOUIS A. TURNER, *Princeton University.*—The wires of two self-extinguishing alcohol-filled Geiger-Müller counters[1] are connected in parallel to the grid of a 57 tube and to the grid bias through a resistance (30,000 ohms) and a radiofrequency choke (0.085 *H*). The extremely rapid onset of current in one of the counters produces a damped oscillation of high frequency in the grid circuit. Coincident discharge of both counters produces an oscillation of double amplitude when the counter voltages have been adjusted so that both give impulses of the same size. The grid may be biased so far past cut-off that no current whatsoever flows in the tube unless the double pulse of a coincidence occurs. The output of this tube may be applied directly to a thyratron or further amplified. With counters having cylinders six cm long and two cm in diameter and applied voltages 150 volts above threshold, a grid bias three volts larger than that for cut-off is necessary for making the tube insensitive to single counts, a bias of 4.5 volts greater than cut-off is suitable for recording coincidences. The resolving time for accidental coincidences is determined by the frequency of the oscillation. With the above choke and resistance it is found to be 3×10^{-6} sec. The same principle may be used in connection with ordinary counters and the Neher-Harper circuit for improving the resolving time for coincidences. A closely similar method was developed independently and applied in this manner by Maze.[2]

[1] A. Trost, Zeits. f. Physik **105**, 399 (1937).
[2] R. Maze, J. de phys. et rad. **9**, 162 (1938).

120. A Camera for the Study of Nuclear Scattering. T. R. WILKINS AND G. KUERTI, *University of Rochester.*—We have utilized the fact that suitable photographic emulsions record the tracks of alpha-rays, protons and deuterons and designed a camera to study the scattering of sharply limited beams of these particles brought out from a cyclotron to a position where the magnetic field is negligible. The camera is about 30 cm in diameter and four cm in depth. Foils of various elements placed at the center scatter the particles through small holes in a circular ring. Plates are placed at five-degree intervals around the circumference so that the particles enter these plates at a glancing angle (4°) and give flat tracks distributed over a very restricted area (1×0.1 cm). The narrowness of these patches makes it possible to view the complete patch-width when the plate is examined by a microscope with a 16-mm objective. Shutters make it possible to close off any of the apertures if exposures of differing times are desired or if different scattering foils are used with some of the plates. The parallelism and characteristic lengths of the tracks serve to eliminate all strays and make energy distribution studies possible while the differential grain spacing of protons and deuterons[1] may prove of considerable importance in the study of deuteron scattering. The new emulsions developed for these studies will shortly be generally available.

[1] T. R. Wilkins and H. J. St. Helens, Phys. Rev. **54**, 783 (1938).

121. The Ionization Produced in Thimble Chambers by Fast Neutrons. PAUL C. AEBERSOLD* AND GLADYS A. ANSLOW,† *University of California.*—Experiments with thimble ionization chambers were conducted using a collimated beam of fast neutrons[1] for which the contribution to the measured ionization due to gamma-rays is relatively small.[2] The effects of varying the wall material, the enclosed gas, the gas pressure, and the collecting field were observed. The Bragg-Gray relationship between the ionization in a gas cavity inside a medium to the energy absorbed in the medium was tested. Chambers small enough and with gas pressure low enough to allow C, N, or O recoils from the walls to lose only a fraction of their energy in crossing the chamber, as demanded by the relationship, were not feasible. However, the conditions demanded for the validity of the relationship hold approximately for protons ejected from hydrogenous walls, and when the ionization due to recoil protons alone is determined by comparison of hydrogenous and carbon-walled chambers satisfactory agreement with the relationship is obtained. It is noted that the ratio of the stopping power of hydrogenous material to that for air is greater for protons than for electrons and that this ratio increases with decrease of particle velocity. The consequences of this in the use of thimble chambers for measuring the relative ionization in biological material with neutrons and x-rays is considered.

* Finney-Howell Research Foundation Fellow.
† Research participated in while on sabbatical leave from Smith College.
[1] P. C. Aebersold, Phys. Rev. **55**, 596 (1939).
[2] P. C. Aebersold and G. A. Anslow, Bulletin of American Physical Society **14**, No. 1, 14 (1939).

122. A Device for Compounding Sine Functions. LOUIS R. MAXWELL, *Bureau of Chemistry and Soils.*—A device has been constructed for evaluating the series $\Sigma A_n \sin a_n x$ where the coefficients A_n and a_n are freely adjustable. For each term there is constructed one compounding element composed of three coils; a long solenoid (primary, 60-cycle a.c.) within which are mounted two short secondary coils, one a rotor (order of 1/5 r.p.m.) and the other a stator. Current in the primary is made proportional to A_n while the slow angular speed of the rotor is governed by a_n. The mutual inductance between the primary and rotor varies as the sine of the angle $a_n x$ of rotation. The voltages (60-cycle) induced in the rotor and stator are in phase during the first half-turn of the rotor and 180° out of phase during the second half-revolution giving a resultant peak voltage whose variations are proportional to $A_n \sin a_n x$. Variations of the resultant r.m.s. voltage from all of the elements about a constant value are proportional to the sum of the series. A record of the sum is then made on photographic paper by means of a vacuum tube voltmeter circuit. Tests have been made on a two-element system by adding $\sin x + \sin 2x$; also $\sin x + 2 \sin 2x$ for x values up to 30 radians. Positions of the maxima and minima obtained agree with the calculated values within less than 0.09 radian and the complete curves were also closely reproduced. $\sin x + 1.77 \sin 1.45x$ was satisfactorily traced by the compounder. Extension to many terms simply involves a repetition of the present units with sets of interchangeable gears. The compounder can be used in connection with structure determinations of gas molecules by electron diffraction, and it has been found to work satisfactorily for CO_2.

123. An Electron Lens Type of β-Ray Spectrometer. C. WITCHER, E. HAGGSTROM, J. S. O'CONOR AND J. R. DUNNING, *Columbia University.*—A β-ray spectrometer has been constructed utilizing the lens action of a long solenoid, 152 cm long, 25 cm diameter. The radioactive source and the G-M counter for detecting the β-rays are located 86 cm apart on the axis of the solenoid. A baffle system consisting of aluminum disks and rings is interposed between source and counter to restrict within specifiable limits the dimensions of the helical paths which electrons may traverse in passing from source to counter. The magnetic field of the solenoid is homogeneous within approximately 1.0 percent over the region between source and counter, and its maximum value under present operating conditions is 1200 gauss, corresponding to a β-ray energy of 5.0 Mev. There appear to be four major advantages inherent in a spectrometer of this form. (1) The relatively great distance between source and counter greatly reduces background from gamma-rays. (2) The total thickness of absorbing material in the electron path consists solely of the counter window, which may be made as thin as one or two microns. (3) Theory indicates, and preliminary experimental results verify, that a better combination of intensity and resolution can be obtained with this type of instrument than with the conventional type. (4) Sources in the form of disks 2.0 cm in diameter may be used.

124. An Electron Spectrograph. W. T. HARRIS, *Princeton University.*—A magnetic spectrograph embodying some new features has been constructed. The magnet, constructed of Armco iron and Alnico, maintains a permanent field of 4000 oersteds or less in a pole gap 15×15×2 cm. For studying a spectrum the magnetization can be changed in large steps by energizing the windings for a few seconds, and in fine steps by using iron shunts. Two deflection chambers have been constructed for use interchangeably. One is of the 180° photographic type to be used for survey work. The other is of the 90° type for use with counters. This latter type has some advantages over the 180° type. For the same $H\rho$ only half as large a magnet is required, the source and detector are separated farther, and are both well away from the magnet where space is plentiful. The solid angle of the beam is 2×10^{-3} steradian. The resolution (dispersion/spread) is $(2/\alpha^2)(\Delta H\rho/H\rho)=0.13$, where α, half the angle of divergence of the beam from the source, equals 10° and $\Delta H\rho/H\rho=0.019$, as calculated for the slit width of 0.6 cm and ρ of 11 cm used. The same result would be obtained with a 180° spectrograph of like aperture.[1]

[1] W. E. Stephens, Phys. Rev. **45**, 55 (1934).

125. Beta-Spectra Associated with Iodine. GERALD F. TAPE, *University of Michigan.*—Continuing the detailed investigation of the radioactive isotopes of tellurium and iodine, the momentum distributions of beta particles emitted from several radioactive iodine isotopes have been studied. Activated samples mounted on filter paper were placed inside of a large hydrogen-filled cloud chamber. The inspection upper limit of I^{128} (25 minutes) has been checked at 2.2 Mev. This value is in agreement with the findings of other investigators.[1] The iodine isotope associated with the 8-day half-life[2] was chemically separated from a deuteron-activated Te sample. By inspection the upper limit was found to be 0.74 Mev. This is to be compared with a value of 0.80 Mev by extrapolation on a K-U plot. I^{126} produced by $(n,2n)$ reaction from I^{127} has been chemically concentrated for cloud-chamber work. The upper limit of this spectrum was observed at 1.17 Mev.

[1] Alichanian, Alichanow, Dzelepow, Physik. Zeits. Sowjetunion **10**, 78 (1936); Bacon Griesewood, van der Merwe, Phys. Rev. **54**, 315 (1938).
[2] Tape and Cork, Phys. Rev. **53**, 676 (1938); Livingood and Seaborg, Phys. Rev. **53**, 1015 (1938).

126. Gamma-Rays from Aluminum Due to Proton Bombardment. G. J. PLAIN, R. G. HERB AND R. E. WARREN, *University of Wisconsin.*—A study has been made of the excitation of gamma-rays from thin films of aluminum bombarded by protons in the energy region 0.45 Mev to 2.59 Mev. Practically all of the radiation in the lower half of the energy region is due to resonance excitation. The resonance peaks are sharply defined and are comparable in half-width to those observed from fluorine. In the upper part of the energy region the resonances are too closely spaced for good resolution, but peaks are still distinct up to the maximum proton energy. The average spacing between resonance peaks is considerably less than that observed from fluorine. More than thirty distinct peaks have been established.

127. The Beta- and Gamma-Ray Spectra of Cu^{64} and Eu^{152}. A. W. TYLER, *University of Michigan. (Introduced by J. L. Lawson.)*—The radiations emitted from Cu and Eu have been studied with a magnetic spectrometer having a resolving power of about two percent. Cu^{64} has been reported[1] to decay with a half-life of 12.8 hours by either positron or electron emission. This has been verified. The observed upper limits of the positron and electron spectra are 0.659 ± 0.003 and 0.578 ± 0.003 Mev, respectively. The positron spectrum having the higher upper limit is in definite disagreement with the previously published values.[1] There is no definite indication of an associated gamma-ray other than the positron annihilation radiation. Eu^{152} gives rise to a continuous electron spectrum with an upper limit of $1.88^5\pm0.015$ Mev and a half-life of 9.2 hours. There are also several gamma-rays present in addition to those previously reported.[2] One of them is internally converted. The K and L peaks are easily resolvable above the continuous electron spectrum and indicate a gamma-ray energy of 122 ± 1 kev. A possible energy level diagram of Gd^{152} is proposed.

[1] S. N. Van Voorhis, Phys. Rev. **50**, 895 (1936).
[2] J. R. Richardson, Phys. Rev. **53**, 942 (1938).

128. The Beta-Ray Spectra of Radioactive Phosphorus, Sodium and Cobalt. J. L. LAWSON, *University of Michigan.*—The momentum distributions of emitted particles associated with a few artificially induced radioactivities have been obtained by means of a magnetic spectrometer of high resolution. These distributions have been corrected for window absorption, counter efficiency, source decay, and the spectrometer resolution. The effect of back-scattering from various source mountings is demonstrated. The beta-ray spectra of radioactive phosphorus and sodium obtained with sources weighing approximately three mg per square cm are shown. The observed endpoints are $7210H\rho$ and $6150H\rho$, respectively. The positron spectrum of radioactive cobalt (18 hours half-life) has also been obtained, indicating an upper limit of $6500H\rho$. An example of an internally converted gamma-ray occurring in indium demonstrates the resolution of the spectrometer. The K and L shell conversion electrons occur in well-separated groups.

129. The Gamma-Radiation from Radioactive Cobalt. B. R. CURTIS, *University of Michigan.*—The energy of the gamma-radiation produced by radioactive cobalt obtained by bombarding iron with deuterons[1] has been investigated using a large hydrogen-filled cloud chamber. The momentum distribution of the electron ejected from a carbon radiator of 35 mg/cm² thickness shows that in addition to the annihilation radiation due to the positive electrons from the 18-hour activity of cobalt, there is a strong line of 0.8 Mev and evidence of a weaker line of 1.2 Mev, the relative observed intensities of the three lines being 1, 0.5 and 0.1, respectively. Preliminary results from the momentum distribution of electrons emitted from a lead radiator of 20 mg/cm² thickness indicate that at least two additional lines are present of 0.1×4 and 0.22 Mev energy, with equal intensities of 0.1 and 0.1.

[1] B. T. Darling, B. R. Curtis and J. M. Cork, Phys. Rev. **51**, 1010(A) (1937).

130. Radioactivities Induced in Molybdenum by Fast Protons. DOUGLAS EWING, TOM PERRY* AND RALPH MCCREARY, *The University of Rochester.*—Radioactivities of half-lives 53 ± 3 minutes and 110 ± 10 hours are obtained when molybdenum is bombarded with 6.5-Mev protons. They give rise to β-particles whose maximum energies are 2.3 and 0.6 Mev, respectively. Both activities are accompanied by γ-rays. The 110-hour activity is found to follow the chemistry of element 43. Excitation functions for the two reactions will be shown.

* Now at Bennington College, Bennington, Vermont.

131. Radioactivity in Cadmium and Indium. J. M. CORK AND J. L. LAWSON, *University of Michigan.*—When cadmium is bombarded with 7.5-Mev deuterons several radioactive isotopes of cadmium and indium are formed. The inter-relation of these isotopes and the energies of their radiations have been studied by means of an ionization chamber, a cloud chamber, and a magnetic beta-ray spectrometer of high resolution. There now appear to be four radioactive cadmium isotopes and at least eight indium activities. Two of the periods in indium grow in chain reactions from the cadmium. There is evidence that both stable indium isotopes of mass 113 and 115 may exist in excited states. Gamma-rays associated with these activities are largely internally converted and are beautifully resolved on the beta spectrometer. The energies of certain of the beta-spectra and at least five gamma-lines have been precisely determined.

132. The Heat of Dissociation of Carbon Monoxide. HOMER D. HAGSTRUM AND JOHN T. TATE, *University of Minnesota.*—A mass spectrometric study of the C^+ and O^- ions produced in CO by electron impact indicates, in complete agreement with Lozier,[1] that the following processes occur:

$$CO \rightarrow C+O^- \quad \text{at 9.5 volts,}$$
$$CO \rightarrow C^+ + O^- \quad \text{at 21 volts,}$$
$$CO \rightarrow C^+ + O \quad \text{at 22.8 volts.}$$

As pointed out by Lozier these results in themselves, because of uncertainty about the states of excitation of the products formed, do not discriminate between 9.6 and 11.6 volts as a possible value for D(CO). In the present work the formation of O^+ ions was examined. The absence of C^- ions precludes the process $CO \rightarrow C^- + O^+$. If the process is assumed to be $CO \rightarrow C+O^+$, our measurements indicate that after deducting the kinetic energy of the products an upper limit for the energy involved is 23.55 volts. This leads to the conclusion that D(CO) is less than 10 volts and therefore, in connection with the results noted above, fixes the heat of dissociation of CO at 9.6 volts. This value is in reasonable agreement with thermochemical data and fixes the heat of sublimation of carbon at 5.9 volts (136 cal.). This result also indicates that the O^- ion formed in the above processes has an excitation energy of about 2.2 volts.

[1] W. W. Lozier, Phys. Rev. **46**, 268 (1934).

133. Separation of Gas (Isotope) Mixtures by Irreversible Processes. L. ONSAGER, *Yale University.*—The potentialities and limitations of processes like diffusion and

thermal diffusion as means of separating gas mixtures (isotopes) are brought out by the observation that the physical laws which govern such a process impose an upper bound for its *entropy efficiency*, just like the small ratio of reversible to irreversible heat limits the efficiency of power production by thermopiles. In separating two gases by differential diffusion, the ratio of the decrease in the entropy of mixing, $S_m = R(-N_1 \log c_1 - N_2 \log c_2)$, to the entropy of expansion $\Delta(R \log V)$ will be at most $(c_1c_2/4) \times (\Delta D/D)^2$, proportional to the square of the relative difference between the coefficients of diffusion. In the case of thermal diffusion, the decrease of S_m is to be compared to the increase $S_\lambda = (Q/T_1) - (Q/T_2)$ due to heat conduction, and $-\Delta S_m/S_\lambda \leqq \alpha^2(c_1c_2/4)(PD/\lambda T)$, where P = pressure, λ = heat conductance and $\alpha = d \log (c_1/c_2)/d \log T$. The ratio $(PD/\lambda T) = (R/C_v)(D/D_\lambda)$ varies but little for simple molecules; it never exceeds $\frac{1}{4}$. While the fundamental efficiency of this method is low (10^{-4} to 10^{-3}), it can be approached remarkably well by simple means (50–70 percent times Carnot factor). To this end, an even compromise must be struck between quality and quantity of the product, and the low concentration of the desired component in the first stages of extraction must be compensated by greater numbers of units in parallel. Since the efficiency depends on the concentration, the necessary power is not measured by the entropy, but instead by the change of the function $\Sigma((N_1 - N_2) \log (c_1/c_2))$.

134. Theory of Isotope Separation by Thermal Diffusion. W. H. FURRY AND R. CLARK JONES, *Harvard University*, AND L. ONSAGER, *Yale University*.—A description is obtained for the convection and diffusion processes occurring in a continuous flow apparatus such as that of Clusius and Dickel,[1] and Brewer and Bramley,[2] which consists of two concentric tubes, the inner one heated and the outer one cooled. An expression is found for the net transport of a single isotope which is valid for arbitrary macroscopic properties of the gas, and can readily be put in finite terms if viscosity and heat conductivity are proportional to temperature, which is usually a good approximation. The positive term in the transport is proportional to the fractional difference of molecular masses and to p^2a^2, where p is pressure and a is difference in radii of the tubes. This term essentially determines the speed of production at any specified concentration. The separation factor obtainable with a given length depends on the ratio of this positive term to the sum of the negative, or remixing, terms. One of these is proportional to p^4a^7, and the other is independent of p and proportional to a. A sizable temperature difference is necessary, but application of extreme temperatures would not be advantageous. Calculated separations and speeds indicate that the method should be a useful one.

[1] K. Clusius and Dickel, Naturwiss. **26**, 546 (1938).
[2] A. K. Brewer and A. Bramley, Phys. Rev. **55**, 590(A) (1939).

135. The Diffusion of Hydrogen Through Oxygen Free Copper. W. R. HAM, *The Pennsylvania State College*.—A precise determination has been made of the diffusion of hydrogen through copper that is spectroscopically oxygen free. The range of temperature is from 450°C to 1050°C. The copper appears perfectly homogeneous over the entire range, the equation followed being $\text{Rate} = Ap^yT^ze^{-b/T}$, where p is pressure, T absolute temperature, and A and b constant characteristics of copper. The value of z is about $+0.5 \pm 0.2$ as was found in pure nickel. The principal point to be noted is that $y = 0.50 \pm 0.01$ even at 450°C. It is well known that copper containing any appreciable amount of oxygen shows isotherms in this region with a value of y as large as 0.8 in some instances when $\log R$ is plotted against $\log p$. It now appears that the removal of all traces of oxygen from copper has the same effect on low temperature hydrogen diffusion isotherms as the removal of all carbon from iron and nickel, *viz.*, these isotherms become perfectly normal, the rate varying exactly as the square root of the pressure. A chemical theory applicable to the variation of the slope of hydrogen diffusion isotherms in contaminated iron, nickel and copper will be found in another paper by Ham and Simons.

136. The Diffusion of Gases Through Metals from a Chemical Point of View. J. H. SIMONS AND W. R. HAM, *The Pennsylvania State College*.—On the basis of chemical equilibria existing in the interior of the metal and without reference to the surface conditions the usual laws of diffusion are derived. Fick's linear diffusion law is shown to be a consequence of the hypothesis. The theory is then applied to the diffusion of a diatomic gas through a metal in the case where the rate of diffusion at constant temperature equals KP^y and y is greater than $\frac{1}{4}$. Further consequences of the theory are discussed and it is applied to additional examples.

137. Repulsive Forces in Van der Waals Adsorption. W. G. POLLARD, *University of Tennessee*.—The Hamiltonian for an atom with one valence electron in the surface field of a metal is averaged with a determinantal wave function completely antisymmetric in the positional and spin coordinates of the outer electron of the atom and of all the electrons in the conduction band of the metal. The resulting expression includes the usual Coulomb, exchange and overlap terms common to molecular binding. The exchange and overlap terms appear as summations over each electron in the metal with the same spin as that in the visiting atom. The terms are evaluated approximately for a simple free electron model of the conduction band by replacing these summations in the usual way by integration consistent with the exclusion principle. The exchange terms are repulsive and depend on a parameter which is proportional to the ratio of the radius of the "s sphere" in the solid to the mean radius of the electron cloud in the visiting atom. The results are applied to H_2 and He by using the classical image force for the attractive Coulomb terms and the above terms for the exchange repulsion.

138. Van der Waals Forces in Helium. HENRY MARGENAU, *Yale University*.—Different methods for computing the dispersion forces in helium give widely discordant results. In view of current interest in the low temperature properties of helium, a fairly accurate knowledge of these

forces is desirable. The most important parameter in the force law $V=Ae^{-\lambda r}-c_1r^{-6}-c_2r^{-8}$ is c_1. Previous calculations have led to values for c_1 ranging from 1.20 to 1.60×10^{-60} erg cm^6. In the present investigation it has been calculated with the use of Wheeler's[1] absorption f values, the result being $c_1=1.49\times10^{-60}$. This happens to be in exact agreement with the formula of Slater and Kirkwood. It turns out, however, that the same f values give the result $\alpha=2.11\times10^{-25}$ cm^3 for the static polarizability, whereas the best empirical value appears to be 2.02×10^{-25} cm^3. To obtain a correct result for α, Wheeler's f values were corrected by suitably changing the relative weights of the discrete and the continuous spectrum, leaving the sum rule valid and assuming the same trend of the f's in the continuous spectrum. Recalculation with these adjusted f values yields $c_1=1.39\times10^{-60}$. The coefficient c_2 may be taken from the work of several investigators, all of whom agree sufficiently well. A and λ have been calculated by Slater. We conclude that the best expression for V is, in the face of present evidence,

$$V=\{770\,e^{-4.60\,R}-1.39\,R^{-6}-3.0\,R^{-8}\}10^{-12}\text{ erg},$$

if R is measured in A.

[1] J. E. Wheeler, Phys. Rev. **43**, 258 (1933).

139. Electrolytic "Polishing" of Tungsten. J. M. Hughes and E. A. Coomes, *University of Notre Dame.*—Electrolytic polishing as described by Vernon and Stroud[1] has been carried out for tungsten, as a possible method for the preparation of filaments for electron emission studies. Sodium hydroxide was used as electrolyte. The process was studied for 50-mil rods, and 0.7-cm×0.7-cm bars as well as three-mil wires, and over a range of concentrations from about 0.02 to 2.0 normal. The form of the current density *versus* voltage curves was essentially the same as that previously reported, and appeared to be independent of the geometry of the specimen, the concentration of solution, and the spacing of the electrodes. All of the curves exhibit a steep initial rise and a fairly sharp maximum, followed by a plateau. Polishing takes place at the constant current density represented by the plateau; on other parts of the curve etching is observed. For specimens in which the surface imperfections are small compared to the total area there is a definite current density at a given concentration, regardless of the shape or size of the specimen. In the case of fine wires apparently a much higher current density is necessary. The time required for polishing decreases with current density, and bears an approximate inverse proportion to it. A 50-mil tungsten rod polishes in 30 minutes at a current density of 32 ma per cm^2 (0.25 normal solution), and in 20 minutes at a current density of 52 ma per cm^2 (0.5 normal solution). The polishing time depends directly on the area of surface exposed to the electrolyte, and is very short for fine wires.

[1] W. H. J. Vernon and E. G. Stroud, Nature **142**, 477 (1938).

140. The Equation of State of the Frozen Rare Gases. Brother Gabriel Kane, *Catholic University of America.* (*Introduced by K. F. Herzfeld.*)—The constants in the expression for the potential energy between two atoms of the rare gases, neon and krypton, were calculated from the lattice distance and the heat of sublimation. The form of energy function used was $-Ar^{-6}+AB\exp -r/\rho$. For ρ, the values 0.2091A and 0.345A were taken, the former having been found theoretically by Mayer and Bleick for neon, the latter being the value applicable in alkalihalide crystals according to Born and Mayer. In addition argon was recalculated. The results are:

	$\rho=0.2091$			$\rho=0.345$		
	Neon	Argon	Krypton	Neon	Argon	Krypton
$NA\times10^{28}$	1.486	5.27	8.924	0.844	7.55	12.61
$B\times10^{-65}$	1270	9500	14700	6.9	12.8	15
θ (Calc.)	60.1	105	91.1	52.7	80.5	68
θ (Exp.)	64	80	63	64	80	63

Here θ is the characteristic Debye temperature. With the above data, the equation of state of the crystals was calculated, treating them as completely ordered.

141. Specific Heat, Heat of Sublimation, and Vapor Pressure Constant of Tantalum. D. B. Langmuir and L. Malter, *RCA Manufacturing Co., Inc.*—The specific heat C_p of tantalum between 1650°K and 2800°K was determined by measurements of the ripple in the light output and in the electron emission of a tantalum filament heated with alternating current. Within the limits of experimental error, the specific heat over this range is expressed by $C_p=(0.0264+8.5\times10^{-6}\ T°\text{K})$ cal./gram. The results of these measurements together with existing data for lower temperatures were combined with vapor pressure data[1] to determine the heat of sublimation at absolute zero and the vapor pressure constant from the relation

$$\log P-\frac{5}{2}\log T+\frac{1}{4.573}\int_0^T\frac{dT}{T^2}\int_0^T C_p dT=-\frac{l_0}{4.573T}+i,$$

where l_0 is the heat of sublimation at absolute zero, i is the vapor pressure constant and P the vapor pressure in atmospheres. Between 2200°K and the melting point, P is given by: $\log P=6.978-\frac{39{,}780}{T}$. The values obtained were

$185{,}100\ \frac{\text{cal.}}{\text{mole}}$ for l_0, and 2.46 for i. In the computations a value of 250°K for the Debye temperature was used. This is the mean of values computed from melting point[1] and compressibility data.

[1] D. B. Langmuir and L. Malter, Phys. Rev. April 15, 1939.

142. The Vapor Pressure and Rate of Evaporation of Barium Oxide.* J. P. Blewett, H. A. Liebhafsky and E. F. Hennelly, *General Electric Company.*—The most extensive investigations[1, 2] reported in the literature of the rate of evaporation of barium oxide are in serious disagreement. In these experiments the oxide was allowed to evaporate from an exposed surface into a vacuum, a method which for this particular case may involve large tempera-

ture uncertainties. Consequently the method of Knudsen has been applied; the oxide escapes through a small aperture in the wall of a "blackbody" at a rate so small that the equilibrium vapor pressure is not sensibly disturbed. The final results are in exact agreement with those of Claassen and Veenemans.

* Supplementary Program Paper No. 181 is to be called for after Paper No. 142.
[1] A. Claassen and C. F. Veenemans, Zeits. f. Physik **80**, 342 (1933).
[2] G. Herrmann, Zeits. f. physik. Chemie **35B**, 298 (1937).

143. A Method of Determining Thermal Conductivity Suitable for Solid or Molten Metals. Values for Zinc from −250°C to 720°C. C. C. BIDWELL, *Lehigh University.*—A metal rod or hollow graphite cylinder containing molten metal is packed in silocel contained in an outer iron cylinder. Downward heat flow is established and vertical gradients measured differentially by thermojunctions in quartz tubes together with radial temperature drops across the silocel at all levels. At low temperatures the iron cylinder is surrounded by constant temperature baths, at high temperatures by additional silocel contained in magnesia pipe lagging. The differential junction measurements were obtained by raising one junction progressively while the other was left at the bottom. High temperatures were obtained by a heater winding directly on the specimen or graphite cylinder but insulated electrically. For either low or high temperature arrangements the gradient changes are found to be constant, meaning that radial temperature drops across the silocel are constant from bottom to top. This was checked experimentally. The equation is

$$k_s A dG/dx = K k_s \Delta T.$$

G is the gradient at level x, k_s the thermal conductivity of silocel at the particular temperature, k_s the desired thermal conductivity. Previously published values for solid zinc are verified and extended through the melting point to 730°. The drop in conductivity at the melting point agrees with data of Konno[1] (the only data found in the literature). The values in the liquid state decrease slightly with temperature. Konno's data suggested this but did not extend far enough to prove it.

[1] Konno, Phil. Mag. **40**, 542 (1920).

144. On Thermal Dependence of Elasticity in Solids. LÉON BRILLOUIN, *Collège de France, Paris, France.*—A rigorous analysis of thermal agitation[1] in a strained solid body is necessary to give correct information on the whole thermodynamics of solids and especially on the influence of temperature on elasticity coefficients. The general results are the following: (1) The microscopic elasticity coefficients which rule the propagation of hypersonic waves (thermal agitation) are given by the derivatives of the elastic potential energy and will be affected only in an indirect way by the thermal expansion. They should accordingly show a slow decrease with increasing temperature. (2) The macroscopic elasticity coefficients as measured in the propagation of acoustical or suprasonic waves are to be derived from the free energy instead of from the purely potential energy. These coefficients are directly influenced by thermal agitation. It is rather difficult to predict the variation of the λ-coefficient but the rigidity coefficient μ should show a very peculiar decrease with increasing temperature. This decrease, while slow at low temperatures, should become faster and faster as the temperature increases. For room temperature and for solids not too near their melting points the decrease is of the order of 50 to 100 times RT/V. The rigidity should decrease very rapidly and fall to zero at the melting point. However, this is true only for the macroscopic rigidity, whereas the microscopic rigidity would be but little affected. Thus the specific heat should remain nearly 3 R as for solids. There is good experimental evidence for the correctness of these predictions.

[1] L. Brillouin, Phys. Rev. **54**, 916 (1938).

145. The Specific Heat of Monatomic Liquids. W. J. ARCHIBALD,* *Yale University.*—If one assumes that the law of force between two spherically symmetrical molecules is known, then it is possible to derive an expression for the translational part of the partition function of such a molecule in the liquid state. For the case of a monatomic liquid, this partition function yields immediately all the equilibrium properties of the liquid. The law of force between two argon atoms as determined from experiments on the gaseous and crystalline state[1] enables one to calculate the specific heat of argon by the above proceedure. The computed values agree satisfactorily with the experimental values (allowance being made for the uncertainties in the law of force used) except near the melting point where the measured specific heat is larger than that given by the present theory. This discrepancy may be due to the neglect of the internal energy due to disorder which exists in this region.[2]

* Sterling Fellow.
[1] R. A. Buckingham, Proc. Roy. Soc. **168**, 264 (1938).
[2] J. E. Lennard-Jones and A. F. Devonshire, Proc. Roy. Soc. **169**, 317 (1939).

146. Determination of Quenching Rates in an Aluminum Alloy of the Duralumin Type.[1] HUGH L. LOGAN, *National Bureau of Standards.*—The quenching rate used in the heat treatment of an aluminum alloy of the duralumin type has a very important influence on some of the characteristics of the finished material, particularly its corrodibility. Such rates have been calculated from photographically recorded time-temperature cooling curves obtained by means of an Einthoven string galvanometer connected in series with a thermocouple that was peened into the sample material.[2] A commercial aluminum alloy having the nominal composition Cu 4.4 percent, Mg 1.5 percent, Mn 0.5 percent, was used in this work. Samples of this sheet material were quenched from the solution temperature, 493°C±5°C, into water at temperatures ranging from 22°C to 100°C. Susceptibility to intergranular corrosion was determined, after age-hardening at room temperature, by metallographic examination of samples exposed to accelerated corrosion in an oxidizing sodium chloride solution. Samples quenched through the range 485°C to 125°C at a rate in excess of 1200°C/sec. were immune to intergranular corrosion, whereas comparison samples quenched at an appreciably slower rate were severely attacked. The time required to transfer the sample under treatment from the heat-treating

furnace to the quenching bath must be sufficiently short so that the temperature of the sample does not fall below 415°C before the sample enters the bath if the material is to be immune to intergranular corrosion.

[1] This report is to be published in the *National Bureau of Standards Journal of Research*.
[2] H. J. French and O. Z. Klopsch, Trans. Am. Soc. Steel Treating 6, 251 (1924).

147. The Momentum of Electrons in a Metal Crystal. W. V. HOUSTON, *California Institute of Technology*.—The interpretation of Peierls' conservation theorem in the theory of electrons in metals has been obscured by the fact that the electron wave functions ordinarily used do not represent precise values of the momentum, and the ion lattice is usually treated as fixed. This has made it difficult to recognize the theorem as that of the conservation of momentum. This becomes easier when it is realized that the theorem imposes no restrictions whatever on the distribution of momentum over the possible values represented in an electron function. When the Hamiltonian function for the whole system is written down, a number of other conservation theorems can be established, and it becomes evident that Peierls' "umklapprozesse" represent the transfer of momentum to the lattice from a single electron without the excitation of a vibration. It also becomes evident that such processes can take place involving a large number of electrons. On this account no restrictions are imposed on the form of the electron energy as a function of wave-number because of the observed resistance at low temperatures.

148. The Effect of High Pressure upon the Order-Disorder Transformation in Cu-Zn and Cu-Au Alloys. THOMAS C. WILSON, *Yale University*.—Since the change of entropy with pressure is equal to the negative of the change of volume with temperature, a definite prediction may be made of the effect of pressure upon the order-disorder transformation. By using electrical resistance as an index of disorder, these predictions have been examined over a temperature range of 40°C to 430°C and over a pressure range of 0 to 10,000 kg/cm². Two copper-zinc and two copper-gold alloys (75 and 50 atomic percent copper) were used. In all cases, the resistance decreased more rapidly with pressure as the temperature was raised. The definite but relatively small change observed in beta brass is to be expected, but the similar result in alpha brass unexpectedly suggests an ordered phase stable only at high pressures and temperatures. Similar abnormalities in the copper-gold alloys were noticeable at low temperatures and became very large as the transition point was approached, confirming prediction. Moreover, in the case of both these alloys the transition point was raised by approximately 15°C at maximum pressure. Clapeyron's equation when applied to the Cu_3Au alloy gives a value for the volume change consistent with x-ray measurements of Jones and Sykes,[1] using a value of 1.3 cal./g for the latent heat. In Cu-Au the same simple treatment leads to an anomalous result.

[1] Jones and Sykes, Proc. Roy. Soc. June (1938).

149. The Dependence of Internal Friction in Metals on Grain Size. R. H. RANDALL, F. C. ROSE AND C. ZENER, *College of the City of New York*.—Experiments have been performed to test the theory previously developed* for that part of the internal friction of polycrystalline metals which arises from the flow of heat back and forth between adjacent crystals. Measurements were made upon annealed strips of brass and zinc, with a range of grain size of 0.0006 to 0.4 cm. These specimens were kindly prepared by the American Brass Company and the New Jersey Zinc Company. The strips were set into longitudinal vibration by means of an electromagnetic driver of variable frequency. A symmetrical pickup, with amplifier, was used to measure the response. The frequency of measurement was varied from the first to the sixth harmonic (6000 to 36000~). The internal friction was found to be a maximum for those combinations of grain size and frequency where the vibration is half isothermal and half adiabatic. The experiments indicate that at room temperatures that part of internal friction in annealed, non-ferrous, polycrystalline metals which arises from microscopic thermal currents is of a larger order of magnitude than that due to all other causes, barring possible macroscopic thermal currents.

* Phys. Rev. **53**, 97 (1938).

150. The Anisotropy of Electric Conductivity of Metals. E. M. BARODY, *Cornell University*. (*Introduced by H. A. Bethe.*)—A theoretical investigation of the contributions of various factors to the observed anisotropy in the conductivity of the divalent, hexagonal close-packed metals has been begun. The source of this anisotropy is to be sought in the dependence of (1) the electron energy and (2) the scattering probability on the direction of the electron wave vector. The second effect will be due partly to the anisotropy of the electron wave functions and partly to that of the lattice waves. If we assume that the directional dependence is due to the lattice waves only, the conductivity at low temperatures should be largest in the direction of smallest velocity of sound. This is the opposite of Houston's theory[1] of 1928. For cadmium and zinc the result is of the order of magnitude of the observed effect and in the opposite direction. For magnesium it follows from the values of the elastic constants that the lattice waves are themselves isotropic. We therefore believe that the anisotropy of the electron wave functions and energy is important for the effect and a study of its influence has been begun.

[1] W. V. Houston, Zeits. f. Physik **48**, 449 (1928).

151. Excited Electronic States and Compressibility of Metallic Beryllium. A. G. HILL AND CONYERS HERRING,* *Massachusetts Institute of Technology*.—Results of a calculation of the binding energy of metallic beryllium have already been reported.[1] Now calculations of the energies of electronic states near the top of the Fermi distribution have been made in sufficient detail to give an approximate picture of the form of the Fermi surface and the variation of energy E with wave vector k. It is noteworthy that the wave functions of the upper of the two filled energy bands are rather less like plane waves than those of the lower. Calculations have been made of the lattice constant and

compressibility, but these calculations cannot be made as precise as for monovalent metals, for two reasons: (a) the shape of the Fermi surface is irregular and varies considerably with lattice constant; (b) the deviations from the usually assumed formula $E=\alpha k^2$ are large. The importance of (b) is illustrated by the fact that the compressibility calculated assuming $E=\alpha k^2$ is 4 to 5 times the value 0.80 $\times 10^{-12}$ cm²/dyne (at room temperature) observed by Bridgman,[2] whereas a calculation using the directly calculated energies of electrons near the top of the Fermi distribution gives a value near the experimental.

* National Research Fellow.
[1] New York Meeting, Feb. 1939, Abstract No. 8.
[2] P. W. Bridgman, Proc. Am. Acad. Arts Sci. **68**, 27 (1933).

152. A Dynamic Measurement of the Elastic, Electric and Piezoelectric Constants of Rochelle Salt. W. P. MASON, *Bell Telephone Laboratories.*—The elastic, electric, and piezoelectric constants of Rochelle salt have been measured at low field strengths by measuring the resonant frequencies and impedance of vibrating crystals. It is shown experimentally that the resonant and anti-resonant frequencies of the crystal are both considerably below the natural mechanical resonant frequency of the crystal in disagreement with the usual derivation of the frequencies of a piezoelectric crystal. By assuming that the piezoelectric stress is proportional to the charge density on the electrodes rather than the potential gradient as usually assumed, theoretical frequencies are obtained which agree with those found experimentally. This theoretical derivation together with the measured frequencies supplies values for the piezoelectric constants. The elastic constants measured dynamically show some differences from those measured statically. A large difference is found for the dynamically measured piezoelectric constants from those statically measured, which may be attributed to the finite relaxation time for the piezoelectric elements.

153. Crystallization and Melting of Rubber at High Pressure. R. B. DOW, *The Pennsylvania State College.*—The normal rate of crystallization of crude rubber at atmospheric pressure is retarded by application of pressure. Bekkedahl has shown previously that the transition from amorphous I to crystalline I is completed normally in about 13 days at 0°C, the volume decrease being 2.2 percent for crude smoked sheets. At a pressure of 8000 kg/cm² a sample of smoked sheet kept at 0° for 14 days showed no detectable change of volume. If the curve for rate of crystallization *vs.* temperature is merely shifted by pressure, an increase of 8000 kg/cm² would lower the rate to a negligible amount at 0°. The inhibition of crystallization is due doubtless to high viscosity since it is known that the pressure coefficient of viscosity increases with molecular weight. The transition of crystalline I to amorphous I, however, appears to be an equilibrium phenomenon. Crystallized smoked sheet melted at 77.5°C at 1270 kg/cm², giving $dT_m/dp = 0.0484$ on the assumption that the normal transition point is 16°C.

154. The Dependency of the Stress-Strain Relationship for Rubber Upon the Rates of Stretching. F. E. DART AND E. GUTH, *University of Notre Dame.*—The influence of the rate of stretching upon the stress-strain curves was investigated for a pure gum compound and for a loaded stock at three different degrees of vulcanization for each. A photographically recording stress-strain apparatus was used. Rates of stretching of 2.5, 5, 10, 20 (standard testing speed), 45, 90, 180 and 1200 inches per minute were used. For all speeds but the last the rate of stretching was uniform. For very high speeds a non-uniformity of the rate of stretching is not as serious as it is for lower speeds. Hysteresis curves for first extensions and for repeated stretchings were taken at the lower speeds. The high speed curves lie, in general, above the low speed ones. For purely elastic deformation such a behavior is to be expected according to thermodynamics. The ratio of the adiabatic to the isothermal modulus which is equal to the ratio of the specific heats at constant force and constant elongation respectively, is larger than one. This relationship is expected to hold only for cases without hysteresis. In all cases there is the possibility of obtaining polytropics instead of adiabatics and isothermals. From truly adiabatic and isothermal stress-strain curves the complete free energy function of stretched rubber can be obtained without any caloric measurements. The influence of the rate of stretching upon the stress-strain relationships is, therefore, important not only from the point of view of routine testing, but also for the basic physical properties of rubber.

155. The Dielectric Properties of Dielectrics Dispersed in Water and Anomalous Dispersion in Bound, (Oriented) Water. HUGO FRICKE, *The Biological Laboratory, Cold Spring Harbor, New York.*—Over the last few decades there are found scattered through the literature dielectric observations on various kinds of dispersed systems showing the occurrence of anomalous dispersion in the low radio and audible frequency range. These observations have generally been explained on the basis of either solute ions bound electrostatically at the interphases (Debye-Falkenhagen effect) or—for the case of colloids—revolving dipolar colloidal particles. We have carried out an extensive investigation of this phenomenon which shows its general occurrence in dispersed systems and evidence is given to show that it originates in the multimolecular layer of oriented water molecules at the interphases. This effect becomes less pronounced as we pass into the range of molecular dispersion, but it is still present quite strongly in solutions of the dispersion of proteins and it appears to account essentially for the high polarizability of gelatin at low frequency, to which many investigators have recently drawn attention. The importance of this phenomenon for the dielectric properties of many systems of wide interest such as soil, living cells and hygroscopic electric insulators of the gelatinous or fibrous type is remarked upon.

156. An Experimental Method for Measurement of Shearing Stresses in Turbulent Air Flow. HAROLD K. SKRAMSTAD, *National Bureau of Standards.*—In turbulent air flow, the shearing stress due to velocity fluctuations is given by: $\tau = -\rho\overline{u'v'}$, where τ is the shearing stress, ρ the density of the fluid, u' and v' the fluctuations from the

mean value of the velocity components in the direction of the mean flow and in the direction of the gradient respectively, the bar representing a time average. This shearing stress may be measured by a special type of hot-wire anemometer, consisting of a short, fine wire at about 45° to the direction of the mean velocity mounted on a holder which permits the wire to be placed in various planes with respect to the direction of the velocity gradient. The velocity fluctuation of the air is converted into an alternating current which is amplified and whose mean square value is measured by a thermal type milliammeter. For small fluctuations, the response in the position of maximum reading may be regarded as proportional to $Au'+Bv'$, and in position of minimum reading to $Au'-Bv'$, where A and B are experimentally determined constants of the wire. The difference between the mean square values of these expressions multiplied by $\rho/4AB$ is equal to the shearing stress. The apparatus has been used to measure the distribution of shearing stress in the boundary layer of a flat plate. This work is being done in cooperation and with the financial assistance of the National Advisory Committee for Aeronautics.

157. Refinements in Atmospheric Transmission Measurement for Solar Constant Determination. BRIAN O'BRIEN, *Institute of Optics, University of Rochester.*—The spectral transmission of the atmosphere which enters into determination of the solar constant introduces the chief uncertainty because of variations in transmission during a set of observations. The greatest variations occur in the lower half (by weight) of the atmosphere because of higher dust and water content. An airplane instrument has been developed to measure the intensity of the direct solar beam at two wave-lengths, in the ultraviolet and red, respectively, with relatively high precision. Two barrier layer photo-cells are provided with filter systems transmitting the desired spectral regions. A temperature-controlled housing surrounds both cells and filters. Means are provided for maintaining a constant state of fatigue of the cells. By synchronizing observations with identical measurements from the ground, transmission of that part of the solar radiation path between airplane and ground station can be determined with some precision. By combining this with the measurement of transmission of the total atmosphere by conventional methods from the ground, much of the uncertainty in solar energy determination can be eliminated. Preliminary flight tests have been completed and an observing procedure developed.

158. The Approach to Saturation of Iron and Nickel. A. R. KAUFMANN, *Massachusetts Institute of Technology.* (*Introduced by F. Bitter.*)—A new arrangement for measuring magnetization in high fields has been developed by which all systematic errors are reduced sufficiently to allow a relative accuracy of one part in 50,000 to be obtained. The apparatus consists of a large air-cored solenoid at the center of which are two similar search coils connected in opposition. The specimen in the form of a long, thin rod extends through one of the search coils and entirely through the solenoid. Observations are made by jumping the field from some standard high value to any desired lower field. The ballistic charge from the search coil is counteracted by simultaneously breaking a current through a mutual inductance in the circuit, the degree of compensation being observed with a ballistic galvanometer operating as a flux meter. The results show that the magnetization curve in fields between 600 and 7000 oersted can be accurately represented by an equation of the form: $I=I_s-(a/H)-(b/H^2)+CH$, where I_s is the intrinsic saturation value at room temperature. The coefficients a and b are found to vary greatly with the treatment of the sample but C is relatively constant. The theoretical value for b agrees satisfactorily with experiment but the measured value of C is about 10 times greater than the calculated value. The constant a is purely empirical.

159. Susceptibility Measurements of Cu-Fe Alloys in Fields from 0–40,000 Gauss. F. BITTER AND A. R. KAUFMANN, *Massachusetts Institute of Technology.*—An air core water-cooled solenoid will be described in which fields of the above magnitude can be kept constant to about ±20 gauss for indefinite periods of time. The solenoid has an inside diameter of 1¼" and can dissipate 500 kw. Susceptibility measurements on copper containing 0.003 percent, 0.094 percent, and 0.71 percent of iron have been made at room temperature using the Gouey method. These measurements will be continued at high and low temperatures in order to follow in detail the process of solution and precipitation. In all samples there is a ferromagnetic, and one or more para- or diamagnetic constituents. The results are summarized below. The annealed samples were

	Cold Worked Samples			Annealed Samples		
Total iron content	.003%	.094%	.71%	.003%	.094%	.71%
Saturation moment of ferromagnetic constituent	.0042	.0050	1	.002%	.002	.042
Total para- or diamagnetic-volume susceptibility $\times 10^6$	−.714	.22	?	−.709	.221	3.7

heated to 850°C (which supposedly put all the iron into solution) and were then slowly cooled. The above saturation values indicate, in confirmation of earlier results by Tammann and others, that only a small fraction of the total iron present is ferromagnetic. In general the ferromagnetic constituent is characterized by the following: (a) remanence small compared to the saturation intensity I_s, (b) initial susceptibility$\sim I_s\times 10^{-3}$ and more or less constant in fields up to a few hundred gauss, and (c) saturation not complete until the field reaches 10–20,000 gauss.

160. Ferromagnetic Anisotropy in Nickel-Iron Alloys near Ni_3Fe. E. M. GRABBE AND L. W. MCKEEHAN, *Yale University.*—The effect of heat treatment on the magnetic anisotropy and saturation magnetization in nickel-iron alloys near the composition Ni_3Fe has been investigated.

Oblate spheroids of axial ratios greater than 15 to 1 were prepared from single crystals of alloys containing 65, 70 and 75 percent by weight of nickel. High precision measurements using a pendulum magnetometer showed differences between magnetization curves for different directions even for very small anisotropies. The changes observed can be explained by order-disorder transformations. Specimens cooled rapidly from 720°–750°C had the anisotropy reported by Kleis.[1] Baking at temperatures from 430°–500°C for long periods of time produced an increase in saturation magnetization. The maximum increases in saturation values are greater than those first reported,[2] amounting to 5.8, 4.2 and 3.4 percent respectively for the 75, 70 and 65 percent alloys. A 75 percent specimen having negligible anisotropy when rapidly cooled had anisotropy of the type characteristic of nickel when baked, with $K_1 = -2.30 \cdot 10^4$ erg cm^{-3} and $K_2 = 1.65 \cdot 10^4$ erg cm^{-3}. For lower nickel content [100] is the direction of most difficult magnetization at low fields. Near saturation the [100] curve crosses the [110] and [111] curves and becomes the direction of easiest magnetization. Several other crossovers not reported previously have been observed on curves which are nearly coincident.

[1] J. D. Kleis, Phys. Rev. **50**, 1178–1181 (1936).
[2] L. W. McKeehan and E. M. Grabbe, Phys. Rev. **55**, 505 (1939).

161. The Hall Effect and Change of Resistance in a Magnetic Field. L. Davis and W. V. Houston, *California Institute of Technology.*—Change of resistance in a magnetic field cannot be interpreted in terms of a free electron picture. Since such a change is observed in the alkalis it is of interest to see if it can be understood as a small departure from the free electron situation. A rigorous formulation of this idea can be obtained by expanding the electron energy and the relaxation time as a series of spherical harmonics that have the symmetry of a cubic crystal. This permits the necessary integrals to be carried out to any desired degree of approximation. When only the first two harmonics are retained, the computed change of resistance and Hall effect are close to the observed values. However, contrary to the available observations, the ratio of the transverse to the longitudinal change of resistance shows a minimum value of about four. It seems improbable that this result could be changed in any material way by the inclusion of higher series members, so that if the experimental results are to be taken as reliable, doubt is thrown on the general method of treatment.

162. Investigations of Ferromagnetic Impurities in Metals. F. W. Constant and J. M. Formwalt, *Duke University.*—As previously described, a method has been developed whereby a permanent magnetic moment as small as 10^{-7} per cc may be measured. Practically all the various metals tested by this method showed slight ferromagnetic impurities. To determine whether the impurity was a surface or volume one, the specimens were dissolved away in successive steps in various acids. In many cases the effect was only a surface one, in others partly so, but in the case of copper, brass and silver a linear relationship between magnetic moment and volume was found. With aluminum the volume impurity appeared to be nonmagnetic but could be dissolved out in HCl and deposited on the surface in a ferromagnetic state. Further measurements have also been made on the character of the hysteresis curves for the impurities in copper, brass and silver, on their Curie temperatures and on the effect of annealing. Heat treatment appears to dissolve ferromagnetic impurities into a nonmagnetic state and to render what little is still magnetic much "softer."

163. The Isotopic Constitution of Iron and Chromium. Alfred O. Nier, *University of Minnesota.*—A study of the isotopic constitution of iron and chromium has been made with a mass spectrometer similar to that previously described.[1] Although the apparatus had sufficient sensitivity and resolving power to detect extremely rare isotopes, none was found. In a search for isotopes of chromium it was possible to set the following upper limits for abundances relative to Cr^{52}: Cr^{54}, 1/100,000; Cr^{50}, 1/15,000; Cr^{51} and Cr^{49}, 1/100,000. A trace of calcium present as an impurity prevented a search for Cr^{48}. For iron the following upper limits of abundances relative to Fe^{54} were found: Fe^{59}, 1/30,000; Fe^{58}, 1/7000; Fe^{55}, 1/20,000; Fe^{53} and Fe^{52}, 1/50,000. The relative abundances measured for the known isotopes are given in the tables. The positive ions of iron were formed by bombarding a molecular beam of iron vapor with electrons. In the case of chromium it was found that by merely heating chromium metal in a tantalum furnace to about 1200°C positive ions were emitted.

Stable Isotopes of Chromium

Mass Number	50	52	53	54
Relative Abundance	5.36	100	11.26	2.75

Stable Isotopes of Iron

Mass Number	54	56	57	58
Relative Abundance	6.6	100	2.30	0.31

[1] A. O. Nier, Phys. Rev. **53**, 282 (1938).

164. Some Evidence for the Existence of Higher Hydrates of Gamma and Alpha Ferric Oxide.[4] Lars A. Welo, *Tottenville, Staten Island, New York,* and Oskar Baudisch, *Saratoga Springs Authority, Saratoga Springs, New York.*—On heating ferromagnetic gamma ferric oxide along with water in sealed tubes the susceptibility (concentration of gamma oxide) decreases linearly with time. Depending on the temperature, within the range 40°C to 70°C, the entire curve may consist of one, or two, or even three straight-line segments. The transformations (reactions), being of zero order, must occur by way of transition between intermediates which are considered to be the well-known monohydrates and the higher hydrates, heretofore unobserved, that are needed to complete the analogy between the oxide and oxide hydrate systems of iron and aluminum.[1] All but two of the slopes (rates) so far observed group themselves upon three separate straight lines on plotting their logarithms against temperature. At 41°C the susceptibility decreases to 87 percent of its initial value and then ceases to change. At 56° and 69°C the times to near zero susceptibility are, respectively, 325 and 80 days. In open tubes, at the temperatures of

225° to 250°C necessary for comparable transformation rates, the susceptibility is an exponential, not a linear, function of time.

* These experiments were performed in the Research Laboratory of the Consolidated Gas, Electric Light and Power Company of Baltimore.
[1] F. Haber, Naturwiss. 13, 1007 (1925).

165. Thermionic Constants of Tungsten for Various Crystallographic Directions. MYRON H. NICHOLS, *Massachusetts Institute of Technology.* (*Introduced by W. B. Nottingham.*)—By a suitable heat treatment,[1] a long single tungsten crystal has been grown in a five-mil tungsten wire. One of the face diagonals of the unit cube lay along the axis of the wire. The single crystal wire was mounted so that it could be rotated in front of suitable collimating slits. The variation of emission around the wire was measured and showed perfect cubic crystal symmetry. Richardson and Schottky plots were made for each maximum and minimum found in the polar plot. The data were fitted to the empirical formula $i = AT^2 \exp(-e\varphi_0/kT)$, thus determining A and φ_0. Preliminary calculations gave the following values for A and φ_0:

MILLER INDICES	110	111	112	116	001
φ_0	4.65	4.38	4.66	4.35	4.53
A	15	38	125	56	117

These results show that the values of A and φ_0 obtained from the usual measurements on polycrystalline wire are characteristic of a weighted average of the properties of the various crystal surfaces, and have, therefore, only empirical value indicating that all attempts to relate observed to theoretical values of emission constants have so far no great significance.

[1] R. B. Nelson, M.I.T. Doctor's Thesis.

166. A New Circuit for Accurate Control of Current-Intensity and Time Used in Spot-Welding. W. B. NOTTINGHAM, *Massachusetts Institute of Technology.*—As a result of experience with the use of a spot-welder control designed to give accurate timing of the welder current over the range from zero up to one-half of a sixty-cycle wave,[1] it became evident that accurate control of timing for much longer periods of time than this is needed in order to fabricate the metal parts used in research. Such a circuit has been developed which can be constructed from parts which may be purchased at reasonable cost. The timing control is a unit which operates from the 115-volt a.c. lines and, by means of vacuum tube circuits, it controls the starting of two pool-type mercury arcs connected parallel-inverse so that current is delivered to the welder any arbitrary number of half-cycles from one to sixty. Circuit constants may be chosen so that only even numbers of half-cycles are used if that is desired. The pool-type mercury tubes used control peak currents up to 150 amp. in circuits with a line voltage of 230 volts a.c. or more.

[1] T. S. Gray and W. B. Nottingham, Rev. Sci. Inst. 8, 65 (1937).

167. A Mechanical Model for Electron Motion in a Uniform Magnetic Field. ALBERT ROSE, *RCA Manufacturing Company, Inc.* (*Introduced by B. J. Thompson.*)—A mechanical model in the form of a gyroscope may be used to trace the path of an electron in a uniform magnetic field, acted upon by transverse electric fields. In using the model to find the electron path the following substitutions are employed: the uniform magnetic field vector is replaced by the spin velocity vector of the gyroscope, the electric fields are replaced by magnetic fields which give the same field configuration, the electron is replaced by one pole of a permanent magnet mounted on the axis of the gyroscope. Depending upon the dimensions of the gyroscope, the strength of the permanent magnet, the spin velocity of the gyroscope, and the scale factor used in setting up the mechanical model, the strength of the magnetic field in the model is adjusted to correspond to the strength of the electric field in the actual case. The path described by the magnetic pole then corresponds to the actual path of the electron. Since the error involved in identifying the equations of motion of the gyroscope with those of the electron is of the order of θ^2 where θ is the half-angle of the cone through which the spin axis is allowed to move, the range of observations must be restricted accordingly. By periodically reversing the current through the field magnets, a qualitative picture of the path of the electron in an alternating electric field may be obtained. Some familiar structures for which electron paths may readily be obtained are deflection plates in a uniform magnetic field, a diode in an axial magnetic field and a split-anode magnetron.

168. Limiting Currents in a Ring Discharge. C. G. SMITH, *Raytheon Manufacturing Co., Medford, Massachusetts.*—Currents from 50 to 800 amperes were passed through mercury vapor in a large ring discharge at a frequency of 980 cycles and at pressures between 10^{-3} and 10^{-4} mm. About 5 volts e.m.f. were used. A definite limit to current flow accompanied by very high electronic temperature (up to 250,000°K) was encountered. Current carrying capacity of the gas seems to be in approximate agreement with observations by A. W. Hull on current through constrictions in mercury vapor.[1] Saturation current at about 2×10^{-4}-mm pressure seems to be 4 amp. per sq. cm. At the ultimate currents sharp fluctuations with a frequency of approximately 50,000 per sec. were observed. A permanent type of gaseous clean-up was encountered, and also a temporary type as observed by Kenty.[2] At the high electronic temperatures the two forbidden lines of mercury λ2655.8 and λ2269.8 were observed. Spectra of Hg II, Hg III were brilliant; Hg I was always the brightest. Hg IV was weak. The current limiting factor acts too quickly to be accompanied by changes in pressure. Evidence indicates it is not caused by magnetic fields. The phenomena occurring in a closed ring wherein the usual space charge limitations are ruled out, and electrical pumping phenomena are of no avail, make it apparently a characteristic of the gaseous medium.

[1] A. W. Hull, Electrical Engineering, November 1934.
[2] Carl Kenty, J. App. Phys. 9, 765 (1938).

169. Electron and Potential Distributions Near the Anode of a Mercury Discharge. LLOYD P. SMITH AND PAUL L. HARTMAN, *Cornell University.*—The electron energy distribution and potential in the plasma has been measured by means of probes located on the cathode side of the anode for various arc currents and mercury vapor pressures. At the same time the energy distribution of electrons arriving at the anode was measured by means of a collector behind a small hole in the anode. The combined results of both measurements indicate that on approaching the anode the potential first drops below the plasma potential by an amount V_m and then rises sharply to the anode potential which is considerably higher than the plasma potential. The value of V_m determines the concentration of the slow electrons in the plasma and the arc current according to the relation $i = i_0 \exp V_m e/kT$ where i_0 and T are the random current density and temperature of the plasma electrons. The measurements also indicate that some electrons arriving at the anode have energies well above that corresponding to the potential difference between anode and cathode. The lower the mercury vapor pressure the greater the number of these excess energy electrons.

170. Variation of the Anode Effect with Temperature. PAUL L. COPELAND, *Armour Institute of Technology.*—That the plates of vacuum tubes can acquire surface charges which alter the contact potential relative to a hot filament (called the anode effect) is known.[1] This effect has been studied by means of a diode in which the cathode is a straight tungsten wire and the anode is a nickel spiral, which itself may be maintained at elevated temperatures by the passage of a current through it. The most prominent feature of the results is the rapid decrease of the observed anode effect with anode temperature.

[1] W. B. Nottingham, Phys. Rev. **39**, 183 (1932); and **44**, 311 (1933).

171. The Effect of Wall Charge on the Progressive Breakdown in Long Discharge Tubes. J. R. DIETRICH,* *University of Virginia.*—The charge left on the walls of a long discharge tube after a discharge has occurred had been measured. Also its effect on the speed of negative potential propagation in subsequent impulsive breakdowns[1,2] has been studied. The wall charge was measured with an electrometer and electrostatic pickup over a short section of a 750-cm tube of 5 mm internal diameter. The tube was surrounded by a concentric metal shield of 76 mm diameter. The charge varies with pressure in the tube, applied potential, and the time constant on the discharge circuit considered as a unit. At pressure 0.46 mm (dry air), applied potential 25.6 kv negative, the walls of the tube are left at potentials varying from 300 volts when the output end of the tube is short-circuited to 7700 volts when the output end is insulated. The corresponding variation in the speed of potential propagation is from 18×10^8 to 15×10^8 cm per sec.

* Charles A. Coffin Fellow.
[1] J. R. Dietrich, L. B. Snoddy and J. W. Beams, Phys. Rev. **53**, 923 (1938).
[2] L. B. Snoddy, J. R. Dietrich and J. W. Beams, Phys. Rev. **52**, 739 (1937).

172. Discharges Between a Stationary and a Moving Electrode. L. B. SNODDY AND J. W. BEAMS, *University of Virginia.*—The discharge in air at atmospheric pressure between a moving surface and a stationary rod electrode has been investigated by means of a rotating drum camera and an oscillograph. The rotating disk electrode was supported and driven in a manner previously described.[1] Surface speeds from 1 to 2×10^4 cm/sec. were used. Disks of copper, bronze, Duralumin, Dow metal and steel gave the same general results. Single impulses were applied to the rotating electrode gap from a highly damped series circuit consisting of a 1 mfd condenser, spark gap and resistance. At low currents (1 or 2 amps.) with the rotor either cathode or anode the luminous column is carried around on the rotor surface, the current decreasing during the process. Rotating film photographs show this extension to take place in a fairly continuous manner. The arc finally breaks and reforms approximately under the stationary electrode and is again carried around the rotor. This is repeated several times. The arc extension was found to depend (critically when the rotating electrode was anode) upon the gap width which indicates an effect of air currents. Also it was changed when the arc was formed to the inside surface of a rotating cup electrode. At high currents (30 amp.) the extension of the arc with rotor anode was very much less than with it cathode.

[1] Phys. Rev. **55**, 504 (1939).

173. The Positive Column of the Nitrogen Arc. ALBERT M. STONE, KARL T. COMPTON, AND EDWARD S. LAMAR, *Massachusetts Institute of Technology.*—Extending earlier work of one of us,[1] a theory of the positive column of an atmospheric arc in nitrogen has been developed from considerations of energy balance, and applied to cases where convection can be neglected; i.e. to low current arcs and to arcs in gravity-free space. Justification for applying a power extreme hypothesis as a means of determining the axial temperature is discussed. From the theory a functional relationship between the potential gradient E in volts/centimeter and the current I in amperes is obtained as $E = 65.8/I$, with the axial temperature 6200°K, determined from the hypothesis above. Preliminary computations, neglecting convection, for arcs at 10 and 100 atmospheres are presented, together with a discussion of the applicability of the power extreme hypothesis to these cases. In the 10 atmosphere case, tolerable agreement with the experimental value of power input/cm and axial temperature is reached; we have available no experimental results at 100 atmospheres. Finally, attempts to include convection in a more general theory of the nitrogen positive column are discussed and some preliminary results are presented. At least one such attempt permits a theoretical check of the experimental atmospheric nitrogen arc characteristic from 0–10 amperes.

[1] E. S. Lamar, Phys. Rev. **49**, 861 (1936).

174. The Dispenser Cathode, a New Type of Thermionic Cathode for Gaseous Discharge Tubes. A. W. HULL, *General Electric Company.*—Modern oxide-coated cathodes have the characteristic that the initial high electron emis-

sion decreases gradually with time of operation. This characteristic is avoided by using initially-uncoated cathode members to which a coating material is dispensed at uniform rate from a "dispenser" located within the common heat-shield. Such cathodes, after initial aging, show an electron emission equal to the initial emission of oxide-coated cathodes, which does not decrease with time. In the cathodes which have been tested, the dispenser was a closely woven "stocking" of fine molybdenum wires, filled with granules of fused $BaO-Al_2O_3$ eutectic. It was maintained at 1150°C by current through it, and served as a radiation heater for the cathode. The electron-emitting members were clean molybdenum. These cathodes show undiminished electron emission at the end of 3-years life test with no indication of exhaustion.

175. Autoelectronic Emission in Metal Arcs. W. S. HUXFORD, S. G. ESKIN, AND R. W. JONES, *Northwestern University.*—Recent measurements by one of us* show that restriking of the arcs formed between slowly separating contacts occurs during the interruption of low voltage a.c. circuits containing non-inductive loads. These observations have been supplemented by oscillographic determinations of current, potential, and energy of these arcs for the case of silver electrodes. At a contact opening speed of 0.024 in. per sec. the probability of reignition increased with rise of current and with increase of potential from 110 to 220 volts at constant current. Seven cases of reignition were observed in fourteen trials at this speed, but none at the two higher speeds used. The potential gradient and not the potential across the gap at the instant of arcing appears to be the determining factor in reignition. In the seven cases for which measurements were made the value of the field was $0.30\pm0.11\cdot10^6$ volts/cm when restriking occurred; the potential range was from 72 volts to 170 volts. Presumably the arc is initiated by field emission of electrons from the cathode. The field required to start an arc between electrodes having a fixed separation of the order of 0.001 cm was approximately $0.20\cdot10^6$ volts/cm for freshly cleaned silver contacts.

* S. G. Eskin, "Effect of Contact-opening Speed on Arc Energy in a.c. Switching," Gen. Elec. Rev. **42**, 81–86 (1939).

176. The Effect of Electron Bombardment on the Electrical Conductivity of Zincblende Crystals.* MERRIL DISTAD, *University of Minnesota.*—Two opposite sides of a transparent zincblende crystal were coated with semitransparent layers of copper. A potential difference V_c was maintained between these electrodes. When the negative crystal electrode was bombarded by electrons whose energy V_e ranged from 5 to 900 electron volts, a current i_c flowed through the crystal. This current depended on the bombardment time and asymptotically approached an equilibrium value which was proportional to the bombarding current and independent of the crystal temperature. The variation of i_c with the bombardment time was apparently caused by a space charge in the crystal near the bombarded electrode. The equilibrium magnitude of this space charge was practically independent of the magnitude of the bombarding current and of the crystal temperature. It had relatively large negative values for small V_e and was practically zero for V_e greater than 400 electron volts. Electron bombardment produced a crystal current even if V_c was zero. When the positive crystal electrode was exposed to electron bombardment, small crystal currents were observed which were positive or negative depending on V_e and V_c. If the electrons entering the crystal have sufficient energy, they can also liberate other electrons in the crystal.

* Supplementary Program Paper No. 182 is to be called for after Paper No. 176.

177. Measurement of Pain Threshold with Thermal Radiation. J. D. HARDY, H. G. WOLFF AND H. GOODELL, *Russell Sage Institute of Pathology in Affiliation with the New York Hospital, Cornell University Medical College.*—Using the following technique the threshold for pain has been studied in three normal individuals. The light from a 1000-w bulb was focused upon the blackened foreheads of the subjects. A shutter arrangement was provided to allow exposure to the radiation for exactly three seconds. The intensity of the radiation was varied until the subject barely felt pain at the end of the exposure. The intensity of the light was then measured radiometrically in cal./cm²/sec. and called the pain threshold. The results of the studies are: (1) The intensity of radiation required to evoke a painful sensation in three seconds was 0.218 ± 0.004 g cal./sec./cm². (2) The threshold stimulus was the same regardless of the size of area stimulated. This lack of spatial summation is in contrast to other modalities, heat, cold, sight, touch, etc. (3) The time required to evoke pain was a function of the reciprocal of the light intensity. (4) Pain produced by this method was not dependent entirely upon how high the skin temperature was raised. (5) Changes in threshold produced by drugs were studied.

178. Displacements and Depolarization Factors of the Raman Lines of Di-Normal- and Di-Iso-Ethers. FORREST F. CLEVELAND, M. J. MURRAY, JULIA SHACKELFORD, AND HERSCHEL H. HANEY, *Lynchburg College.*—The Raman spectra of di-*n*-propyl, di-isopropyl, di-*n*-butyl, di-*n*-amyl, and di-isoamyl ethers have been obtained by use of a spectrograph having a dispersion of 33A/mm at 4500A. High,[1] who previously studied all except di-*n*-butyl ether with an instrument giving less dispersion, reported only a few lines. For example, he reported only 6 lines for di-*n*-amyl ether, whereas the present investigation yielded 24, most of which were obtained with both Hg 4047A and Hg 4358A. Part of this increase is due to resolution of broad lines into two or more components. In di-*n*-amyl ether, for example, the $-CH_2$-frequency near 1450 cm^{-1} is resolved into four components and eight frequencies are observed in the region 2700–3000 cm^{-1}. The large number of lines observed in the latter region is probably due in part to resonance interactions with the first overtones of the fundamentals near 1450 cm^{-1}. The depolarization factors of the more intense lines have been determined by use of the method described in Paper No. 16. This paper covers part of a research program which has been aided by grants from the Virginia Academy of Science, Sigma Xi, and the American Association for the Advancement of Science.

[1] M. E. High, Phys. Rev. **38**, 1837–1844 (1931).

179. On Alleged Discontinuities in the Diffuse Scattering of X-Rays from Crystals at Small Angles. G. G. HARVEY, *Massachusetts Institute of Technology.*—In a short note Laval[1] claims to have found that the diffuse scattering from a large number of crystals varies in a discontinuous manner as the scattering angle is increased. He used "monochromatic" radiation obtained by reflexion from a crystal and worked in regions where the Bragg law was not satisfied for the particular wave-length (Cu $K\alpha$) and scattering materials used. A large number of discontinuities are reported. We wish to point out that in every case the positions of these alleged discontinuities coincide with the positions of reflected lines of $\frac{1}{2}$, $\frac{1}{3}$ and $\frac{1}{4}$ the primary wave-length, which strongly suggests that the incident beam was not really monochromatic. The results may be completely explained if Laval used a potential of about 35 kv on his tube, a not unusual value for a copper target tube. (He gives no experimental details.) The experiment has been repeated photographically for the case of aluminium, for which Laval reported nine discontinuities. Weak second-order reflexions of half the primary wave-length might be mistaken for edges if one did not map out the immediate vicinity too carefully. It is suggested that the effect reported by Laval does not exist.

[1] J. Laval, Comptes rendus **201**, 889 (1935).

180. The Paschen-Back Effect in the Spectrum of Neon. J. B. GREEN, *Ohio State University*, AND J. A. PEOPLES, JR., *Lehigh University.*—The methods developed in Paper No. 78 have been applied to the spectrum of neon. The transformation coefficients in this spectrum can be easily determined since parameters have been calculated for several of its configurations. When applied to several lines of the p^5p–p^5s and p^5p–p^5d transitions, results are obtained which are in extremely good agreement with observed patterns.

181. Use of Surface States in Solids to Explain Activated Adsorption. W. G. POLLARD, *University of Tennessee.*—In addition to the usual Bloch functions $e^{i\mathbf{k}\cdot\mathbf{r}}u(\mathbf{k},\mathbf{r})$ for stationary states in a solid, there exist stationary solutions with real energy of the type $e^{i(k_x x+k_y y)-\mu z}u(k_x,\ k_y,\ \mu;\ \mathbf{r})$ representing an electron confined to the surface of the solid. These states, first introduced by Tamn,[1] are investigated for actual solids with respect to their form, energy spectrum, and the conditions under which they can exist. Application is made to adsorption by showing that the conditions for stability of these states can be satisfied when a visiting atom gets close enough to the surface. The atom can then transfer its electron to the surface state with large decrease in total energy of the whole system. The transfer is shown to be feasible in that it gives rise to no serious electrical disturbance in the solid. The probable location in energy of these states is shown to be favorable. The extent to which exchange can take place between the two states is determined. The interactions are calculated approximately for H on a metal. An H_2 molecule with sufficient activation energy can split into two H atoms which become bound to surface states.[2] The computed binding energy leads to the right order of magnitude for the heat of activated adsorption of H_2 on various adsorbates.

[1] Ig. Tamn, Physik. Zeits. Sowjetunion **1**, 733 (1932).
[2] Lennard-Jones, Trans. Faraday Soc. **28**, 341 (1932).

182. Dielectric Anomalies of Zincblende Crystals. MERRIL DISTAD, *University of Minnesota.*—The dark current I in a zincblende crystal depends on the time T the potential difference has been on the crystal electrodes. In transparent zincblende crystals at the temperature of dry ice, it was found that the observed current agreed with the empirical equation $I=(I_f+K/T)$ for values of T from 1 to 100 minutes. K is a constant and I_f is the equilibrium dark current. The dark current in colored zincblende crystals, however, does not agree with this equation.

183. Experiments on the Condensation Rate of Mercury Vapor. JOSEPH SLEPIAN AND W. M. BRUBAKER, *Westinghouse Electric and Manufacturing Company.*—The rate of condensation of mercury vapor on to various surfaces has been investigated under conditions of cleanliness which are obtained in ordinary laboratory practice. As other investigators have found, the rate is usually much less than the maximum predicted by kinetic theory. When water-cooled, freshly sandblasted steel probes were suspended above the mercury, the observed rate of condensation was always less than eight percent of that predicted by the simple kinetic theory. If an arc was run in the chamber (as in an Ignitron) and the probe held at a negative potential with respect to the cathode, the rate of condensation increased many fold. This higher rate continued after the arc was turned off, but fell rapidly toward its initial value. The rate of fall depended upon the length of the previous conditioning period. The behavior of a nickel probe is different from that of a steel probe. Although initially the same, the yield of condensed mercury from a nickel probe has been observed to increase to approximately five times that observed simultaneously from a steel probe, when no arc was run in the chamber.

Author Index to Abstracts of the Washington Meeting

Aebersold, Paul C. and Gladys A. Anslow—No. 121
Albertson, W. E. and G. R. Harrison—No. 45
Alder, Robert L.—see Evans, Robley D.
Allen, James S.—No. 115
Anderson, Wilmer C.—No. 90
Anslow, Gladys A.—see Aebersold, Paul C.
Archibald, W. J.—No. 145

Barker, E. F.—see Owens, Ralph G.
Baroody, E. M.—No. 150
Baudisch, Oskar—see Welo, Lars A.
Bayley, D. S.—see Ellett, A.
Beams, J. W.—see Snoddy, L. B.
Beck, C. A. and W. F. Radle—No. 49
Beeman, W. W.—see Friedman, H.
Beeman, W. W. and H. Friedman—No. 29
Beese, N. C.—No. 80
Bell, P. R.—see Harkins, W. D.
Bethe, H. A.—No. 100
Beutler, H.—No. 43
Beutler, H.—see Metropolis, N.
Beyer, Harold G.—see Whitaker, Martin D.
Bidwell, C. C.—No. 143
Birge, Raymond T.—No. 47
Bitter, Francis—see Harrison, George R.
Bitter, F. and A. R. Kaufmann—No. 159
Blewett, J. P., H. A. Liebhafsky and E. F. Hennelly—No. 142
Bloch, F.—No. 39
Bohr, N. and John A. Wheeler—No. 71
Bonner, L. G.—see Kirby-Smith, J. S.
Bonner, L. G., A. P. Cleaves and H. Sponer—No. 18
Booth, E. T., J. R. Dunning and F. G. Slack—No. 68
Borst, L. P.—see Harkins, W. D.
Boyd, Edward and William D. Harkins—No. 105
Brackett, F. S.—see Kuper, J. B. H.
Brackett, F. S. and Alexander Hollaender—No. 53
Brady, Lynn J.—No. 116
Breit, G.—see Share, S.
Brillouin, Léon—No. 144
Brown, Sanborn C. and Robley D. Evans—No. 117
Brubaker, W. M.—see Slepian, Joseph
Buck, J. H.—see Livingston, M. S.
Buehl, R. C. and A. von Hippel—No. 61

Campbell, J. S. and J. R. Davis—No. 74
Carpenter, B.—see Harkins, W. D.
Carroll, K. G.—No. 94
Cartwright, C. Hawley and A. Francis Turner—No. 92
Cleaves, A. P.—see Bonner, L. G.
Cleaves, A. P. and E. K. Plyler—No. 17
Cleveland, Forrest F. and M. J. Murray—No. 16
Cleveland, F. F., M. J. Murray, J. Shackelford and H. H. Haney—No. 178
Cohen, V. W.—see Goldsmith, H. H.
Collins, G. B.—see Waldman, B.
Collins, G. B., B. Waldman and W. Polye—No. 64
Compton, K. T.—see Stone, A. M.
Constant, F. W. and J. M. Formwalt—No. 162
Coomes, E. A.—see Hughes, J. M.
Copeland, Paul L.—No. 170
Cork, J. M. and J. L. Lawson—No. 131
Cowie, D. B.—see Montgomery, C. G.
Crane, H. R.—see Halpern, J.
Crane, H. R. and N. L. Oleson—No. 5
Curtis, B. R.—No. 129

Dart, F. E. and E. Guth—No. 154
Davis, F. J.—see Winans, J. G.
Davis, J. R.—see Campbell, J. S.
Davis, L. and W. V. Houston—No. 161
Dawson, L. H. and E. O. Hulburt—No. 91
Dieke, G. H.—see Wood, R. W.
Dietrich, J. R.—No. 171
Distad, Merril—No. 176, No. 182
Dow, R. B.—No. 153
Duffendack, O. S.—see Lifschutz, Harold
Dunning, J. R.—see Booth, E. T.
Dunning, J. R.—see Goldsmith, H. H.
Dunning, J. R.—see Witcher, C.

Eichelberger, J. F.—see Green, J. B.
Eisenbud, L.—No. 98
Ellett, A., J. A. Van Allen and D. S. Bayley—No. 97
Ellis, Cecil B.—No. 21
Enns, T.—No. 42
Eskin, S. G.—see Huxford, W. S.
Evans, R. D.—see Livingston, M. S.
Evans, Robley D.—see Brown, Sanborn C.
Evans, Robley D. and Alder, Robert L.—No. 118
Ewing, D., T. Perry and R. McCreary—No. 130

Fisher, Russell A.—No. 12
Fisk, J. B.—No. 35
Formwalt, J. M.—see Constant, F. W.
Fricke, Hugo—No. 155
Friedman, H.—see Beeman, W. W.
Friedman, H. and W. W. Beeman—No. 28
Furry, W. H. and R. Clark Jones—No. 134

Gamertsfelder, Carl—No. 31
Gamertsfelder, G. R.—see Shoupp, W. E.
Gill, Piara S.—No. 6
Gill, Piara S.—see Schein, Marcel
Gingrich, N. S. and C. N. Wall—No. 32
Ginsburg, N.—No. 13
Glasoe, G. N. and J. Steigman—No. 70
Goldhaber, M.—see Waldman, B.
Goldhaber, M., R. D. Hill, P. G. Kruger and F. W. Stallmann—No. 36
Goldsmith, H. H.—see Manley, J. H.
Goldsmith, H. H.—see Primakoff, H.
Goldsmith, H. H., V. W. Cohen and J. R. Dunning—No. 69
Goodell, H.—see Hardy, J. D.

Gorrill, Stirling—No. 58
Grabbe, E. M. and L. W. McKeehan—No. 160
Green, J. B. and J. F. Eichelberger—No. 78
Green, J. B. and J. A. Peoples, Jr.—No. 180
Grönblom, B. O.—No. 101
Guth, E.—see Dart, F. E.

Haggstrom, E.—see Witcher, C.
Hagstrum, Homer D. and John T. Tate—No. 132
Hale, Donald H.—No. 56
Halpern, J. and H. R. Crane—No. 66
Halpern, O., M. Hamermesh and M. H. Johnson—No. 73
Ham, W. R.—No. 135
Ham, W. R.—see Simons, J. H.
Hamermesh, M.—see Halpern, O.
Haney, H. H.—see Cleveland, F. F.
Hardy, J. D. and A. I. Ryer—No. 14
Hardy, J. D., H. G. Wolff and H. Goodell—No. 177
Harkins, W. D., H. W. Newson, R. J. Moon, A. H. Snell, L. A. Slotin, L. P. Borst, S. L. Simon, B. Carpenter and P. R. Bell—No. 1
Harkins, William D.—see Boyd, Edward
Harris, W. T.—No. 124
Harrison, G. R.—see Albertson, W. E.
Harrison, George R. and Francis Bitter—No. 76
Hartman, Paul L.—see Smith, Lloyd P.
Harvey, G. G.—No. 25, No. 179
Haskins, C. P.—see Scott, G. W., Jr.
Hebb, M. H.—No. 20
Hebb, M. H.—see Nordheim, L. W.
Hemmendinger, Henry—No. 46
Henderson, W. J.—see King, L. D. P.
Henderson, W. J., L. D. P. King and J. R. Risser—No. 3
Hennelly, E. F.—see Blewett, J. P.
Herb, R. G.—see Plain, G. J.
Herring, Conyers—see Hill, A. G.
Hill, A. G. and Conyers Herring—No. 151
Hill, J. E.—No. 38
Hill, R. D.—see Goldhaber, M.
Hippel, A. von—see Buehl, R. C.
Hippel, A. von—see Merrill, F. H.
Hoisington, L. E.—see Share, S.
Hollaender, Alexander—see Brackett, F. S.
Hornbostel, J.—see Manley, J. H.
Houston, W. V.—No. 147
Houston, W. V.—see Davis, L.
Hudson, G. G.—No. 60
Hughes, J. M. and E. A. Coomes—No. 139
Hulburt, E. O.—see Dawson, L. H.
Hull, A. W.—No. 174
Huxford, W. S., S. G. Eskin and R. W. Jones—No. 175

Jauch, J. M.—No. 109
Johnson, M. H.—see Halpern, O.
Johnson, Thomas H.—No. 9
——see Pomerantz, Martin A.
Jones, R. Clark—see Furry, W. H.
Jones, R. W.—see Huxford, W. S.

Kane, Gabriel—No. 140
Kaufmann, A. R.—No. 158
——see Bitter F.
King, G. W. and J. H. Van Vleck—No. 48
King, L. D. P., W. J. Henderson and J. R. Risser—No. 41
——see Henderson, W. J.
King, Ronold—No. 83
Kip, Arthur F.—No. 59
Kirby-Smith, J. S. and L. G. Bonner—No. 19
Kruger, P. G.—see Goldhaber, M.
——see Shoupp, W. E.
——**F. W. Stallmann and W. E. Shoupp**—No. 96
Kuerti, G.—see Wilkins, T. R.
Kuper, J. B. H. and F. S. Brackett—No. 93

Lamar, E. S.—see Stone, A. M.
Landé, Alfred—No. 110
Langer, L. M., A. C. G. Mitchell and P. W. McDaniel—No. 67
Langmuir, D. B. and L. Malter—No. 141
Lawson, J. L.—No. 128
——see Cork, J. M.
Leitzke, V. A.—see Winans, J. G.
Liebhafsky, H. A.—see Blewett, J. P.
Lifschutz, Harold and O. S. Duffendack—No. 113
Livingston, M. S., J. H. Buck and R. D. Evans—No. 2
Loeb, Leonard B.—No. 57
Logan, Hugh L.—No. 146
Luyet, Basile J.—No. 112
Lyman, Elisabeth Reed—No. 81
Lyman, Ernest M.—No. 65

Mack, J. E.—see Roberson, J. H.
Malter, L.—see Langmuir, D. B.
Manley, J. H., J. Hornbostel and H. H. Goldsmith—No. 33
Margenau, Henry—No. 138
Mason, W. P.—No. 152
Maxwell, Louis R.—No. 122
McCreary, R.—see Ewing, D.
McDaniel, P. W.—see Langer, L. M.
McKeehan, L. W.—see Grabbe, E. M.
Meek, J. M.—No. 63
Merrill, F. H. and A. von Hippel—No. 62
Metropolis, N. and H. Beutler—No. 15
Mimno, H. R.—see Pierce, J. A.
Mitchell, A. C. G.—see Langer, L. M.
Montgomery, C. G., W. E. Ramsey, D. B. Cowie and D. D. Montgomery—No. 37
Montgomery, D. D.—see Montgomery, C. G.
Moon, R. J.—see Harkins, W. D.
Munier, J. H.—No. 30
Murray, M. J.—see Cleveland, Forrest F.
Murray, M. J.—see Cleveland, F. F.

Newson, H. W.—see Harkins, W. D.
Nichols, Myron H.—No. 165
Nielsen, H. H.—see Shaffer, W. H.
Nier, Alfred O.—No. 163
Nordheim, L. W. and M. H. Hebb—No. 8

Nottingham, W. B.—No. 166
Nusbaum, C.—No. 26

O'Brien, Brian—No. 157
——see Stewart, Harold S., Jr.
O'Conor, J. S.—see Witcher, C.
Oleson, N. L.—see Crane, H. R.
Olsen, Leonard O.—No. 82
Onsager, L.—No. 133
Overbeck, C. J. and E. Wiler—No. 85
Owens, Ralph G. and E. F. Barker—No. 44

Packer, Donald M.—No. 55
Page, Chester H.—No. 107
Parratt, L. G. and C. A. Randall—No. 23
Peoples, J. A., Jr.—see Green, J. B.
Pepinsky, Raymond—No. 27
Perry, T.—see Ewing, D.
Pielemeier, W. H. and D. Telfair—No. 84
Pierce, J. A. and H. R. Mimno—No. 89
Placzek, G.—No. 102
Plain, G. J., R. G. Herb and R. E. Warren—No. 126
Plyler, E. K.—see Cleaves, A. P.
Pollard, W. G.—No. 137
——No. 181
Polye, W.—see Collins, G. B.
Pomerantz, Martin A. and Thomas H. Johnson—No. 10
Preston, William M.—No. 75
Primakoff, H. and H. H. Goldsmith—No. 34

Radle, W. F.—see Beck, C. A.
Ramsey, W. E.—see Montgomery, C. G.
Randall, C. A.—see Parratt, L. G.
Randall, R. H., F. C. Rose and C. Zener—No. 149
Richardson, J. Reginald—No. 99
Risser, J. R.—see Henderson, W. J.
——see King, L. D. P.
Roberson, J. H. and J. E. Mack—No. 77
Rose, Albert—No. 167
Rose, F. C.—see Randall, R. H.
Rydbeck, Olof—No. 88
Ryer, A. I.—see Hardy, J. D.

Sachs, R. G.—No. 108
Sanders, F. H.—No. 87
Saxton, Harold L.—No. 86
Schein, Marcel and Piara S. Gill—No. 7
Scott, G. W., Jr. and C. P. Haskins—No. 11
Shackelford, J.—see Cleveland, F. F.
Shaffer, W. H., H. H. Nielsen and L. H. Thomas—No. 104
Share, S., L. E. Hoisington and G. Breit—No. 103
Shive, J. N.—No. 114
Shoupp, W. E., P. G. Kruger, F. W. Stallmann and G. R. Gamertsfelder—No. 40
——see Kruger, P. G.
Simon, S. L.—see Harkins, W. D.
Simons, J. H. and W. R. Ham—No. 136
Sklar, A. L.—No. 52
Skramstad, Harold K.—No. 156
Slack, F. G.—see Booth, E. T.
Slepian, Joseph and W. M. Brubaker—No. 183
Slotin, L. A.—see Harkins, W. D.
Smith, C. G.—No. 168
Smith, Lloyd P. and Paul L. Hartman—No. 169
Snell, A. H.—see Harkins, W. D.
Snoddy, L. B. and J. W. Beams—No. 172
Sponer, H.—see Bonner, L. G.
Stallmann, F. W.—see Goldhaber, M.
——see Kruger, P. G.
——see Shoupp, W. E.
Steigman, J.—see Glasoe, G. N.
Stewart, Harold S., Jr. and Brian O'Brien—No. 54
Stone, A. M., K. T. Compton and E. S. Lamar—No. 173
Strong, John—No. 22
Stubblefield, E. M.—see Waldman, B.

Tape, Gerald F.—No. 125
Tate, John T.—see Hagstrum, Homer D.
Telfair, D.—see Pielemeier, W. H.
Thomas, L. H.—No. 4
Thomas, L. H.—see Shaffer, W. H.
Turner, A. Francis—see Cartwright, C. Hawley
Turner, Louis A.—No. 119
Tyler, A. W.—No. 127

Van Allen, J. A.—see Ellett, A.
Van Vleck, J. H.—see King, G. W.

Waldman, B., G. B. Collins, E. M. Stubblefield and M. Goldhaber—No. 95
——see Collins, G. B.
Wall, C. N.—see Gingrich, N. S.
Warren, R. E.—see Plain, G. J.
Weisskopf, V. F.—No. 106
Welo, Lars A. and Oskar Baudisch—No. 164
Wheeler, John A.—see Bohr, N.
Whitaker, Martin D. and Harold G. Beyer—No. 72
Whitmer, R. M. and H. J. Yearian—No. 24
Wiler, E.—see Overbeck, C. J.
Wilkins, T. R. and G. Kuerti—No. 120
Williams, Dudley—No. 50
Wilson, Thomas C.—No. 148
Winans, J. G., F. J. Davis and V. A. Leitzke—No. 79
Witcher, C., E. Haggstrom, J. S. O'Conor and J. R. Dunning—No. 123
Witmer, Enos E.—No. 111
Wolff, H. G.—see Hardy, J. D.
Wood, R. W. and G. H. Dieke—No. 51

Yearian, H. J.—see Whitmer, R. M.

Zener, C.—see Randall, R. H.